STUDIES IN THE DESIGN AND DEVELOPMENT OF MINIATURE OPTICAL-FIBRE *IN-VIVO* SENSORS: WITH APPLICATIONS IN OBSTRUCTIVE SLEEP APNOEA SYNDROME AND ARTERIAL RESTENOSIS

Thesis submitted for the degree of

Doctor of Philosophy

at the University of Leicester

by

Paul David Goodyer B.Eng. (Hons)

Department of Engineering

University of Leicester

June 1995

ProQuest LLC
789 East Eisenhower Parkway
P.O. Box 1346
Ann Arbor, MI 48106-1346

A man's reach should exceed his grasp

Robert Browning

STUDIES IN THE DESIGN AND DEVELOPMENT OF MINIATURE OPTICAL-FIBRE *IN-VIVO* SENSORS: WITH APPLICATIONS IN OBSTRUCTIVE SLEEP APNOEA SYNDROME AND ARTERIAL RESTENOSIS

by

Paul D. Goodyer

Declaration of originality

This thesis is submitted in fulfilment of the requirements for the degree of Doctor of Philosophy in the Department of Engineering, University of Leicester, UK. All work recorded in this thesis is original unless otherwise acknowledged in the text or by references. No part of it has been submitted for any other degree, either to the University of Leicester or to any other University.

Paul D. Goodyer

June 1995

I dedicate this Ph.D. to my Mum and Dad. Without their love and motivation this would never have been possible

Acknowledgements

There are so many people that have helped and advised me during the past three years that it is difficult to know where to begin. Firstly I would especially like to thank Dr. John Fothergill who stimulated my interest in the area, and provided the support and motivation for three years even when the project was not running quite as smoothly as I had envisaged, his guidance and encouragement is unsurpassed. A big thank you also to Dr. Chris Hanning for his advice in clinical issues and ongoing enthusiasm in the project, especially in his willingness to test the prototypes on himself in the early design stages. Prof. Barrie Jones has provided constant support thoughout the three years. He has given me the opportunity to attend international conferences to help to establish the work in the biomedical field and has always been able to find time to discuss the project at remarkably short notice given his heavy work load; for this I give him a special mention. Prof. David deBono provided invaluable clinical support with chapters 6 to 8, and was kind enough to help in proof reading the thesis.

Numerous bodies have supported the research and include The British Lung Foundation, The British Heart Foundation, Simms Portex Ltd and EPSRC.

The technical support has been so wide spread it is difficult to describe each of the individual contributions. Anthony Piper and Matthew Billingham, both of whom exceeded their duties as biomedical technicians and contributed a considerable amount of thought and ideas to the project. The following groups of people who provide technical support during the research. Engineering: Alan Wale, Tony Forryan, Adrian Payne, Ian Bromley, Jeff O'Connor, Barry Chester, Chris Day, Pete Barwell, Phil Brown and Paul Smith. Anaesthetics: Dr.Chris Secker and Andy Key. Cardiology: Dr.A.Gershlick, Dr.R.Aggarwal, Liz, Debbie and Allison.

I should also mention my friends in engineering who have made life both bearable and sometimes unbearable during the last three years. David Sewell and Tuan Tran, for their constant ribbing sessions and abuse deserve a special mention. The biomedical research group past and present: Dr.S.Q.Wang, Yuehe Wang, Man Ho Kim, Dr.Gareth Loudon, Dr.Sangeet Loudon, Eric Worrall, Paul Keaton, Chen Pang Wong, Kien Seng Wong, Dr.Mike Pont, Dr.Fernando Schlindwein. Also in the control systems research group: Ghassan Murad, Dr.Chris Edwards, Neale Foster and Dr.Tim Fitzpatrick.

Finally I should like to thank Andrea Judge for her love and support without which life would have been very much different, especially during the writing of this thesis.

STUDIES IN THE DESIGN AND DEVELOPMENT OF MINIATURE OPTICAL-FIBRE *IN-VIVO* SENSORS: WITH APPLICATIONS IN OBSTRUCTIVE SLEEP APNOEA SYNDROME AND ARTERIAL RESTENOSIS

Contents

STUDIES IN THE DESIGN AND DEVELOPMENT OF MINIATURE OPTICAL-FIBRE *IN-VIVO* SENSORS: WITH APPLICATIONS IN OBSTRUCTIVE SLEEP APNOEA SYNDROME AND ARTERIAL RESTENOSIS

by

Paul David Goodyer

ABSTRACT

The current *state-of-the-art* of *in-vivo* optical fibre sensors is reviewed. There then follows a review of techniques for pressure measurement and for diagnosis of obstructive sleep apnoea syndrome (OSAS). A catheter containing seven optical fibre pressure transducers for use in the diagnosis of OSAS is described which has been designed, modelled, built and successfully tested both in the laboratory and on six subjects. The transducer has a range of ±5kPa, a resolution of 10Pa and a potential bandwidth of >1kHz. Oral and nasal breathing, snoring, peristalsis and airway collapse were distinguished using the system.

After a review of angioplasty techniques and subsequent healing or arterial restenosis (AR), another optical fibre sensor is described which was designed and built for monitoring the healing of the endothelium and for the detection of AR following percutaneous transluminal coronary angioplasty. The sensor used a fluorescent antibody antigen reaction and its potential was successfully demonstrated both *in-vitro* and using mammalian models. The resolution was better than 107pMoles of antibody. It was shown that the use of a similar radio-labelled reaction was not feasible for *in-vivo* use.

The study concludes that there is significant scope for development of optical fibre *in-vivo* physical sensors and biosensors.

Glossary of terms

Acromegaly	-	An excess of growth hormone leading to abnormal airway
Adiabatic	-	Without heat loss or transfer
Adonotonsillectomy	-	Removal of the adenoids and tonsils
AHI	-	Apnoea-hypoapnoea index
Anisotropic	-	Crystalline material where atoms are not parallel
APD	-	Avalanche photodiode
Arterial Restenosis	-	Reoccurrence of stenosis or blockage of the arteries after surgery
Atonic	-	Lack of muscular tone
Biosensor	-	A sensor, optical or otherwise, involving a biological reaction as part of its transduction element
Birefringence	-	Polarisation conserving anisotropic material
CAT	-	Computer aided tomography
CCD	-	Charge-coupled device
CW	-	Continuous wave (refers to a laser)
DCA	-	Direct coronary angiography
DLA	-	Direct laser angioplasty
Duplex	-	A pair of unidirectional or bi-directional optical fibres
ECG	-	Electrocardiogram (Recording of the electrical activity of the heart)
ECL	-	Emitter-coupled logic
EDS	-	Excessive daytime sleepiness
EEG	-	Electroencephalogram (Electrical activity from the brain)
EMG	-	Electromyogram (Electrical activity from myocardial tissue)
Enuresis	-	Incontinence of urine
EOG	-	Electro-oculogram. The recording of the electrical activity arising due to eye movement
Evanescent	-	A short range optical wave occuring at the interface of two materials of differing refractive index
Extrinsic	-	An optical fibre sensor whereby the light leaves the fibre core
HeNe	-	Helium Neon laser (632nm)
Hypoxia	-	Diminished oxygen in the tissues
In-vitro	-	Within a glass or artificial environment

In-vivo	-	Within living tissue
Intrinsic	-	An optical fibre sensor whereby the light is confined in the optical fibre core
ID	-	Inner diameter
Idiopathic hypersomnia	-	As Narcolepsy but neurologically based
IR	-	Infrared (refers to light of a wavelength longer than visible red)
Ischaemia	-	Insufficient blood supply causing tissue damage or death
Isophotal	-	A line or contour of constant light flux
LAA	-	Laser assisted angioplasty
Laser	-	Light amplification by stimulated emission of radiation
LDV	-	Laser Doppler velocimeter
LED	-	Light-emitting diode
Medulla	-	Upper part of the spinal cord (refers to nerve endings)
NA	-	Numerical aperture
Narcolepsy	-	EDS Sleep disorder. Patient lapses into brief episodes of sleep throughout the day.
Nd-YAG	-	Yttrium-aluminium-garnate solid-state laser rod doped with neodymium (Nd^{3+}) ions
NREM	-	Non-rapid eye movement
OD	-	Outer diameter
OSAS	-	Obstructive sleep apnoea syndrome
Patency	-	The extent to which a vessel is open.
PMT	-	Photomultiplier tube
PTCA	-	Percutaneous Transluminal Balloon Angioplasty
PW	-	Pulsed wave (refers to a laser)
QE	-	Quantum efficiency
REM	-	Rapid eye movement
Scintillation	-	The generation of a photon arising as a result of a radioactive element decaying
Simplex	-	A single unidirectional or bi-directional optical fibre
Thrombosis	-	Intravascular formation of a blood clot
Transduction element	-	Element of the transducer responsible for modulating the electrical or optical activity
UV	-	Ultraviolet (refers to light of a wavelength shorter than visible violet)
VCVS	-	Voltage-controlled voltage-source

Chapter 1

Optical measurements taken from the human body and current biomedical techniques

1.1 Introduction

The aim of this research was to explore some aspects of the important and growing field of optical fibre sensors for *in-vivo* use[1]. Two lines of investigation in the University departments of local hospitals provided vehicles for this research: namely sensors for the diagnosis of Obstructive Sleep Apnoea Syndrome and for monitoring arterial restenosis. The first sensor gives the opportunity to compare fibre optic sensors with existing "conventional" sensor technology in a new application, the second an opportunity to tackle a problem as yet unsolved by existing technology. In order to allow some basis for comparison it was decided to make both sensors extrinsic and amplitude modulated.

Optical fibre technologies derive from the principle of optical confinement using materials of differing refractive index which was first proposed by Tyndall in 1870. However it was not until 1966 that optical fibres were produced with acceptable transmission losses[2] (Grattan., 1987).

Optical fibres are used in medicine either as light guides to conduct laser energy to an operative site, to visualise specific details of a site directly or, in the development of transducers, to measure physiological and biological parameters. In some cases this means providing an alternative transducer to complement currently available technology and further assist in the diagnosis of a patient, or alternatively inventing an entirely new concept for the measurement. The high bandwidth of an optical fibre

[1] An *in-vivo* sensor is a sensor designed for use within a living organism and can be either invasive (placed in tissue) or semi-invasive (placed within a hollow organ, e.g. the gut).

[2] Current silica optical fibres used for communications have an attenuation of < 0.2dB km^{-1}

means distributed sensor systems, comprising a single unbroken optical fibre, can be constructed to collect information from a large number of remote sites. Optical fibre sensors for *in-vivo* use are either invasive or semi-invasive and are used in cardiology, gastroenterology, neurology and respiratory medicine for example (Baldini and Mignani., 1994). The applications of optical fibres in the biomedical field are extensive, and are not reviewed fully in this chapter. Issues only concerning optical fibre sensors for *in-vivo* use, and the transducer designs discussed in this thesis are addressed.

Optical fibres have advantages which cannot be rivalled and are often particularly applicable to medical applications (Mignani and Brenci., 1991). The major advantages are:

Geometric versatility - This is important in highly invasive probes where size is a dominant factor, for example, where restriction of blood flow past a sensor in a blood vessel is undesirable.

Dielectric material - The material of the optical fibre core and cladding is either a polymer or silica. The optical signal cannot be disrupted by electromagnetic interference (although the polarisation in a birefringent fibre can be changed).

Intrinsic safety - The materials used in the manufacture of the optical fibre are chemically, biologically and electrically inert which allows safe operation inside the human body.

This chapter introduces some of the concepts that optical fibre *in-vivo* sensors use and describes the modulation techniques used in their design, including amplitude, phase, frequency and polarisation. This is presented with reference to currently available optical fibre transducers designed for use both inside and outside the human body. Optical fibre transducers are classified as either intrinsic or extrinsic devices (Tracy., 1991 and Jackson and Jones., 1986). The intrinsic optical fibre sensor usually uses a communication grade monomode silica optical fibre and usually encompasses frequency, phase and polarisation modulated sensors, although amplitude modulated

sensors are possible (Gambling., 1991). The extrinsic sensor involves the light leaving the confinement of the optical fibre core temporarily, it is then modified by a transduction element before being intercepted again by the optical system. The transduction element may be either physical, chemical or biological and normally requires that a multimode optical fibre be used. Amplitude modulation is also usually more appropriate.

1.2 Measurements taken from the human body

There are a wide range of signals which can be obtained from the human body. The type of signal depends on whether the measurement is taken externally, such as conventional imaging and blood flow, or invasively, such as intramuscular pressure. Generally biomedical and physiological measurement is classified as electrical, chemical or physical.

1.2.1 Electrical measurements

Electrical measurements from myocardial and neurological tissue can be taken from many sites on the human body. The electrocardiogram is the characteristic electrical activity of the heart and produces a peak-to-peak voltage of approximately 1mV. The rhythmic nature of the signal and the large amplitude makes detection a relatively simple task (Guyton., 1981)[3]. Similarly measurements can be made from other muscles, the name of the measurement being specifically attributed to the muscle under study, e.g. electro-oculogram (eye-movement) and electro-myogram (activity of the skeletal muscles). The measurement of the electrical activity from the brain is called the electroencephalogram (EEG). The acquisition of such data is usually obtained by surface electrodes coupled to a location close to the signal source. The site is treated to remove dead surface skin and hair, and an impedance matching medium, usually in the form of a gel, is interposed. The signal amplitude and the site of the measurement

[3] The measurement is usually performed using a *12-lead* configuration where one unipolar electrode is placed on each limb, and a fifth is placed in different positions on the chest (Bhullar., 1992).

will depend on the type of electrodes used and whether they are *active* or *passive*. Waveform extraction is optimised by strategic placement of the electrodes and carefully screened cables. The addition of an active element in the electrode design increases the signal-to-noise ratio of the signal due to the early pre-amplification close to the measurement site. Intelligent *knowledge-based* signal processing techniques can then be used to decompose the raw signals using digital filtering techniques and signal averaging. Loudon (1991) used these techniques to make a diagnosis of muscle fatigue and disease by decomposing the EMG signal.

1.2.2 Chemical measurements

Analysis of blood and other bodily fluid constituents can provide a significant amount of information about the operation of the internal organs and evidence of disease. Analysis of soft tissue is usually performed by removing a sample or section and examining it in a pathology laboratory. Chemical constituents in the body are measured by one of two methods:

- Biochemical analysis,
- Immunoassay.

Biochemical analysis involves the extraction of the required constituent directly using techniques such as *titration* and *secondary chemical reaction* which are able to isolate chemicals such as cholesterol, iron and glucose. Other constituents are commonly of significantly lower concentrations than can be determined by these methods (10^{-6} to 10^{-15} Moles, compared with 10^{-3} to 10^{-6} Moles detectable with the former techniques). Immunoassay is used is these cases, and is able to detect the presence of steroids, hormones and drugs which are present at these concentrations by using a specific reversible reaction, such as:

$$Ab + Ag \leftrightharpoons Ab\,Ag \qquad \text{(Eqn 1-1)}$$

where antibody (Ab) reacts with an antigen (Ag).

The labelled antibody[4] or *tracer* is added to the sample and is then detected using secondary techniques such scintillation counting (Harmer., 1987). Such techniques are expensive to perform and often use expensive, toxic chemicals such as radioisotopes. Analysis may take several hours to produce a result due to the filtration and purification procedure required during the analysis. A system for use in real-time which could produce "instant" analysis is economically desirable.

The more novel type of chemical sensor is that relying on an electrochemical reaction to measure a molecular reaction. These sensors are classified as *electron-transfer type* devices (a sub-set of these devices are the optical fibre biosensors discussed in section 1.5.2). The selectivity of the sensor is determined by the exploitation of bio-molecules (enzymes and antibodies) able to recognise their counterparts but which respond to virtually nothing else. The aggregation of electron laden enzymes permits a current to flow into the surface of an electrode which is coated with a conductive polymer (Figure 1-1).

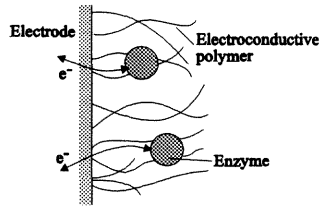

Figure 1-1 Electron transfer of an enzyme on an electrode surface (Aizawa., 1991)

This type of electrode is typically used *in-vitro*, and has in the past been used to detect the presence of toxic gases (Aizawa., 1991).

Sensors designed for chemical analysis are usually limited to the aforementioned *in-vitro* systems, however it could be envisaged that such sensors systems could be used inside the body (see chapters 6 to 8). A sensor described by Narayanaswamy (1993) was able to measure humidity and could be used for measuring the efficiency of the nose in humidifying the inhaled air for example.

[4] The label is a radioisotope, enzyme or fluorophor.

1.2.3 Physical measurements

The group of transducers designed to measure physical properties include those for flow, pressure, force and temperature. There is a wide variety of transducers available to measure physiological parameters. The diversity of measurement devices means that both *in-vivo* and external measurements are possible.

The most common transducer for the measurement of force and stress is the silicon strain gauge. One example is the measurement of force exerted by the myocardium. This may be measured by an array of transducers, the limitation is in the manner in which the physical movement is conducted to the measurement device. The electrical activity (electromyogram) does provide evidence of muscle activity, but in order to measure physical movement, expansion or contraction, an element must conduct the movement to the transducer (Figure 1-2).

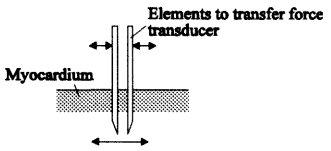

Figure 1-2 The physical members transferring expansion and contraction of myocardium to the force transducer.

One of the most valuable measurements which can be taken from the human body, both *in-vivo* and externally, is pressure. The first biomedical pressure measurement taken was that of blood. This was published by Stephen Hales in 1733 and involved inserting a tube into the carotid artery of a mare and observing the pressure head of the blood as it rose up the vessel lumen (Nichols and O'Rourke., 1990).

An animal body consists not only of a wonderful texture of solid parts, but also of large proportion of fluids, which are continually circulating and flowing, thro' an inimitable embroidery of blood vessels and other inconceivably minute canals. (Hales., 1733).

Current technology has permitted the miniaturisation of devices which may be inserted not only into the major arteries, but into the smaller vessels such as the

coronary arteries. Silicon microstructures are often designed for use inside a catheter, and have been used with significant success. Such silicon sensors are manufactured using etching techniques and can be made with high precision, however optical fibre transducer designs can be manufactured small enough to be passed down the lumen of a needle (0.35mm) (Emanuelsson *et al.*, 1991).

A system developed by McNally *et al* (1992), described a strain-gauge system to measure the pressure at the centre of the intervertebral disc. The strain gauge was mounted on the tip of a needle 1.3mm in diameter with a pressure range of 0 to 3MPa (±0.2% linearity). The frequency response was however limited, and had a working dynamic range of only 0 to 10Hz. The introduction of miniature transducers constructed using optical fibres has permitted intramuscular and intravascular pressures to be measured more accurately without significantly impairing the measurement (section 1.5.1).

1.3 Optical techniques in medicine

The use of lasers has provided a means of conducting safe and highly selective investigative and therapeutic surgery. Several types of laser are used and include Nd:YAG, argon ion and excimer systems. The choice of the laser is dependent on the medium through which the laser energy propagates prior to striking the target, and the purpose of the surgery: ablative or investigative. Recanalisation of stenotic arteries has been performed by many researchers (section 6.5.2 - laser angioplasty). The therapeutic use of a laser is dependent on the following three factors (Kaplin *et al.*, 1985):

- Laser power density
- Absorption coefficient of the target
- Absorption coefficient of the medium through which the laser light travels to reach the target.

Trials with argon ion lasers in *continuous-wave* mode have highlighted problems of localised heating leading to further vessel and tissue damage. Also the absorption of

the argon ion laser at the higher energy wavelengths (488nm and 514nm) by the blood means that the vast majority of the energy is absorbed by the red blood cells. Kaplin and his co-researchers (1985) found that in order for therapeutic laser surgery to be performed with an argon ion laser, 99% of the red blood cells must be displaced from view. To minimise these problems a *pulsed-wave* excimer laser system is currently used (White *et al.*, 1993).

One of the most promising applications of lasers and high power coherent light sources is that of light activated drug therapy and photopolymerisation of materials for *in-vivo* use. One of the most heavily researched areas is that of locating malignant cells using UV activated molecules trapped by the tumour (Hematophorphyrin Derivative, HpD). It is envisaged that photo-dynamic drug therapy could be used in a similar manner to destroy the malignancy (Colussi *et al.*, 1994). Lasers are now also used extensively in dentistry using photopolymerisation technology. A study by Potts and Petrou (1991) described a scheme for photopolymerisation of resin used to fill the root canals of human teeth using an argon ion laser carried by a fibre optic cable as an alternative to the conventional non-coherent UV curing lamps. Careful choice of the wavelength (477nm and 488nm) and efficient optical coupling permitted a low power laser (50mW) to be used. The use of an argon ion laser in dentistry is made viable because of the lack of red blood cells in the medium conducting the laser beam: the dentine being able to transmit the laser energy with a minimum of absorption.

The pulse oximeter, used to measure the oxygenation of haemoglobin, has become an invaluable tool in medicine and was one of the early applications of optical fibres in biomedical engineering (see section 1.5.2). The system relies on measuring the absorption at visible-red and infrared wavelengths whereupon a ratio is obtained and checked against a look-up table (Eqn 1-2):

$$\frac{\Delta \text{ red}}{\Delta \text{ infra - red}} = \Omega \rightarrow [\text{Look - up table}] \rightarrow SpO_2 \qquad \text{(Eqn 1-2)}$$

where Δ red - Absorption at red wavelengths
Δ Infra-red - Absorption at IR wavelengths
Ω - A variable defined by the absorption of haemoglobin
SpO_2 - Oxygen saturation of the tissues

Such a system has inherent problems in its design because of the requirement for a look-up table. This requires an extensive amount of research into the pre-calibration process. A system developed by Leuthner (1994) attempted to simulate the presence of blood using varying dilutions of red and black dye and relating the extinction coefficient to that of real arterial blood (Prys-Roberts., 1969), however a standard method of calibration is yet to be established. Other systems have been developed to measure other chemical constituents and pH, and are discussed in section 1.5.2.

1.4 Light modulation techniques in an optical fibre sensor

1.4.1 Intensity modulated sensors

The simplest optical fibre transducer to visualise is the amplitude or intensity modulated sensor, where the amplitude of the light contained inside the optical fibre is modified in sympathy with the measurand. The optical fibre is usually multimode and hence has limited *down-lead* sensitivity[5].

Fibre / transduction element displacement: The path of light coupled through an optical pathway of a receiving and emitting fibre is modulated by either mis-alignment or impairment of the optical path by an external means. This can be achieved by either adjusting the position of the receiving optical fibre, or introducing a secondary optical component such as a prism or grating (Medlock., 1987). Similar to this is the reflective sensor where the light encounters a reflective surface on its journey to that receiving.

Fibre loss: The most prominent characteristic of the amplitude modulated sensor system is the susceptibility to bend loss. Bending of an optical fibre is classified as either micro or macro-bending[6]. The occurrence of bending can lead to one of two

[5] *Down-lead* sensitivity is when the signal is more likely to degrade due to intermodal dispersion when using multimode optical fibre. The signal is also more susceptible to noise.

[6] Macro-bending is when both the optical fibre core and cladding is bent. Micro-bending is said to occur when the bend radius is comparable to the dimensions of the optical fibre core (Powers., 1993).

occurrences, either the high order modes are coupled out of the optical fibre core and dispersed, or the high-order modes are coupled out of the core into the cladding momentarily and then back into the core. The latter usually occurs at a critical bend radius and is known as the whispering gallery effect (Haran *et al.*, 1994). As a result the power transmitted through the optical fibre bent at a given bend radius changes periodically as a function of wavelength (Berthold., 1994).

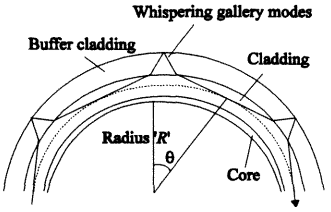

Figure 1-3 An optical fibre given a macro-bend gives rise to the light being coupled out of the core momentarily known as the whispering gallery effect (Haran *et al.*, 1994).

The principle of bend loss can be used directly to construct a physiological transducer. Micro bending sensors were used by Stenow and Öberg (1994). A micro-bending cantilever structure was constructed and mounted on the surface of a limb, the limb venous blood flow was then occluded and the radial expansion observed (<0.1% change in volume could be easily observed).

The intensity sensor is now a well established technique for determining the level of a liquid in a vessel (Watson., 1989). Sensors of this type rely on the light conductor coming into direct contact with the fluid. If the refractive index of the liquid is greater than that of the optical fibre light modes will be lost. The level sensor consists of either a closed loop of optical fibre with the cladding removed or a prism inserted into the circuit, the internal reflection of which is changed when the prism is immersed in a fluid. If an optical fibre with a core refractive index which is dependent on temperature (such as polymer) is used, loss due the interface between the two materials can be measured and hence temperature quantified (Thursby *et al.*, 1992).

A more elegant method of constructing an intensity modulated system is by exploiting the evanescent field present at the interface of two surfaces of differing refractive index. The extraction of the energy from the system takes place at the point at which internal reflection occurs (Figure 1-4), and where an absorbing surface is located. Similarly a reflective surface may be used to modulate the evanescent wave directly[7] (Hale and Payne., 1994). This method is usually used where the operating distance is small as the evanescent wave decays exponentially with distance (negligible at ≈1μm) (Medlock.,1987). This technique is often used in conjunction with sensors based on fluorescence quenching (section 1.5.2) (MacCraith *et al.*, 1993).

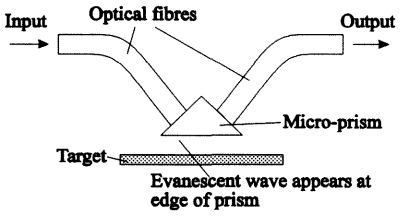

Figure 1-4 An optical fibre sensor based on the evanescent wave of an optical fibre coupled micro-prism.

The use of amplitude modulation means there can be inherent problems with the interruption of the signal *en route* giving rise to apparent changes in the signal which are not due to the transduction element; hence causing ambiguous results. To overcome this problem a dual-reference or dual-wavelength *hybrid* can be used. This design uses more than one optical fibre to determine a *ratiometric* signal, the signal-to-noise ratio of which is conserved at larger distances away from the transduction element. Alternatively a *colourmetric* technique may be adopted where two wavelengths are coupled into the optical fibre simultaneously, one which is highly modulated by the transduction element and another which is not affected. The ratio

[7] The process of absorbing the evanescent wave is known as *frustrated total internal reflection*, where reflection of the wave is known as *Attenuated total reflection.*

between the two may then be calculated to improve the signal-to-noise ratio (Libo and Anping., 1991).

1.4.2 Interferometry

Interferometry is a well established technique for measuring temperature and strain for example with high accuracy and resolution (<1nm). The process of interferometry relies on the constructive and destructive interference of light waves when they combine in and out of phase respectively.

An optical fibre sensor using interferometry is a phase modulated system, but the process of demodulation produces a signal which changes in amplitude due to the interference of the wave-fronts. Optical fibre *high coherence interferometers* are classified as either Mach-Zehnder, Sagnac, Michelson or Fabry-Perot named after their inventors (Jackson., 1987) (Figure 1-5).

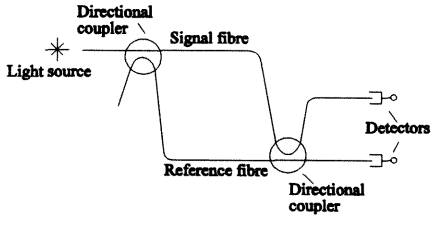

Figure 1-5a
The Mach-Zehnder interferometer

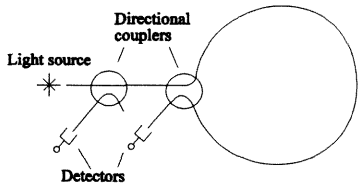

Figure 1-5b
The Sagnac interferometer

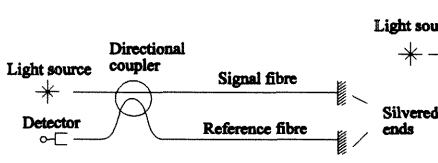

Figure 1-5c
The Michelson interferometer

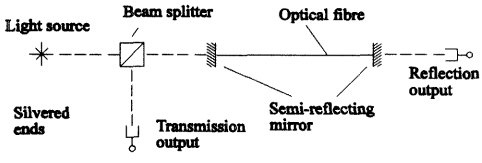

Figure 1-5d
The Fabry-Perot interferometer

The most common configurations are the Mach-Zehnder and Michelson. Both designs are a variations on the Rayleigh refractometer developed in the late 1800s. Parameters are measured with respect to a reference arm which is in stable conditions by a signal fibre: the light of which is modified by an external influence (Rogers., 1988). The Fabry-Perot device uses a pair of semi-reflecting mirrors which set up an optically resonant cavity; this may be used to perform lasing action if an appropriately doped fibre is used (section 1.4.3) (Gambling and Poole., 1988). The Sagnac interferometer is used in the design of gyroscopes (Yu and Siddiqui., 1993), and is a loop of optical fibre through which light is launched in both clockwise and anti-clockwise directions. The phase shift due to the *Sagnac effect* observed upon rotating the loop is then measured.

1.4.3 Frequency and wavelength modulated sensors

Perhaps one of the most promising developments in the optical fibre industry for sensor applications is the fluorescent optical fibre. The fibre core is doped with a fluorescent material which is responsive to the measurand. A sensor described by Maurice *et al* (1994) was able to measure temperature changes over the range 200K to 1200K in this way. A short length of Erbium and Ytterbium doped silica fibre was excited with a argon ion laser at 488nm. The ratio of the spectra of the returned light with respect to a reference was then used to produce a measure of temperature. A similar system was developed by MacCraith and McAleavey (1994), light at near-infrared wavelengths was used to estimate the absorption of a sample of water.

Optical fibres have now been developed which are able to perform lasing action, having been pumped with cheap semiconductor lasers, to produce several tens of watts of power (Poole., 1992). One of the most recent developments is that of the *up-conversion* optical fibre laser where a Ho^{3+} or Pr^{3+} doped fluoride glass fibre is pumped with a longer wavelength than the lasing wavelength. This is particularly useful in biomedical applications where visible light is used to stimulate fluorescence, and benefits from the associated low coupling loss between correctly terminated fibres.

Fluorescence is used extensively in the development of *in-vivo* biosensors sensors, see section 1.5.2 for further discussion.

1.4.4 Polarisation modulated sensors

Birefringence of a medium is observed in anisotropic materials, where the molecules in the material acting as the waveguide, typically quartz or calcite, are in different directions throughout the structure (Wilson., 1989). The polarisation of an electromagnetic wave is determined by observation of the electric field vector. The speed of light travelling though an anisotropic material is dependent on the direction and polarisation, i.e. the direction of the electric field vector with respect to the crystal lattice. In practical terms this means that the refractive index of the material is dependent on the polarisation of the wave travelling through it. These materials are said to be *birefringent* and can be *biaxial* or *uniaxial* [8]. Birefringence can be introduced into the optical fibre by either geometrically changing the fibre core and cladding or introducing axial stress across the fibre core (Figure 1-6).

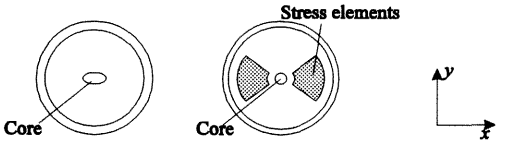

Elliptical core optical fibre "Bow-tie" optical fibre

Figure 1-6 Configurations of stress-induced birefringent optical fibre (Ourmazd *et al.*, 1983)

Birefringence[9] $B = (n_x - n_y) = \left(\frac{\lambda}{2\pi}\right)\Delta\beta$ (Eqn 1-3)

where n_x = Refractive index of polarisation in axis 'x'
n_y = Refractive index of polarisation in axis 'y'
$\Delta\beta$ = Phase change between orthogonal polarised modes
λ = Wavelength

[8] Uniaxial and biaxial describe a birefringent optical fibre with one or two axes respectively, where the velocity of propagation is the same.

[9] The birefringence of an optical fibre is characterised by its *beat length*. This is defined by the distance between points on the transducer where the polarisation modes are in phase and is typically of the order 0.6mm (Gambling and Poole., 1988).

Birefringent optical fibres are used currently in strain gauge gauges, gyroscopes and current sensors (Varnham *et al.*,1983, Jeong *et al.*, 1994 and Qian *et al.*, 1994). Although systems utilising polarisation conserving optical fibres have yet to be extensively researched in the biomedical field, sensors have been developed to measure hydrostatic pressures (0 to 40kPa) (Gauthier and Dhliwayo., 1992). The development of such sensors is often impractical for miniaturisation for use *in-vivo* because of the size of the transduction element.

1.5 *In-vivo* optical fibre sensors

Optical fibres are perhaps more famous in medical endoscopes than in the communications industry. Their increased bandwidth in comparison with conventional coaxial cable has revolutionised the communications industry, but their infiltration into the biomedical field is less extensive that it could be. Research into the development of optical fibre sensors is widespread, but they are often not developed commercially due to requirements for extensive clinical trials before such a device is regarded as acceptable.

1.5.1 Physical optical fibre sensors

Physical sensors are noted most for their measurement of pressure and flow. The transducer transduction element physically deforms or moves and has the resulting effect of directly modulating the light. The simplest design to envisage is that of the optical displacement transducer, where the optical fibres are perpendicular to a planar reflective target which modulates the light directly.

One of the most promising applications of optical fibre is the development of a transducer to measure intravascular or intramuscular pressure or flow (Tenerz., 1991 and Crenshaw et al., 1989). This is a formidable achievement as miniaturisation must be such that blood flow is not impaired and hence the pressure reading is not exaggerated. Tenerz produced a transducer able to resolve a pressure range of 0 to 500mmHg (67kPa). Optical fibres need not necessarily measure blood flow invasively. The classic device used to calculate blood flow non-invasively is the ultrasonic Doppler

blood flow meter (Satomura., 1959). Using optical fibres as a light guide it is possible to construct an optical Doppler meter, known as a laser Doppler velocimeter (LDV). The LDV uses the Doppler-shift phenomenon with a coherent laser light source (Eqn 1-4). The wavelength is chosen so as to be reflected by the red blood cells in the blood stream as they pass through the vessel lumen. The change in frequency of the light reflected back describes the local flow rate (m/s) of the red cells and hence of the blood. Although a laser is selected at a wavelength not readily attenuated by the intervening tissues (Helium-Neon at 632.8nm), the system is regarded as *in-vivo* as the emitting and receiving optical fibre must penetrate the wall of the blood vessel (Kajiya *et al.*, 1987). The governing equation of the LDV is:

$$\Delta f = \frac{2nV\cos\theta}{\lambda} \qquad \text{(Eqn 1-4)}$$

Where Δf = Doppler shift frequency
n = Refractive index of the blood (1.33)
V = Blood velocity (ms^{-1})
λ = Wavelength
θ = Angle between light beam and flow direction

The miniaturisation of optical fibre sensors has permitted a substantial number of physical parameters to be measured directly, without the need for coupling systems[10]. The early optical fibre manufacturing techniques did not permit fine optical fibre catheters to be constructed, and the limitation of optical receivers and emitters meant that optical fibre bundles had to be used. Even so intravascular sound and pressure could be measured optically (Lindström., 1970 and Ramirez *et al.*, 1969). A system for measuring the length and diameter of elastic vessels *in-vitro* (Papageorgiou and Jones., 1985) was also developed. Such schemes are designed to measure strain and have also been adapted to measure thoracic wall movement (Dahnoun *et al.*, 1994) and limb flexion (Stenow and Öberg., 1994).

[10] For example in pressure measurements a saline filled catheter was used, in early designs, to conduct the pressure signal to a remote site for measurement as the transducer could not be integrated into a catheter (Drorbaugh *et al.*, 1963 and Chu *et al.*, 1964).

The optical fibre sensor is not limited to applications where a transduction element physically moves. The gas content and pH of liquids and gases have been measured by the development of colour modulated optical fibre sensors. Such systems rely on the transduction element changing colour and hence changing its absorption and reflection characteristics. The temperature of a flame for example can be measured in this way (Pitt *et al.*, 1985). These sensors are one of the designs collectively called chemical and biological sensors.

1.5.2 Biosensor systems - chemical and biological sensors

Biosensors are a group of sensors where the primary transduction element utilises a biological system or biochemical reaction. They may encompass any one of the aforementioned modulating systems. For example *in-vivo* optical fibre biosensors have been developed to measure dissolved oxygen concentration (Smith., 1987). Biosensors can be classified under one of two headings:

- Biocatalysts - The binding of a molecule is followed by a chemical reaction. The process is reversible and consequently such transducers based on this concept are often re-usable.
- Bioreceptors - Molecules bind to the receptive component of the biosensor, and the reaction is irreversible (Brooks and Turner., 1987).

The fibre optic reflection oximeter works on a similar principle to all fibre tip biocatalyst biosensors. A transduction element mounted on the tip of an optical fibre changes its optical properties with respect to the measurand. In the case of the reflection oximeter a bundle of optical fibres emits light into the blood and the back scattered light is measured at the visible red and infrared wavelengths. The absorption spectra of haemoglobin and oxyhaemoglobin can then be described: the logarithm of the ratio of the absorption spectra is approximately proportional to the blood oxygen saturation (Landsman *et al.*, 1978).

Optical fibre sensors, or *optrodes*, have been developed to measure a multitude of chemical constituents and properties, including pH (Silva and Werneck., 1994), glucose, enzymes and antibodies (section 1.2.2). The pH sensor uses one, or a bundle of optical fibres, to analyse the absorption of a dye located at the optrode tip. A dye is

chosen so as to be responsive to changes in pH changing the absorption of the dye at a characteristic wavelength. For example bromothymol blue has a peak absorption at 616nm which varies by several orders of magnitude for a small change in pH (Baldini *et al.*, 1987). A sensor developed by Dafu and his co-workers (1993) described a sensor able to distinguish 3.0 to 5.0pH: bromine phenol blue, 7.0 to 8.5pH: phenol red and 8.0 to 10.0pH: bromothymol blue. In a similar manner to the pulse oximeter two wavelengths are generally used, one to measure absorption and one as a reference to overcome problems arising due to bend loss which will degrade the amplitude modulated signal. If the pH sensitive material is replaced accordingly it is also possible to measure partial pressures of carbon dioxide and oxygen. Research by Brenci and Baldini (1992) described a sensor integrating all of the aforementioned systems into a intravascular catheter of 0.65mm in diameter. Devices are enclosed in a gas semi-permeable membrane to make them sterilisable and re-usable. Typically a chemical sensor has a time delay of 15 to 90 seconds. Since conventional biochemical assays may take several hours this is a considerable improvement.

Bioreceptor biosensors rely on the binding of a substance to a substrate. The ensuing chemical change is then detected optically. The enzyme-based fibre optic sensor described by Arnold (1985) used an enzyme amplitude modulated sensor to determine the concentration of the enzyme treated nylon mesh. The absorption of the membrane at varying concentrations was observed and a proportionality was shown. Such sensors are usually limited in their use because of the extensive analytical techniques required to produce a reaction. A system developed by Fothergill *et al* (1988) used a photochemical reaction to monitor levels of DNA in an assay produced an instant result, however this was not a catheter tip device.

Fluorescence is exploited in a large number of sensor systems, some of which are biosensors. In biochemistry and immunochemistry monoclonal antibodies are given a biological label which is optically detectable (a development discussed in chapter 6 to chapter 8). The optical fibre glucose sensor and oxygen sensor both use fluorescence to determine the concentration of each in a sample (Maccraith *et al.*, 1993). The glucose sensor described by Meadows and Schultz (1993) contained two fluorescent chemicals chosen to be fluorescent at two different wavelengths: 485nm and 540nm, to overcome the need for recalibration. A novel fluorescent biosensor sensor was

described by Golden *et al* (1994) using antibodies. The cladding of an optical fibre was removed, the tip was moulded into a taper, and coated with an immobilised antibody. The concentration of a specific antigen in an assay could then be determined using an antibody-antigen reaction which results in antigens binding to the probe which could then be detected by observing fluorescence at 514nm. The development of an optical fibre biosensor with an active element which modulates the fluorescence with respect to the measurand is known as *fluorescence quenching*.

The use of fluorescence in a sensor may not encompass any active transduction element at all, comprising only a single optical fibre or optical fibre bundle to analyse the material at the transducer tip using evanescent wave theory. The light is allowed to leave the sensor and strike a target, the fluorescence of which is the detectable. Analysis of the wavelength of the back-scattered light and that emitted can be used to quantify fluorescence. Such probes have been used extremely successfully as part of *in-vivo* studies analysing the fluorescence of atherosclerotic arterial plaque and dysplasia (Bartorelli *et al.*, 1991 and Cothren *et al.*, 1994) (cf: chapter 6).

1.5.3 Electrical optical fibre sensors

There are a limited number of optical fibre sensors available to measure electrical signals in the human body. Electrical current sensors have been developed, and operate on the Faraday effect which induces birefringence into an optical fibre (section 1.4.4). Such sensors rely on magnetically induced birefringence, and hence require a high magnetic field strength arising from a high current density: such sensors are used in power stations to measure the field in the insulation between the primary and secondary turns of a transformer operating at 440kV (Jackson *et al.*, 1992). The high field strengths required mean that such a scheme is not suitable for detection of low amplitude signals such as are present in the EEG or ECG for example.

1.6 Discussion and motivation

The improvements in many commercial transducers are small in comparison with optical fibre transducers as the limits of such devices have been reached and the

technology is established. Although optical fibres are currently approaching the theoretical transmission limits (Figure 1-7), the efficiency of receivers and emitters are constantly being improved.

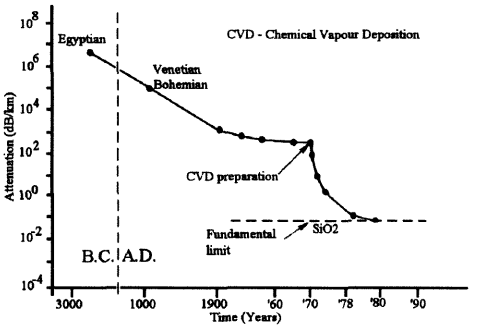

Figure 1-7 Optical fibre loss in an historical concept (Kao., 1988)

Patent description	Patents
Biological constituents	66
Chemical constituents	239
Defects, flaws presence or absence	403
Density	11
Dimension	219
Electrical and/or magnetic parameters	55
Flow	29
Force, stress, strain	47
Laboratory measurements	140
Liquid level	33

Patent description	Patents
Medical parameters	56
Movement (excluding flow)	389
Optical properties	229
Physical properties	81
Proximity, position	234
Pressure	28
Smoke, turbidity	45
Temperature	47
Unspecified parameters	49
Other	317

Figure 1-8 Distribution of optical sensor patents in the US during 1989 (Grattan., 1989)

The number of active US patents in 1989 was large: 2717. Interest in fibre optic sensors has steadily increased in the area of biomedical engineering and the bias has come away from the military which provided the vast majority of the original funding (Grattan., 1989) (Figure 1-8).

The use of optical fibre transducers in surgery or by the general practitioner means that major operations can be replaced by minor clinical interventions. The miniaturisation and hence less invasive nature of systems using fibre optic technology means that the patient recovery time is substantially shorter and this will reduce nursing costs (McGeehin., 1987). There is also the ability to learn more during a single study by measuring more physiological parameters simultaneously to produce a more reliable diagnosis.

1.6.1 Aims and objectives

It is important for researchers to gain a good understanding of the key fields of development when designing a sensor, optical or otherwise, for *in-vivo* use. Catheter systems for medical diagnosis must, as far as possible, not affect the parameter being measured and this usually implies that it should be as small as possible. One of the original main advantages of the optical fibre was its intrinsic isolation from the signal acquisition and processing equipment. Current technology means that a large range of isolation apparatus is available, however this feature is desirable as it does mean that cost is reduced. Moreover the low cost of optical fibre means that the whole transducer arrangement may be deemed disposable.

The aim of this research is to contribute to the understanding of physical and biochemical sensing using optical fibres, by using two optical systems as vehicles to investigate some of the main design considerations during the development of sensors for *in-vivo* use.

Optical fibre sensors are available to measure a multitude of parameters which can be classified as either electrical, chemical or physical. The latter group of sensors: chemical (biosensors) and physical, have been developed by applying novel techniques to construct transducers to aid in the diagnosis of specific medical disorders. The marked differences were targeted to explore the broad range of parameters which must be considered when designing a device for use in the human body.

1.6.2 Scope of research

Given the wide choice of modulation techniques available, the research was restricted to amplitude modulated sensors, the two selected were diverse as possible so

as to explore the capabilities and limitations for each device *in-vivo*. The first sensor selected attempted to apply and improve current technology in the development of a pressure transducer intended for use in the upper airway. The second is a biosensor and is intended to be considerably more invasive being for use in the coronary arteries.

The aim was not to develop commercial systems for either of the devices, but purely to examine the clinical feasibility of each, and to clarify the design lessons which should be addressed. The work is intended to explore and extend the *state-of-the-art* by review and detailed examination of the major issues associated with the production and testing of the working prototypes.

1.7 Thesis overview

Chapter 1 has introduced the rationale for the research, and introduced some of the current technologies exploited in contemporary physiological biomedical measurement, both optical and otherwise. Having addressed optical fibres for use in the development of sensors for *in-vivo* use the modulation techniques of light have been summarised with reference to the demodulation techniques currently available in optical fibre systems. It has been proposed that two optical fibre sensors be developed as vehicles to contribute to the understanding in such systems: investigating both physical and biosensors. The research was restricted to amplitude modulated and extrinsic systems.

Chapter 2 to chapter 5 describe a catheter containing seven optical fibre pressure transducers which is intended to aid in the diagnosis of obstructive sleep apnoea syndrome. Chapter 2 is the motivation behind the catheter development and gives a brief overview of the problem from a physician's aspect. The overview of sleep and sleep disorder leads to the specific sleep disorder *Obstructive Sleep Apnoea Syndrome* (OSAS) and the physiology of the airway which causes the problem. The current investigative methods for diagnosing OSAS are discussed and include invasive and non-invasive methods as well as the fibre optic endoscope for direct visualisation of the airway components. One motivation for the work reported here is the current primitive nature of pressure transducer techniques for examination of the upper airway and the

unsatisfactory results produced from X-ray. This then leads to chapter 3 where the use of a fibre optic pressure transducer is addressed. A brief summary of some of the research concepts and industrially available transducers is given before describing the development of the multiple transducer catheter. The transducer was designed to be inserted through the naso-pharynx and must encounter a bend radius of typically 100mm through 180°, and so suffers from macro bending losses. The design overcomes problems associated with bending loss, as it typically occurs in amplitude modulated sensors, and incorporates design features required to achieve a sensitivity of 10Pa of static water pressure. The design details regarding the integration of seven pressure transducers in a catheter and the system electronics are discussed with reference to the original design specification. A single channel more portable device is also presented for use in pre-term babies and neonates. A series of mathematical models was developed to aid in the design process. This includes a simplified two-dimension algorithm, and a more complex three-dimensional system. The latter model encompasses the Gaussian non-Lambertian distribution of light emanating from an optical fibre, and the convex reflective transduction element of the transducer. Results used to assist in the design procedure are presented. Chapter 5 presents the clinical trials performed using the pressure transducer catheter with both static and dynamic testing. Experiments were conducted on patients under both general and local anaesthesia. Results of tests on a catheter of low thermal mass containing a single device are compared to results from a seven channel device with a significantly higher thermal mass (time constant = 78 seconds) Problems of such a device for use *in-vivo* are addressed with reference to the expected temperature change of the airway mucosa during inspiration and expiration. It was found that the device could observe the palatal vibration characteristic of snoring patients which may also be characteristic of OSAS.

As a comparison and contrast with the pressure transducer a second device was developed, also for *in-vivo* use and amplitude modulated, but more invasive. Chapter 6 develops the rationale for the probe development in a similar manner to chapter 2. Restenosis of the coronary arteries may follow percutaneous transluminal balloon angioplasty (PTCA) and is attributed to the migration of the smooth muscle cells into the vessel lumen during the healing process. The haemodynamics of the pulmonary and

systemic circulatory system are presented as are the effects of stenosis on blood flow and its prognosis. The current techniques for investigating blood flow and arterial damage are reviewed with reference to both invasive and non-invasive imaging techniques. It was proposed that an optical fibre probe be developed for intravascular use which could monitor the healing process of the endothelium: the lining of the vessel wall. The antibody-antigen complex is introduced as a means of locating endothelial cell damage by the use of a biochemical label. Biosensors are widely developed as extrinsic amplitude modulated systems, and although the sensor is designed for use in a completely different application, the concept is the same as the pressure transducer. Chapter 7 evaluates two possible optical technologies for the detection of biologically labelled monoclonal antibodies using scintillation and fluorescence respectively. The latter design was selected for development because of the non-toxicity of the chemicals used and the potentially higher sensitivity due to the excitation light source. The reasoning behind the choice of the biochemical label is discussed, and the formal probe development including optic and hardware specification is presented. The results obtained from the endothelial cell damage probe are summarised in chapter 8. The highly invasive nature of the endothelial cell damage probe in comparison with the optical fibre pressure transducer limited the extent of the clinical trials, but detailed investigations were performed on both simulated vessels and mammalian models. Experiments were conducted with vessels perfused with blood and heparin, and vessels perfused with saline. Living endothelial cells were investigated *in-vitro* using sodium fluorescein labelled monoclonal antibodies, the ensuing antibody-antigen complex made visualisation of the damaged region by the probe possible.

Chapter 9 draws conclusions from the design lessons learnt during the development of each of the optical fibre transducer designs. The pressure transducer, although for *in-vivo* use, is not as invasive as the endothelial probe. The endothelial probe is extremely simple, containing two optical fibres and relying on a biological reaction taking place external to the probe, the optics, detector and light source are however considerably more complex. In contrast the pressure transducer is more complex to construct due to the integration of a transduction element into the probe tip, however the optics are simpler. The pressure transducer is an addition and modification to existing technology, whereas the endothelial cell probe is operating at

the limits of current technology and required expensive detection apparatus. Both transducers may be considered disposable, and both are amplitude modulated. The designs highlight the limitations of amplitude modulated sensors in some applications which become immaterial in others.

Chapter 2

Rationale for the optical fibre pressure transducer - An overview of Obstructive Sleep Apnoea Syndome and upper airway physiology

2.1 Introduction

This chapter discusses the anatomy and physiology of the human upper airway, paying particular attention to characteristic anatomical changes which may lead to the occurrence of Obstructive Sleep Apnoea Syndrome (OSAS), and is the rationale for the development of the optical fibre pressure transducer catheter. A general overview of the upper airway is presented and the differences between patients with a healthy and abnormal airway are discussed. Sleep is a significant contributory factor in OSAS and consequently current methods of sleep stage classification are summarised, and related to the occurrence of the disorder. The currently practised surgical procedures are summarised and the advantages and disadvantages highlighted. Currently available transducers to measure pressure and flow in the upper airway are briefly reviewed, and the advantages and disadvantages discussed. The final part of the chapter justifies the development of a system using optical fibre technology to make a diagnosis of altered airway impedance and to determine the location and extent of airway obstruction.

2.2 Anatomy and physiology of breathing in the upper airway

The human extrathoracic upper airway describes the route though which inhaled air travels when entering the nose or mouth to the point at which it enters the trachea. Control of the upper airway during a wake or sleep state can be considered to be by a series of three valves, each controlling the volume of airflow and the route through which it propagates (Edelman *et al.*, 1986).

Air enters the body through the nose or mouth, passing through nares or lips respectively. The lips are able to completely block or regulate air flow, whilst the nasal

valve is only able to change flow rate by constricting or relaxing to adjust the cross-sectional area of its orifice. The second valve, further into the respiratory system, is the soft palate. Serving as a *switchable* valve it is able to select the proportion of nasal or oral airflow. The larynx is the third and final regulatory valve before the air enters the trachea (Figure 2-1). It is able to regulate flow by behaving as a variable orifice (Rodenstein *et al.*, 1986). The nasal and oral cavities must combine to perform three separate tasks: breathing, ingestion of food and speech. The airway must be able to perform each task without affecting the remaining two.

Interest in OSAS has led to extensive study of the rôle of the soft palate in respiration and as a source of obstruction (Rodenstein *et al.*,1986). A change in posture or physical abnormality may increase the probability of airway collapse (section 2.3.3).

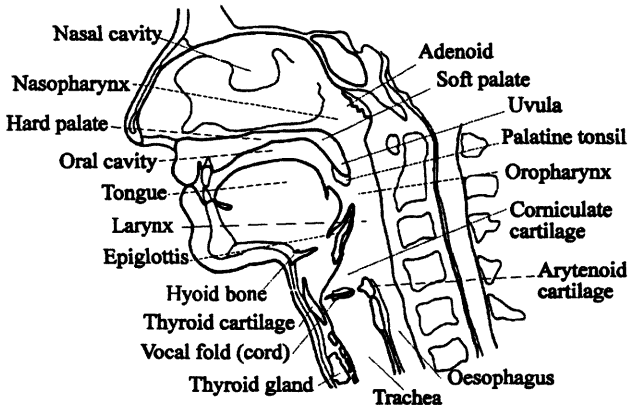

Figure 2-1 Lateral view of the head

The use of the electroencephalogram (EEG) to study the level of brain activity and hence depth of sleep of a patient in an overnight sleep study drew attention to the significant effect of sleep on breathing (Lydic *et al.*, 1988). The airway impedance, nominally 60 to 70mmH_2O per l/s at the end of inspiration (Figure 2-2) (Guyton.,

1981), may increase up to three times as the subject passes from wakefulness to NREM (Non-rapid eye movement) sleep (Hudgel., 1993)[1].

Resistance of the upper airway segments (mmH_2O per l/s)		
Region of upper airway	Peak inspiratory pressure	At 0.01 l/s flow
Nasal	2.92 ±0.67	2.11 ±0.56
Transpalatal	2.03 ±0.37	0.90 ±0.40
Hypopharyngeal	1.31 ±0.40	0.78 ±0.29
Total Supralaryngeal	6.26 ±0.56	3.79 ±0.50

Figure 2-2 The impedance of the upper airway segments during normal and forced flow showing mean and standard deviation
(Hudgel and Hendricks., 1988)

The physiology of the airway encompasses the processes of oral ingestion of food and oral/nasal breathing cross-over (Figure 2-1), consequently the airway is rigid in the nose and trachea, and compliant in the pharynx[2]. The patency of this portion of the airway is dependent on the muscles controlling dilation and constriction. The work required by the dilator muscles is determined by the compliance of the pharyngeal wall, which is dependent on airway abnormality and excessive fat: a highly compliant airway requires increased effort of the dilator muscles. During sleep the muscles holding the upper airway open may decrease their activity and go out of phase with the inspiratory muscles. This is further complicated in REM sleep when then muscles become atonic, increasing the probability of a collapse. The increased airway impedance leads to the thoracic *pump* muscle activity increasing. Obstructive Sleep Apnoea Syndrome

[1] It is normal for the airway to narrow during sleep, the effort required by the subject to inhale being characterised by airway impedance.

[2] The ideal airway would be rigid, but crossover and need to vocalise means the pharynx is compliant.

(OSAS) is a consequence of these parameters combining to obstruct the airway at a site specific to the patient and preventing gas exchange[3] (Hudgel., 1993).

Obstruction may occur at a number of different sites. Previous studies have analysed the profile of respiratory impedance along the upper airway as a means of isolating regions of probable collapse (Rodenstein *et al.*, 1990). A study conducted by Hudgel *et al* (1988) found that in approximately half of OSAS patients studied, the site of collapse was at palate level, whilst the remainder obstructed at the hypopharyngeal level. Obstruction is usually due to the back of the tongue resting against the soft palate or pharyngeal wall where the tissue is most compliant. The obstruction is promoted by an abnormally narrow airway typically occuring in obese patients or patients with acromegaly. Once obstruction occurs the site of blockage may travel further into the airway as the patient attempts to inhale. It is also reported that obstruction may occur due to a misshapen or over-sized soft palate, allowing the uvula to rest again the back of the tongue (Horner *et al.*, 1989 and Pringle and Croft., 1993). In such circumstances surgery may be applicable (section 2.3.5).

Snoring represents partial obstruction of the airway with the *fluttering* of the palate and pharyngeal wall, and may be heard in the early stages of an apnoea before the onset of total obstruction moments later. For this reason snoring is often a symptom of the condition.

The probability of a collapse occuring is also dependent on other parameters beyond that of physical abnormality and dysfunction. Passive neck flexion describes the angle and curvature of the neck. The resulting deformation of the airway may promote collapse. The infant has a reflex action to increase muscular tone as a counter-acting measure which instinctively restores the airway, this instinctive reaction diminishes with age (Cherniak *et al.*, 1988). The change of blood flow due to gravity and posture can cause swelling of the tissues and hence an increase in respiratory impedance, e.g. swelling of the nasal mucosa can cause partial obstruction.

---

[3] Apnoea is defined a the transient cessation of breathing for a period of typically ten to thirty seconds.

2.3 Sleep disorders and obstructive sleep apnoea syndrome

2.3.1 A brief overview of sleep disorders

Sleep disorders can be split into three distinct groups and classified under the following headings:

- Disorders of initiating and maintaining sleep 'DIMS' - e.g. Insomnia
- Disorders of excessive sleepiness 'DOES' - e.g. OSAS, Narcolepsy and Idiopathic hypersomnia
- Parasomnia - e.g. nightmares, night terrors and sleep walking

Such disorders can be classified further as *primary* or *secondary,* i.e. *is the disorder a cause or consequence of further medical complications?* It can often be impossible to determine whether a patient is experiencing a primary or secondary sleep disorder by observation alone.

A primary sleep disorder's only symptom is the disorder itself (Hauri., 1977). An example of this is primary insomnia. A patient's inability to sleep may be due to a neurochemical disorder and, although yet to be proved, it is thought to be inherited (Thorpy *et al.*, 1991). The secondary sleep disorders are harder to diagnose, often due to a patient's unknown medical and psychiatric history. Causes include depression, schizophrenia and neurologic problems (Mendelson *et al.*, 1977).

A serious sleep disorder can lead to problems in the work or home environment. The sufferer is unable to relax and has a constant feeling of tiredness and fatigue. It was reported by Hauri (1977) that a patient who is deprived from sleep for a long period of time, perhaps several days or more, will begin to suffer from *micro-sleeps.* Initially these may only last a few seconds, but as tiredness progresses these will increase in duration. Eventually the micro-sleeps will become completely intertwined such that it is no longer possible to determine whether the subject is awake or asleep. Activities usually associated with a wake state, e.g. walking, no longer provide direct evidence of consciousness. If micro-sleeps occur the patient may be a danger to themselves and others.

2.3.2 Sleep stage classification

Sleep consists of a combination of two distinct stages, known as NREM or orthodox sleep and REM or paradoxical sleep. The differences between the two are comparable to the difference between a wake or sleep state (Edelman *et al.*, 1986). NREM sleep is a passive state reflecting low neuromuscular activity, however the muscular system is still responsive to cortical activity. REM sleep, colloquially referred to as *dream sleep,* is a time of very high brain activity, although this is not apparent by observation of the EEG alone. The voluntary muscular control system is disabled completely, apart from those muscles associated with respiration and excretion of body fluids [4]. Both types of sleep can be broken into several more stages, each distinctly different from the preceding stage.

NREM is the sleep state that any human will enter following drowsiness. A typical duration may be up to ninety minutes; the young middle aged adult spending up to one quarter of their total sleep in this state. NREM may be further classified into four more stages. Classification is achieved by visual inspection of the unipolar EEG taken from the occipital area. Whilst awake the EEG is primarily that of sinusoidal alpha waves[5], this activity decreases as the subject becomes more drowsy. During the onset of stage 1 the alpha waves disappear and the waveform is comprised of mainly beta[5] and the lower frequency theta waves[5] which interrupt periodically. Stage 2 is recognised by the presence of sleep spindles[6] and K-complexes[7]. These features disappear when the subject is in stages 3 and 4. These two stages are often grouped together and referred to collectively as *delta* sleep (Figure 2-3).

[4] The standard for the classification of sleep stages by observation of the electroencephalogram, electromyogram and electro-oculogram is that defined by Rechtschaffen and Kales, 1968.

[5] Alpha waves 8-14Hz; Beta waves 15-35 Hz; Theta waves 4-7Hz; Delta waves 0.5-3Hz.

[6] A sleep spindle is a brief burst of high frequency (12-14Hz) waves typically of duration of over 0.5 seconds.

[7] A K-complex is a high amplitude negative wave followed by a high amplitude positive wave.

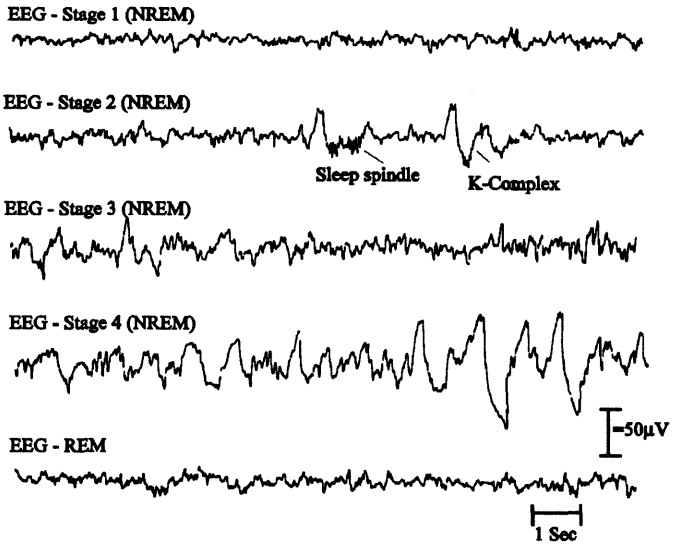

Figure 2-3 Electroencephalogram (EEG) of sleep stages during REM and NREM (Mendelson *et al.*, 1977)

2.3.3 Obstructive Sleep Apnoea Syndrome

OSAS was first recognised as a clinical disorder in the French literature in 1965 (Gastaut *at al.*, 1965), although a good case was also described by Charles Dickens as early as 1836[8]. Periodic hypoxia and poor quality sleep was attributed to intermittent occlusion of the upper airway. In extreme cases it was thought to be the cause of acute heart failure. Apnoea, obstructive or otherwise, is graded by an *Apnoea-Hypopnoea Index* (AHI). Severe OSAS typically occurs in 0.3 to 1% of adult males (over 50 obstructive episodes per hour) (Douglas., 1990 and Stradling., 1993).

Apnoea in OSAS occurs as a result of an abnormally narrow airway. The constriction in the pharynx promotes a negative gauge pressure to develop across its orifice forcing it to collapse in onto itself. The sufferer then awakes and *gasps* for air

[8] Pickwickian Syndrome describes obese patients who commonly suffer from OSAS (elevated CO_2 levels, and abnormally low blood oxygen levels). The condition is named after a character "Joe the Fat Boy" in the book "The Posthumous Papers of the Pickwick Club" by Charles Dickens (Dickens., 1836 and Thorpy and Yager., 1991).

before falling back to sleep, the muscular tone being returned to the muscles as a consequence of arousal. These brief interruptions to the sleep pattern, typically 10 to 15 seconds duration, are so short that the patient does not remember them occuring. *Micro-arousals* may occur several hundred times during the course of one night. Consequently the subject is unable to reach the deeper sleep stages (stages 3 and 4 NREM and REM sleep). There is not a consistent anatomical site for the occurrence of OSAS. The region posterior to the soft palate is recognised as being one of the most common (Horner *et al.*, 1989). The extent of a collapse will vary between patients, a severe collapse being over 20mm in length (cf: pressure transducer spacing in catheter - section 3.3.1).

Apnoeas may also occur due to failure of the respiratory centre (central apnoea), these are however extremely rare. Central apnoea has in the past been either mis-diagnosed or occurs as a result of combined effects arising as a result of OSAS. The condition is caused by a failure of the inspiratory neurones in the medulla. The brain either fails to evoke the necessary neuromuscular signal, or the respiratory system fails as part of reflex action. Reported cases may usually be attributed to neuromuscular disease or underdevelopment of the brain stem, and are common in pre-term babies and neonates (Thorpy *et al.*,1991).

A mixed apnoea begins as a result of the pharyngeal muscles becoming atonic whilst asleep causing an obstructive apnoea (section 2.2), but is complicated by an imbalance of the blood gases: CO_2 and O_2. Carbon dioxide stimulates respiration, hence an increase in $PaCO_2$ will increase the respiratory effort and tidal volume. During the apnoea the blood carbon dioxide level steadily rises to an abnormal level. When the patient wakes, returning tone to the dilatory muscles, the sudden increase in breathing reduces the $PaCO_2$ to less than the limit necessary to stimulate respiration. The apnoea then re-occurs as part of a reflex action. Mixed obstructive sleep apnoea is a cyclic process. It has been reported that mixed apnoea accounts for between 53 and 71 percent of apnoeic episodes in pre-term infants (Santiago *et al.*, 1986).

The lack of *good quality* sleep, i.e. sleep not persistently impaired by micro-arousals, causes symptoms including excessive daytime sleepiness (EDS) and cognitive impairment. If OSAS is allowed to persist it may lead to hypertension, headaches and

in some sufferers, enuresis and impotence (Guilleminault *et al.*, 1990). There are several groups of patients which are at risk, each has in common sleep related occlusion of the upper airway. Obese adults are known to suffer from nocturnal hypoxaemia caused by the reduced lung tidal volume due to increased effort to breathe. This factor combined with an abnormally large collar size makes them among those at highest risk (Crumley *et al.*, 1987). Young children may suffer as a result of enlarged tonsils and adenoids, a condition which may be easily remedied by routine surgery. Older patients (over 60) may also be considered to be a high risk group. Studies of volunteers over 60 years of age concluded that a large percentage of patients suffered from OSAS arising from the reduced response time of the pharyngeal dilator muscles (Santiago *et al.*, 1986). It was suggested that prolonged OSAS may contribute to brain dysfunction and senility. Other symptoms include pulmonary, cardiac and neurological disease.

The associated reduced pressure across the larynx of a patient suffering from OSAS promotes *fluttering* of the palatal region and pharyngeal wall, producing often loud and unbearable snoring for the partner.

2.3.4 Invasive and non-invasive assessment techniques

The known cause of OSAS is the abnormally narrow airway. Prior clinical investigations of the condition have previously been conducted using two and three-dimensional imaging techniques to produce a cross-section of the airway in question.

Cephalometry is a two-dimensional static image of the skeletal tissue and palatal region. An X-ray is taken with the patient in a seated or standing position at the end of expiration. Using this technique it is possible to determine the exact location of the tissues at the end of a respiratory cycle. Known reference points are measured and a narrowing or occlusion may be measured directly (Sheppard *et al.*, 1991). Features of interest include obvious deformation such as elongation of the soft palate and a narrowing of the posterior air space. Although they provide only a limited amount of information, cephalograms are cheap and easy to perform. Complications do arise because of the orientation of the patient, making comparison of the data to that occuring during sleep difficult.

Somnofluoroscopy is an extension of cephalometry. It is able to provide a dynamic illustration of the location of the soft palate in a patient whilst asleep and in a supine position (Suratt *et al.*, 1983). This is usually facilitated by the coating the relevant tissues with a radio-opaque dye such as iodine. Unfortunately the image is still two-dimensional and given the number of frames required for animation, the patient is subjected to a considerable dose of ionising radiation. It has however provided invaluable information regarding the role of the soft palate as a gate in the oropharynx (Pepin *et al.*, 1992).

A **CAT** scan (Computer-aided tomography, also called CT) takes a series of radiographic slices through the tissue or organ under study. A series of two-dimensional pictures may then be collated to produce a three-dimensional image. A typical human head requires 8 to 15 slices to produce reasonable anatomical resolution (Haponik *et al.*, 1983). The patient is subjected to radiation, but modern techniques are able to perform a fast-CAT scan in 50ms, making exposure time minimal.

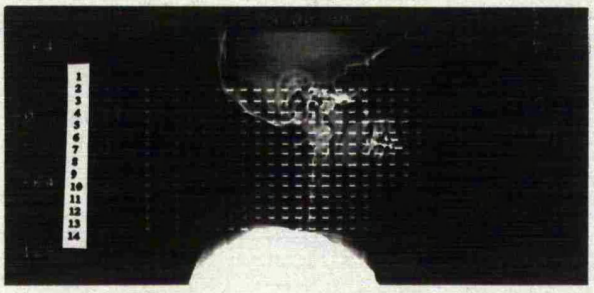

Figure 2-4a An X-ray of the upper airway

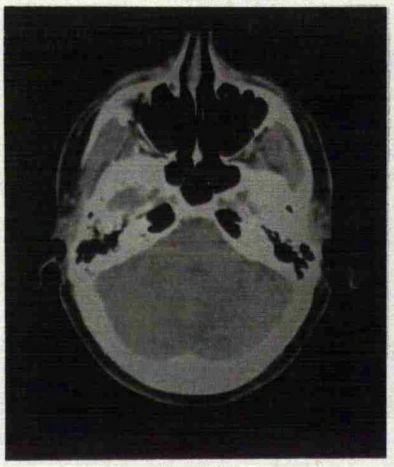

Figure 2-4b

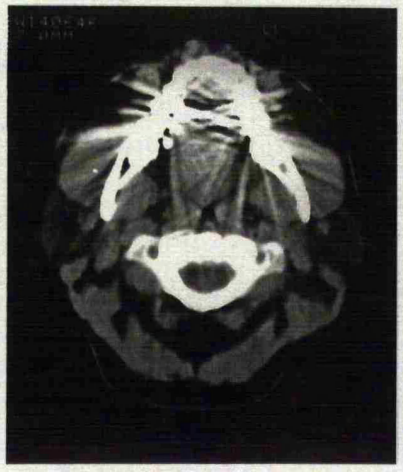

Figure 2-4c

Figure 2-4d

Figure 2-4b-d CAT scans of the upper airway
(Complements of Dr. C.Hanning - see acknowledgements)

The diagrams shown in Figure 2-4 show a cephalogram and three CAT scans at three different levels through the airway of an OSAS patient. The first CAT slice, Figure 2-4b, is high in the airway (corresponding to slice number '1' in Figure 2-4a) and illustrates the nasal cavities and sinuses. At this level the airway is apparently normal and there are no obvious abnormalities. The second slice, Figure 2-4c, (corresponding to CAT slice number '7' in Figure 2-4a) shows the airway narrowing. The constriction can be visualised if it is compared to the third slice, Figure 2-4d, (corresponding to slice '9' in Figure 2-4a). The airway has now widened.

The substantial reduction in radiation exposure is advantageous. The resulting image is of excellent clarity and anatomical detail, whilst being non-invasive (Crumley *et al.*, 1987). Studies have been performed during wakefulness and as part of sleep studies (R.L.Horner *et al.*, 1989). Installation, maintenance and running costs are high.

Nuclear magnetic resonance imaging (NMRI) is the most recent of the imaging techniques used to date. In a similar manner to CAT, NMRI is able to construct a three-dimensional image from a series of two-dimensional slices. It is also able to scan in more than one direction of the axial plane, such that adjacent slices need not be parallel (Rodenstein *et al.*, 1990). Problems associated with ionising radiation are not applicable, the energy source being a powerful radio frequency magnetic field (2 to 10MHz). The image produced is static, but with excellent anatomical detail (Payne., 1987). Currently a full scan of the upper airway may take up to 5 minutes. With increased computer power and more efficient mathematical algorithms this time scale should be reduced to a fraction of a second making real-time images possible.

Fibre-optic pharyngoscopy is able to investigate the mucosa of the upper airway in close detail with a minimum of discomfort (see chapter 3). Features of interest include the presence of polyps, septal deviation and narrowing of the nasal valve region (Sheppard *et al.*, 1991). Direct visualisation of the uvula and soft palate are possible with the patient relaxed and in any posture. Crumley *et al* (1987) observed the airway of a group of patients with and without OSAS. A narrowing from 15 to 3mm was reported in the posterior tongue base region, depending on whether the subject was in a supine or upright position. Such findings have been validated by many papers and widely accepted (Bradley *et al.*, 1986, Hudgel and Hendricks., 1988). The

use of endoscopy as an explorative technique has proved successful. It is possible to insert a device through the nostril and collect data with the patient asleep under sedation (Pringle and Croft., 1993). The main disadvantage is the full extent of the collapse may not be easily determined. The full length and severity of the collapse cannot be viewed.

Imaging techniques, although useful, produce data dependent on the patient's posture. The conditions under which the scan is performed are often dissimilar to those under which the disorder occurs. The result is uncertainty between physicians. It has been suggested that an image of the airway whilst the patient is awake is not a reliable method of predicting the site of OSAS. The conflicting results lead to the following conclusions (Hudgel., 1992):

- Anatomical disorder can lead to OSAS, but not in all patients;
- The current techniques are too crude to define anatomic abnormality accurately.
- Pharyngeal size may not be a primary factor in OSAS.

2.3.5 Corrective surgical techniques

Revision of the upper airway is now a routine method for eliminating or reducing the effects of OSAS, however for a surgical technique to be successful a careful diagnosis of the patient must be performed. An incorrect choice of surgery may not only inconvenience the patient, but also make the snoring and apnoeic episodes more frequent and severe. The goal is to be able to reliably identify the site of obstruction so that it may be logically treated.

The use of lasers in medicine permits accurate, precise and hygienic surgery to be performed. Lasers coupled to optical fibres are able to reduce the number of necessary incisions; hence reducing the length of patient recovery time. There are two types of laser surgery. The first method involves using the laser as an optical scalpel to cut or modify tissue (Kamami., 1994). The second, less extreme form of surgery, modifies the tissue by causing superficial damage which leads to the generation of scar tissue. The function of the soft palate is modified by scarring it along its length. The resulting

increase in rigidity reduces movement and helps to prevent vibration during respiration as occurs in snorers.

A considerable number of sleep studies have been conducted involving the screening of sleep apnoea patients prior to surgery. Some patients respond more positively to alternative treatments such as continuous positive airway pressure[9] (CPAP), or the nasal dilator (Keenan *et al.*, 1994). Surgery is reported to increase the life expectancy of a patient suffering from OSAS (Keenan *et al.*, 1994). The excessive strain on the heart as a result of periodic apnoea being reduced.

2.4 Sleep monitoring

2.4.1 Current techniques

There are currently a wide variety of clinical diagnostic aids available to characterise the existence and extent of upper airway impairment in OSAS patients. Prior to the commitment of the physician to a radiological scan, it is usual for the patient to be admitted for an overnight sleep study. At this early stage of investigation physiological parameters are recorded such as oxygen saturation[10], abdominal movement, body-trunk movement on the bed, oral and nasal airflow and sound. Occasionally a polysomnograph may also be conducted, involving an unipolar EEG, EOG[11] and EMG[12], to examine during which level of sleep (section 2.3.2) apnoeic episodes occur.

[9] CPAP operates by monitoring airflow and applying a positive gauge pressure into the top of the airway through a face-mask to prevent an airway collapse and apnoea.

[10] Oximetry measures the level of oxygen in the haemoglobin using spectrophotometry. The presence of more oxygen renders the red blood cells *redder* in appearance, hence changing the optical absorption and reflection characteristics of given wavelengths (see chapter 7).

[11] EOG: Electrodes are attached to the outer corners (canthi) of the eyes, the differential between each and a reference is recorded. The signal recorded from each eye is the reverse of that of its neighbour in a normal patient.

The efficiency of respiration may be monitored by analysing the airflow into the body through the nose and mouth. A tightly fitting mask is fitted over the nose and mouth, the output of which may then be fitted to a pneumotachograph (a device which will measure the constituents of the gas entering and leaving the body, and the frequency at which breathing takes place). Analysis then provides information on lung tidal volume. The presence of the mask over the face causes problems when attempting to measure breathing patterns over a long period of time: condensation and other secretions will collect in the mouth piece. The presence of the mouth piece may also inherently effect the characteristic breathing of the patient, this is particularly significant it the patient is conscious.

An alternative to the mask is a ventilated canopy which encloses the entire head. Oxygen and carbon dioxide are monitored and tidal volume calculated. This technique correlates to within 96% of the direct measurement of the pneumotactograph.

Both techniques clearly have some major disadvantages. Practically they are only useful for taking quantitative measurements as part of energy studies (Wilmhurst and Shah, 1994). Pneumotachography also only indicates the presence of apnoea, giving no information on the collapse site, only severity. The only quantitative method of measuring the extent of airway collapse and its location, independent of patient posture, is by pressure and hence flow measurement in the pharyngeal space. Accurate measurement of the tidal volume is not usually necessary. It is normally sufficient to measure airflow by placing a thermistor at the nose and mouth, or by monitoring chest wall and abdominal movement.

2.4.2 Airway pressure measurement - diagnosing OSAS

The continuous measurement of pressure throughout the varying sites in the upper airway produces important diagnostic information on a collapse as it occurs in patients suffering from OSAS, including the extent and location.

---

[12] EMG: The electromyogram is taken from beneath the jaw to measure the muscular tone of the chin.

A detailed sleep study, performed by Koike *et al* (1992), used a single channel pressure transducer to measure pressure in the hypopharynx. The study was conducted to investigate the existence of OSAS and its influence on respiratory pressure. Oximetry, abdominal movement, oral airflow and sound were also measured. Recordings of pressure were observed in a group of 201 patients during the pre-operative period in the age range 7 months to 14 years. Patients were then classified depending on the extent of snoring and duration of apnoea. Following an adonotonsillectomy the peak pressure was seen to fall from 130cmH_2O, in the severest case, to just 30cmH_2O. Although the technique was useful in this application, the use of a single transducer is limited. It is unable to provide information regarding the site of collapse should an obstructive apnoea occur. Tvinnereim and Miljeteig (1992) proved that multiple measurements were possible using a catheter into which were integrated five solid state semiconductor pressure transducers at 35mm intervals. The transducer reported apnoeic episodes due to OSAS from between 8 and 25 seconds in duration. Occurrences of snoring and nasal stenosis were also observed.

A similar study was conducted by Woodson and Wooten (1992), using an identical device as described above, but with only four transducers. Each transducer in the catheter comprised a solid-state ultra-miniature semiconductor sensor enclosed in a stainless steel housing. The transduction element was an elastic diaphragm. The condition of the airway was also monitored with the aid of an optical fibre endoscope. The images received were used to confirm the prognosis implied by the pressure transducers. Partial or total obstruction was observed as a reduction or absence of respiratory artefact observed on the transducers above the obstructed site. Below the occlusion increased amplitude of the signal due to increased muscular effort from the respiratory motor units in the abdomen was observed (Figure 2-5).

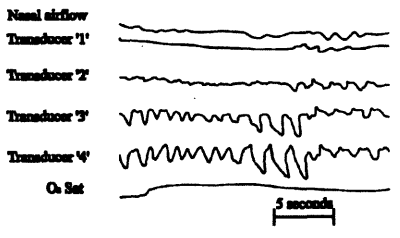

Figure 2-5 A obstructive apnoea occuring at the distal palate (Woodson and Wooten., 1992)

The above figure illustrates the occurrence of an apnoea due to an occlusion of the distal palate (uvula), in this case transducers '1' and '2'. The pressure on transducers '3' and '4' steadily increase until the obstruction is cleared.

Work by Skatvedt (1993) has been able to validate the conclusions drawn from the study discussed above. A series of transducers were placed in the pharyngeal space and oesophagus and recording taken with the patient in an unconscious state. A separate exploration was conducted on the same set of patients with a nasopharyngoscope. The results showed that visual inspection of the mucosa lined airway was able to predict the occurrence of apnoeic episodes in 25% of patients. The use of the pressure transducer was able to isolate 55% of patients suffering from OSAS, considerably more efficient than the former method. An earlier study by the same author (Skatvedt., 1992) analysed 18 subjects in a pre-operative study at 6 sites along the oesophagus and upper airway. The purpose of the study was to examine the reduction of airway impedance after surgery. The catheter used during the research was chosen so as to be able to respond to transient pressures with bandwidths of up to 500Hz, adequate to provide all necessary dynamic information.

2.5 Motivation

OSAS is clearly cause for concern in extreme sufferers. If it is left untreated OSAS may be either life threatening , or result in a reduction in life expectancy. A report by Keenan *et al*, (1994) suggested that the life expectancy of a patient suffering from OSAS may be reduced by as much as five years. The clinical and physiological problems of OSAS may be investigated by a selection of diagnostic equipment including imaging and polysomnography. The advantages with the direct measurement of pressure and hence flow and airway impedance are clearly that of a more representative picture of an apnoeic incident. The combined forces of muscular tone and gravity render the results taken with the patient in an upright and supine position incomparable when performing an accurate diagnosis. Skatvedt (1992) showed that patients are able to sleep with a catheter in the pharynx if the device is small enough. The devices currently available range from 2 to 3mm in diameter. Unfortunately,

although they do produce high quality data which is both repeatable and representative of the pressure profile in the nasopharynx and hypopharynx, there are still some disadvantages. It would be unwise to perform a NMRI or CAT scan of the subject whilst the catheter is in place. The presence of metallic objects will distort the image, and in the case of NMRI may lead to localised heating which may damage the airway mucosa. Metallic objects are desirable when performing cephalometry, serving as radio-opaque markers indicating the location of the catheter inside the throat. The catheters currently produced are also extremely expensive due to the micro-electronics required to integrate a large number of devices into a single catheter.

The motivation stimulating the research discussed in the first part of this thesis is the application of optical fibre technology to OSAS in the development of a multiple pressure transducer catheter to overcome some of the aforementioned problems. The scope for miniaturisation is vast. The optical fibre, being an inherently dielectric material, does not suffer from the radiographic problems associated with metallic objects. The cost of optical fibre is low. The cost of the active optical components is still relatively high, however once purchased, optical devices should not need to be replaced for normal use. The catheter, being considerably less expensive, may be considered disposable whilst still being viable for use as part of a routine pre-surgical procedure.

Chapter 3

Design of the optical fibre pressure transducer for use in the upper airways

3.1 Introduction

This chapter discusses the currently available pressure transducer technology for addressing the problem of obstructive sleep apnoea syndrome. Specific design considerations are outlined, and with reference to chapter 2, a series of design factors particular to optical fibres is presented. The objective of this chapter is to summarise the full design process and give the reasoning behind choice of materials and the physical constraints of the optical fibre pressure transducer when designed for use in the human body. The design begins with the development of a single *pigtailed* device. This is then integrated into a catheter housing seven pressure transducers. Details regarding the selection of materials, hardware design and the design of a catheter for *in-vivo* use are discussed. The clinical methods and results are reported in chapter 5.

3.2 Pressure transducers

3.2.1 Pressure measurement

Pressure transducers are used to measure *in-vivo* pressures in many situations including the muscles, gastro intestinal tract, airway and the cardiovascular system. There are a wide variety of pressure transducers, however each possesses a transduction element which modulates a signal, electrical, optical or otherwise into a signal which is monitored by a detector. There may also be some further signal conditioning circuitry (Figure 3-1).

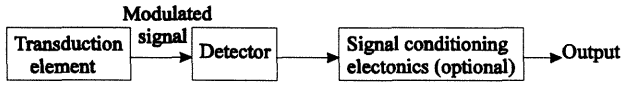

Figure 3-1 A block diagram of the elements of a pressure transducer (Bicking., 1982)

Selection of an appropriate pressure transducer for a specific task may involve a compromise between selecting the most relevant properties at the expense of others. The general requirements and physical construction restraints will often significantly reduce the choice of transducers available. Performance is characterised under the following headings:

- Pressure range
- Sensitivity and resolution
- Long-term drift and hysteresis
- Resilience to vibration, shock and transient over-pressures
- Reliability and cost

Transducers for use in the biomedical field must also be assessed for size, sterilisability, toxicity and electrical isolation (Priest., 1979). In order to describe the dynamic limitations as well as those under static conditions the transfer function and slew-rate must also be considered.

Pressure[1] is measured either with respect to a vacuum: absolute pressure or with respect to atmosphere: gauge pressure. A differential pressure transducer measures one pressure with respect to another.

3.2.2 Current commercial pressure transducers

One of the most popular pressure transducers available is the long established thin-film strain gauge transducer. The action of such a transducer is essentially electromechanical. The transduction element is an elastic diaphragm with either a thin film strain gauge or strain-gauge bridge bonded to it. As the diaphragm distorts under pressure the resistance of the strain-gauge is modulated (Rajanna *et al.*, 1993). Long term use of such a device may be unreliable due to ageing of the adhesive binding the strain gauge to the diaphragm. To overcome these problems the strain gauge is either suspended and a linkage used to deform it, or the semi-conductive material is deposited directly onto the diaphragm using gas glow discharge techniques. Strain-gauge transducers are both reliable and accurate, a simple device is also extremely cheap to produce. Using silicon etching a strain gauge may be etching directly onto a

[1] The SI unit of pressure measurement: 1 Pascal (Pa) = 1 N/m^2

silicon wafer making single chip solutions possible. The pre-processing circuitry and transducer can then be integrated into the same device (Kim *et al.*, 1992).

The diaphragm is the most common transduction element, however the Bourdon tube, named after its inventor, is an alternative. It consists of a collapsed, twisted tube which applies torque on the onset of pressure onto one end. The ensuing mechanical movement may then be detected.

The remaining transducer designs, using linear-variable differential transformers (LVDT), variable-reluctance transformers, capacitance (Kudoh.,1991), piezo-electric and resistance (Roberts and Burton., 1992), all rely upon electrical properties (magnetism, charge, capacitance etc). Consequently at least two electrical conductors are required to carry the signal. If transducers such as these are to be miniaturised there are inherent problems associated with the physical space required for the transduction element and the wiring. The transducer is also susceptible to short-circuiting due to dampness or wetness.

3.2.3 Optical fibre pressure transducers - an overview

As discussed in chapter 1, optical fibre transducers operate on a multitude of different modulation principles. Typically optical fibre pressure transducers are amplitude modulated, although interferometry is not uncommon. The depth of an optical cavity is measured by examination of the constructive and destructive interference of light following two optical paths, where one of the paths changes with respect to pressure: the Fabry-Perot interferometer (Wolthuis., 1991) (section 1.4.2). It may also be argued that a birefringent optical fibre is, in itself, a pressure transducer. Monomode high birefringent optical fibres are used in interferometry to ensure that only one mode of polarisation is populated. The high sensitivity produced by interferometry makes the technique useful where the transduction element displacement is small ($<<1\mu m$). Such devices are seldom used for direct pressure measurement, but there has been significant success in the construction of hydrophones to measure pressure arising from sound waves (Jackson., 1987). Studies involving multimode optical fibre have been conducted, their application in interferometric

transducer design is yet to be exploited as the *speckle pattern* produced is not easily quantified (Taniguchi., 1991).

The photoelastic pressure sensor differs from other pressure transducers. The transduction element is solid state and its optical properties directly modulate a light source. Hydrostatic pressures of 95Pa were reported to have been detected by Spillman (1982). The optical absorption of polarised light is dependent on the applied pressure to a glass transduction element. In a similar manner a gallium-arsenide (GaAs) crystal is able to shift its absorption edge (cut-off wavelength) when exposed to high pressures (~100MPa) (Bock., 1992). The orientation of the optical fibres in such designs cannot be miniaturised sufficiently so as to be integrated into a catheter. The frequency response is also limited. Such transducers are designed for hydrostatic pressures in environments where temperature is stable: a temperature change of 65° produced an apparent pressure change of 200MPa in the system described by Bock (1992).

A transparent silicone rubber optical fibre to measure force, pressure and displacement has been described by Muhs *et al* (1991). The optical fibre was able to cope with over 200% strain by changing the elongation of the optical fibre core. The design relies on the deformation of the silicone rubber optical fibre core. As pressure increases the cross-sectional area of the fibre core decreases causing a proportional increase in transmission loss. The applications in pressure sensing are limited, but have the advantage of almost complete immunity from temperature drift: <5% from 0 to 100°C (Muhs., 1992).

The optical fibre pressure transducer without an elastic diaphragm was first described by Jones and Papageorgiou (1988). The system replaces the standard diaphragm associated with amplitude modulated optical fibre systems with a gas / liquid interface. A column of gas is trapped inside the transducer housing and is compressed or expanded as the liquid is compressed and expended respectively. The deformation of the gas/liquid interface is then detected optically. Such a system is potentially cheaper and easier to manufacture than a diaphragm alternative, and there is potential for miniaturisation. There were however problems associated with bend loss. The original system used a single optical fibre to both transmit and receive light from

the gas / liquid interface. If the design were to be viable unquantifiable losses must be compensated (section 1.4.1).

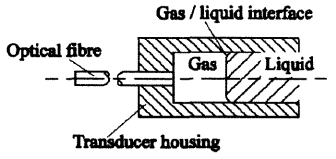

Figure 3-2 The optical fibre pressure transducer without an elastic diaphragm (Jones and Papageorgiou., 1988)

The main disadvantage of amplitude modulated optical fibre pressure sensors is their susceptibility to loss during bending, giving rise to *phantom pressures* (section 3.3.2). Several researchers have attempted to overcome this problem with the addition of extra optical sources at secondary wavelengths (Wolthuis *et al.*, 1991). A ratio is taken between incoming wavelengths to overcome loss and produce a linear characteristic. The pressure transducer discussed in the remainder of this chapter exploits this idea to produce a sensor which is immune from bending loss using the transducer described by Jones and Papageorgiou as a starting point.

3.3 Design criteria

3.3.1 Physical constraints

The specification of the transducer, as defined by the Department of Anaesthesia[2], described a multi-transducer catheter containing an array of seven pressure transducers. The system was to be designed for real-time monitoring of the upper airway as part of an overnight sleep study, to aid in the diagnosis and evaluation of Obstructive Sleep Apnoea Syndrome. It was hoped that the device would provide information on the occurrence of an airway collapse, its location and severity. The following was proposed:

[2] University Dept. of Anaesthesia, Leicester General Hospital, Gwendolen Road, Leicester. LE5 4PW

- Each transducer should have an operating range of ±400mm of water gauge pressure (3.9kPa).
- The resolution of each transducer should be better than 10mm of water pressure (98Pa).
- One transducer to be located at the tip of the catheter, a second 200mm from the first and the remaining five to be spaced at 20mm intervals thereafter in order to distinguish the collapse of the airway adequately as occurs during OSAS (see chapter 2).
- The tip of the longest channel to the conditioning circuitry no less than 1m in length.
- Outside diameter of catheter containing transducers ≤ 3mm.
- All materials should be non-toxic if ingested.

It was proposed that the catheter be inserted through the nasal passage; consequently to be able the cope with the curvature of the pharynx (almost 180° through a radius of curvature of approximately 100mm): the device should be flexible and without any sharp edges.

One of the most fundamental physical constraints was that of the catheter diameter. If it is too large it will not only be uncomfortable for the patient, but the data produced will not be an accurate representation of the pressure in the airway: the catheter itself promoting collapse.

3.3.2 Transducer design: location of the optical fibres in the transduction element

To fully understand the operation of the optical fibre pressure transducer it is useful to consider the principle of the optical fibre displacement transducer as it forms the basis of the design.

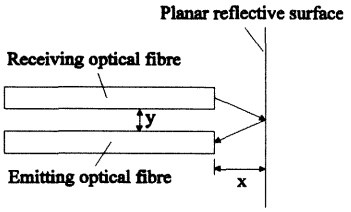

Figure 3-3 An optical fibre displacement transducer with duplex fibre orientation

A simple optical fibre displacement transducer consists of a single emitting optical fibre, and a second separate unrelated receiving fibre (Figure 3-3). This gives rise to three distinct operating zones (as shown in Figure 3-4, labelled '1', '2' and'3' respectively). The first zone is a *dead-spot* and occurs when the fibres are too close to the reflecting surface. Light emitted from an optical fibre emanates within a cone whose solid angle is a function of the numerical aperture (NA) and cross-sectional area of the optical fibre. Only light within this *cone of acceptance* can be successfully launched into an optical fibre. In the dead-spot zone the projections of the cones of the receiving and emitting fibres onto the reflecting surface do not overlap. A second zone occurs when the reflecting light traverses across the face of the receiving optical fibre, i.e. the projections of the cones partially overlap. In this area the gain is potentially very high and may be suitable for applications where the displacement of the reflecting surface is small. The width of zone '2' is a function of the diameter of the core and NA of the optical fibres. Zone '3' occurs when the face of the receiving optical fibre is fully illuminated by that emitting. The light received then decays with distance. This region may be approximated by the inverse square law, the received light being a ratio between the cross-sectional area of the receiving optical fibre and the effective area of the emitted light due to the fibre NA at a fixed distance away (chapter 4 - 2D model). Zone '3' is a more desirable operating region for the design of the optical fibre pressure transducer, not only is it wider, but the positions of the of the fibres are less critical.

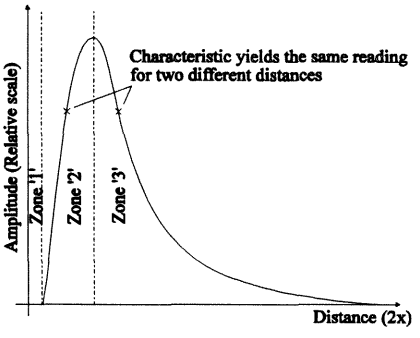

Figure 3-4 The operating characteristic of a duplex optical fibre displacement transducer

Once the appropriate part of the operating characteristic is selected: zone '3', it is important to ensure that the transducer does not wander into any other zone which may give rise to a false reading. If the receiving optical fibre gets too close to the reflective surface zone '2' will be breached. Should this occur there will be two distances, and hence two pressures, which will give the same reading (Figure 3-4). The unwanted reading is rejected by offsetting the emitting optical fibre from that receiving: distance 'l_2' (Figure 3-5).

Considering the bend-radius the optical fibre must go through *en-route* to the oesophagus, measures must be taken to ensure *phantom pressures* arising due to bending loss do not occur.

The design of the pressure transducer uses three optical fibres: one emitter and two receivers.

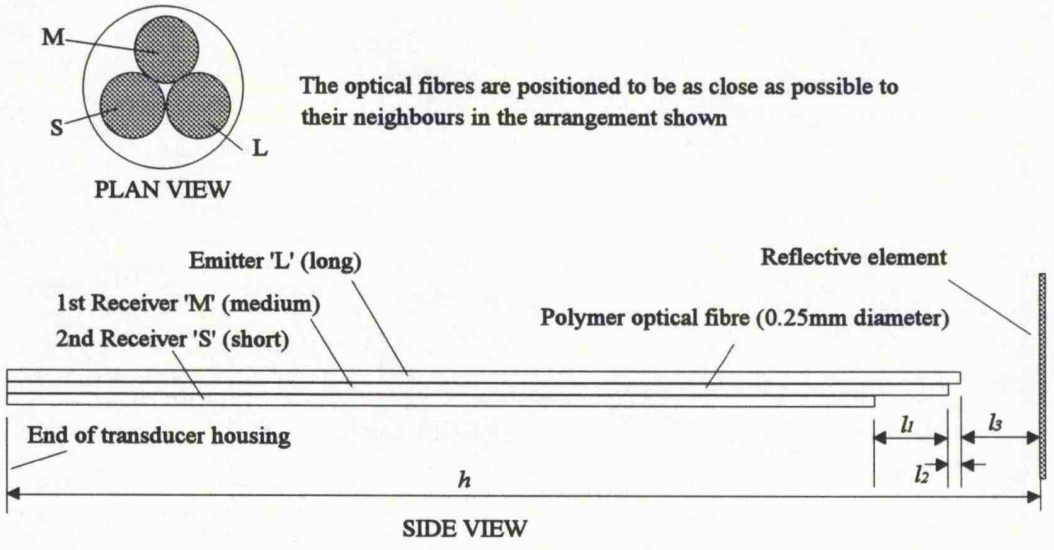

Figure 3-5 The location of the optical fibres in the transducer housing

Consider an optical fibre spaced distance 'l_3' from the reflecting surface with one further offset by a distance 'l_2' (Figure 3-5) (cf: Figure 3-3).

Light path length 'x' $= (2l_3+l_2)$

also from Figure 3-3:

Fibre spacing 'y' = (Fibre diameter 'ϕ_s') - (Fibre spacing across centres 'ϕ_d')

where 'l_2' = Offset between emitting and receiving optical fibres
'l_3' = Distance from emitting optical fibre to surface

In the boundary case: $(\phi_s - \phi_d) = (2l_3 + l_2)\tan\theta_c$ (Eqn 3-1)

where θ_c = Angle at which the light leaves the optical fibre (defined by NA).

hence $l_3 = \frac{1}{2}\left(\frac{\phi_s - \phi_d}{\tan\theta_c} - l_2\right)$ (Eqn 3-2)

The distance from the emitting optical fibre to that receiving, via the reflective surface, is ($2l_3$+l_2) which implies that the variable path length can never fall to zero (l_3 being the only variable). If the distance 'l_3' is set to at least half the sum of the distance defined by zones '1' and '2' (Eqn 3-2) of the operating characteristic, zones '1' and '2' will never be reached.

The second stage of the design process was the introduction of a second auxiliary optical fibre in a different location and distance from the transduction element.

If two optical fibres are located in the same position in a catheter, it is reasonable to assume that they should bend through the same radius of curvature, and hence suffer the same bend loss. The two signals may then be combined to produce an output independent of bend radius assuming the fibres are not bent too far. Research by Libo and Anping (1991) used a pair of optical fibres with a *white light* source and a diaphragm transduction element in a similar manner.

The simplicity of the LED micro-lens system launching light into the optical fibre means the light is also able propagate along the cladding as well as the core of the optical fibre. The length of the optical fibre used for each receiver (≈1m) is not sufficient to attenuate these cladding modes completely. Optical fibres suffer from two types of loss due to bending, known as *micro* and *macro* bending (see chapter 1). Micro bending occurs when the bend radius of the fibre is comparable to the

dimensions of the optical fibre core: in practice the fibre will usually fracture before the critical radius is reached (Eqn 3-3) (Powers.,1993).

$$r_{critical} \approx \frac{3n_2\lambda}{4\pi(NA)^3} \qquad \text{(Eqn 3-3)}$$

n_2 = Refractive index of fibre
λ = Wavelength of source
NA = Numerical Aperture

A solution is a mode stripper, however these are expensive to buy commercially and awkward to make reliably in laboratory conditions. Such an addition to the manufacturing process would also further increase the complexity of the design and is undesirable. Given the number of optical fibres inside a pressure transducer catheter (21) it is also impractical since the mode stripper itself is large and cumbersome[3].

Macro bending gives rise to appreciable loss in the optical fibre due to a small angular change in direction of the optical fibre (Figure 3-6)

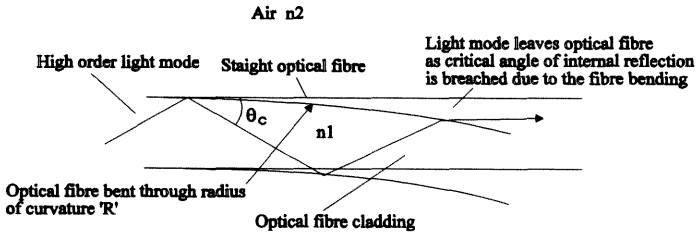

Figure 3-6 High order modes escaping from the optical fibre due to bending

The light contained within the core of the fibre changes direction changing the angle of internal reflection. The energy of one mode is shifted to another: mode coupling. High order modes, with their modal angle 'θ_c' close to the angle of total internal reflection will be refracted out of the fibre and lost. In a similar manner light in the cladding is lost (Figure 3-6). The detection system : a PIN diode and micro-lens,

[3] There are various methods for implementing a mode stripper, but the most common comprises a cone which has the optical fibre wound around it in order to vary the radius of bending and hence remove all cladding modes.

will detect the presence of *secondary* light modes in the optical fibre cladding and is a significant portion of the signal (≈5%).

To compensate for bend-loss, a second receiving optical fibre was integrated into the design: offset distance 'l_1' from the first receiving fibre (Figure 3-5). The location of the auxiliary fibre is important. If it is placed too far away from the reflective surface an unacceptably low light level will be detected, making the fibre worthless as a reference. Alternatively if the two receiving fibres are placed too close to one another the difference between them will be so small that the high gain required in the pre-amplification stages may make the system unstable and force it too close to the noise floor. It was also found that in order for the approximation for the difference between optical fibres to be linearly related to the ratio, the signal in the second fibre should be considerably less than that in the first (section 3.4.5.2).

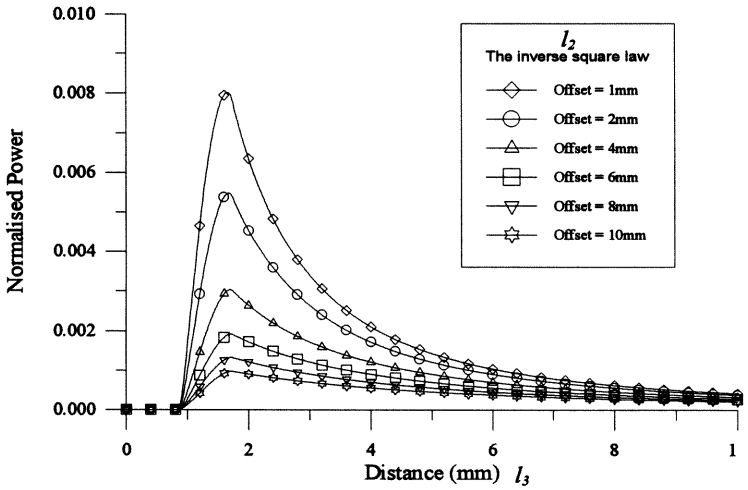

Figure 3-7 The light received by an optical fibre displaced by different distances (l_2): 1mm to 10mm from the emitting optical fibre. "Normalised power" is the proportion of light received by the receiving optical fibre to that emitted from the emitting optical fibre.

Figure 3-7 is a prediction of the light received by an optical fibre from the emitting optical fibre following the inverse-square law (see chapter 4 - mathematical modelling in two-dimensions) for the following conditions:

NA=0.5; Fibre spacing 'ϕ_s'=1mm; Fibre diameters'ϕ_d'=0.5mm

As the distance from the emitting fibre to that receiving decreases (Distance 'l_2' for the first receiving optical fibre and distance 'l_1+l_2' for the second receiving optical fibre in Figure 3-5) the amplitude of the received signal falls. The transducer combines two of these characteristics to produce a single output.

3.4 Concept design

3.4.1 The pressure transducer transduction element

The design of the amplitude modulated optical fibre pressure transducer relies on the deformation of a reflective surface. Although others are used, the most common transduction element used for pressure transducers is an elastic membrane (section 3.2). Although it is possible to make a small diaphragm, such a device would be extremely delicate and to make reproducibly would be expensive. An optical fibre pressure transducer constructed by Papageorgiou and Jones (1988), described a fluid filled device. The transduction element was a saline meniscus, the transducer requiring priming prior to use. The early prototype designs attempted to duplicate this design without success. It was concluded that such a device would be extremely cumbersome to use, and it was felt doubtful that saline would prove to be a sufficient reflector to modulate the light arriving from an emitting optical fibre. Ideally a low viscosity *white liquid* should be used as the reflecting medium. *White liquids* as such do not exist: they are either suspensions which tend to settle-out, or emulsions (requiring an emulsification agent) which *crack* and separate.

Early prototype designs used a soybean oil emulsion and a glycerol with titanium dioxide (TiO_2) suspension. The apparent *whiteness* of the fluid did provide sufficient reflection to produce a signal, and the frequency response was extremely high (>1kHz). However it was found that the device was not very reproducible, and did suffer from the aforementioned problems of *cracking* or settling. A more practical problem found was that of transducer agitation during use, invalidating any prior calibration as the fluid will either shift inside the tube or leave the tube completely. This was found to occur should the subject cough whilst the device was in position. Several alternatives for replacement of saline with a more stable element were considered,

including a ferrous suspension which may be restored by magnetism and replacing the saline with higher viscosity oils or water-based products with a high boiling point.

The design chosen for the final device used an inert silicone gel. Preliminary prototypes used the gel alone, however the small volume used (0.5μl) permitted the light to be reflected off both the meniscus closest to the optical fibres and that furthest away making the output unpredictable. The Young's modulus 'σ' of the gel, summarised in Figure 3-8, is affected by any residual element suspended in it: the addition of small reflective particles such as titanium dioxide make the suspension *stiffer*. This will affect the frequency response. To overcome this problem the meniscus closest to the optical fibres was coated with fine grade titanium dioxide to prevent the light reaching the second, more reflective[4], meniscus (section 3.4.3).

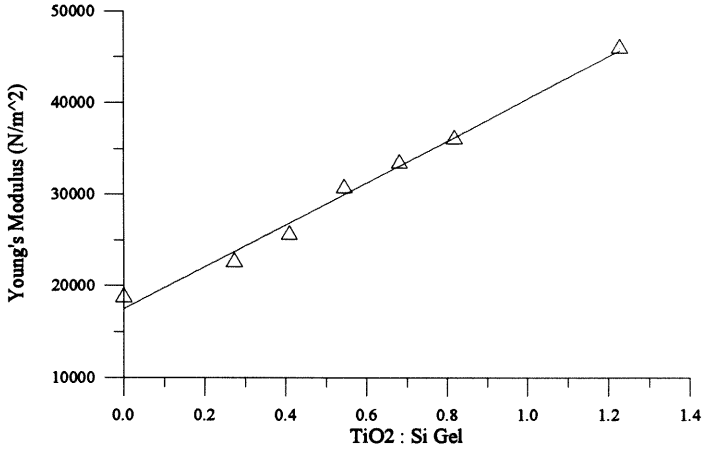

Figure 3-8 The Young's modulus of silicone gel/titanium dioxide suspension

Figure 3-8 shows the increased Young's modulus of the gel as the quantity of titanium dioxide (TiO_2) in the silicone (Si) suspension is increased. The relationship is approximately linear.

[4] The greater the change in refractive index (n) of the conducting medium, the greater the change in direction of an incident beam of light. Light travelling from a higher to a lower RI will be deflected towards the normal to the incident beam. Above a critical angle the light will be reflected back into the optically denser material.

3.4.2 Design to achieve sensitivity and resolution

The optical fibre pressure transducer relies on a column of trapped air being compressed or expanded on the introduction of a pressure difference across an elastic transduction element (Figure 3-9).

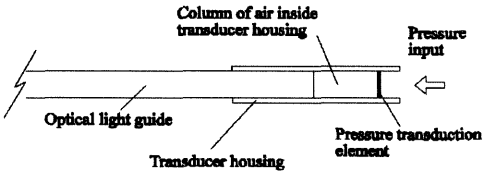

Figure 3-9 An optical fibre pressure transducers air column and transduction element

In order to meet the specification the volume of the column of air must be chosen to allow the pressure transduction element to deform sufficiently to produce a signal within the elastic limit of the gel. The diameter of the transducer housing is fixed (0.76mm ID), hence the only variable is the length of the tubing.

As a first approximation, the transduction element was assumed to be planar and free to move perpendicular to the transducer housing wall. It was also assumed that the pressure required to deform the gel is insignificant with respect the force required to compress the gas (Note: very low Young's modulus, Figure 3-8). The column of air trapped inside the transducer housing was assumed to be a perfect gas for low pressure changes.

The ideal gas law $P_0 V_0^{\gamma} = P_1 V_1^{\gamma}$ (Eqn 3-4)

where P_0, P_1 = Pressure before and after respectively (N/m^2)
V_0, V_1 = Volume before and after respectively (m^3)

Assuming adiabatic conditions ($\gamma \approx 1.5$ for adiabatic conditions) and the contact angle between the fluid and tube wall is 90° (Eqn 3-5):

$$(P_0 V_0)^{\gamma} = (P_0 + x)(V_0 - yA)^{\gamma} \quad \text{(Eqn 3-5)}$$

where x = Change in pressure (N/m^2)
y = Displacement of liquid gas interface (m)
A = Cross-sectional area of interface

Linearising $P_0 V_0^{1.5} \approx (P_0 + x)(V_0 - yA)^{1.5}$ (Eqn 3-6)

$\Rightarrow \quad P_0^2 V_0^3 = P_0^2 V_0^3 + 2P_0 x V_0^3 - 3P_0^2 A V_0^2 + \ldots\ldots$

$\Rightarrow \quad y = \frac{2V_0}{3AP_0} x$ (Eqn 3-7)

The starting pressure P_0 is dependent on the atmospheric conditions under which the transducer was primed ($\cong 101\times10^3$ kPa). The tube's diameter is constrained so as to be able to fit into a catheter 3mm in diameter. The tube chosen was 0.76mm ID and 0.94mm OD. Polymethylmethacrylate multimode optical fibre (0.25mm OD) was selected due to the restricted space in the transducer housing. The working range of the pressure transducer was designed to be ±500mm of water pressure (4.9kPa).

Optical fibre radius 'r_{fibre}'	=	0.125mm
Transducer housing radius 'r_{tube}'	=	0.38mm
Atmospheric pressure 'P_0'	=	1.01×10^5 N/m^2
Closest fibre to meniscus	=	3mm (section 3.3.2)
Permitted displacement 'y'	=	1mm
Cross-sectional area 'A'	=	0.454mm^2

Distances l_1, l_2 and l_3 see Figure 3-5

$$V_0 = \pi r_{tube}^2 - \pi r_{fibre}^2 (3h - 3l_3 - 2l_2 - l_1) \quad \text{(Eqn 3-8)}$$

substituting (Eqn 3-8) into (Eqn 3-7) (see Figure 3-5)

$$\text{Length of transducer housing } h = \frac{\left(3yAP_0 - 2\pi\, r_{fibre}^2 x(l_1 + 2l_2 + 3l_3)\right)}{2\pi x\left(r_{tube}^2 - 3r_{fibre}^2\right)} \quad \text{(Eqn 3-9)}$$

From Eqn 3-9 for pressure ±4.9kPa (500mm of water pressure)

$\therefore$ Transducer housing length = 44mm

It is important to note that the final transducer design used a silicone gel (section 3.4.4). Consequently the surface does not displace, it changes in curvature (chapter 4). The approximation did however prove to be satisfactory for selection of

the transducer housing for the final design where the apex of the gel meniscus is displaced (0.28mm for a pressure of ±4.9kPa)

3.4.3 Construction of a single channel *pigtail* pressure transducer

To avoid a poor frequency response caused by the use of a suspension (Figure 3-8), only the meniscus closest to the optical fibres was *dusted* with titanium dioxide, chosen because of its high reflectivity and inert properties[5]. A 0.5µl column of silicone dielectric gel was then injected into a 100mm length of 0.76mm∅ ID autoclavable Nylon tubing at 25mm from the tube orifice and allowed to cure. A small amount of titanium dioxide was tipped into the longer portion of the tube and agitated to ensure that it comes into contact with the meniscus, the excess titanium was then the removed by inverting the tube. Having removed the loose material there remained a coating of titanium on the meniscus as shown in Figure 3-10.

The second stage of the transducer production was the mounting the three optical fibres, one emitting and two receiving, into the end of the tubing. Three two metre lengths of 0.25mm∅ polymethylmethacrylate optical fibre were placed as follows[6]:

Distance between emitter & first receiver = 1mm (±10%)

Distance between first and second receiver = 5mm (±10%)

(Section 3.3.2)

The three optical fibres are from here onward referred to as 'M', 'L' and 'S', representing medium, long and short are connected to the first receiver, emitter and second receiver respectively (Figure 3-10). The transduction element and housing were then slid over the three optical fibres, titanium coated meniscus end first, where upon the distance from the coated meniscus is 3mm (±10%) away from the emitting optical fibre 'L'. The fibres were held in place using a two part epoxy resin sealing the tube at the end where the fibres emanate.

---

[5] Further details of the manufacture of the transducers is given in appendix A. Summaries are presented in section 3.4.3and section 3.4.4.

[6] Using a two-dimensional simulation (Figure 3-7, section 3.3.2), this yields a difference of 33% between the two signals at a displacement of 3mm if the transduction element is assumed to be planar.

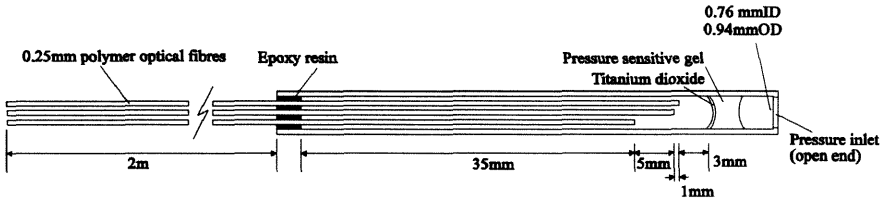

Figure 3-10 The construction of a single *pigtailed* optical fibre pressure transducer.

3.4.4 Fibre-optic pressure transducer catheter manufacture

The following section gives details on the catheter constructed to house seven *pigtailed* pressure transducers. Prior to catheter construction a radio-opaque marker was attached to each individual transducer body, this was a short length of gold leaf (2mm × 5mm) which was held 10mm from the transducer tip.

A 1.5m length of PVC tube was then slid over the twenty-one fibres of the seven transducers until it was 5mm away from the tip of transducer '7', the top-most device (Appendix A.2). When the tube was in position a flowable silicone sealant was administered through a 5cc syringe with a dispensing needle.

The second stage of the skeleton construction is the addition of the nylon supporting collars which also act as the seal between adjacent transducers[7]. Each collar consisted of a 10mm length of 3mm∅ OD nylon tubing sealed in a similar manner to that described above. A collar was fitted between the following sets of transducers: 7-6, 6-5, 5-4, 4-3 and 3-2, and sealed where upon transducer '7' is the topmost transducer. The result is the isolation of transducers 7-3 in separate windows by air-tight seals at each end, but still exposed to atmosphere. In order to isolate transducers '2' and '1' in a similar manner to '7' to '3' the lower section of the catheter must be added. This consisted of a 200mm length of PVC tube with two 10mm windows cut at each end 10mm from the ends (Figure 3-11). Two 30mm lengths of silicone filled nylon tube were secured on each window to reinforce the construction. Transducers '1' and '2' are hence located in their respective windows, and separated by an air-tight seal.

[7] The layout of the individual transducers in the catheter housing is detailed in Appendix A.4.

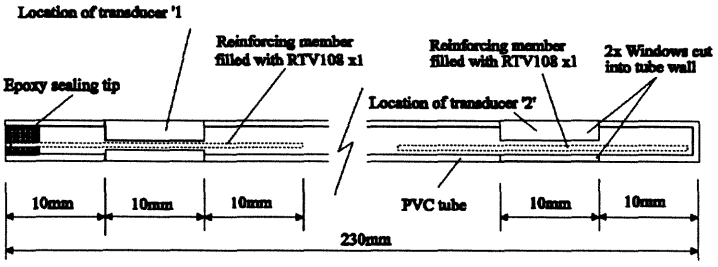

Figure 3-11 The PVC tube used for the lower half of the catheter.

Prior to the addition of the optical connectors the catheter *skeleton* was enclosed in a latex sheath (Appendix A.1). A 130mm length of 4mmØ latex tube was slid along the length of the skeleton so as to cover transducers '2' to '7' leaving equal portions of tubing at each end. The sheath was held in place temporarily by a series of cotton ties: two ties at each end (5mm apart) and two over each of the collars (5mm apart). In a similar manner a shorter length (50mm) of 4mmØ latex was fastened over transducer number '1'. Acrylic sealant was used to fill each of the ten 5mm long chambers to form an air-tight seal (Figure 3-12).

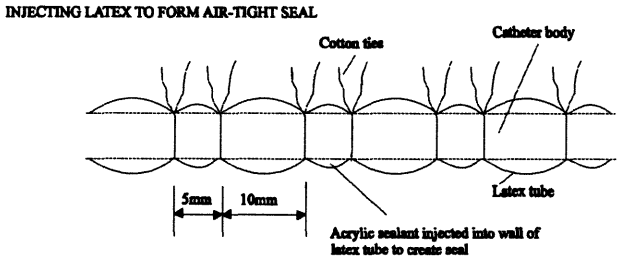

Figure 3-12 The ties to isolate adjacent pressure chambers when introducing sealant into the latex seal.

The result is seven air-tight chambers, each containing a transducer, isolated from the atmosphere and each of its one or more neighbours. Prior to coating the catheter with latex solution, four 10mm collars made from 3mmØ latex were stretched over the ends of the 4mmØ sheath and onto the PVC tube to create a smoother finish.

The device was then painted with latex solution over 1m and air dried for twenty-four hours and coated with french chalk for storage.

The final stage of production was the addition of modified 21 SMA905 optical connectors (appendix A.3). Each connector was held in place using a two-part epoxy resin and polished to 0.3μm. The weakest section of the catheter design was that of the grouping of the 21 fibres into sets of 3, corresponding to each transducer. To remedy this each set was encased in a custom built, epoxy resin filled fibre optic clamp. The seven clamps then held together in a clamp holder (appendix A.5). Figure 3-13 shows a semi-constructed transducer.

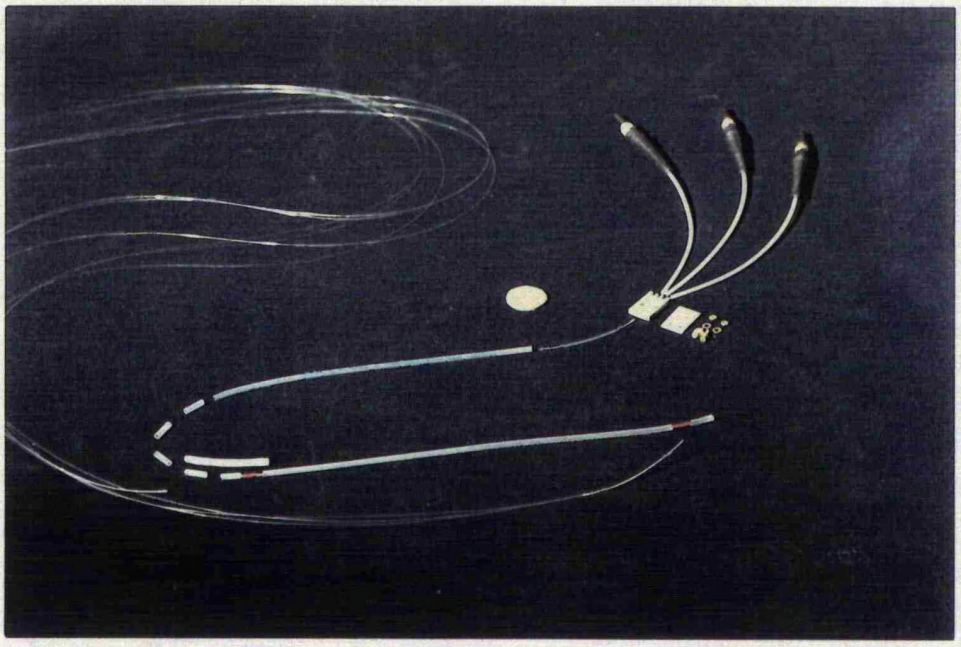

Figure 3-13 A photograph of the unassembled catheter. A single *pigtail* pressure transducer, 3 optical fibre connectors, the transducer housing and a fibre optic clamp for a single transducer is shown.

3.4.5 Electronic hardware design

The hardware design of the optical fibre pressure transducer may be sub-divided into several parts, and for reasons discussed below, is also split between two boxes for clinical use. The output of the circuit had to be unipolar DC so as to be compatible with the existing data acquisition system in the hospital sleep laboratory. The single channel device, for use in a secondary application in pre-term babies and neonates, is

exactly the same as the multiple transducer design, but the signal conditioning electronics are one seventh of the size[8]. The electronics for each channel are summarised below (Figure 3-14).

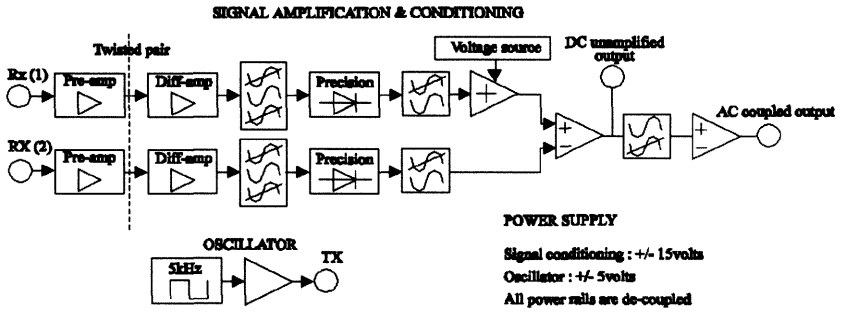

Figure 3-14 A block diagram of the signal conditioning electronics for the optical fibre pressure transducer.

As part of a sleep study a patient is required to spend a night at the hospital in order to monitor the occurrence of a disorder and is required to duplicate a typical *relaxed* sleep pattern as would occur in the home environment. If this is not the case the diagnosis produced from the study will not be reliable. The minimum of equipment was made visible to the patient, the majority of the apparatus being stored in a large container out of sight. A small *bed-side* pre-amplification box, containing pre-amp stages and the optical devices (PIN diodes and emitters) was constructed and placed next to the patients head (Figure 3-15).

[8] The single channel device (section 3.5) was split between two boxes, the first containing pre-amplification and signal conditioning, and the second the power supply.

Extra care with electrical isolation is not necessary, the transducer itself being an insulator.

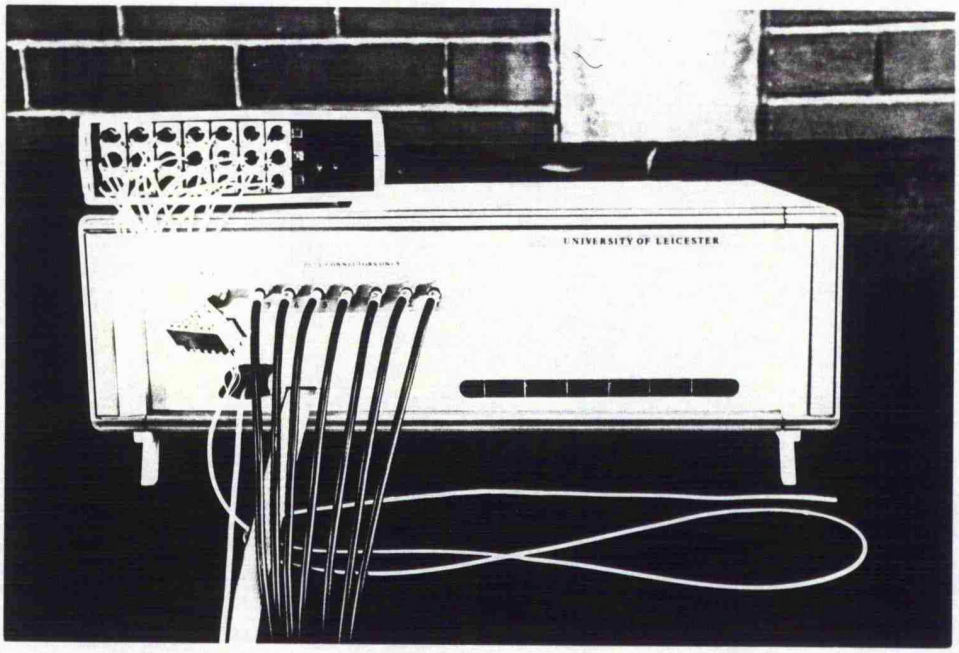

Figure 3-15 The bedside *patient-friendly* pre-amplification stages of the optical fibre pressure transducer.

3.4.5.1 The signal modulating circuitry

As discussed in chapter 1, techniques for modulating light include phase, frequency, polarisation and amplitude. The design of the optical fibre pressure transducer uses amplitude modulation. The transduction element translates a significantly large distance in comparison with the wavelength of light, hence interferometry is not appropriate. An amplitude modulated system involves the modulation of a carrier with respect to the signal. Amplitude modulated systems are susceptible to external effects, such as bending of the optical fibre waveguide (this problem is addressed in section 3.4.3). The system used an LED and micro-lens designed for coupling to optical fibres to light at a wavelength of 850nm. This provides sufficient coupling as the diameter of the fibre was large: 0.25mm multimode (core and cladding).

The emitting LED was modulated at 5kHz so as to avoid interference from mains frequencies and artificial lighting and provide sufficient bandwidth to permit the transducer to have a frequency response equal to or better than currently available

transducers (>1kHz). At peak the emitting LED draws 100mA, and hence an appropriate driving transistor circuit was selected, and driven by a relaxation oscillator implemented using an CA3140E operational amplifier which has a fast slew-rate: 9V/μS.

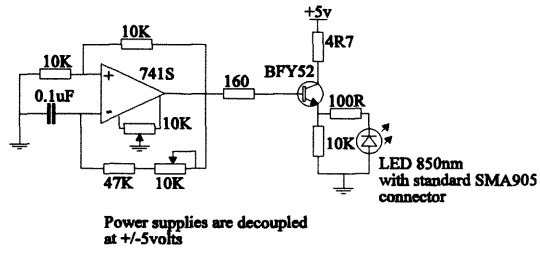

Figure 3-16 The circuit diagram of the oscillator for the optical fibre pressure transducer modulating the LED fibre optic light source

The receiving circuitry comprised a PIN diode and a high gain FET-input current amplifier (AD712N). The output was then fed into a non-inverting amplifier with a variable gain (Figure 3-19).

3.4.5.2 The signal conditioning circuitry

When designing circuitry for use in medical applications it is a legal requirement to isolate all equipment from the patient[9]. The use of optical fibres and their inherent electric isolation deems this unnecessary and so considerably reduces cost. The optical emitters, receivers and pre-amplifiers were fixed in a small box, whilst the remaining conditioning circuitry, power supplies etc. were located elsewhere. Signal lines connecting the pre-amplification stages to the signal conditioning were constructed using *twisted pairs*. The receiving PIN diode was connected to the input of a FET input amplifier, and the earth and output of each amplifier was connected to an

[9] IEEE standard for transient voltage protection (472-1974: surge withstand capability) requires equipment to withstand 5kV 10ms pulses. Underwriter's laboratory (UL544) standard for safety in medical and dental equipment limits leakage current from the mains to 35μA. In order to meet UK safety requirements ISO (International Standards Office) regulations are adopted.

appropriate twisted pair. In order to minimise noise further all PCBs were constructed with a ground plane and conductors were screened. On arrival to the signal conditioning stage a differential amplifier was used to take the difference between associated signal and ground lines to remove noise that may have been induced in transit.

A bandpass filter was used to select the 5kHz carrier frequency. A biquad implementation was used for ease of adjustment since the centre frequency and Q-value could be adjusted independently (Horowitz and Hill., 1990).

The next stage of the circuitry rectifies the amplitude modulated 5kHz carrier using a precision rectifier, comprising a diode bridge in the feedback loop of an inverting unity gain amplifier loading a resistor. The voltage drop across the resistor is measured using a differential amplifier. The final stage of the signal conditioning prior to the amplification is that of the low-pass filtering to remove the carrier. The design of this filter is important as it will determine the phase distortion and frequency response of the output. Three filter designs were considered:

- Butterworth - This design has the flattest response in the passband, and a fast cut-off. Phase characteristics are poor.
- Chebyshev - In a similar manner to the Butterworth filter, the phase characteristics are poor. The cut-off is extremely sharp and there is ripple in the pass-band.
- Elliptic - There is ripple in both the pass-band and stop-band. The phase characteristics are poor.
- Bessel - The Bessel filter has linear phase, resulting in a constant time-delay for all frequencies in the pass-band. The cut-off of the filter is the poorest of the three designs.

The Bessel filter configuration was selected for the linear phase characteristics and lack of distortion due to overshoot *ringing*. The poor time-delay and cut-off required the use of an eighth order filter (appendix A.4). The pre-amplifier, differential amplifier, bandpass filter, precision rectifier and lowpass filter are duplicated for each of the fourteen PIN diodes contained in the *bedside* unit as are the emitters. Each

transducer requires the output from two PIN diodes connected to the two receiving optical fibres fitted in each optical fibre pressure transducer in the catheter. In order to conserve the signal, the ratio between the two receiving optical fibres should be calculated. Assuming both fibres are attenuated by the same factor, the ratio between them is conserved. In order to simplify the electronics the differential between the two fibres may be taken as a first order approximation to the ratio (see below).

if a = Output from channel '1'
b = Output from channel '2'

$$\frac{a}{b} \equiv \left(1-\frac{x}{a}\right)^{-1} \quad \text{where } x = (a-b) \qquad \text{(Eqn 3-10)}$$

Expanding into a Taylor series (Munday and Farrar, 1979):

$$(1+z)^{\alpha} = 1+\alpha z+\frac{\alpha(\alpha-1)}{2!}z^2+\frac{\alpha(\alpha-1)(\alpha-2)}{3!}z^3+\ldots.. \qquad |z|<1 \qquad \text{(Eqn 3-11)}$$

Re-arranging (Eqn 3-10) to form first two terms of series (Eqn 3-11)

$$\frac{a}{b} \approx 1+\left(\frac{x}{a}\right) \qquad \left|\frac{x}{a}\right|<1 \qquad \text{(Eqn 3-12)}$$

substituting for x in (Eqn 3-12)

$$(a-b) \approx a\left(\frac{a}{b}-1\right) = a\frac{a}{b} - a \qquad \left|\frac{a-b}{a}\right|<1 \qquad \text{(Eqn 3-13)}$$

The ratio and difference are linearly related under the conditions specified in (Eqn 3-13) (see Figure 3-17).

If the change in channel 'a' is kept small with respect to channel 'b', 'a' is less than 'b' and 'b' does not change too much (<50%) the approximation is valid (Figure 3-17). In the case of the pressure transducer, channel 'a' is the lower gain channel and

does not change as much as the higher gain channel 'b'. Channel 'b' changes more than channel 'a', but not sufficiently to invalidate the approximation (<5%) (See chapter 5).

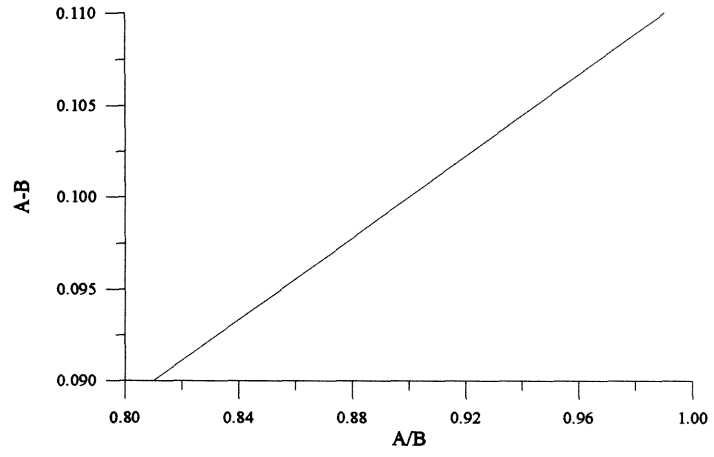

Figure 3-17 The difference between two receiving optical fibre as a first approximation to the ratio.
B<A; B=0.1; A=1 (±10%)

The final part of the circuitry is that involving the gain of the output and the coupling. The nature of the pressure transducer design, i.e. a column of air trapped inside the transducer, means that it is susceptible to temperature drift; this phenomenon is discussed in chapter 5. To compensate for this the output is fitted with an RC network configured as a highpass filter; the output being coupled with a time constant of 30 seconds. The output of the channel with the higher gain is also fitted with a summing amplifier, summing the signal with a regulated voltage. The purpose of this is to provide the output with an offset control, and was also used for diagnostic purposes during the development process.

A full circuit diagram of the signal conditioning circuitry is given in Figure 3-19. The PCB is depicted in Figure 3-18.

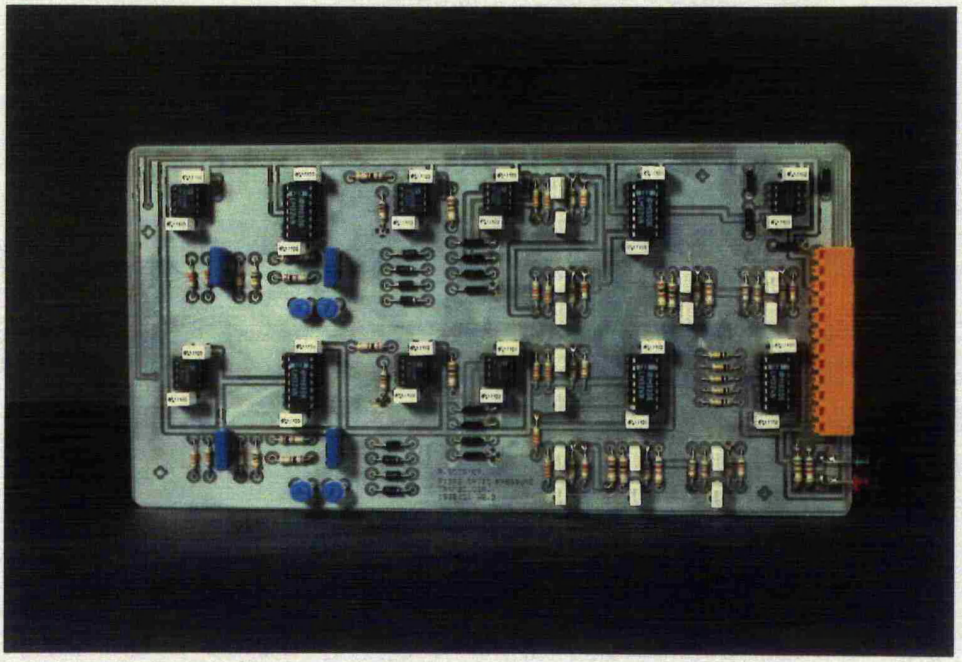

Figure 3-18 A photograph of the signal conditioning PCB, note ground plane to reduce noise and single edge connector to allow easy PCB interchange

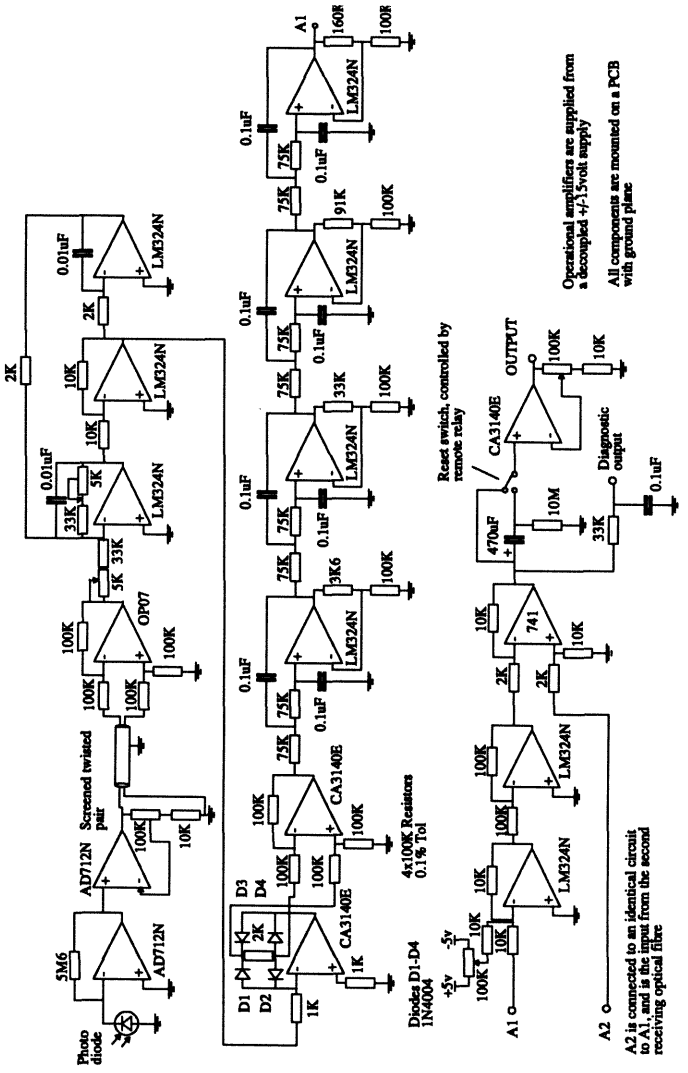

Figure 3-21 The circuit diagram of the PIN diode receiver, pre-amplifier and signal conditioning.

3.5 A portable single transducer for use in pre-term infants

It is not possible to measure pleural pressure directly in infants. Lung compliance and pulmonary resistance maybe calculated by measuring oesophageal pressure. Early studies by Drorbaugh *et al* (1963) and Chu *et al* (1964) used liquid-filled catheters and air-filled balloons. The limited frequency response, susceptibility to movement and necessary flushing of liquid-filled devices make their used limited. The suggested design criteria of a single channel device for use in pre-term babies was as follows:

- A single channel catheter diameter less than French Gauge 8 (<2.5mm)
- A length of 1.35m, penetration typically being 0.35m.
- Easily sterilisable.
- Design should be robust and realistically priced.

A single channel device was constructed from the *pigtailed* design detailed in section 3.4. A side hole was used to allow the airflow into the catheter , and the tip modified to allow ease of insertion into the airway (OD=0.94mm). The signal conditioning electronics were housed in a single *portable* box, and the power supply provided separately. This system was used to acquire data using the single optical fibre pressure transducer (see chapter 5).

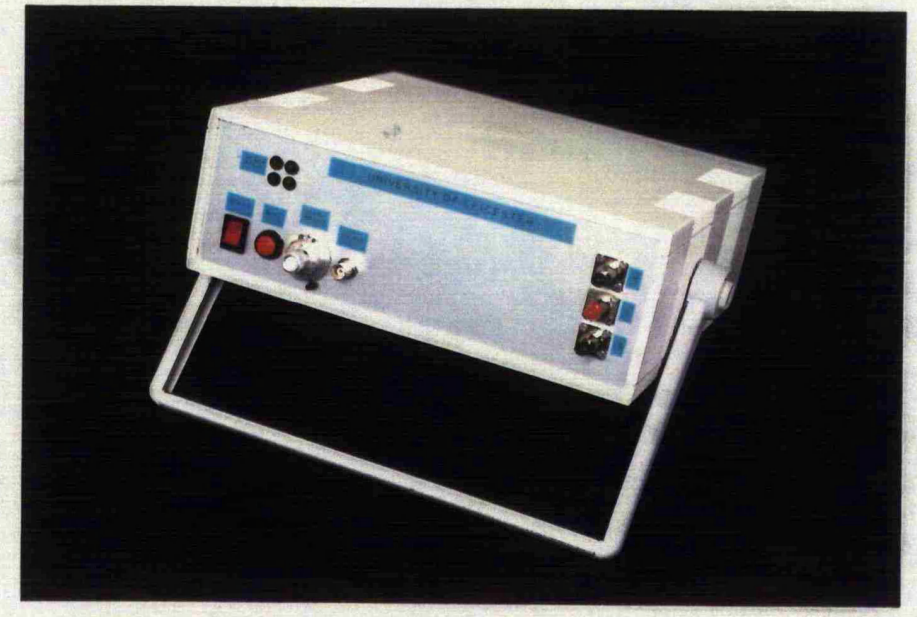

Figure 3-20 The single channel optical fibre pressure transducer instrumentation for use in pre-term babies and neonates.

3.6 Summary

After careful consideration of the commercially available pressure transducers it was decided that an optical fibre pressure transducer had the greatest potential for development into a device for assisting in the diagnosis of Obstructive Sleep Apnoea Syndrome (chapter 2). The potential for miniaturisation is limited by the physical strength of the optical fibre, the volume of air required in the transducer housing to achieve the required sensitivity and the type of gel transduction element used. The inherent electrical isolation achieved by optical fibres cannot be matched by any other technology.

The optical fibre pressure transducer first suggested by Jones and Papageorgiou (1988) has been developed considerably. The problems associated with amplitude modulation have been conquered by adding a secondary receiving optical fibre at a different distance away from the reflective transduction element. The location of the optical fibres was chosen specifically to select the appropriate part of the operating characteristic. From the design of a *pigtailed* device two separate transducers were developed: a multiple pressure transducer catheter containing seven devices, and a single channel device for use in pre-term babies and neonates (results from both are shown in chapter 5). The transduction element suggested by the aforementioned researchers: gas / saline interface, was not found to be adequate for the development of this transducer. The integration of each transducer inside an enclosed catheter renders the transducer housing inaccessible, and hence cannot be *primed* with saline minutes before use. A *white* low viscosity liquid to increase reflectivity and hence sensitivity is either a suspension or emulsion. The low viscosity also made the transducer impractical for insertion into the upper airway due to the loss of the liquid when the catheter was agitated. The final design used a two-part silicone gel which was liquid when administered, but cured in the transducer housing: adhering to the transducer housing wall. To increase sensitivity and prevent secondary reflection from the meniscus furthest from the optical fibres the meniscus closest to the optical fibres was *dusted* with titanium dioxide.

All materials selected during the design of both the multiple and single transducer catheters were inert and harmless if ingested.

Chapter 4

Mathematical modelling and analysis of the optical fibre pressure transducer

4.1 Introduction

The following chapter is a detailed examination of the operation of the optical fibre pressure transducer. It attempts to further the understanding of the physical transduction element operation. A mathematical model using ray-tracing techniques was developed to assist in the design of the transducer and to validate its operation. The transduction element of the transducer is not a planar surface, a first order approximation to a curved surface is presented. Prior to the development of a three-dimensional model a two-dimensional model was developed. The role and limitations of this model as a tool in the transducer design process are discussed. Finally the advantages and disadvantages of both of the models are examined and regions of future improvement are presented. Results validating the model by comparing it to data taken from an actual transducer are illustrated in chapter 5.

4.2 Ray-tracing

Ray tracing is a method most commonly associated with three-dimensional graphic animation. Computer languages exist purely for the purpose of ray tracing. The concept involves the tracing of physical rays from a source back to the viewer (or screen). If secondary objects are obscuring the path of the ray back to the viewer shadows and reflections will be formed, it is this effect that gives a ray-traced object a three-dimensional appearance.

The two-dimensional representation on a computer screen is a means of simulating perception. Graded shading of two-dimensional objects is dependent on the angle at which a ray hits the surface. If the ray is perpendicular to the surface the resulting pixel will be of maximum brightness, should the contact angle be less the apparent brightness is represented as a darker shade (Figure 4-1).

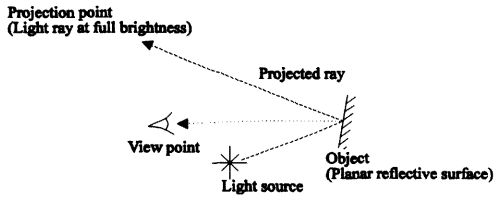

Figure 4-1 Commercial ray-tracing showing the principle of deception of the eye.

Most ray tracing is produced using three-dimensional vectors. Any point on the *graphic* is defined by both position and direction. The discrete manner in which ray-tracing is implemented involves the calculation of the intercept between lines and planes. The change in direction of a ray, represented by a vector, should it strike a reflective, semi-reflective or transparent surface, is calculated by the solving of the equations describing the planes, objects and surfaces.

A dedicated mathematical package is used to optimise this process (Jennrick *et al.*, 1989). It was felt necessary to develop an algorithm dedicated to the optical fibre pressure transducer due to the specific requirements of the light source (emanating from an optical fibre) and the receiver (a second optical fibre). Such packages are designed for creating visual effects and cannot account for such tight constraints. The ray-tracing algorithm developed uses the techniques mentioned above, but is not limited to a Lambertian or spherical light source.

4.3 Model design

4.3.1 A two-dimensional analysis

The simplest way to view an optical fibre pressure transducer is to consider the optical fibre displacement transducer (chapter 3). If the reflective surface is planar and perpendicular to the optical fibres and is free to move laterally the light received may be approximated to by an inverse square law[1] (Eqn 4-1).

[1]The inverse square law assumes that the distribution of light leaving the emitting optical fibre is uniform throughout the face of the fibre.

$$\text{Power received } 'I' \propto \frac{1}{\text{Ray path length}^2} \qquad \text{(Eqn 4-1)}$$

The ray path length is the distance from the emitting to the receiving optical fibre via the planar reflective surface. If separate optical fibres are used to receive and emit the light there are two regions where the acceptance cones of each fibre partially, or fail to overlap (chapter 3). These three zones of the operating characteristic were modelled as a first order approximation to the pressure transducer.

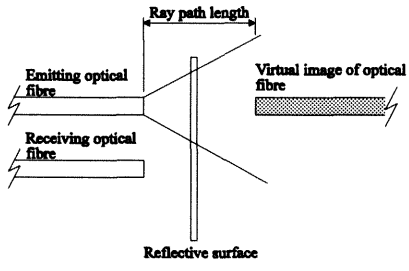

Figure 4-2a
The virtual image of a duplex optical fibre displacement transducer

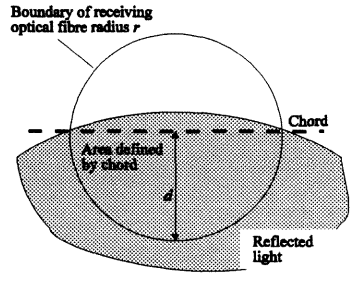

Figure 4-2b
The light arriving on the face of the *virtual* optical fibre

The partial overlap of the acceptance cones of the optical fibres was defined by calculating the sector cut by the chord of the of the edge of the reflected light on the face of the receiving optical fibre (Figure 4-2).

The area of the light defined by the chord defining the edge of the light traversing across the face of the receiving optical fibre and the fibre boundary (Figure 4-2b) is defined by Eqn 4-2:

$$\text{Area defined by chord } = \frac{1}{2}r^2\left(2\cos^{-1}\left(\frac{r-d}{r}\right) - \sin\left(2\cos^{-1}\left(\frac{r-d}{r}\right)\right)\right) \qquad \text{(Eqn 4-2)}$$

where 'r' is the radius of the optical fibre and 'd' is the distance from the centre of the chord to the boundary of the optical fibre perpendicular to the chord.

When the receiving optical fibres are fully illuminated the intensity of the light is defined as an inverse square law dependent on the numerical aperture of the optical fibre. The two receiving optical fibres present in the pressure transducer give rise to the following two equations:

$$\text{Intensity '}I_1\text{' at fibre offset '}l_1\text{'} \approx \frac{k_1}{(2x+l_1)^2}$$

$$\text{Intensity '}I_2\text{' at fibre offset '}l_2\text{'} \approx \frac{k_2}{(2x+l_2)^2}$$

Assuming the difference between intensity is an approximation to the ratio (chapter 3, section 3.4.5.2) then the signal received by the pressure transducer is defined in Eqn 4-3:

$$\text{Difference between intensities} = \frac{k_1}{(2x+l_1)^2} - \frac{k_2}{(2x+l_2)^2} \qquad \text{(Eqn 4-3)}$$

where 'k_1' and 'k_2' are constants of proportionality and the receiving optical fibres are offset distances 'l_1' and 'l_2' from the emitting optical fibre respectively, which is placed distance 'x' back from the reflective surface.

4.3.2 The significance of transduction element dimensions

Consider a column of fluid held in a length of tubing by capillary action, the interfacial tension gives rise to a contact angle between the fluid and vessel wall (Fell., 1988). This phenomenon is best known as the cause of capillary action: when a tube of very narrow diameter is lowered into a low viscosity solution , the solution is seen to climb up the lumen (Moore., 1974). The curvature of the liquid meniscus arises because the forces of cohesion between the molecules in the liquid are different to the adhesive forces between the tube wall and the liquid. If the adhesive forces are stronger than the cohesive forces, than the liquid will prefer to stick to the vessel wall rather than itself.

On introduction into the transducer housing, the gel transduction element has fluid properties including contact angle and interfacial tension. The gel then stays in equilibrium, held in place by capillary action until it cures. Once cured the gel is no longer able to shift longitudinally due to its adhesion to the vessel wall (See Figure 4-3). As the size of the vessel containing the reflective fluid falls in diameter the surface meniscus may no longer be treated as a planar surface and may be approximated to a continuous curved surface.

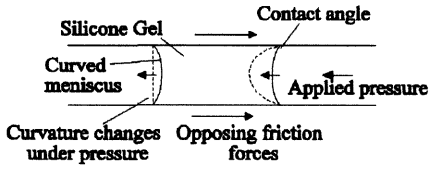

Figure 4-3 The process of adhesion of the fluid to the vessel wall giving rise to a contact angle which is maintained after the gel has cured.

When exposed to a pressure difference on opposite ends the gel will deform changing the meniscus curvature. This was observed under the microscope (Figure 4-4): the tube is made from nylon with and internal diameter of 0.76mm and an outer diameter of 0.94mm.

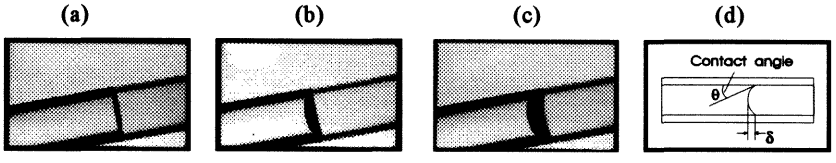

Figure 4-4 The silicone gel transduction element changing curvature with respect to pressure.

Although the fluid does not physically shift, the curvature was observed to increase or decrease as pressure was increased or decreased respectively. This was felt to be difficult and unnecessary to model mathematically. Difficult because not only does the gel distort in a non-linear and non-uniform manner, but also the pressure of the gas trapped between the fibres and gel changes. This pressure change is also non-

linearly related to its volume. It was also felt unnecessary since its measurement was straightforward. An approximation to the curvature of the fluid meniscus was calculated by measuring the distance 'δ' between the apex of the meniscus and the highest point of the gel adhering to the tube wall from the apex (Figure 4-4d).

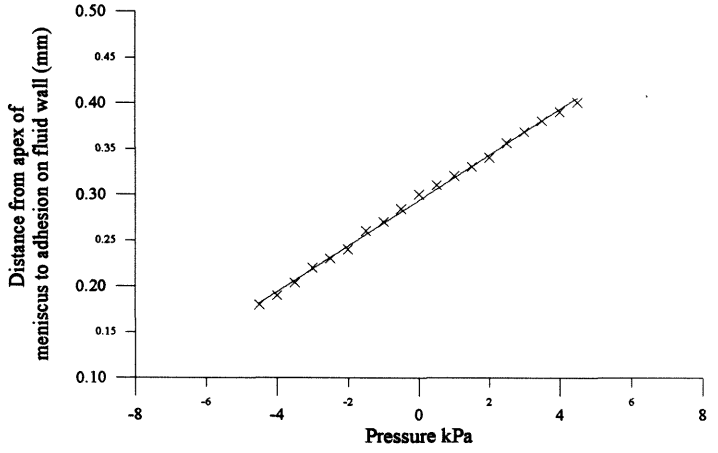

Figure 4-5 The variation of curvature of a column of silicon gel transducer transduction element as a function of height of apex.

A reasonably linear relationship between the displacement at the centre of the meniscus and pressure was established, Figure 4-5. This apparent linearity is, perhaps, surprising but may be due to the restricted range of displacement found within the required pressure range.

It is probable that the meniscus is parabolic, especially at high pressures. To simplify the calculations, the meniscus was approximated by a spherical surface (Hecht., 1987). This is justified by considering a sphere offset by a radius 'R':

$$y^2 + (x - R)^2 = R^2 \qquad \text{(Eqn 4-4)}$$

$$\Rightarrow \quad x = R \pm \sqrt{\left(R^2 - y^2\right)} \qquad \text{(Eqn 4-5)}$$

Binomial series expansion:

$$x = \frac{y^2}{2R} + \frac{1y^4}{2^2 2! R^3} + \frac{1 \cdot 3y^6}{2^3 3! R^5} + \ldots \qquad \text{(Eqn 4-6)}$$

Considering the first term only

$$\Rightarrow \quad y^2 = 2Rx \qquad \text{(Eqn 4-7)}$$

cf: equation for a parabola $y^2 = 4fx$, where the vertex is at the origin and has a focal length 'f', then $f=R/2$ (i.e. $y^2=2xR$ if $2R >> x$).

A spherical surface was fitted to these measurements after establishing this is a reasonable approximation by making measurements at various points along the surface. A series of photographs were taken of the gel whilst under pressure to establish distance 'δ'. The diameter of the transducer housing 'ϕ' is known (0.76mm). Eqn 4-8 was then used to determine the radius of curvature for the spherical fit to the reflecting meniscus.

$$\text{Spherical curve fit } r(\delta) = \frac{\delta^2 + \phi^2/4}{2\delta} \qquad \text{(Eqn 4-8)}$$

The minimum radius of curvature is restricted to the radius of the transducer housing. It was also found by measurement that the reflecting meniscus did not become convex within the limited pressure range for which it was designed for (±5kPa). Having determined the appropriate fit this was validated by measuring the depth of a sector cut by a chord joining the apex of the meniscus to the point where the gel meet the vessel. The contact angle may then be measured.

4.3.3 Power distribution of optical fibres

The power distribution of light leaving an optical fibre is dependent on the numerical aperture. This was found to be Gaussian in appearance, and confirms the findings by Perlin (1992) (experimental results - Figure 4-6).

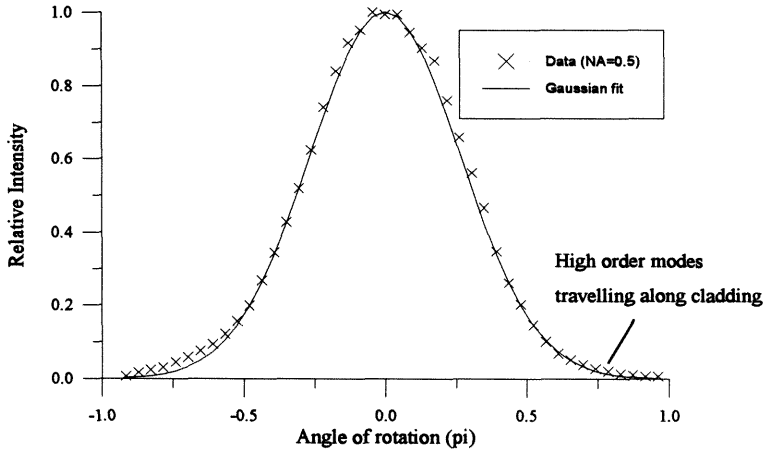

Figure 4-6 A plot of the light emitted from the core of a polymethylmethacrylate optical fibre compared to the fitted data derived from the Gaussian curve fit (NA=0.5).

The duplex orientation of the optical fibres make the effect of the Gaussian distribution significant. The curve contains two sets of data. The majority of the light travels along the core of the fibre, but there some high order modes also travelling along the cladding confined by the air/cladding interface.

A scaled Gaussian distribution, Eqn 4-9, was fitted to the data shown in Figure 4-6 to model the intensity of the light leaving the optical fibre at a given angle (Mean error = 0.011984).

$$\Phi(z) = \frac{1}{\sqrt{2}} e^{-\frac{1}{2}z^2} \qquad \text{(Eqn 4-9)}$$

4.4 Model implementation

4.4.1 Ray tracing using vectors

The mathematical model was implemented using a set of weighted trajectories corresponding to light rays emitted from the tip of the optical fibre. A series of points on the surface of each optical fibre were traced through their path from the emitting optical fibre to the reflective surface and back to the receiving optical fibre. The launch angle at each point was defined by the numerical aperture. The model was split into several different stages, each covering different aspects of the path of the ray on its journey to the receiving fibre or otherwise. The model consists of the following features:

- Location of ray origin on the surface of the emitting optical fibre and tracking to a point on the reflective medium.
- Course adjustment of the light ray depending on contact angle of ray against reflective surface.
- Tracing of ray back to receiving optical fibre.

The ray tracing process was calculated using three dimensional vector algebra. A set of points launched from the same radial distance around the central longitudinal axis of the emitting optical fibre was described as an *isophotal*.[2]

The cylindrical co-ordinate system is simple to visualise, the transducer housing being cylindrical. In order to handle the spherical fluid meniscus easily (minimising computation time) a Cartesian co-ordinate system was selected. The power of each isophotal was selected depending on its location on a normalised radius on the emitting optical fibre as defined by Eqn 4-9.

To minimise computation time further a series of *exploratory* points were traced as a part of a low resolution isophotal, the computation process moved to the successive isophotal if at least one point did not lie within the face of the receiving

---

[2] The power along each isophotal is constant. When each point in the isophotal strikes the reflective surface the points will either reflect straight back in the boundary case, converge or diverge depending on the angle at which they strike.

optical fibre. If this condition was true the exploratory points, evaluated using a COST function (below), were used as the initial guesses for the numerical optimisation. The intersection of each point with the spherical reflective surface was calculated using (Eqn 4-10) to (Eqn 4-12)[3]:

Consider a vector of position $\begin{pmatrix} x_1 \\ y_1 \\ z_1 \end{pmatrix}$ and direction $\begin{pmatrix} x_2 - x_1 \\ y_2 - y_1 \\ z_2 - z_1 \end{pmatrix}$

and a spherical surface: $x^2 + y^2 + z^2 = R^2$

Intersection of trajectory with spherical surface is given by:

$$Y = aX + b \qquad \text{(Eqn 4-10)}$$

$$Z = cX + d \qquad \text{(Eqn 4-11)}$$

$$Y^2\left(\frac{1}{a^2} + \frac{c^2}{a^2} + 1\right) + Y\left(\frac{2cd}{a} - \frac{2b}{a^2} - \frac{2c^2 b}{a}\right) + \left(\frac{b^2}{a^2} - \frac{2cbd}{a} + \frac{c^2 b^2}{a^2} + d^2 - R^2\right) = 0 \qquad \text{(Eqn 4-12)}$$

where

$$a = \frac{y_2 - y_1}{x_2 - x_1} \qquad b = x_1\left(\frac{y_1 - y_2}{x_2 - x_1}\right) + y_1$$

$$c = \frac{z_2 - z_1}{x_2 - x_1} \qquad d = x_1\left(\frac{z_1 - z_2}{x_2 - x_1}\right) + z_1$$

which may be solved analytically. The two roots of Eqn 4-12 give rise to the two points of intersection of the sphere.

[3] A point of intersection is the intersection of three planes, the intersection of two planes is the path the trajectory travels before striking the reflective surface.

The algorithm used to determine the change in direction of the of a ray upon striking the reflective surface was determined by calculating the angle of the trajectory vector '$\bar{a}$' to a normal vector '$\bar{n}$' perpendicular to the spherical surface. Vector '$\bar{b}$' is the path of the trajectory reflecting at the same angle at which it struck the tangent to the spherical surface.

$$\bar{n} \times \bar{a} = \bar{n} \times \bar{b} \qquad \text{(Eqn 4-13)}$$

i.e. a vector $\perp$ to $\bar{a}$ and $\bar{n}$ is also $\perp$ to $\bar{b}$ and $\bar{n}$ where $\bar{a}$, $\bar{b}$ and $\bar{n}$ are unit vectors

$$\bar{n} \times \left(\bar{a} - \bar{b}\right) = 0$$

$$\Rightarrow \quad \bar{b} = \bar{a} - \lambda\, \bar{n} \quad (\lambda \text{ is a scalar such that } |\bar{b}| = 1) \qquad \text{(Eqn 4-14)}$$

Solving for λ

$$|\bar{a} - \lambda\, \bar{n}|^2 = (a_1 - \lambda n_1)^2 + (a_2 - \lambda n_2)^2 + (a_3 - \lambda n_3)^2 = 1^2 \qquad \text{(Eqn 4-15)}$$

Discounting trivial solution, λ=0

$$\lambda = 2(a_1 n_1 + a_2 n_2 + a_3 n_3) = 2(\bar{a} \cdot \bar{n})$$

hence $\bar{b} = \bar{a} - 2(\bar{a} \cdot \bar{n})\bar{n}$ (Eqn 4-16)

$\bar{a}$ and $\bar{n}$ are unit vectors and are known, $\bar{b}$ is the unknown and describes the new trajectory of the ray after striking the reflective meniscus and uniquely defines its direction (Figure 4-7).

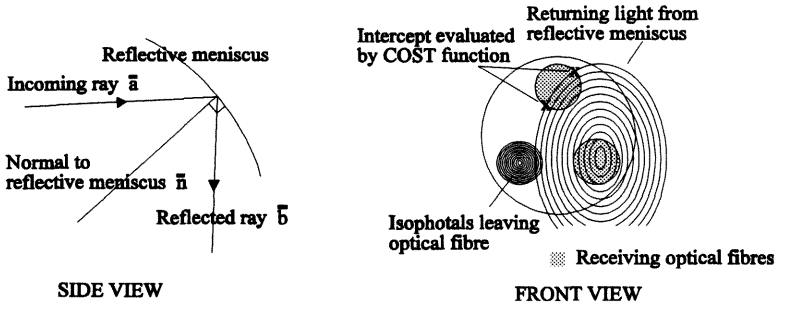

Figure 4-7 Reflected isophotals striking a receiving optical fibre after being reflected off the spherical transduction element.

The intercepts between the reflecting isophotal and the boundary of the optical fibre were established by numerically calculating the point at which a COST function (Eqn 4-17) has a root. The function is defined as the difference between the radius of the optical fibre and the distance between the centre of the receiving optical fibre and each reflected point. If the modulus of this function is found, the minimum (Figure 4-8) indicates the points of interception[4].

Reflection algorithm = f'(Ray origin, Curvature, NA)
≡ f(X0,Y0,Z0,$\Re$,NA)
Optical fibre radius = Fr

hence

COST function : $|f(X0,Y0,Z0,\Re,NA)-Fr|=0$ (Eqn 4-17)

[4] The minima is found using a Nelder-Meade simplex algorithm (Whidborne *et al.*, 1994)

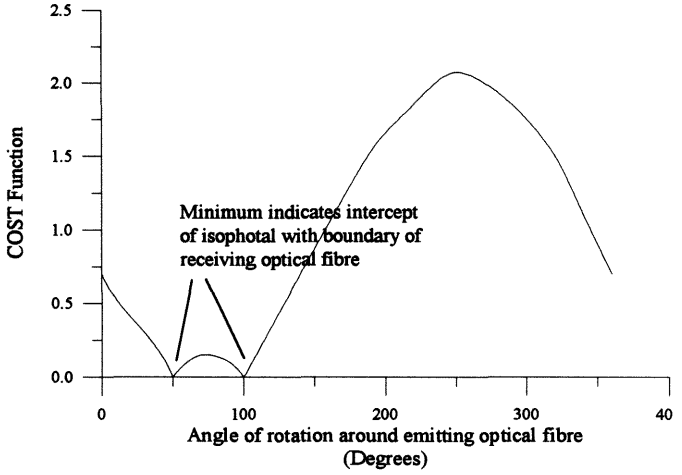

Figure 4-8 The cost function evaluated for a single isophotal.

The redirected trajectory was then traced back to a position level to the surface of the appropriate receiving optical fibre to check whether it lies within it and that the numerical aperture has not been exceeded.

4.4.2 The isophotal weighting function

The significance of the proportion of each isophotal is calculated by combining its weight (Eqn 4-9) with the change in effective area and integrating numerically over the fibre surface.

$$\text{Power} = \sum \frac{\text{Current isophotol area}}{\text{Original isophotol area}} \times \text{Weight} \times \text{Fraction inside fibre} \qquad \text{(Eqn 4-18)}$$

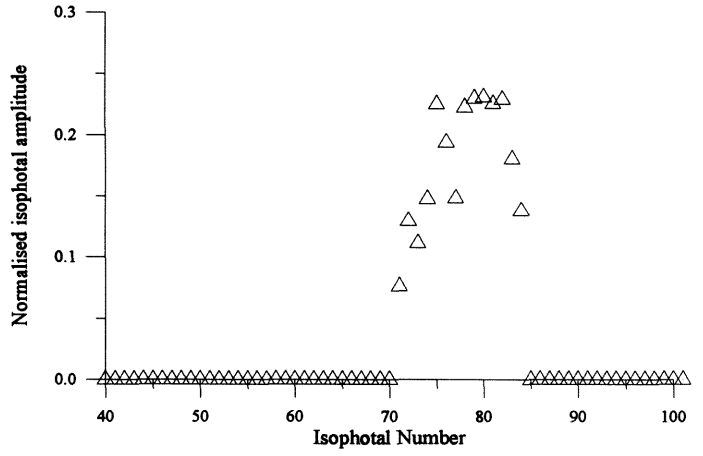

Figure 4-9a Unweighted isophotals

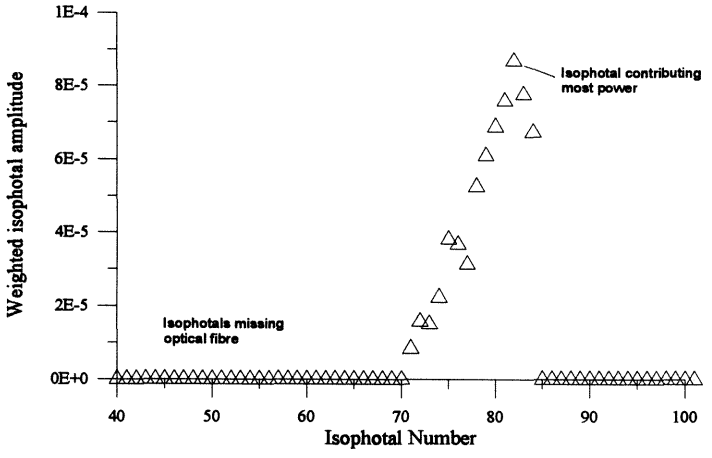

Figure 4-9b Weighted isophotals

Figure 4-9 The proportion of the light received by the receiving optical fibre and weighted according to the Gaussian power distribution of the optical fibre

The graphs in Figure 4-9 illustrate the proportion of weighted isophotals lying within the face of the receiving optical fibre. An Optical fibre 250μm OD (10μm cladding) was used, with a NA of 0.5 (the NA was normalised and used to determine

the weight of each isophotal). The nature of the discrete numerical calculation implies that the model has error related to the number of isophotals used in each simulation and the number of points in each simulation. If the optical fibre is small with respect to the effective area of each band defined by the boundary of two isophotals the error may be up to 50%: the receiving fibre being equally dissected by the isophotal. The error is non-linearly related to the number of isophotals defined in each simulation and the extent at which they disperse or converge. The error can be seen in Figure 4-9a as a lack of curve continuity.

The significance of the error with respect to the received light is dependent of the weight of the associated isophotal. Both curves shown in Figure 4-9 show that 15 isophotals (#72 to #87) of a possible 250 were captured by the face of the receiving optical fibre. Any isophotals outside these boundaries are lost. Figure 4-9a illustrates a trend, isophotal normalised amplitude increases steadily from 7% to 23% where there is a plateau before tailing off. Each of the isophotals are given a weight in Figure 4-9b. The plateau region becomes a peak due to the higher associated power of the higher order isophotals. It is apparent from this simulation that of all of the power received by the receiving optical fibre, the greatest contribution is by isophotal #84. Although higher orders have a higher power, the area of each is not sufficient to exceed the aforementioned lower powers.

4.5 Results

The following section presents the results from the two dimensional and three dimensional model respectively. The validation is performed by comparing simulated data to a displacement transducer with an ideal planar reflective surface. This is intended to show the improvement of the later model design using a Gaussian flux distribution across the face of the emitting optical fibre. Results comparing the model to a pressure transducer are presented in chapter 5, section 5.6.

4.5.1 Two-dimensional modelling

4.5.1.1 Comparison with a displacement transducer

As part of the preliminary research an optical fibre displacement transducer was developed. The device comprised an optical fibre probe made from 1mm∅ duplex optical fibre (see chapter 3). The faces of the optical fibres were *lapped* to 0.3μm. This was then mounted onto a travelling micrometer. The distance from the tip of the probe to the face of a surface planar mirror was then measured. The data obtained was compared to the two-dimensional mathematical model using the inverse-square law

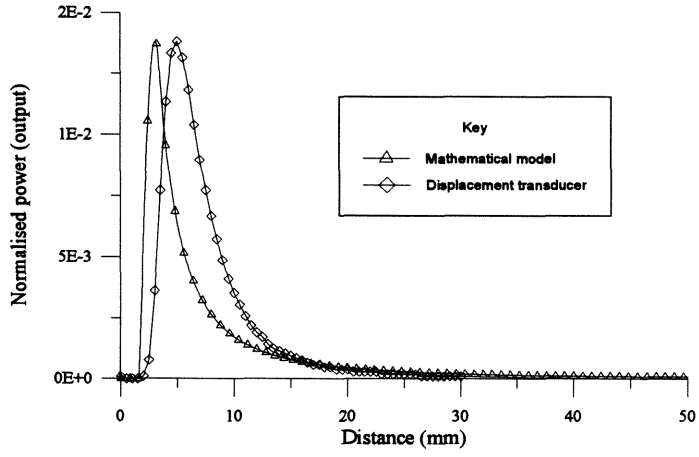

Figure 4-10 The comparison of two-dimensional simulated data to actual data obtained from a displacement transducer mounted in front of a surface planar mirror.

The displacement transducer was averaged during 5 cycles over 50mm and the mean was calculated (Figure 4-10). The standard deviation was insignificant and is not displayed on the graph. The mathematical model did not require any averaging. Although the general topology of the two graphs are similar, the two-dimensional model is a gross approximation to the displacement transducer. The dead-spot at the start of the each of the curves is 2mm in both cases. The model assumes that there is a uniform power distribution across the face of the emitting fibre, and hence when the acceptance cones of the receiving and emitting fibres overlap there is a step indicating the onset of the reflected light traversing across the receiving fibre. As shown in section 4.3.3, the power distribution is Gaussian in appearance. For this reason the

transition from the dead-spot to the first part of the operating region is more gradual. The sensitivity of the left-hand side of the characteristic is similar in each case, $8.0\times10^{-3}mm^{-1}$ and $5.3\times10^{-3}mm^{-1}$ for simulated and actual data respectively. The peaks of each curve are at different distances, 3.5mm and 6mm respectively. This is also a feature of the non-Gaussian distribution.

The second part of the operating characteristic, that chosen for the pressure transducer operation (right-hand-side of the peak), has the same gain initially (although translated 2.5mm). The simulated data attenuates quicker than the recorded data. This is due to the uniform spreading of the power over the effective area of the light spot once reflected. The mean error was measured to be 0.62% normalised power (44% of peak value[5]) over the range 2mm to 8mm (cf: section 4.5.2).

4.5.1.2 Comparison with the pressure transducer

Although the two-dimensional model is limited it was found to be useful in the early design stages when determining the location of the receiving optical fibres within the transducer housing with respect to one another.

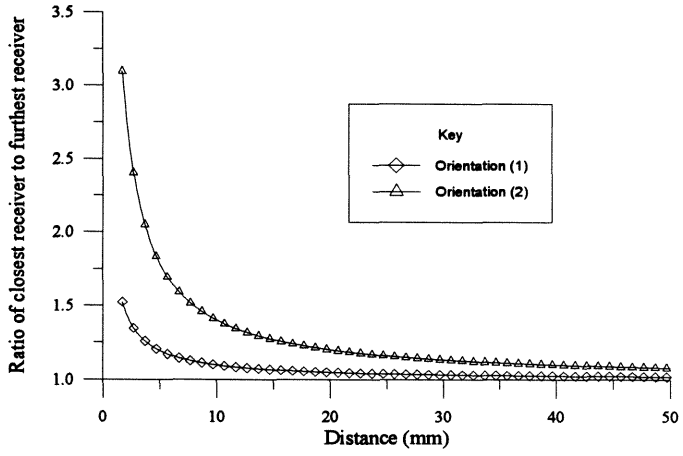

Figure 4-11 A comparison of the ratio between receiving optical fibres when offset differences from the emitting fibre.

Orientation (1) - Offset from receiver '1' to emitter = 0mm

[5] Peak value was measured from the base-line (0% power) to the peak of the curve (1.4%)

		Offset from receiver '2' to emitter	=	1mm
Orientation(2)	-	Offset from receiver '1' to emitter	=	1mm
		Offset from receiver '2' to emitter	=	5mm

Figure 4-11 illustrates the importance of selecting the offset between the receiving optical fibres so to ensure that the ratio between them has a high enough to achieve adequate sensitivity.

If the difference between the two signals is to be a first order approximation to the ratio, the amplitude of the signal received by the second receiving optical fibre must be considerably less than that received by the receiving optical fibre closest to the reflective element (<10%) (see chapter 3). This model was also able to illustrate the importance of making the emitting optical fibre closest to the reflective surface. If this is not the case the peak of the characteristic will translate along the x-axis when the difference is evaluated.

4.5.2 Three-dimensional modelling

4.5.2.1 Comparison with a displacement transducer

The first three-dimensional simulation modelled the optical fibre displacement transducer (chapter 3). The planar reflecting surface was represented by a curved surface with a large radius of curvature (100mm) with respect to the diameter of the optical fibres. Having produced a set of simulated data, an optical fibre displacement transducer was used to produce a set of data for comparison (Figure 4-12). The dimensions used were: a duplex pair of 0.25mm diameter optical fibres, spaced 0.25mm apart across their centres. The distance was then varied over the range 0 to 50mm. It was expected that this investigation would demonstrate the improved accuracy achieved by modelling the Gaussian distribution of the light leaving the optical fibre.

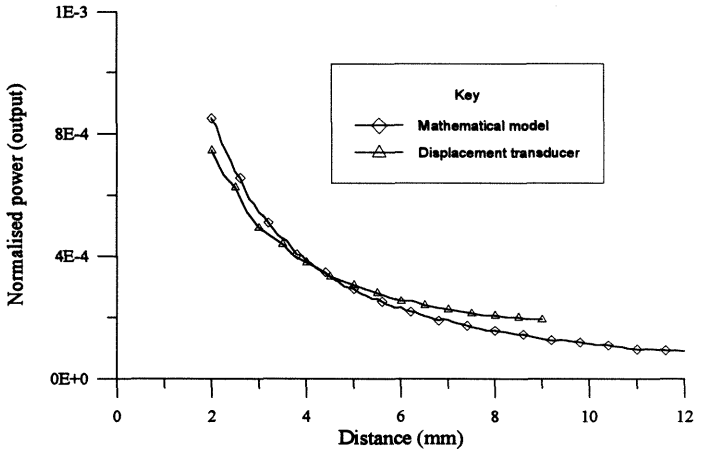

Figure 4-12 A comparison of data taken from a duplex fibre optical displacement transducer with actual data.

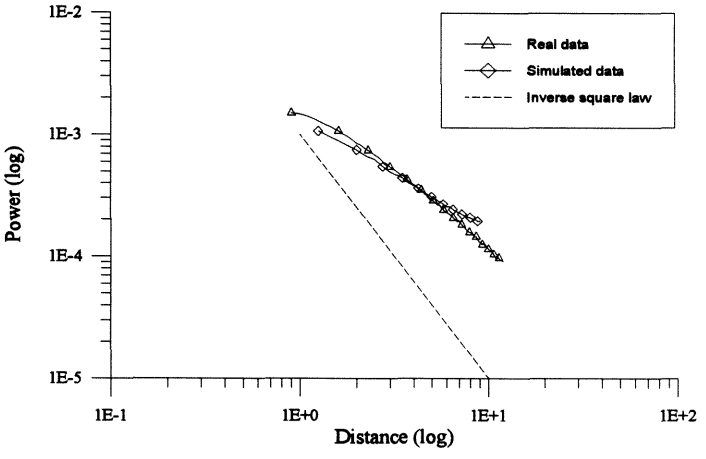

Figure 4-13 The pressure transducer operating characteristic modelled on a planar surface in comparison with the two-dimension square law approximation.

Figure 4-12 illustrates the three-dimensional model compared against the displacement transducer plotted on a linear axis. The optical fibre was 250μm (10μm cladding), NA of 0.5. The peaks of both curves are in the same position, and the gain of the left-hand-side of the curve is to within 0.62% of the recorded data peak value (1.465×10^{-3}). Both of these factors are attributed to the closer approximation to the

Gaussian light flux power distribution across the face of the emitting optical fibre in comparison to the uniform distribution assumed in the former two-dimensional algorithm. Figure 4-13, illustrates the same set of data on a log-log plot in order to identify the deviation away from the inverse square law. The gradient of the model, recorded data and inverse square law were measured to be -1.03, -1.38 and -2 respectively using a best straight line fit.

The error of the model is due to the non-ideal characteristics of the experiment. The model does not take account of the reflection on the face of the cleaved fibre or the angle of the cleave. It is also unlikely that the location of the optical fibres in the transducer are going to be exactly those specified in the model. The model also assumes that all light striking the face of the receiving optical is collected which is not true in the ideal case: a proportion of the light (the high order modes) will be refracted straight out of the fibre core.

4.5.2.2 Variation of reflective surface curvature

The compensation for curvature of the reflective transduction element is the second main design feature of the three-dimensional model. To examine this phenomenon, the distance from the face of the emitting fibre to the transduction element apex was kept constant and curvature varied in order to simulate pressure change.

The pressure transducer comprises three optical fibres, one to emit light and two to receive. Each of the receiving fibres is offset a different distance from the emitter (chapter 3, section 3.3.2). A selection of offsets between the emitting and receiving optical fibres were investigated, two of which were later combined to produce the final output from the pressure transducer.

The titanium dioxide gel transduction element adheres to the vessel wall and hence changes curvature when exposed to a pressure difference (see section 4.5.2.2). The apex of the gel meniscus then translates along the vessel perpendicular to the optical fibres.

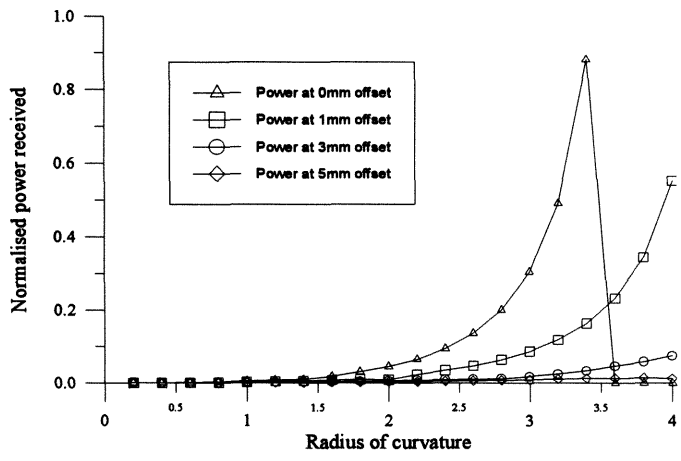

Figure 4-14 Data obtained from the three dimensional model using a single optical fibre to receive light offset 0mm, 1mm, 3mm and 5mm from a similar fibre emitting light

The data obtained and illustrated in Figure 4-14 used a single optical fibre to receive and a second to emit. The graph shows the effect of offsetting the two fibres whilst varying curvature given the following dimensions:

Optical fibre diameter	=	0.25mm
Optical fibre location	=	Adjacent and spaced 0.25mm across their centres in the centre of the housing
Distance from emitting fibre to transduction element	=	3mm
Numerical aperture	=	0.5

The offset between the emitting and receiving optical fibre means the characteristic is translated along the x axis. This is due to the increase in light ray path length that the light must encounter before being received

The optical fibre pressure transducer discussed in chapter 3 combines the output from two receiving optical fibres offset 1mm and 5mm from the emitting fibre respectively; these results are presented in chapter 5, section 5.6. The graph also shows the problems which would be encountered should the fibres be placed too close to the gel and is characteristically illustrated as a peak in the characteristic at an offset of

0mm. At this point the desired operating region is breached and the output will become unpredictable (cf: Figure 3-4, chapter 3).

The addition of the curved gel transduction element considerably complicates the path of each light ray within the transducer housing in comparison with the idealised two dimensional model using a planar reflective surface (see section 4.3.1).

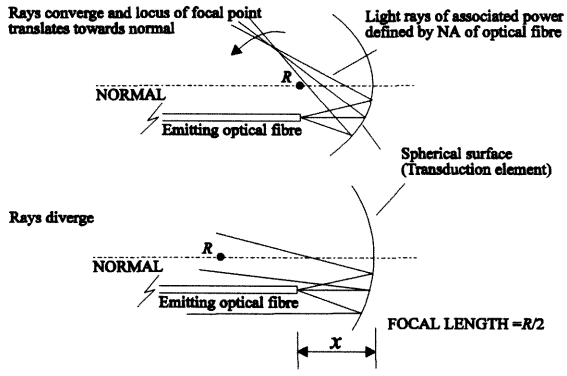

Figure 4-15 Ray diagram indicating the deformation of an isophotal when striking a spherical surface whilst varying radius of curvature 'R' and keeping the distance 'x' from the apex of the spherical surface to the face of the receiving optical fibre constant.

Examination of the geometry of the reflective transduction element and the location of the optical fibres defines whether the isophotals converge or diverge. When the radius of curvature is comparable with the dimensions of the optical fibre, and the emitting fibre is not on the normal to the transduction element, the image will be focused on the opposite side of the normal (Figure 4-15). As the curvature increases the locus of the image will traverse across the normal, at which point the radius of curvature is large in comparison with the dimensions of the fibre and the transduction element approximates to a planar surface.

The size of the image at a fixed distance away is dependent on the focal length of the gel surface and hence the radius of curvature[6]. The isophotals will diverge or

[6] A spherical mirror with radius of curvature R has a focal length $R/2$.

converge, depending of whether the light emanates from inside or outside the radius of curvature respectively.

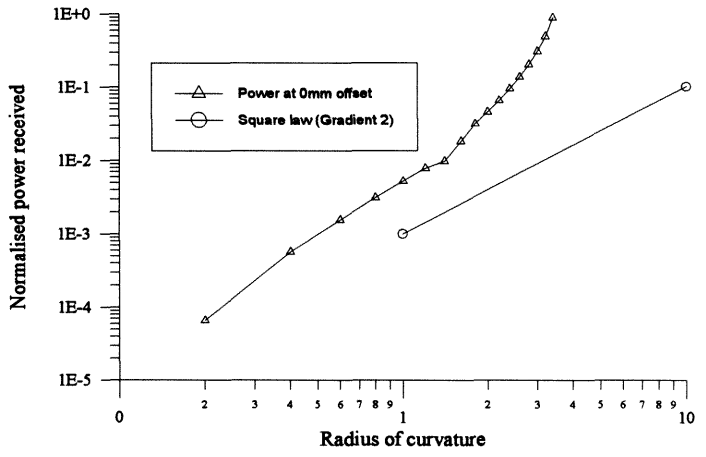

Figure 4-16 Comparison of the mathematical model to a square law

The graph shown in Figure 4-16 is the comparison of data obtained from the model by variation of curvature to a square law. Earlier models used an inverse square law as a first approximation, the output decaying as a function of distance. The graph shows the same phenomena, but transposed. As the radius curvature increases the centre of the meniscus moves closer towards the optical fibres and the signal increases in amplitude (cf: inverse square law, section 4.3.1). The results show that initially the mathematical model has a mean error of 24.4 % of the idealised square law (gradient = 2.61), however beyond 1.5mm the gradient is more positive (gradient = 8.47).

The size of the transducer housing (0.76mm ID), the contact angle and the distance from the emitting optical fibre to the transduction element (3mm) means that the transduction element cannot be treated as a planar surface when forming an accurate model of the pressure transducer.

4.6 Discussion

The development of two numerical models to describe the optical fibre pressure transducer have been presented to assist in the development of the hardware. The inverse-square law, two-dimensional approach, was found to be useful to determine the optimum location of the optical fibres inside the transducer housing: providing a fast solution due to the small amount of computation involved. The three-dimensional approach was able to improve the mean error from 44% to 0.62% in the case of the optical fibre displacement transducer indicating that the Gaussian weight function is an effective method for improving the accuracy of the model.

The radius of curvature of the transduction element cannot be neglected due to the contact angle between the gel and the vessel wall. As the radius of curvature becomes increasingly large with respect to the dimensions of the optical fibre, the change in light received will become increasingly less with change in curvature as it then approximates to a planar surface. Beyond this threshold and the transduction element becomes convex. In practice this was only found to occur when the transducer was exposed to pressures of over 5kPa, outside the original design criteria, and hence neglected for the purposes of the simulation.

Validation of the model was performed by measuring the dimensions and location of the optical fibre transduction element under varying static pressure, and implanting them into the model. These results are presented and discussed in section 5.6, chapter 5.

Chapter 5

Validation of the optical fibre pressure transducer catheter

5.1 Introduction

The following chapter details both the clinical investigations and the laboratory trials performed on the optical fibre pressure transducer designed to assist in the diagnosis of OSAS. Two transducer designs are discussed, a single and a seven channel device. Static and dynamic testing were performed. Results were obtained from patients and volunteers under both local and general anaesthesia, and are grouped accordingly. The clinical significance of the data obtained in each subject is discussed with the physiological explanation of each subject regarding catheter position in the pharynx.

In the final section of the chapter the usefulness of the optical fibre pressure transducer in the diagnosis of obstructive sleep apnoea syndrome is explored, outlining the main design lessons learnt in the design of the catheter. In chapter 9 these are compared to those of the endothelial cell damage probe. The aim is to present the usefulness of a *physical* optical fibre transducer, and validate its usefulness as a clinical tool for *in-vivo* applications.

5.2 Static and dynamic evaluation

5.2.1 Static analysis

5.2.1.1 Calibration data

All transducers were calibrated prior to conducting both the clinical and laboratory trials. A pressure chamber was constructed to contain either the single or seven channel system. Pressure was varied using an air-loaded syringe and measured using either an analogue Bourdon gauge or water-filled manometer. In the case of the seven channel device, all channels were zeroed at 0Pa gauge pressure and a 10 second epoch recorded on all channels simultaneously at a known pressure using a data

acquisition system currently used to acquire data from an overnight sleep study (Cardas, Oxcams™) (See chapter 2). The calibration data obtained was then used to scale the recordings to provide a quantitative output by removing the mean of the signal and linearly interpolating over the pressure range of interest.

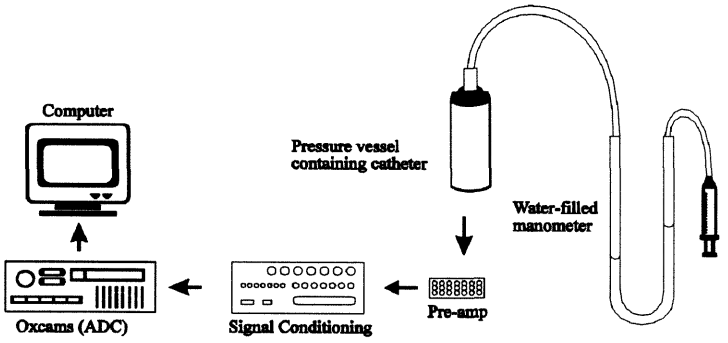

Figure 5-1 The semi-automatic arrangement for calibrating the seven channel transducer prior to clinical use.

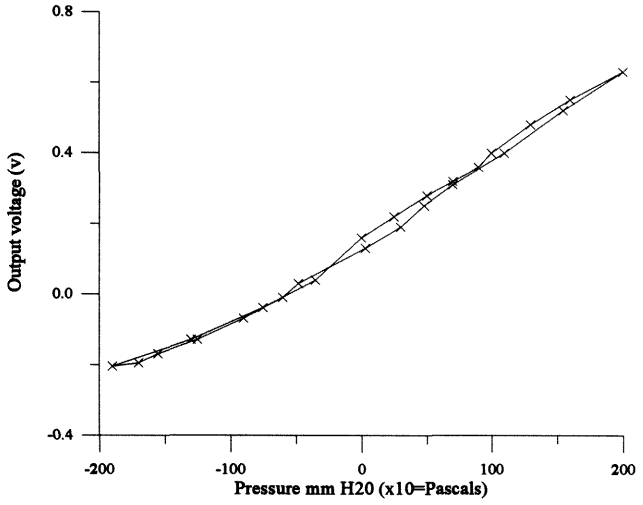

Figure 5-2 Calibration of a single channel optical fibre pressure transducer showing hysterisis and non-linearity.

The operating characteristic of the pressure transducer is not linear, and was predicted so by the mathematical model (see section 5.6). Linearity was found to be 8% over the pressure range ±2kPa, given Eqn 5-1:

$$\text{Linearity} = \frac{\text{Max. deviation from straight line fit}}{\text{FSD}} \times 100\% \qquad \text{(Eqn 5-1)}$$

Characteristics over ±2kPa range (Figure 5-2):

Hysterisis = 5.1%

Sensitivity = <10Pa

5.2.1.2 Long-term drift and usage

A criticism of using low-viscosity *white-liquids* for use in the transducer is their existence only in the form of a suspension or an emulsion; both systems suffering from instability during long-term storage, i.e. they will either settle out or *crack*. The use of a gel prevents the suspension settling out, however the operating characteristic is dependent on the atmospheric pressure and temperature of the operating conditions since the signal measured is dependent on the conditions under which the *pigtail* transducer was *initially* primed. A set of calibration data was taken from a single channel pressure transducer using the arrangement in section 5.2.1.1, atmospheric pressure, temperature was recorded over 110 days.

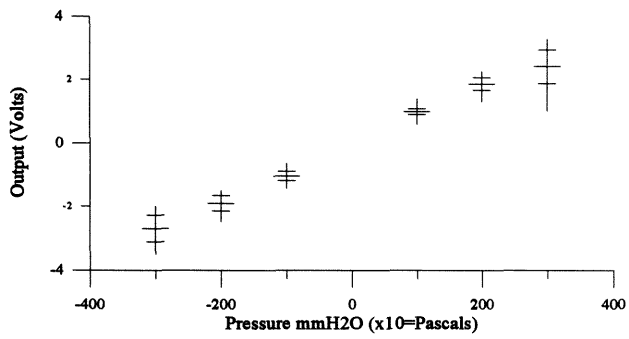

Figure 5-3 The long-term testing of a single channel pressure transducer over 110 days showing the mean and standard deviation.

The atmospheric pressure varied over the range 728.1mmHg to 769.7mmHg, whilst the ambient temperature varied 17.9°C to 24.9°C.

Pressure → (Pa)	-3kPa	-2kPa	-1kPa	0kPa	1kPa	2kPa	3kPa
Mean μ	-2.710	-1.921	-1.048	0	0.987	1.868	2.419
Std Dev σ	0.417	-0.254	0.143	0	0.0912	0.202	0.539
Coeff of var (σ/μ)	-0.154	0.132	-0.136	-	0.0921	0.108	0.223

Figure 5-4 The statistical deviation of the output voltage taken from a single channel pressure transducer during long term analysis given varying atmospheric pressure and temperature

The results show that the transducer is dependent on the ambient conditions at the time of the recording, and hence to produce quantitative results the calibration data from preceding use should not be deemed reliable. The deviation is due to the non-linearity of the pressure transducer. The change in temperature and pressure of the operating conditions translates the calibration curve along the pressure axes (see section 5.6 - Validation of the mathematical model).

5.2.2 Dynamic analysis

In order to determine the fundamental frequency 'ω_o' of the pressure transducer a simple spring-mass and damper system may be analysed and related to the mechanical properties of the transduction element.

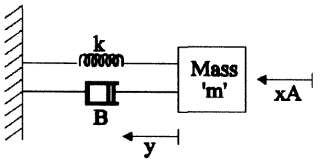

Figure 5-5 The simplified spring-mass and damper system for the optical fibre pressure transducer transduction element

$$m\frac{d^2y}{dx^2} + B\frac{dy}{dx} + ky = Ax \qquad \text{(Eqn 5-2)}$$

which has:

Resonant frequency $$\omega_r = \omega_o\sqrt{1-2\zeta^2}$$ (Eqn 5-3)

Damping ratio $$\zeta = \frac{B}{2}\sqrt{\frac{1}{mk}}$$ (Eqn 5-4)

If the transduction element is a low viscosity fluid, and it is assumed that the fluid meniscus moves perpendicularly to the vessel wall, the spring constant k is dependent on the compressibility of the air in the transducer housing. The approximation becomes less valid when the soybean emulsion is replaced by the gel: the gel adheres to the vessel wall and does not physically shift along the tube. Although it is theoretically possible to estimate these parameters, in practice the only reliable means of determining the fundamental and resonant frequency is to measure them mechanically.

The frequency response of the transducer was analysed using a white noise generator and a mechanical shaker with a frequency response flat to 10kHz coupled to a piston. The system was then driven with white noise and the transfer function calculated using a digital signal processor data acquisition system and a DSP TMS320C25 signal processor at a sampling frequency of 50kHz. The results of the analysis are illustrated in Figure 5-6a and Figure 5-6b.

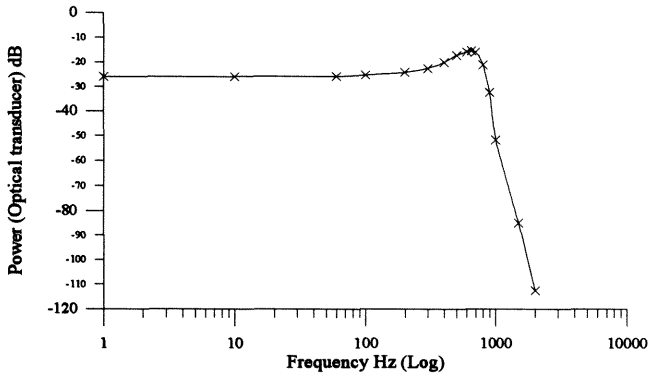

Figure 5-6a The frequency response of an optical fibre pressure transducer with a low-viscosity soybean emulsion transduction element (output fitted with a 1kHz filter).

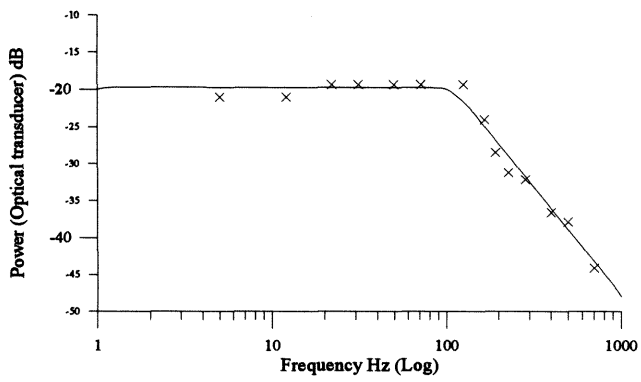

Figure 5-6b The frequency response of an optical fibre pressure transducer with a dusted silicon gel transduction element (output fitted with 100Hz filter to reduce noise and permit low pressures to be measured more accurately).

The results from two transducer designs are shown. Figure 5-6a is the frequency response of a transducer with a soybean oil emulsion transduction element, and illustrates that the design may be used to monitor pressures of at least that frequency as long as the modulating frequency of the light source is at least that to be measured. Figure 5-6b is the frequency response of the transducer used during the clinical trials and illustrates the 20dB roll-off of the first order low-pass filter fitted to the output of the device used to limit the noise to achieve the low-resolution (10Pa) required in the design specification.

5.2.3 Thermal considerations

One of the main features of the optical fibre pressure transducer is that it measures absolute pressure. Its design means that it is susceptible to temperature drift, particularly in the upper airways[1]. The temperature change is dependent on the temperature of the ambient air, efficiency of the airway to warm and humidify the air, and whether the subject is breathing orally or through his nose. Several studies have been performed by researchers to determine the temperature change, including the

[1] The pressure reading recorded by the pressure transducer is measured with respect to the temperature and pressure of the atmosphere at the time that the pressure transducer was sealed.

influence temperature change has on the cross-sectional area of the airway itself. The cross-section of the nasal airway changed from 42.3mm^2 to 37.6mm^2 for a temperature change of -25°C to 23°C respectively (Laine *et al.*, 1994). The change in airway cross-section due to air temperature is not significant if the air is ambient i.e. approximately 20°C.

The temperature of the air is dependent on whether the subject is breathing orally or nasally. Assuming the temperature in the airway is the temperature of the airway mucosa (37°C) (Köhl.,1990) and the ambient temperature is 20°C the worst case scenario would be a temperature change of 17°C. In order to quantify the temperature drift of the optical fibre pressure transducer, a series of two experiments were performed on both the single channel device and the seven transducer catheter (below).

5.2.3.1 Steady-state analysis

The instrument was partially submerged in ice-cooled water (4°C) and allowed to stabilise. When the reading was constant the output was zeroed and a heating element used to heat the water to 50°C. To ensure uniform heating the water was stirred at a constant rate by an automatic stirrer. Also suspended in the chamber was a thermocouple (type B). The reading from this was acquired simultaneously with the optical fibre pressure transducer using an automatic logging system and multiplexer connected to a TMS320C25 digital signal processor (Tran., 1994). The thermocouple was then used to relate the data to temperature.

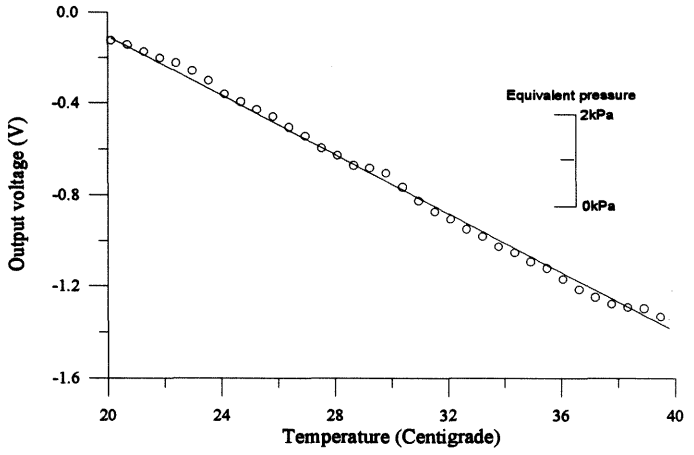

Figure 5-7 The change in output of the single channel pressure transducer with respect to temperature

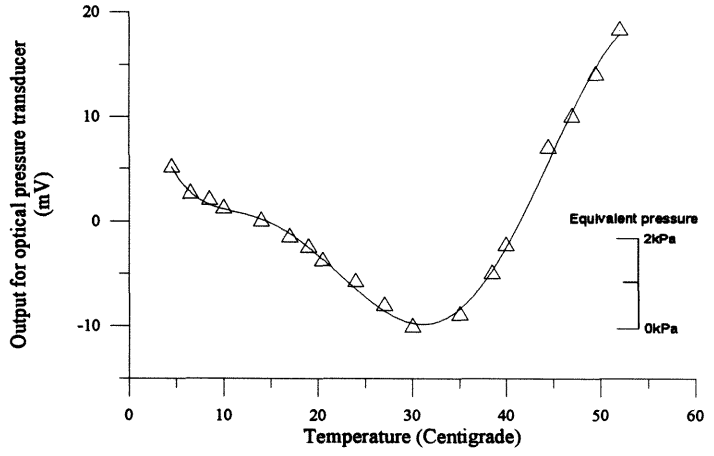

Figure 5-8 The change in output of the bottom-most transducer (#7) of the seven transducer catheter with respect to temperature.

The results obtained in each experiment indicate the different behaviour and nature of the two transducer configurations even though they are, in principle, the same design. Pressure is measured with respect to the gas bubble enclosed in the

transducer housing, and obeys the gases laws: expanding and contracting with increasing and decreasing temperature respectively[2] (Eqn 5-5).

Ideal gas law : $PV=nRT$ (Eqn 5-5)

The titanium dusted gel transduction element is the easiest place to impose volume change due to temperature drift, and hence will also act as a temperature sensor. In order for the transducer to be useful for measuring pressure, temperature drift must be accurately quantified, or the operating conditions must remain constant.

Figure 5-7 shows an approximately linear relationship between temperature and voltage output. This differs from the characteristic illustrated in Figure 5-8. There is a clear peak in characteristic and a plateau region at approximately 35°C. This difference in characteristic may be explained by examination of the construction of the two catheter designs. A *pigtailed* catheter without any external diaphragm enclosing the catheter can be treated as a piston (from here onward referred to as the primary chamber), the transduction element is free to move within the bounds of its elastic limit. In the case on the catheter the *pigtailed* device is enclosed in a further air chamber by the latex jacket of the catheter Figure 5-9 (from here onward referred to as the secondary chamber).

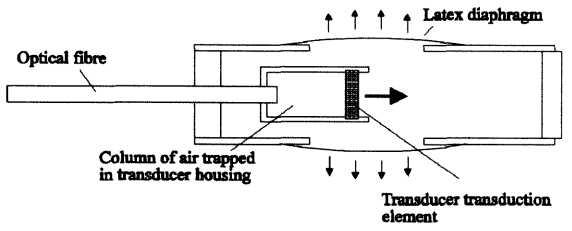

Figure 5-9 A schematic of the thermal expansion of the seven channel optical fibre pressure catheter with the transducer enclosed in a latex jacket.

[2] Air is not an ideal gas and the formula must take into account the specific heat ratio (see chapter 3).

As the transducer heats up the air in both the primary and secondary chambers will expand. Since the wall of the secondary chamber is free to expand, the pressure inside the transducer housing is greater than that in the secondary chamber and gel meniscus moves away from the optical fibres (hence apparent pressure drop). As the temperature rises the latex diaphragm enclosing the catheter tightens increasing the pressure in the secondary chamber and forces the transduction element back into its housing and the meniscus closer towards the optical fibres (hence an apparent pressure rise at higher temperatures).

5.2.3.2 Dynamic considerations

The temperature drift of the transducer is dependent on the frequency of respiration and the temperature change (17°C) in the airway. The significance of the temperature drift is dependent on the time taken for the transducer to respond to the change, i.e. the thermal mass. The time constant of the device was measured by lowering it into water of known temperature and allowing it to stabilise (4°C). The catheter was then removed and the time taken for it to return to ambient room temperature (22°C) measured.

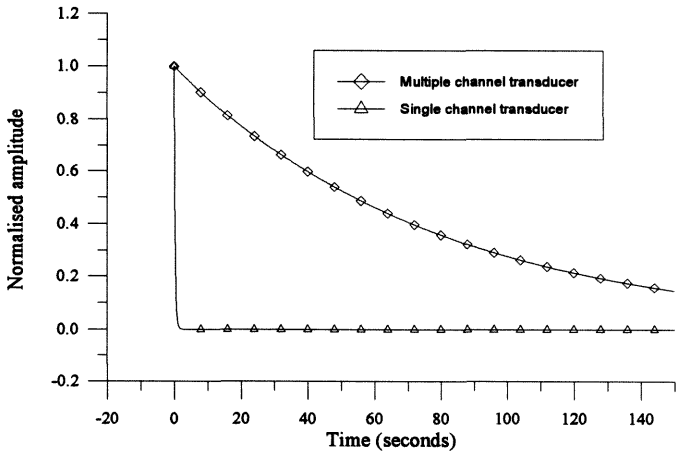

Figure 5-10 The time constant of the optical fibre pressure transducer when used as a single channel device, and integrated into a catheter containing seven devices of a higher thermal mass

Figure 5-10 illustrates the output change with temperature of the single channel pressure transducer and the seven channel equivalent. If the pressure transducer is a first order system (Eqn 5-6) the transfer function is described by (Eqn 5-7):

In the time domain : $y = \frac{A}{T} e^{-\omega_o t}$ (Eqn 5-6)

where $\omega_o = \frac{1}{T}$ and $f = \frac{\omega_o}{2\pi}$

Taking Laplace Transform : $\frac{X(s)}{Y(s)} = \frac{A}{1+sT}$ (Eqn 5-7)

where A = Gain
T = Time constant
ω_o = Angular frequency (radians)

The time constant 'T' for *single channel* device : 0.3 sec

The time constant 'T' for *multiple channel* device : 78.3 sec

Since respiratory signals are usually no less than 0.2Hz ($\omega_{breathe}$ = 1.26rad/s) (see clinical trials: Test CT 6-14) the long time constant makes the temperature dependence less critical. In steady state the apparent pressure change for a temperature change of 20°C to 37°C is 6kPa and 2kPa for the single channel and multiple channel device respectively (Figure 5-7 and Figure 5-8).

The amplitude of the signal at the corner frequency $1/T$ for the transducer is defined by the modulus of the transfer function (Eqn 5-8) (Gain is unity, i.e. A=1):

Modulus of transfer function : $\left|\frac{X(s)}{Y(s)}\right|_{s=j\omega} = \frac{A}{\sqrt{1^2 + \left(\omega/\omega_o\right)^2}} = \frac{1}{\sqrt{2}}$ (Eqn 5-8)

hence:

Temperature drift = $\Delta T \frac{\omega_o}{\omega_{breathe}}$ (Eqn 5-9)

where ΔT = Change in airway temperature
ω_o = Corner frequency
$\omega_{breathe}$ = Frequency of breathing (rad/s)

The time constant associated with each of the two devices hence reduces the effect of temperature drift. A temperature change from 20°C to 37°C produces an error of 15.6kPa and 17.3Pa for the single channel and multiple channel pressure transducers respectively. From these results it is clear that the use of the single channel device must either be temperature compensated, or restricted to areas where the temperature is constant or its thermal mass be artificially increased. In contrast the multiple channel transducer has an extremely long time constant and yields only a very small error (≈1.7mmH2O) even if the temperature change is large. In conclusion temperature effects for the multiple channel transducer maybe neglected for normal use, whilst measurements taken from the single channel transducer are only reliable if the air is reasonably stable due to nasal breathing. The reading will become more reliable as the transducer penetrates further into the airway[3].

5.3 Clinical methods and sterilisation

Systems for use in the upper airway, although capable of being sterilised, need not be clinically sterile. The standard method of sterilisation is auto-claving. The transducer's housing and adhesives are not able to withstand the high temperatures necessary for auto-claving, also the air column trapped behind the transduction element will expand plastically deforming the gel and either impairing operation or destroying it completely. Sterilisation was performed using a 20:1 dilution of sodium hypochlorite (Milton™) in water and a different transducer was used on each patient.

Calibration was performed prior to each test using the equipment illustrated in section 5.2.1.1. The catheter was referenced to zero and pumped to a series of known pressures and calibration curves plotted. In the case of the seven channel device each channel was calibrated against its neighbours to ensure adjacent channels had a similar sensitivity.

[3] All experiments detailed in the successive parts of this chapter involving subjects using the single channel pressure transducer were performed by nasal breathing only.

5.4 Tests on the single channel transducer

5.4.1 Specification and operation conditions

The transducer was 0.94mm OD and, to minimise cost, was not fitted with a pressure transmitting diaphragm, the gel maintaining the seal. A side window (1mm∅) was cut into the side of the device to allow transmission of pressure, and the tip coated with epoxy resin to ensure smooth entry into the airway and oesophagus (Figure 5-11). The open end of the catheter was initially felt to be a cause for concern being a potential site for the accumulation of bacteria , however the cost of the material for a single device (~£15 incl. 3× optical SMA905 connectors. This cost would be considerably reduced if the catheter was manufactured commercially) makes the device disposable eliminating the problem. The single channel pressure transducer was designed for use with the equipment discussed in section 3.5, chapter 3 targeted for use in pre-term babies and neonates.

5.4.2 Clinical trials

The single channel device (Figure 5-11) was constructed and passed into the nasal pharynx and oesophagus. The nasal passage was anaesthetised locally using a Lignocaine spray by a hospital anaesthetist. The subject was seated in an upright posture, and the catheter fed in a series of 50mm steps marked along the length of the transducer housing. The pressure inlet was 10mm from the transduction element, (50mm away from the first marker) (Figure 5-11). When the tip of the transducer was located at the back of the soft palate, it was swallowed with the assistance of water. The subject was then allowed to relax for several minutes before readings commenced. A series of breathing exercises were then performed with the device in various locations in the pharynx and oesophagus. Due to temperature stability emanating from the transducer's low thermal mass, all experiments were conducted with nasal breathing and hence relied on the efficiency of the nose to warm and humidify the air.

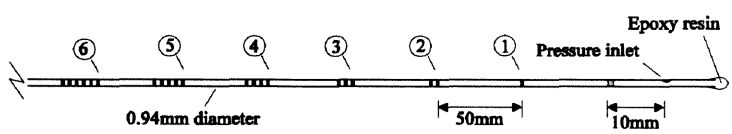

Figure 5-11 The single channel pressure transducer as passed into the oesophagus

5.4.2.1 Test CT1

The first exercise performed was that of normal slow respiration (Figure 5-12). The respiratory signal is periodic at ~ 0.27Hz. The trace has an offset due to the calibration and scaling, however if expiration is assumed to be the base-line, inspiration represents a pressure of 90Pa to 112Pa in this subject. The transducer was located 20mm from the nasal entrance (left-side). It may be concluded that the transducer inlet window is situated slightly below the uvula of the soft palate. The subject was an adult non-obese male, without history of airway disorder.

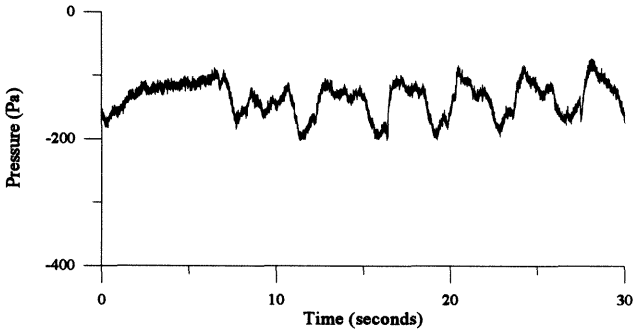

Figure 5-12 Slow respiration
The transducer located with mark '3' at the nasal vestibule

5.4.2.2 Test CT2

The transducer was anchored in the position described in section 5.2.2.1. The right-hand nostril was blocked and the subject instructed to breath normally. The frequency of primary respiration has not changed and remains at ~0.3Hz (cf : Figure 5-12), however the amplitude has changed. The upper airway represents about 50% of the total airway impedance. The apparent halving of the airway orifice increases the pressure in the airway at the lower palatal region significantly in the range 230Pa to 260Pa during inspiration and expiration. In order to overcome the increase in impedance the pressure more than doubled. If the flow in the airway were to be laminar, we would expect the impedance to increase inverse proportionally with

respect to the fourth power of the pipe radius (see conductance of a vessel under laminar flow, section 6.2.1, chapter 6). It is unlikely that the flow will be laminar due to the non-uniform appearance of the airway mucosa. The contribution of impedance by each of the two nasal passages is also unlikely to be equal because of the differing physiological shape of the nasal mucosa.

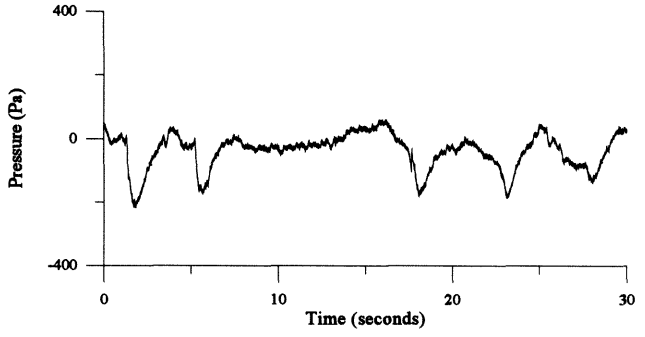

Figure 5-13 Occluded nostril with apnoea
The transducer located with mark '3' at the nasal vestibule

The trace also illustrates a non-obstructive apnoea shown as a 9.6 second pause between inspiration, as opposed to the nominal 2 seconds usually experienced by this patient (Figure 5-13). This was performed by instructing the patient to stop breathing momentarily at the end of expiration. These data shows the limitation of using a single pressure transducer in the evaluation of the upper airway, particularly in OSAS. An obstructive apnoea is characterised by a pressure drop across the occlusion. The pressure information arriving from a single level of the airway only provides an indication of the occurrence of an apnoea and not the occurrence site.

5.4.2.3 Test CT3

The most common symptom of OSAS is loud snoring: representing a partial collapse of the airway through vibration of the soft palate. Snoring was simulated by the conscious patient by forced palatal vibration. Figure 5-14 shows two traces as part of the same diagram. The fundamental frequency of respiration is 0.25Hz (averaged over 4 cycles). The amplitude of the signal is also quite high 312Pa to 380Pa. This is

due to the deep breaths required to execute the snoring manoeuvre. Closer examination of the inspiratory wave shows the snoring or vibration of the soft palate as a high frequency component (see inset). The palatal vibration frequency was found to be 14Hz. Closer examination of the amplitude of the waveform implies evidence of flow limitation. Initially the pressure falls by 220Pa. The partial obstruction causes the pressure to rise by 130Pa at which point palatal vibration begins. This then fades before expiration. From this data it is reasonable to assume that the transducer is slightly above the point where the uvula rests against the back of the tongue. The significance of this to OSAS is discussed further in section 5.5.2.6 (Test CT11), in comparison with the multiple transducer catheter.

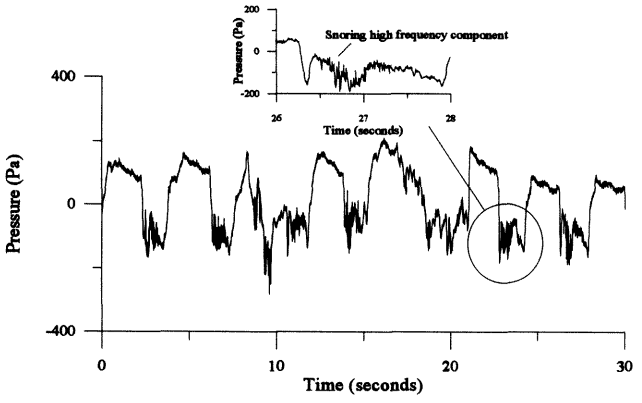

Figure 5-14 Simulated snoring by palatal vibration
The transducer located with mark '5' at the nasal vestibule

5.4.2.4 Test CT4

Although data from the gastro intestinal tract does not yield any diagnostic information about OSAS, the single channel pressure transducer was passed into the oesophagus as the bottom-most transducer of the seven channel device will be anchored mid-oesophagus (Figure 5-15). The presence of respiratory waves is almost completely lost amongst the cardiac artefact which is the most predominant feature. For the first 5 seconds of the recording the peak-to-peak pressure is 370Pa. The lack of muscle tone in the oesophagus means that the oesophageal wall is prone to rhythmic movement due to the heart beating: the transducer is located directly behind the heart.

The transducer has a low mass (0.5g for a 1m device not including the optical connectors). The transducer transduction element, being designed to detect 10Pa is very susceptible to movement and consequently will move when the transducer housing is agitated, recording both pressure and vibration. The frequency of the cardiac cycle, taken from the data, was measured to be 1.4Hz (averaged over the first 5 cycles).

The second main feature of these data is the appearance of a peristaltic wave after 13 seconds in which the pressure increases to 900Pa, peaking at 15 seconds and for a duration 4.9 seconds. The wave is in two halves as first a positive-going and then a negative going cycle. As the oesophagus constricts the pressure increases as the peristaltic wave approaches the transducer inlet, having passed over the transducer inlet a negative gauge pressure is produced momentarily before the pressure returns to its nominal value.

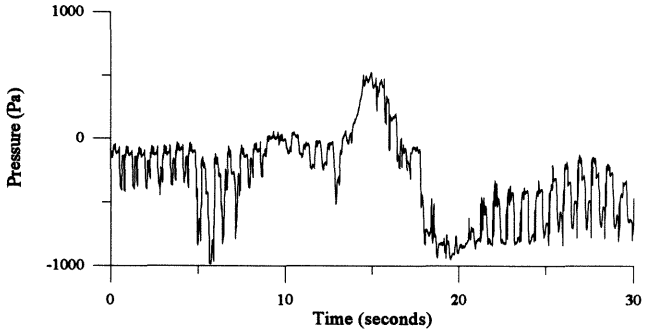

Figure 5-15 Cardiac oscillation and peristalsis
The transducer located with mark '5' at the nasal vestibule

5.4.2.5 Test CT5

The final manoeuvre involved the insertion of the catheter 100mm beyond the sixth mark on the catheter. This would imply that the tip has penetrated the oesophageal sphincter and entered the stomach. Assuming the sphincter forms a reasonably tight seal around the transducer during inspiration the ensuing abdominal movement will compress the stomach and raise the interior pressure. Similarly expiration reduces the pressure. The result is the waveform observed in Figure 5-16.

The waveform is similar to that in Figure 5-12, having a fundamental frequency of 0.2Hz (averaged over the last three cycles). The waveform inversion is apparent (cf: Figure 5-12 and Figure 5-13). The cardiac artefact has fallen to ~10% of full-scale and is no-longer the predominant feature.

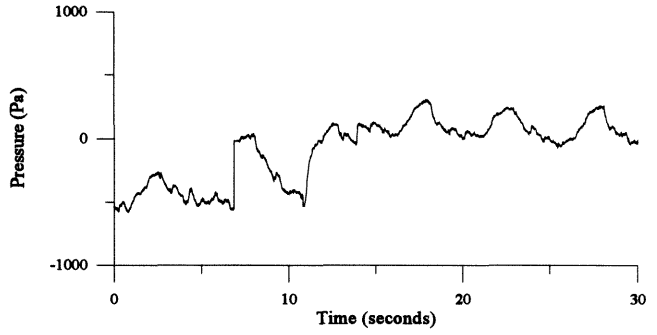

Figure 5-16 Sub-sphinctal (stomach) pressure inversion.
The transducer located with mark '6' 100mm beyond the nasal vestibule

5.4.2.6 Discussion

The single transducer was found to be extremely useful for determining expected respiratory and gastro intestinal data. The signals obtained cannot be considered quantitative in the higher portions of the airway, i.e. in the nasal pharynx the temperature drift will be significant as the air would not have reached a stable temperature at this point.(see section 5.2.3): the ambient room temperature was 24°C at the time of the experiment. Thermal effects become more significant if ambient conditions were cooler as the temperature gradient will penetrate further into the airway.

The single transducer study is also useful in further motivating the development of the multiple transducer catheter. Although the single channel device did provide information regarding the presence of flow limitation during snoring, location information providing a profile of the pressure along the subject area is not available. It is important to anchor the transducer in position to ensure the pressure information is not lost in noise due to vibration.

The resolution of the device is defined by the size of the pressure inlet: 1mm in diameter. A pressure balloon of 30mm or more is usually inflated around the inlet to the transducer to achieve sensitivity during airway manometry, and hence the physiological resolution is limited to 30mm (Beardsmore *et al.*, 1982). The increased resolution due to miniaturisation means the transducer position is critical (resolution of 1mm possible). The location of transducers in the seven transducer device was assisted by the use of a radio-opaque marker (see chapter 3) whereby the resolution was limited to 10mm (the length of each of the pressure balloons confining each of the pressure transducers in the catheter).

5.5 Tests on the multiple channel transducer catheter

5.5.1 A simulated airway

5.5.1.1 Method

Prior to the introduction of the multiple channel optical fibre catheter into the upper airway of a living subject, a series of simulations were performed with different upper airway models. The purpose of these experiments was to ensure that the instrument did not suffer from cross-talk between adjacent transducers, and to confirm that the catheter was indeed able to diagnose airway narrowing by pressure measurement. The models were as follows:

- An airway of rigid construction - A 15mm ID tube with a 20mm long, 5mm ID constriction.
- A non-rigid latex airway (Figure 5-17) which is susceptible to collapse during inspiration.

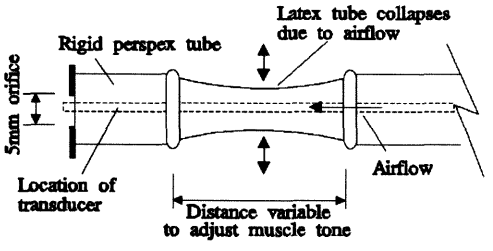

Figure 5-17 An upper airway simulator used for preliminary testing of the multiple transducer catheter.

Figure 5-17 is a schematic of the latex upper airway model. The upper airway is known to become atonic during obstructive sleep apnoea (chapter 2). Given this hypothesis a model airway was constructed using a length of 10mm OD latex tube (0.5mm thick) fixed between two tubes of rigid construction (perspex). Airflow was produced by a 100ml air-filled syringe driven by a motor. "Muscle tone" was adjusted by stretching the latex tube longitudinally. The early experiments replaced the latex diaphragm with a narrow gauge (4mm) rigid tube.

5.5.1.2 Test SA1

During the first experiment (Figure 5-19) airflow was provided by a volunteer breathing normally through a rigid model airway, whilst the catheter was simultaneously withdrawn over the constriction. The catheter was coated with a water soluble jelly to allow the catheter to move freely inside the constriction. The tight fit of the catheter almost completely prevented the air from flowing though the tube. Figure 5-19 shows a series of epochs (labelled '1' to '5') with the catheter in different locations along the airway, and hence different transducers lying across the constriction. By examination of each of the sets of data it is clear that the presence of the catheter was almost completely blocking the flow of air through the constriction.

- Epoch '1' is located with collar separating transducer #1 and #2 across the constriction. Pressure was measured to fall by 88% (788Pa to 97Pa).
- Epoch '2' and '3' show the constriction is located at transducers #3 and #4 respectively. The quantisation error of the data acquisition system means that flow is almost undetectable on the uppermost transducers.
- Epoch '4' clearly illustrates the presence of the constriction by a peak in pressure. The catheter has not occluded the vessel and a local rise in pressure due to a constriction to maintain volumetric flow rate is observed. The constriction is located at transducer #5.

Transducer number against recorded pressure						
#1	#2	#3	#4	#5	#6	#7
OOR≈ 0Pa	OOR ≈0Pa	48Pa	90Pa	1.40kPa	958Pa	461Pa

OOR = Out Of Range due to quantisation error

Figure 5-18 A table of the peak amplitude change observed on epoch '4' (Test SA1)

- Epoch '5' was recorded with a double constriction, the first located between transducers #6 and #7 (50mm below #6), whilst the second was at the entrance to the tube at transducer #1. Both constrictions are apparent by observation of the waveforms, however the amplitude of the pressures recorded is lower when given an identical stimulus to the previous recordings. Transducer #7 is located at 200mm from #6. The catheter is 1mm narrower at this point and consequently air flow is not as severely restricted as when the transducer array is across the constriction: the pressure change in the bottom-most portion of the airway is larger as a result.

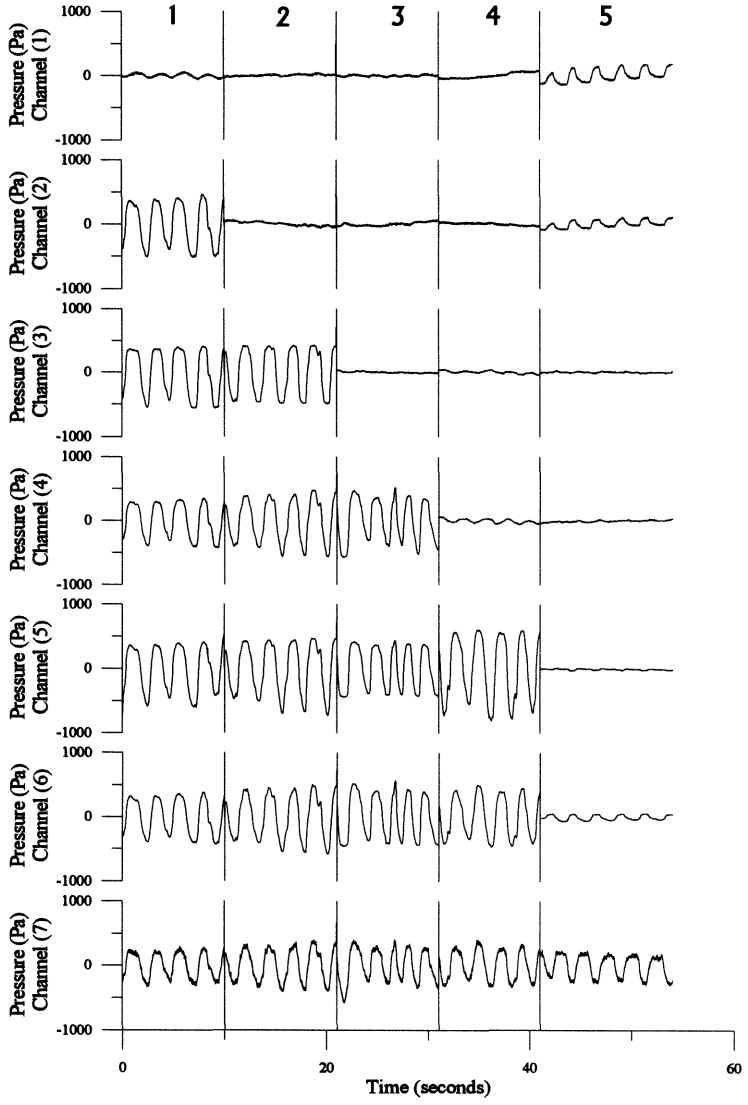

Figure 5-19 A series of five epochs recorded on seven transducers using a simulated upper airway of rigid construction whilst simultaneously withdrawing the catheter over a constriction (Test SA1).

5.5.1.3 Test SA2

A second simulation using the apparatus in Figure 5-17 was performed using a collapsible tube. Airflow was provided by a 100ml syringe driven by a motor to promote collapse of a latex diaphragm representing the upper airway. The peak amplitudes to the recorded pressure in each of the transducers are summarised in the table below (Figure 5-20).

Transducer number against recorded pressure						
#1	#2	#3	#4	#5	#6	#7
82Pa	85Pa	550Pa	3.06kPa	588kPa	353Pa	294Pa

Figure 5-20 A summary of pressure amplitude on seven transducers using a catheter in a simulated latex airway (#7 bottom-most device).

The effect of airway collapse was greatly exaggerated by the model due to the motor being able to supply sufficient torque to force the latex diaphragm to collapse in onto the side of the catheter and then be withdrawn into the airway prior to expiration (Figure 5-21). Consequently the pressure increase at the site of the collapse is greater than would be expected in a real airway.

The results also shown a phase shift between adjacent pressure signals : transducer #1 lags #7 by 160°. This is due to the pressure being introduced at the base of the apparatus, and the low group velocity[4] of the pressure wave.

Distance from transducer #1 to #7 = 300mm

Phase delay = 160°

= 0.53seconds

$\therefore$ Group velocity of air = 566mm/s

[4] The group velocity is defined as the rate of propagation of the atoms in the pressure wave.

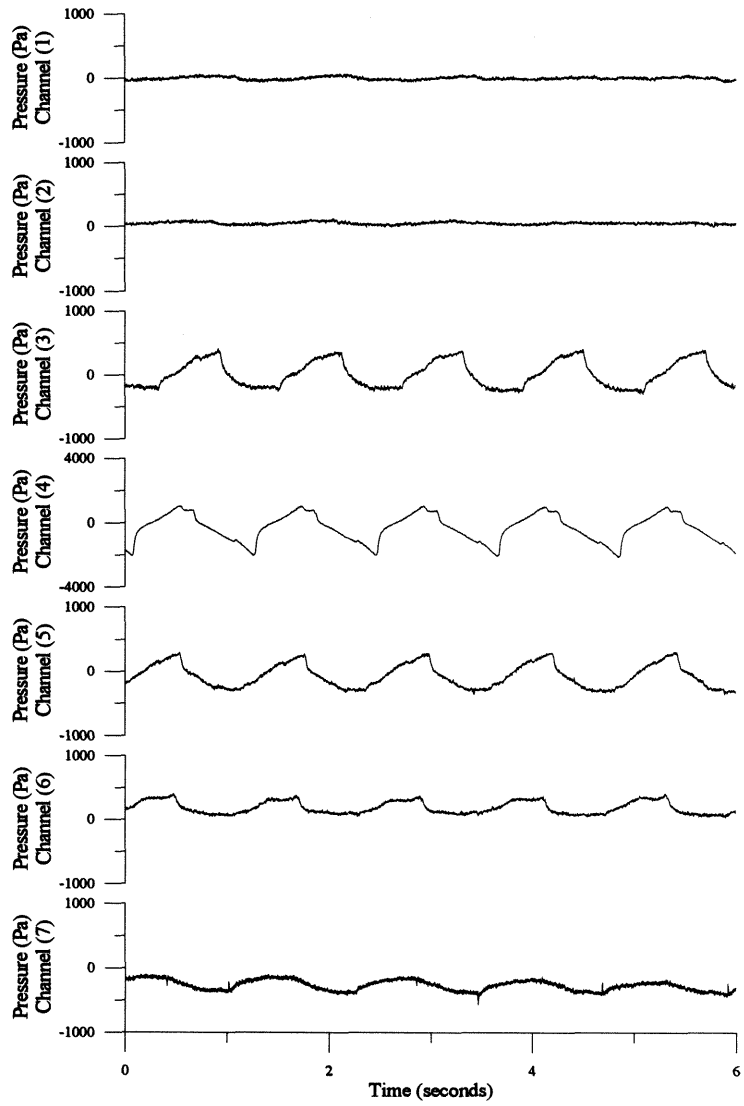

Figure 5-21 Data recorded using a latex model of the upper airway to simulate collapse as occurs in obstructive sleep apnoea syndrome (Test SA2).

5.5.2 Clinical trials

To evaluate the technique fully for clinical use a detailed study should be performed on a large group of patients both with and without airway abnormalities, upon which an unbiased statistical analysis may be performed. A small group of patients was examined with an age range of 40 to 65 years and of mixed sex with the assistance of a consultant anaesthetist. This preliminary study was performed to investigate whether the device warranted such an in-depth, time-consuming investigation.

Patients were investigated under both local and general anaesthesia. The purpose was to provide an accurate reconstruction of the atonic effect of the muscles which occurs during sleep to promote the airway disorder as it occurs naturally. Local anaesthesia was used so to allow the subject to perform a series of respiratory exercises (as in section 5.4). A comparison between consciousness and posture with respect to the airway may then be obtained.

Investigations during general anaesthesia were performed in recovery following a non-sleep related operation. The catheter was inserted 10 minutes prior to the end of the operation to allow it to stabilise, and the location of the transducers behind the soft palate checked by visual inspection. Analysis commenced during a 10 to 15 minute period prior to the patient becoming fully conscious. An X-ray of the catheter in the airway is depicted in Figure 5-22.

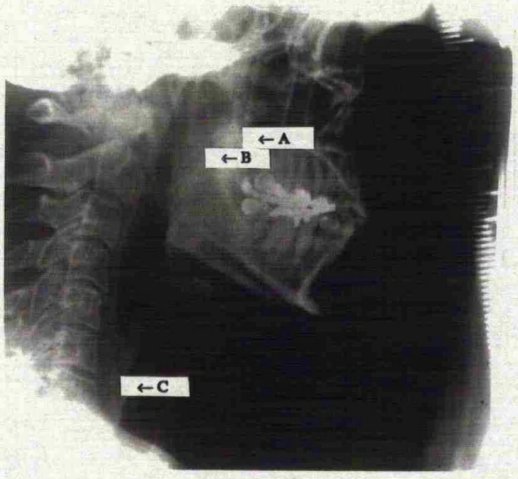

A - The top of the catheter in at the back of the nose

B - Radio-opaque marker below transducer #1

C - Radio-opaque marker at entrance to oesophagus (transducer #6)

Figure 5-22 A lateral x-ray of a subject with the multiple transducer catheter in position: transducer 1 to 6 are illustrated.

Prior to taking the measurement from the airway the catheter was calibrated. Given that the transducer is approximately linear over a limited working range (see section 5.2.1), the catheter was enclosed in a pressure chamber and exposed to a series of sinusoidal varying pressures so as to ensure 1kPa provided a full scale deflection. Calibration data was then collected during a ten second epoch and used to scale the data when the recording was complete. Calibration data and airway data were acquired using the arrangement shown in Figure 5-1 (section 5.2.1.1). The system is capable of simultaneously acquiring data from 16 channels through 16 individually calibrated analogue to digital converters (8 bits): 8 channels patient isolated at 4kV RMS and 8 channels non-isolated (used for pressure transducer). The sample frequency is 100Hz maximum per channel by the serial port of a laptop 386SX PC, and is sufficient for respiration and snoring signals. Once acquired the data was exported as ASCII code into the mathematical modelling package Matlab™ for scaling and then to appropriate graphics software. Data conversion was performed using code written in C.

The nasal passage and soft palate were anaesthetised locally using Lignocaine and the transducer coated with water soluble jelly (KY Jelly™) for analysis of conscious subjects. The catheter was inserted through the nostril and swallowed into place so transducers #1 to #6 were located from the back of the nasal pharynx to the entrance to the oesophagus (Figure 5-22). The patient was then allowed to relax for 5 to 10 minutes to allow the catheter to reach the nominal airway temperature and to allow the oesophagus to become accustomed to the presence of the catheter.

5.5.2.1 Test CT6 - Local anaesthesia

The waveforms illustrated in Figure 5-23 were acquired from a subject breathing normally through the mouth and seated in an upright posture. Normal respiration can be observed on channels #1 to #6, however #1 to #3 are inverted in comparison with channels #4 and #6. This is due to the process of oral breathing, the vast proportion of airflow being over transducers #4 to #6. The frequency of breathing is 0.18Hz. The amplitude for the transducers peak at the level of the soft palate (#4) at 1040Pa. Transducers below the uvula fall in amplitude steadily: #5 at 700Pa, #6 at 520Pa, as do

the transducers above it: #3 at 870Pa, #2 at 430Pa #1 at 170Pa. This peak in amplitude along the length of the six transducer array is characteristic of oral breathing.

Transducer #7 is located mid-oesophagus and shows evidence of cardiac artefact. The ADC of the data acquisition system is clipping because amplitude of the pressure signal has gone too high. The large apparent change in pressure (2500Pa) is due to the deformation of the oesophageal wall as the heart beats and is also due to respiration. The fundamental frequency of the change in pressure due to the heart was measured at 1.2Hz, comparable with the ECG (Figure 5-23). The signal inverts. This implies that the entrance to the oesophagus is partially occluded. As the abdomen expands during inspiration the oesophagus is compressed; the pressure inside increases due to the blockage at the entrance.

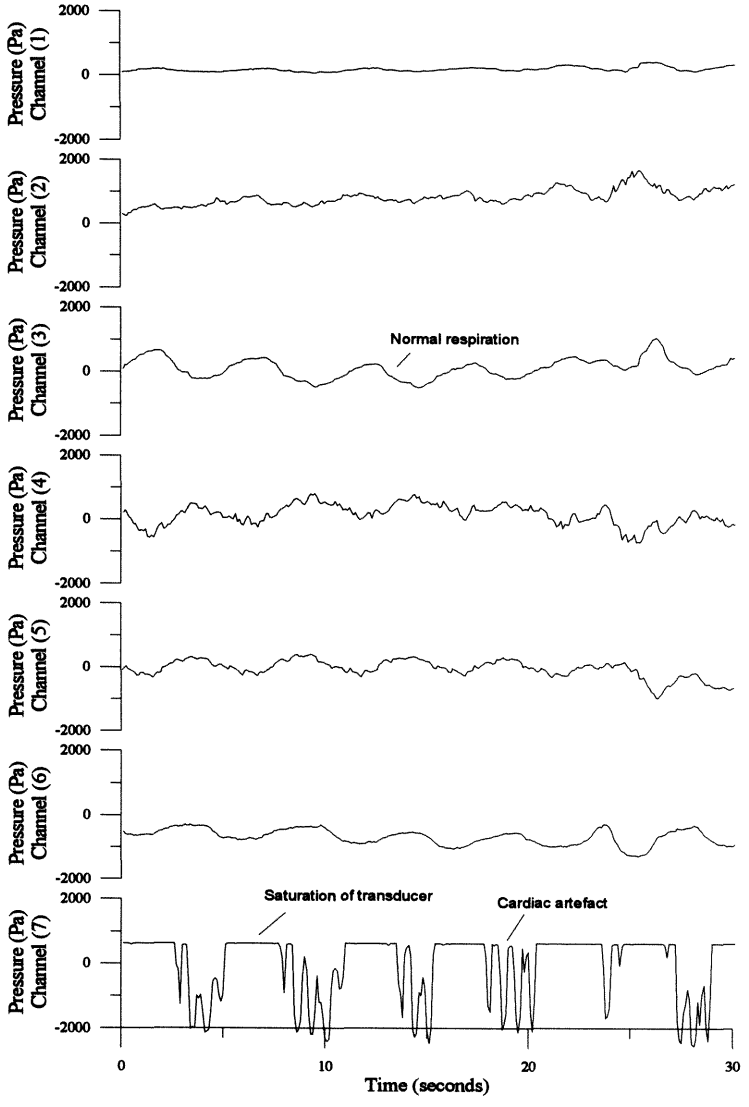

Figure 5-23 A pressure profile of the upper airway of a patient breathing normally illustrating the respiratory and cardiac cycles.

5.5.2.2 Test CT7 - Local anaesthesia

Figure 5-24 illustrates the change in respiratory pressure when simulating snoring by forced vibration of the soft palate, whilst being seated in an upright posture. In order to promote vibration of the soft palate, the vast proportion of air is inhaled through the oral airway, this is characteristically illustrated by the opposing polarity of channels #3 and #4. In the oropharynx the pressure during inspiration and expiration increases to 710Pa, but returns to 170Pa when normal relaxed breathing resumes after 27 seconds. The site of the collapse is illustrated by transducer #4. During inspiration a high frequency palatal vibration is observed (snoring). When the palate strikes the surface of the transducer the pressure inside that particular element rises and is shown as a positive spike (170Pa) immediately after or at the end of the inspiratory part of the cycle on channel #4 (cf: general anaesthesia, test CT9). This is due to the initial negative gauge pressure allowing the tissues to collapse around the device. Consequently, although the pressure is seen to fall initially, the interior pressure of the transducer increases and is reflected in the data.

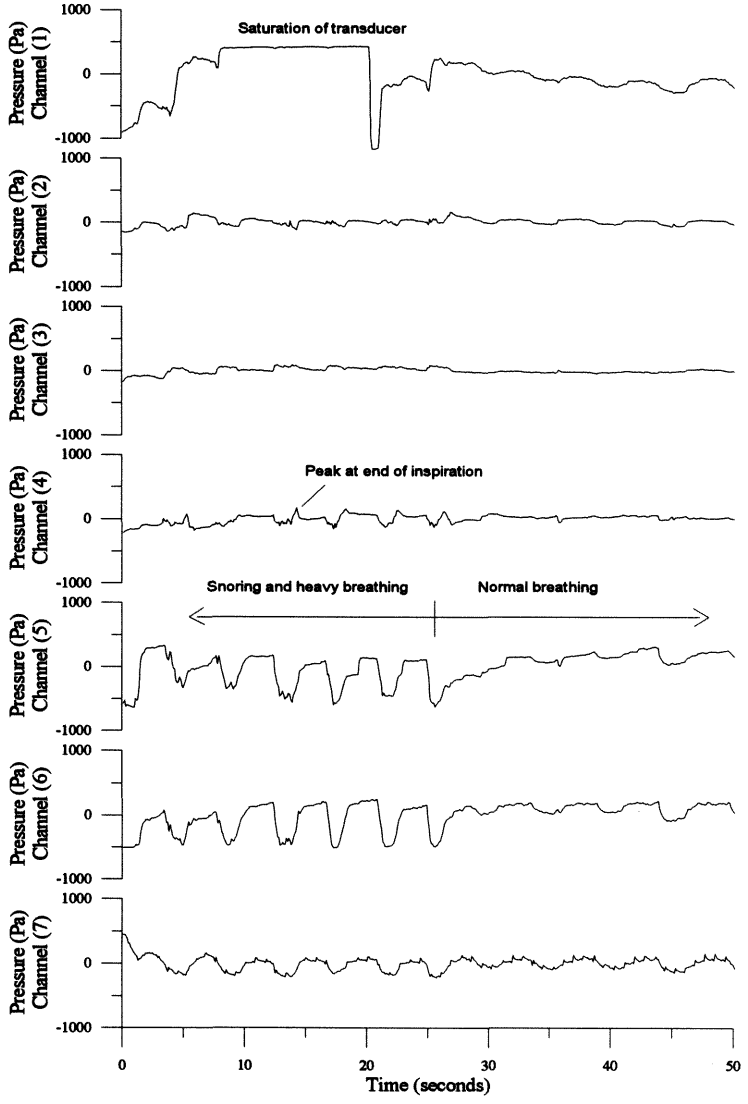

Figure 5-24 Changing amplitude of the respiratory wave during the onset of heavy breathing.

5.5.2.3 Test CT8 - Local anaesthesia

The patient data shown in Figure 5-25 was taken during the same session as Figure 5-24, the transducer was pulled further into the oesophagus by peristalsis. The feature of interest in Figure 5-25 is the phase shift shown between the peaks on transducers #6 and #7 between 55 and 65 seconds. The subject is breathing through the nose normally. This is then interrupted by two swallows causing peristaltic waves to travel down the oesophagus. If all seven transducers were to be located in the oesophagus there would be a phase shift steadily increasing between adjacent transducers. The first action of swallowing is the closure of the soft palate against the back of the throat, i.e. the location of the transducers #1 to #6. The transduction element was designed to detect 10Pa, and so will be susceptible to slight vibration: as the uvula strikes the top of the transducers #1 to #6 register vibration. Transducer #7 is far enough away (200mm) not to register this movement, but does detect the peristaltic wave as it passes. Assuming the wave starts at transducer #6 and passes #7, the speed of the wave is 35.7mm/s (covering 200mm in 5.6 seconds).

Observation of the respiratory waveform of transducers #1 to #6 provides a profile of the airway. A constriction of the airway will require an increased flow rate, and hence pressure will rise. By observation of the data it is apparent that the array of transducers are located between the nasal pharynx and oesophageal entrance. The posterior to the nasal pharynx is narrow in diameter (≈15mm), this is detected by a mean amplitude of 190Pa, falling to 130Pa and 50Pa in transducers #2 and #3 respectively. Unlike test CT6, the transducer is not obstructing the oesophagus, and all waveforms are consequently of the same polarity. Further evidence of the location of the catheter in the airway is the broad peak of the peristaltic wave on transducer #6 (cf: transducer #7). This is not caused by the shock of the uvula striking the catheter, but the wave itself.

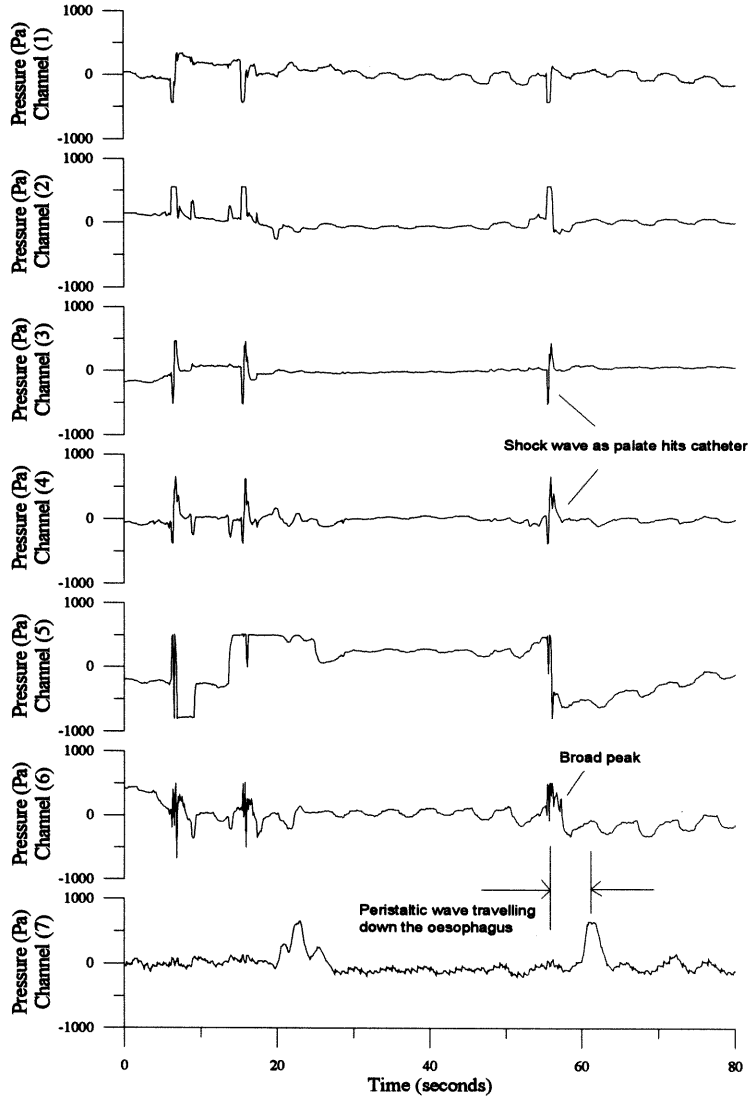

Figure 5-25 The peristaltic wave in the oesophagus.

5.5.2.4 Test CT9 - Local anaesthesia

Results of test CT9 are shown on three graphs. The same subject was used in all cases, but posture and the breathing pattern were varied. Figure 5-29a shows a normal relaxed nasal breathing pattern: transducers #1 to #5 describe the flow of air through the pharynx. The pressure of the higher transducer is lower than that of the bottom (#5). Transducer #2 has a peak-to-peak pressure of 94Pa, which increases successively: #3 at 125Pa, #4 at 110Pa, #5 at 210Pa. Transducer #6 is recording a low amplitude, this may be due to its location in the entrance to the oesophagus. Transducer #7 is saturating. If Figure 5-29a and Figure 5-29b are compared it is possible to observe the effect of posture on airway cross-section. The head of the subject was tipped back and breathing exercised in a similar manner to that in Figure 5-29a. There is little change on transducers #1 and #2, 109Pa to 120Pa and 94Pa respectively. The increase in amplitude as a consequence of orifice constriction is apparent on transducer #3 to #6 inclusive (Figure 5-26).

Transducer	Upright posture (Pa)	Head back (Pa)	Change ΔP (Pa)	Change (%)
#1	117	109	-8	6.8
#2	94	94	0	0
#3	125	194	69	55
#4	109	140	31	29
#5	210	220	10	5

Figure 5-26 Changing pressure observed in the pharynx caused by the adjustment of patient posture.

The table shown in Figure 5-26 illustrates a percentage increase in pressure at maximum at transducer #3, this steadily falls further along the length of the catheter. It may be concluded from these results that the tip of the soft palate (uvula) has closed the orifice at the back of the throat slightly due to gravity. In order to maintain the flow rate the pressure increases.

The head of the subject was tipped back and snoring simulated by forced vibration of the soft palate. In order to exercise this manoeuvre breathing was deeper. The is shown as an increase in respiration amplitude of 198% on transducer #2 falling

to 22% on transducer #5. The percentage increase in amplitude is not linearly related to the change in diameter of the airway, and will be dependent on whether the air flow is turbulent or laminar (chapter 6).

Transducer	Upright posture (Pa)	Snoring (Pa)	Change ΔP (Pa)	Change (%)
#1	117	170	53	45
#2	94	280	186	198
#3	125	250	125	100
#4	109	140	31	28
#5	210	256	46	22

Figure 5-27 Changing pressure during snoring with respect to normal, relaxed, breathing.

By close examination of transducers #2 to #4 it is possible to observe the high frequency component characteristic to snoring (palatal vibration) and was measured to be at 17.3Hz[5]. Examination of the waveform does not show any evidence flow restriction, purely pressure transients due the movement of the palate. This frequency corresponds to the 14Hz measured during snoring when using the single channel device (Test CT3). Snoring was observed on transducers #2 to #5. The occurrence of apnoea, airway obstruction and snoring is discussed fully in section 5.7.

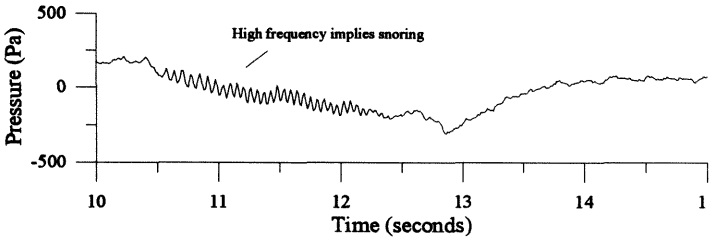

Figure 5-28 High resolution plot of transducer #3, inspiratory cycle 2 (see Figure 5-29c).

[5] The high frequency component is not apparent on Figure 5-29c, this is due to the graph plotting process.

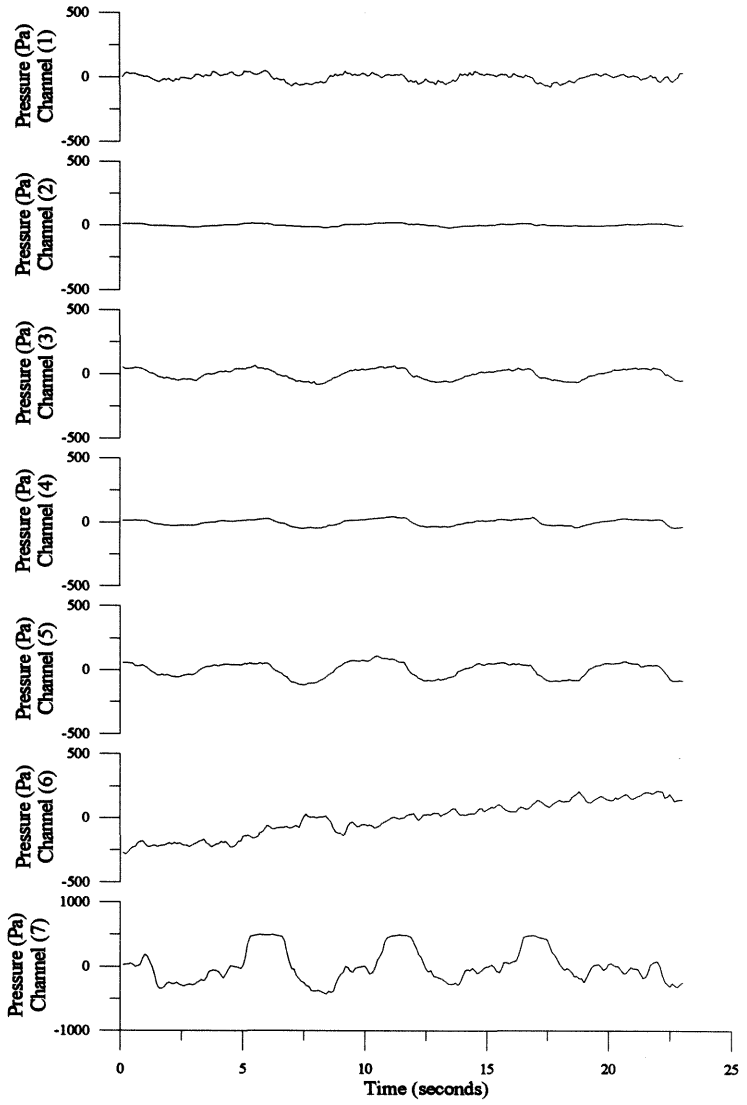

Figure 5-29a The pressure profile of a patient seated in an upright posture and breathing normally.

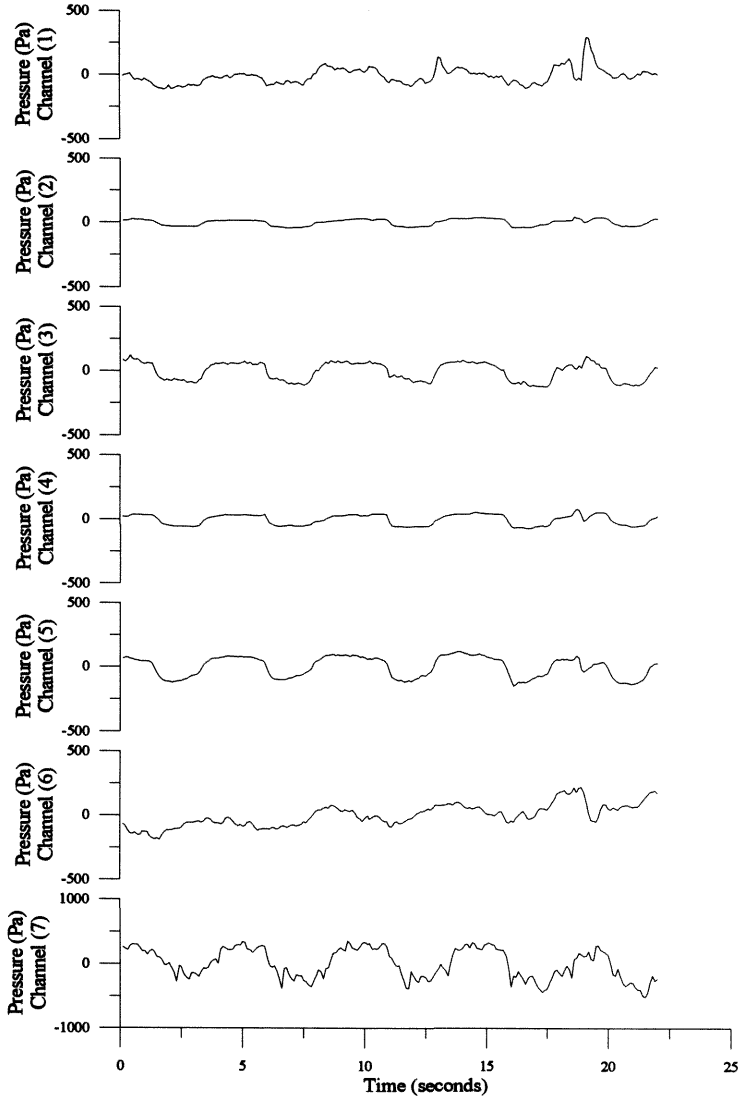

Figure 5-29b The pressure profile of the pharynx with the subject's head tipped back to emulate a supine position.

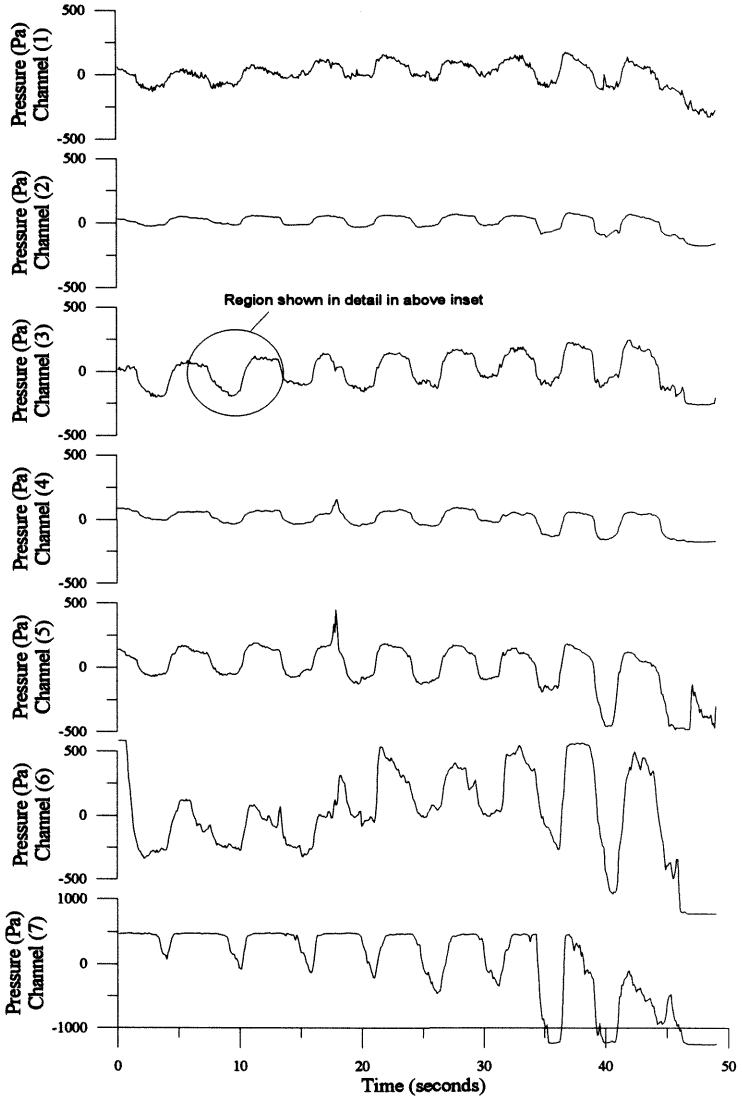

Figure 5-29c The pressure profile of the pharynx illustrating a mean increase in pressure due to the increased effort required to force the soft palate to vibrate (See Figure 5-28 for inset).

5.5.2.5 Test CT10 - General anaesthesia

Patient Profile:

Age	:	50-55
Sex	:	Female
Build	:	Slim

Figure 5-30 illustrates the pressure profile of a patient with a normal airway. Breathing was slow and periodic and primarily through the oral airway. Each of the six upper pressure transducers register extremely low pressures and are approaching the limit of the data acquisition system: this is apparent due to the quantisation error (particularly prominent on transducers #4 to #6). The breathing pattern is almost completely invisible on transducer #3, however above and below shown clear signs of respiration. Transducer #3 is at the back of the mouth and hence in part of the airway with large cross-section. This *dead-spot* is characteristic of the airflow in the pharynx and may be used to determine the location of the transducer in the throat without taking an X-ray. The outputs of the transducers above the *dead-spot* (transducer #3 <10Pa) are of approximately the same amplitude: 17Pa. The pressures below this point successively increase: 38Pa at #4, 55Pa at #5 and 108Pa at #6.

The data also shows the unusual breathing pattern of the patient, transducers #5 and #6 show that whilst the first breath is large the second appears to be a lot shallower.

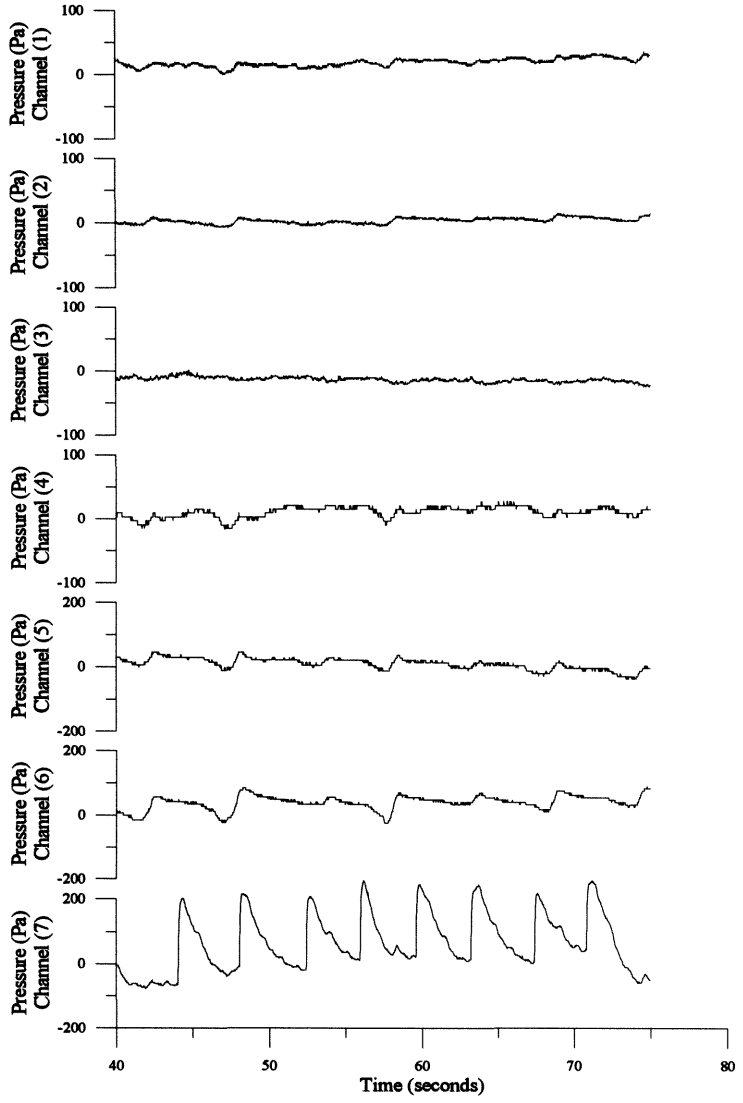

Figure 5-30 The pressure profile of a patient under general anaesthesia breathing through a normal upper airway (Test CT9).

5.5.2.6 Test CT11 - General anaesthesia

Patient Profile: **Age** : **65-70**
Sex : **Male**
Build : **Slim**

The second set of results presented with general anaesthesia illustrate a non-obstructing patient and is the result of the sixth patient investigated in the group of six. The *dead-spot* is clearly visible on transducers #3 and #4. The polarity of the traces changes throughout the airway. Inspiration gives rise to a negative pressure on transducers #3, #4 and #5, whilst there is a positive going pressure on transducers #1, #2, #6 and #7. The posture of the patient lying in a supine position has allowed the entrance to the oesophagus to close around the transducer. The expansion of the chest compresses the oesophageal wall increasing the pressure inside. Transducer #7 shows evidence of the cardiac cycle as a high frequency (1.8Hz) signal superimposed over the respiratory signal at 0.2Hz[6]. The non-uniform compression of the oesophagus also leads to a phase shift between these signals on transducers #6 and #7 of 78°.

The change in polarity of transducers #1 and #2 is surprising, but was also observed test CT1 under local anaesthesia. This may only be explained as the prognosis of a high nasal impedance worsened by the presence of the catheter obstructing airflow in one nostril. When air enters the oral airway it flows both into the pharynx, and also into the nasal pharynx. The air trapped at the back of the nose and sinuses will increase in pressure.

[6] The frequency of respiration has slowed down in all patients under general anaesthesia and is characteristic of natural sleep.

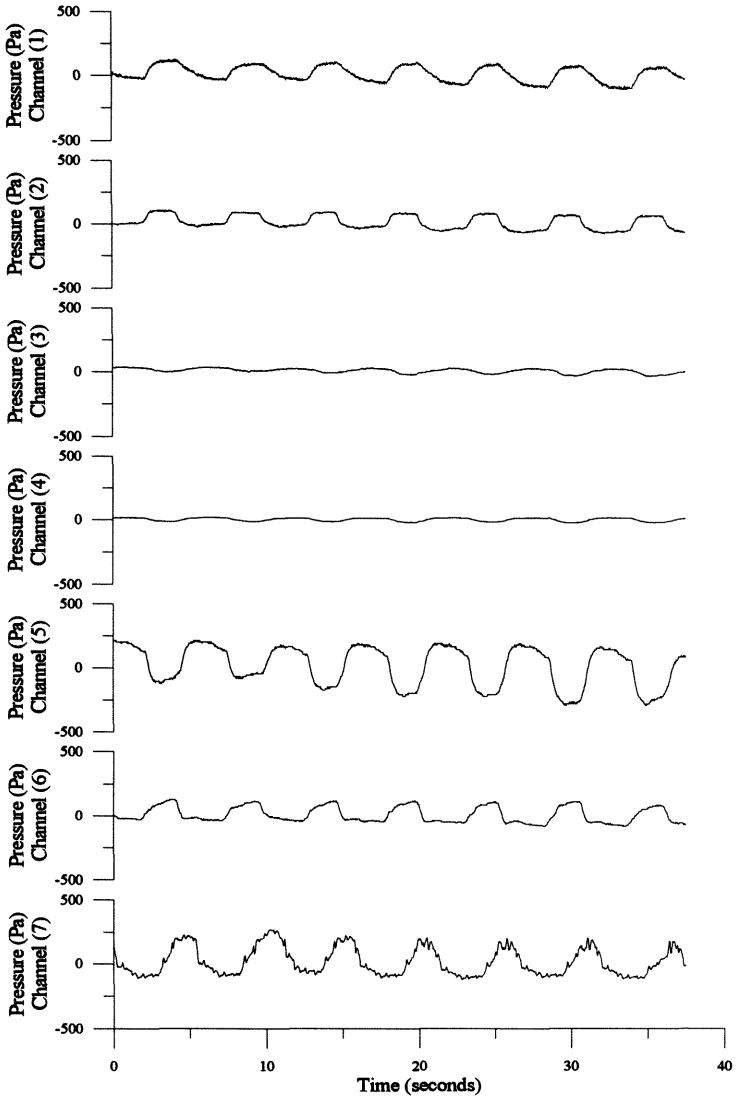

Figure 5-31 The pressure profile of a patient under general anaesthesia breathing heavily through the oral airway (Test CT10).

5.5.2.7 Test CT12 - General anaesthesia

Patient Profile:

Age	:	**55-60**
Sex	:	**Male**
Build	:	**Heavy**

The third patient to be examined under general anaesthesia arrived in the recovery area with audible snoring and possible obstruction. Being of heavy build this patient is a candidate for OSAS.

All traces recorded pressures higher than that illustrated in test CT10 (above). This is due to the heavier breathing. Transducer #1 and #2 are located in the back of the nose and display pressures of similar amplitude: 78Pa and 88Pa respectively. Transducer #3 (illustrated in Figure 5-32) is the site of airway partial obstruction and shows evidence of flow limitation due to palatal vibration. Snoring occurs during inspiration. Initially the flow is maximum and pressure falls by 340Pa: a higher frequency component of 21.2Hz is detectable. As the palate begins to obstruct the flow the pressure rises by 47Pa and stays constant for 0.5 seconds (inspiration occurs for 1.8 seconds).

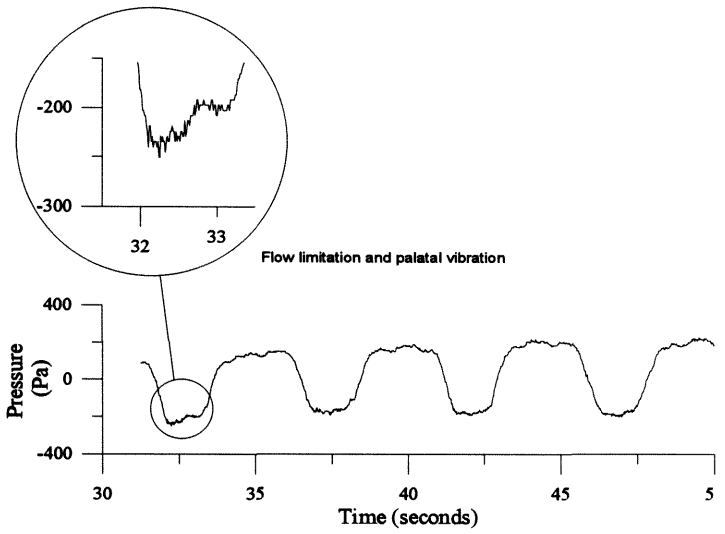

Figure 5-32 Vibration of the soft palate during snoring in a patient under general anaesthesia.

The pressure below the palate rises from 72 Pa to 110Pa on transducers #4 and #5 respectively and is characteristic of the upper airway. The final transducer in the array comprises a null followed by a peak. The negative part of the cycle corresponds to the onset of inspiration, whilst the positive to expiration. Transducer #6 is in the entrance to the oesophagus, the relaxed oesophageal wall resting against the diaphragm of the transducer. During inspiration and expiration the catheter is either compressed further or released momentarily causing the aforementioned waveform. Transducer #7 shows cardiac artefact superimposed on a respiratory wave.

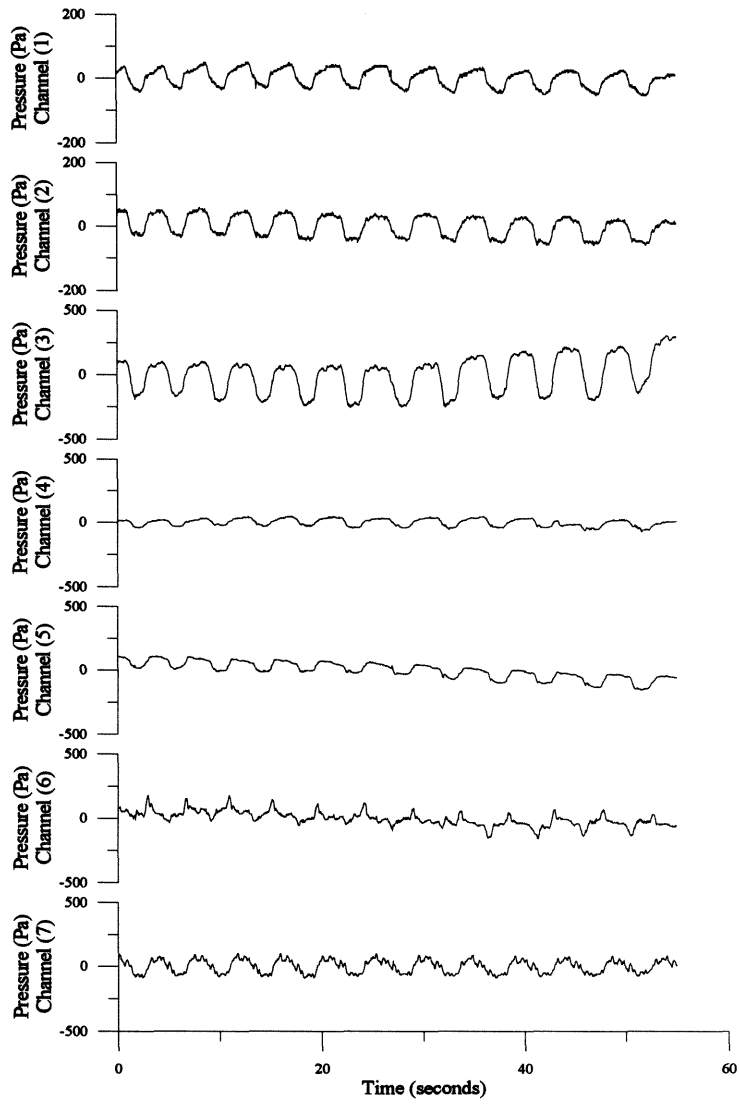

Figure 5-33 The pressure profile of a patient under general anaesthesia with an obstructing airway and snoring (Test CT11).

5.5.2.8 Test CT13 - General anaesthesia

Patient Profile: Age : 70
Sex : Female
Build : Medium

The patient in this study arrived in the recovery area snoring heavily. Evidence of palatal vibration is clear on transducers #3 and #4. Transducer #1, located in the nasal pharynx, does not show evidence of snoring, but can be used to analyse the effect of tidal volume on the vibration of the palate Comparison of breaths '1' and '2' (see Figure 5-35) show two different tidal volumes as different pressures on transducer #1 (the subject is predominantly nasal breathing). Breath '2' has a peak-to-peak amplitude of 96Pa on transducer #1, and examination of the transducers successively lower down the airway show no evidence of palatal vibration. In comparison breath '2' has an amplitude of 183Pa on transducer '1'. The increased pressure is also apparent on transducer #5.

Pressure increases during both breaths through transducers #1 to #4, however during cycle '1', flow is so severely restricted that the plateau region of the flow profile (plotted against time) is clearly visible on transducer #4.

Transducer →	Pressure (Pa) #1	Pressure (Pa) #2	Pressure (Pa) #3	Pressure (Pa) #4
Breath (1)	183	122	52	97
Breath (2)	96	139	261	148

Figure 5-34 A comparison of breaths taken from the same patient illustrating the effect of tidal volume on palatal vibration and occlusion.

The airway of this patient is narrowed behind the soft palate, but is wide at the rear of the nose and below the uvula. A small pressure change lower in airway, i.e. transducer #5 (56Pa), is not sufficient to promote collapse, however if this pressure is increased to approximately 100Pa a collapse will occur in this patient in a supine posture. The oesophageal transducer shows the cardiac cycle superimposed in the respiratory waveform. The waveform is of the same polarity of the proceeding transducers implying that the entrance to the oesophagus is not blocked by the catheter.

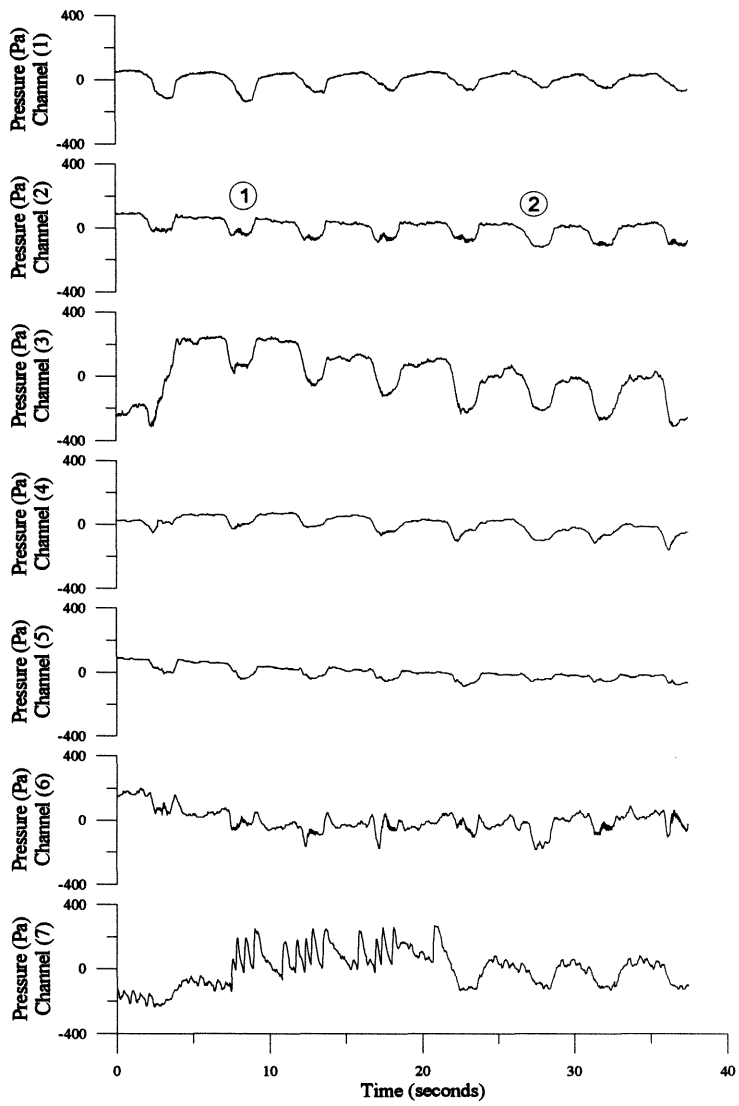

Figure 5-35 The pressure profile of a patient under general anaesthesia with an obstructing airway and snoring (Test CT12).

5.5.2.9 Test CT14 - General anaesthesia

Patient Profile:

Age	:	**57**
Sex	:	**Male**
Build	:	**Medium**

The pressure profile illustrated in Figure 5-36 was taken from a patient suffering from airway obstruction on arrival in the recovery area. Transducer #1 is located in the back of the nose, and shows a low pressure due to the obstruction at the site of transducer #2 which is saturating due to the palate compressing the diaphragm of that particular transducer. This evidence means that the transducer has been either placed further down the airway initially, or peristalsis has pulled it a further 20mm into the oesophagus (transducer #3 being level with the uvula in prior sets of data). This explains the data obtained on transducers #5 and #6 (saturating) which are both in the oesophagus (transducer #5 at the oesophageal entrance, transducer #6 inside oesophagus). The waveform shown on transducer #5 is characteristic to the airway collapsing around the neck of the catheter showing a peak in opposite directions during a single respiratory cycle. Transducer #7 also shows cardiac artefact and is the reverse of transducer #6. This is caused by the manner that the oesophageal wall is deformed by abdominal movement and does not yield any further information about upper airway air flow.

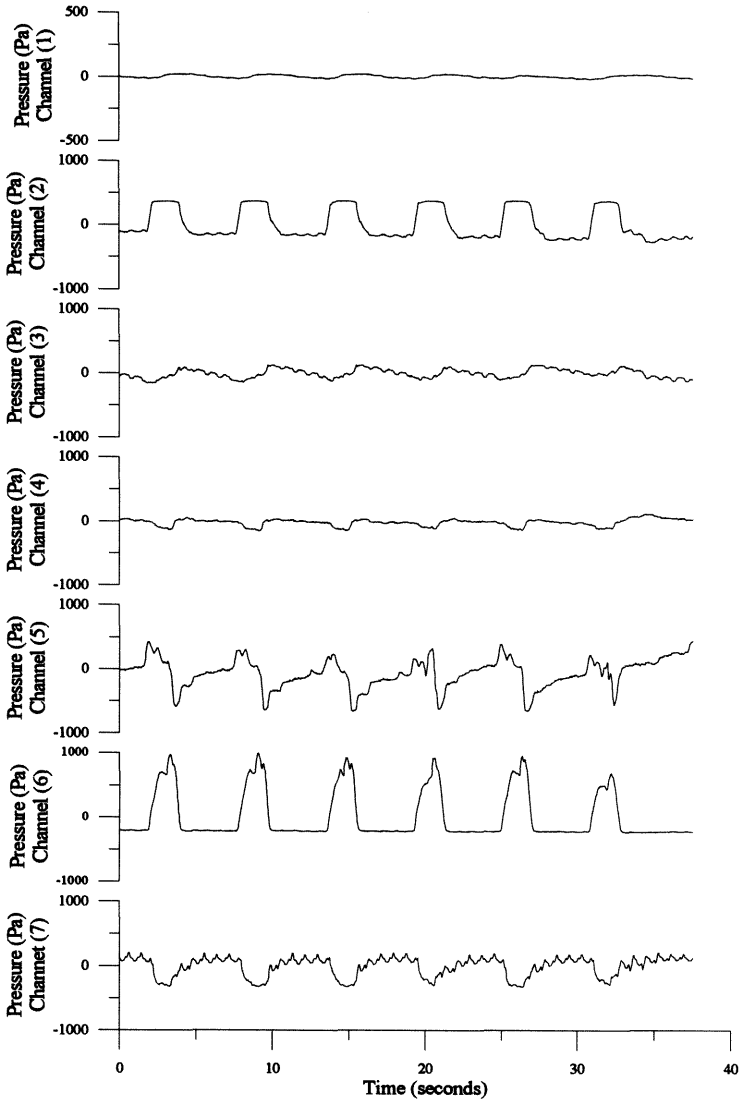

Figure 5-36 The pressure profile of a patient under general anaesthesia with an obstructing airway (Test CT13).

5.6 Validation of the mathematical model

In order to validate the usefulness of the three dimensional mathematical model for determining future pressure transducer designs, the model was compared to a transducer of known characteristic.

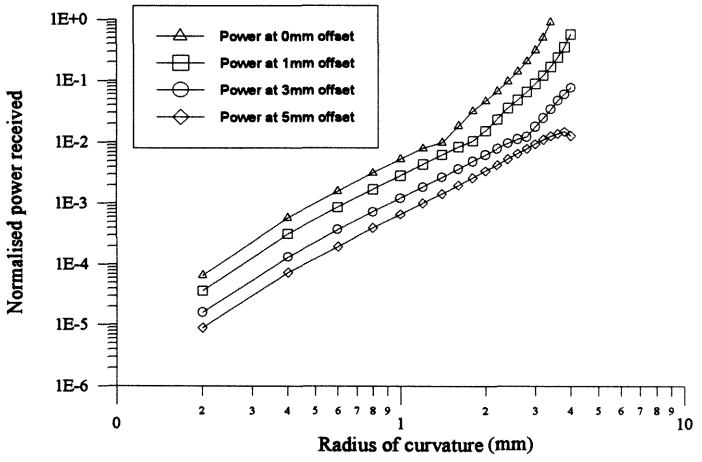

Figure 5-37 The variation of curvature of the reflective transduction element plotted against normalised power whilst keeping the distance to from the receiving optical fibre to the transduction element apex constant

Figure 5-37 presents calculations showing the effect the curved meniscus has on modulating the light emanating from the emitting optical fibre (diameter 0.25mm) of dimensions identical to that of the real pressure transducer. Each of the curves presented is the predicted normalised light received by a optical fibre at different distances back from the transduction element. Two of these curves are combined in the real pressure transducer to overcome bending losses offset 1mm and 5mm from the emitting optical fibre respectively.

The radius of curvature was converted into a pressure axis by examination of the gel transduction element dimensions under various static conditions.

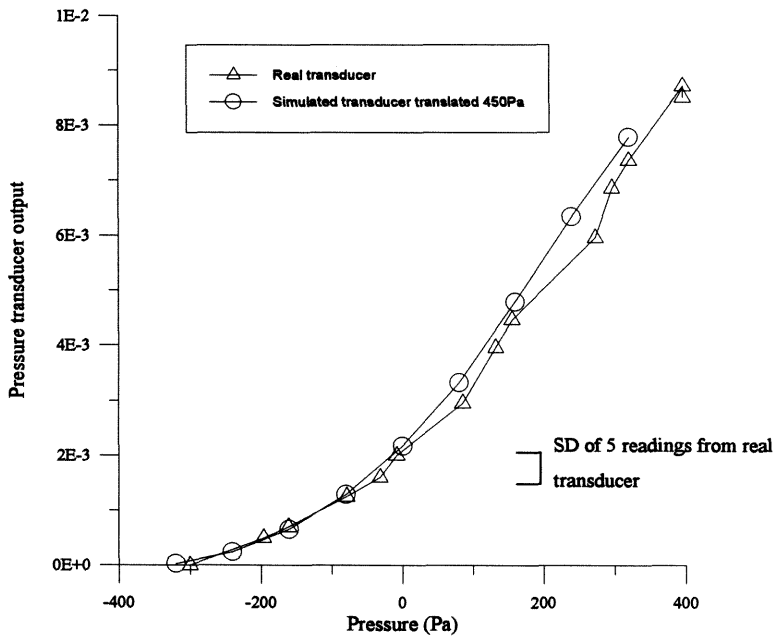

Figure 5-38 Validation of the mathematical model by comparison of real data to simulated data

Figure 5-38 illustrates two curves representing data obtained from a single channel pressure transducer under static conditions, and a transducer of identical dimensions simulated by the tree dimensional mathematical model described in chapter 4. In both cases the emitting optical fibre was placed 3mm away from the gel transduction element. Empirical data was obtained from the device and fed into the model in order to predict the output. The difference between the flux received by two optical fibres, offset 1mm and 5mm respectively, was then calculated to produce a pressure reading.

The atmospheric pressure varied by 450Pa (3.4mmHg) between taking the static calibration and recording the dimensions of the gel transduction element as the reading were taken on different days. The sensitivity of the transducer means that this pressure change can easily be detected and consequently the graphs were mis-aligned by 450Pa. High atmospheric pressure makes the gel meniscus less concave, i.e. the reflective

surface is closer to the optical fibres. If the emitting optical fibre gets too close to the surface the first half of the operating characteristic will be breached and a peak will be observed[7] (see chapter 3, section 3.3.2).

As the pressure falls the reflecting gel is pulled away from the receiving optical fibres becoming concave and the output tails off, this is visible in both curves. If the pressure is increased above that of the enclosed air bubble the gel meniscus becomes less concave, until it becomes planar and beyond that convex. The mean error between the model prediction and the physical data is 0.0284% of the normalised power.

The model is limited in the respect that it cannot simulate a convex surface, however it is useful as an approximation to predict the output from an optical fibre providing the pressure change is within the original transducer design criteria. It is able to detect the operating limits of the transducer, and determine when it should saturate given different ambient conditions.

5.7 Discussion and conclusions

This chapter has summarised both the clinical and laboratory investigations performed on the optical fibre pressure transducer when integrated into a catheter containing seven devices, or used individually. The first set of clinical trials used a single channel 0.94mm OD device to determine the signals expected during respiration using a series of breathing exercises to simulate breathing by tipping the head back and vibrating the soft palate against the back of the tongue. A profile of expected pressures was produced in the upper airway and oesophagus: respiratory, gastric and cardiac signals were observed. This investigation emphasised the limited data that may be obtained using a single channel device. The occurrence of an apnoea may be observed, but location information is not available.

[7] This feature can also be simulated by the mathematical model, see chapter 4, section 4.5.2.2

Following the development of the seven channel design, the two studies were conducted with locally and generally anaesthetised patients respectively. The first set of studies showed the high level of oesophageal activity associated with awake state. Peristaltic waves were not observed in patients under general anaesthesia. By observation of the pressure profile along the airway it was possible to observe the site of airway collapse. The extent of the collapse can be determined by classifying the waveform under one of three headings:

◊ An undistorted respiratory wave, the amplitude of which increases at the site of the occlusion

◊ A negative gauge pressure promotes the airway to completely collapse onto the catheter housing, squeezing the air-filled balloon to raise the interior pressure of the catheter. Such waves are sigmoid in appearance.

◊ Flow limitation due to palatal vibration: this occurs due to the palate vibrating against the back of the tongue during inspiration and gives rise to a high frequency component 15 to 20Hz on the waveform. This represents partial occlusion of the upper airway and may often be observed in transducers below the obstructive site as a negative-going pressure followed by a slight increase in pressure and then a plateau region.

The optical fibre pressure transducer catheter has been shown to work successfully in a small sample of patients with and without history of airway disorder. The main disadvantage of such transducers is their susceptibility to temperature drift. In the case of the single channel system the low thermal mass and hence a short time constant makes temperature drift due to airflow significant, however it is linear and may be compensated using a high speed temperature transducer. The increased thermal mass of the integrated system leads to a time constant of 78 seconds, and hence thermal compensation with normal respiration is not necessary. The increased physical mass of the seven transducer in comparison with the single channel system also

prevented the catheter being agitated in the oesophagus due to cardiac induced motion of the oesophageal wall[8] as drastically.

The final transducer design has satisfied the criteria specified in the initial design protocol. Although the transducer is not currently smaller than recent pressure transducers the potential for miniaturisation is limited only by the mechanical strength of the optical fibres in the transducer housing. The packaging of individual transducers in the catheter was limited by the materials and equipment in the laboratory, using industrially refined techniques it should be possible to reduce the diameter of the catheter to less than 2mm using tin-walled tubing to house the devices. The volume of air contained inside the transducer housing must however be conserved to maintain the sensitivity (10Pa).

For this particular application the frequency response was limited by placing a 100Hz low-pass filter on the output to minimise noise. From the calculations shown in chapter 3 it should theoretically be possible to operate the device at over 1kHz. High accuracy is also not important, even through the catheter has a sensitivity of 10Pa. It is apparent from the waveforms that the physician will only have to look from trends between the pressure readings of each of the transducers to make a diagnosis. The seven pressure transducers inside the catheter must be calibrated against one another in order to make a meaningful diagnosis.

The transducer is disposable, the main cost arising from the optical SMA connectors which may be reconditioned in order to recuperate some of the cost. Currently available transducers comprise a series of miniature components which are too expensive to deem disposable. Although the labour cost for catheter manufacture is high, this would fall should a device be mass-produced commercially.

The quantity of transducers selected for the prototype was chosen by the University Department of Anaesthesia. It can be argued that cost could be minimised further by reducing the number of transducers in each catheter. The site of airway collapse generally occurs at the back of the tongue or soft palate, and consequently the transducers lower than these points provide little more information than those higher

[8] Future miniature designs may be useful for applications were size is extremely important such as applications in pre-term babies and neonates (Skatvedt and Groegaard., 1994).

up the airway. Only one transducer below this point is required to give evidence of air flow limitation. The most distal transducer provided a combination of cardiac and respiratory data. Although it was found to be important to anchor the transducer in the oesophagus for the reasons discussed above, the oesophageal transducer did not provide any information about the occurrence of OSAS. If experiments were to be performed on real OSAS patients a respiratory signal would still be measured on the oesophageal transducer even if the airway was totally occluded.

Chapter 6

Rationale for the optical fibre endothelial cell damage probe - An overview of atheroma, angioplasty and vascular restenosis

6.1 Introduction

The following chapter is the motivation of the development of the optical fibre biosensor for measuring the healing process of the coronary arteries and is a comparison of the former optical fibre pressure transducer (chapters 2 to 5). The anatomy, physiology and histology of the vascular endothelium is introduced as part of the arterial wall. The factors leading to arterial stenosis and restenosis following percutaneous transluminal coronary angioplasty (PTCA) are introduced. Angioplasty using balloon catheters, ultra-sound and lasers are summarised.

Particular attention is paid to the vascular endothelium, and its potential role in causing restenosis following angioplasty. Methods of biologically marking the damaged vessel wall following angioplasty are reviewed as a rationale for the application of optical fibre technology to develop a biological probe to monitor the endothelial healing process.

6.2 Anatomy and pathology of the cardiac arteries and vascular endothelium

6.2.1 Cardiac anatomy and physiology

The adult mammalian heart comprises two muscular pumps acting in series: the right atrium and right ventricle constitute a low pressure pump transferring deoxygenated blood from systemic veins to the pulmonary artery, and the left atrium and left ventricle constitute a high pressure pump transferring oxygenated blood from left atrium to aorta for distribution around the rest of the body Figure 6-1a.

The impedance of the pulmonary and systemic circulation result in mean pressures of approximately 22mmHg (2.9 kPa) and 120mmHg (15.8 kPa) in the pulmonary artery and aorta respectively[1]. Biological vascular pressures are conventionally measured in mmHg (10kPa ≈ 760mmHg). Pressure and flow waveforms in the major vessels are determined both by ventricular output and by the static and dynamic compliance characteristics of the respective arterial trees.

Cardiac muscle is supplied by the coronary arteries, which arise from the aorta just above the aorta valve cusps. The phasic contraction of cardiac muscle causes large changes in the conductance of the coronary circulation down-stream of the arterials - such conductance is very low in systole and large in diastole. As a result distal coronary artery blood flow occurs predominantly during diastole (Figure 6-1b).

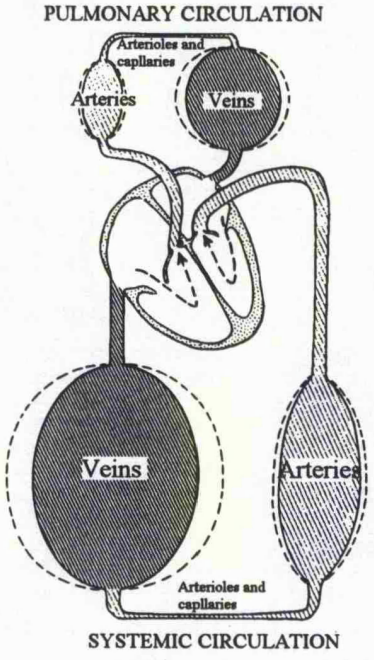

Figure 6-1a

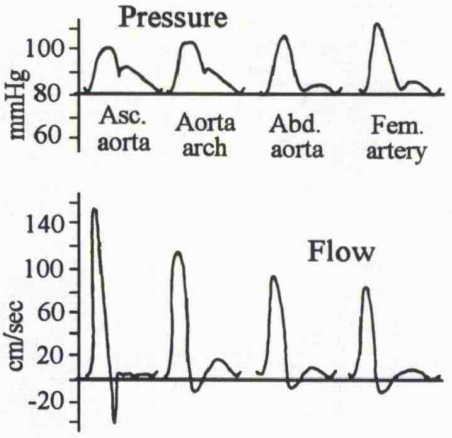

Figure 6-1b

Figure 6-1 Blood flow in the systemic and pulmonary circulatory system (Guyton., 1981 and Wilmer *et al.*, 1990)

[1] The study of the flow, pressure and properties of blood circulation is called haemodynamics.

Figure 6-1a schematically illustrates all of the veins and arteries of the pulmonary and systemic circulatory system grouped together in single chambers. Each of the two chambers are analogously linked by a narrow gauge tube which represents the arteries and capillaries.

Blood flow through a vessel is determined by the following two factors:

- The pressure difference - hence the force of the blood through the vessel.
- Vascular resistance - this is a function vessel diameter and fluid viscosity.

Volumetric flow is closely linked to the metabolic requirements of individual organs. There are currently many systems available to measure blood flow, each of which yields a value either in millilitres or litres per minute (section 6.4).

Each system attempts to describe the following equation:

$$Q = \frac{\Delta P}{R} \qquad \text{(Eqn 6-1)}$$

Q = Volumetric flow rate (ml/sec)
ΔP = Pressure drop (mmHg)
R = Vascular impedance (PRU)

Measured flow is a function of pressure loss, vessel diameter and fluid velocity (Eqn 6-1). The unit of arterial resistance or impedance is stated as *peripheral resistance units* (PRU) :

1 PRU ≡ 1mmHg pressure loss at 1ml/sec

where:	Pulmonary vessels	:	0.12 to 1.00 PRU
	Systemic vessels	:	1.00 to 4.00 PRU

A slight change in vessel diameter by a constriction or otherwise will result in a marked change in vessel resistance (Eqn 6-2 to Eqn 6-5). Steady flow in a narrow vessel implies that the flow is constant in any given concentric ring in a vessel cross-

section. Flow rate Q is defined as velocity V multiplied by cross-sectional area (πr^2) of the vessel (Duncan., 1987 and Nichols and O'Rourke., 1990).

hence: $$Q = V\pi r^2 \qquad \text{(Eqn 6-2)}$$

Poiseuille's law states: $$Q = \frac{\pi \Delta P r^4}{8\eta l} \qquad \text{(Eqn 6-3)}$$

where ΔP = Pressure drop along vessel length l
η = Coefficient of viscosity
l = Length of vessel
r = Radius of vessel

Conductance of vessel: $$C = \frac{\pi r^4}{8\eta l} \equiv kr^4 \qquad \text{(Eqn 6-4)}$$

$\therefore$ Resistance of vessel: $$R \propto \frac{1}{r^4} \qquad \text{(Eqn 6-5)}$$

The flow of blood is also dependent on the vessel lumen surface, and may be either turbulent or laminar flow. The friction between the blood and vessel wall leads to *parabolic laminar* flow. The blood moves at maximal velocity along the neutral axis of the artery, and is almost stationary at the boundary. It is this scenario that a physician would expect to observe in a healthy artery of regular and uniform cross-section. If the artery is partially occluded or bent sharply the flow is disturbed and becomes apparently random in nature (Guyton., 1981). It is impossible to characterise the specific flow details, other than to describe it as turbulent. Turbulent flow is said to be occuring if the blood is both crossing the vessel, forming eddy currents, as well as travelling along it. The result is a further increase in resistance.

The vessel is also pliable, and will introduce a considerable amount of non-linearity. In the extreme case, if the pressure is low enough, the vessel will physically collapse in onto itself. The pressure below which this phenomena occurs is known as the *critical closing pressure*. For normal vessels this is 20mmHg, but will vary if the artery is stimulated by other circulatory reflexes (Guyton., 1981).

The elasticity of the vessel wall will determine the vascular compliance[2] and the vascular distensibility[3] of the artery. If the blood pressure increases due to a constriction or otherwise the heart will be placed under increased stress, and the artery will risk damage. Blood pressure is also determined by the orientation of the subject. If the person is in an upright posture the pressure will either increase or decrease, depending on the location of the measurement instrument.

The cardiovascular system is a finely balanced high pressure system. A blocked narrow gauge vessel, conducting lower pressure blood returning to the heart, can have potentially catastrophic consequences and will be affected more by stenosis than a similar vessel of larger diameter.

6.2.2 The vascular endothelium

A mammalian artery involves the combination and interaction between different types of cell. The artery structure is classified under three headings (Figure 6-2) :

The **Tunica Interna** describes the inner lining of the vessel: the endothelium, basement membrane and internal elastic lamina.

The **Tunica Media** is the centre-most and thickest section of the vessel wall: the external elastic lamina and smooth muscle cells.

The **Tunica Externa** is the outer-most layer, and is principally constructed from elastic fibres.

The combination of each of the vessel components leads the vessel to perform two functions: contractility (vasoconstriction) and elasticity (vasodilation) when vessel stimulation is removed. The force arises from the smooth muscle cells. The proportion

[2]Vascular compliance : A measure of the ability of a mechanical system to respond to an applied force. It is the reciprocal of the system stiffness.

[3]Vascular distensibility : Ability of a vessel to expand

of each of the aforementioned vessel components will vary depending on the type of artery (Tortora and Anagnostakos., 1990) (Figure 6-2).

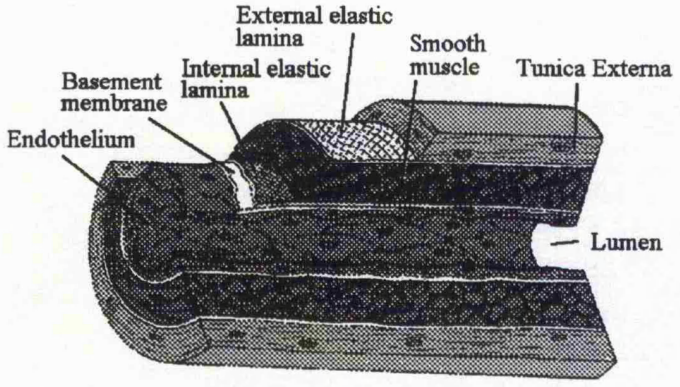

Figure 6-2 The structure of an arterial wall.
(Tortora and Anagnostakos., 1990)

The vascular endothelium is the mediator which controls the tone of the smooth muscle cells, as well as preventing platelet adhesion to the vessel wall (section 6.5.4). If the endothelial cells are damaged the result is localised spasm of the vessel as well as thrombosis (Badimon., 1992). The added complication of endothelial cell death is the secretion of growth components which promote smooth muscle cell proliferation.

Vascular stenosis, and hence the need for interventional cardiovascular surgery, often begins as damage to the endothelium[4]. The fragility of the cells means that they may be disrupted by turbulent blood flow (see section 6.2.1). Endothelial damage allows the aggregation of monocytes on the surface of the endothelial cells which are able to migrate into the sub-endothelium and become loaded with cholesterol. This may be followed by calcification and thrombosis as a result of damage to the endothelial layer.

---

[4] The structure of endothelial cells combining to make the vessel wall is called the vascular endothelium.

6.3 Arterial stenosis

Atheromatous narrowing of the coronary arteries is one of the commonest forms of heart disease in modern society. Narrowed arteries cannot maintain adequate blood supply to heart muscle during exercise, and the result is an accumulation of muscle metabolites causing chest pain. The syndrome of chest pain on exertion is the clinical manifestation of coronary artery narrowing and is called angina.

Calcification occurs when the smooth muscle cells become overloaded with Ca^{2+} ions, destroying the cell mitochondria (Lossnitzer *et al.*, 1984). The pathologically changed cell transforms the arterial wall into a calcified plaque. The eventual accumulation of the calcium in the artery lumen will restrict the blood flow along the vessel, and eventually lead to stenosis of the vessel[5]. The restriction or prevention of blood flow will lead to ischaemia (Figure 6-4). Vascular stenosis is classified by one of two possibilities (Figure 6-3).

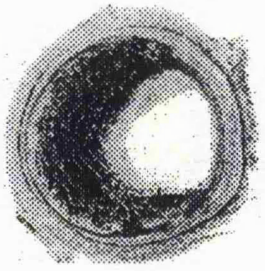

Figure 6-3a

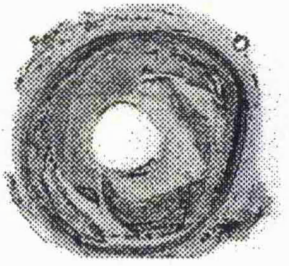

Figure 6-3b

Figure 6-3 Eccentric and concentric stenosis of the coronary arteries occuring on the arterial wall
(after Lossnitzer *et al.*, 1984)

Eccentric coronary stenosis describes the presence of atheroma on only part of the vessel wall through a given cross-section. Concentric coronary stenosis is when atheroma is present on the complete vessel wall through a cross-section.

---

[5] Stenosis is regarded as a loss of approximately 70% of the vessel lumen.

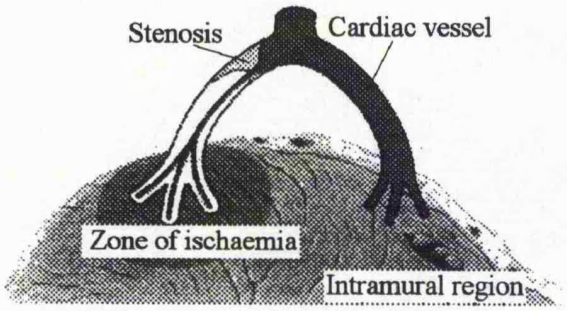

Figure 6-4 Cardiac ischaemia caused by vascular stenosis
(after Lossnitzer *et al.*, 1984)

6.4 Methods of investigating coronary stenosis

The demand for techniques for the examination of the cardiac arteries is extensive. Unlike the initial onset of restenosis, arterial stenosis is easily recognised. The blood pressure along the length of the vessel either changes, or the vessel becomes swollen and deformed. Given these prognoses, current exploratory methods involve either the imaging of the vessel, or the measurement of blood flow and blood pressure.

6.4.1 Angiography

Preliminary investigations of the cardiac arteries typically involve direct coronary angiography (DCA). The technique is the combination of image enhancement by introducing radio-opaque material, such as iodine, intravenously, with image processing and enhancement. The quantity of contrast material present means that a considerable number of X-rays must be taken (> 30 per second). To maximise the signal-to-noise ratio subsequent frames are averaged with previous frames: *mask-mode subtraction.* The duration of the X-ray pulse is short enough to ensure that the patient is not exposed to an excessive dose of radiation and stops the image being blurred due to the blood flowing in the arteries (Mancini., 1994). The technique does provide excellent clarity, however it does lack detail. DCA is useful for determining the presence of arterial stenosis and the extent of the blockage, but it lacks details on the type of occlusion: calcification etc. The clarity of the image permits its use with interventional cardiac catheterisation to determine catheter location with respect to the occlusion. Laser, balloon and ultrasonic catheters are placed in position in this way.

Angiograms are performed in the pre and post-operative period to quantify the success of angioplasty or bypass surgery (Lyon *et al.*, 1987).

6.4.2 Histological investigations

The technique providing the most information about the healing of the vascular endothelium is the histological examination of the vessel post-mortem or by harvesting the vessel during bypass surgery. The vessel is cut into histological slices and examined under the microscope. This technique is able to discover the depth of damage caused to the vessel wall during angioplasty: balloon angioplasty, laser assisted or otherwise (Waller *et al.*, 1992). Initially it was thought that damage was restricted to the intimal layer, however such analysis confirmed that damage can penetrate into the medial vessel wall (Lyon *et al.*, 1987).

6.4.3 Ultrasound

Ultrasound is used in cardiology to both measure blood flow by calculating Doppler shift (Satomura., 1959) and as a tomographic technique (Waller *et al.*, 1992). The Doppler piezo-electric crystal is mounted on the tip of a coronary catheter and placed directly in blood flow. Intracoronary Doppler is able to isolate specific coronary arteries and examine blood flow reduction due to arterial stenosis directly (Serruys *et al.*, 1994). The most recent development in arterial imaging is the application of ultrasound to imaging to investigate localised dissection of an artery following balloon angioplasty (Figure 6-7, section 6.5.3). This is the most common form of arterial damage associated with PTCA, and is closely related to acute complications such as *abrupt closure*. The ultrasonic probe comprises a number of transducers arranged radially around a balloon catheter. The resulting image, arriving in real-time, provides information regarding the extent of arterial damage, and also information on balloon inflation, elastic recoil etc. Modified catheters and the integration of lateral two-dimensional images are able to provide three dimensional reconstructions of the vessel under study. The technique is still in its infancy. If the acoustic transmission path is impaired, details local to this *dead-spot* will be obscured or missed completely. There are also problems associated with the withdrawal of the ultrasonic catheter, should the catheter twist the reconstructed image will be distorted. Blood flow will also distort

the image: flow is not synchronised with catheter withdrawal. Calcified arterial stenosis is easily visualised (Yock *et al.*, 1994).

6.4.4 Angioscopy

Vascular endoscopy was first used in 1913, and is the most common of medical instruments associated with optical fibres. The first prototype endoscopes were of rigid construction and were limited in use due to the non-existence of modern optics and optical fibres (Ramee and White., 1994). The image resolution, flexibility and size are determined by the number of optical fibres contained within the angioscope: 3000 fibres is normal. In a similar manner to PTCA (section 6.5.1), the angioscope is passed from either the femoral or brachial artery into the target site using a guide wire. The catheter is also slowly perfused with saline to prevent platelets accumulating on the end of the scope and impairing the image. Blood flow is halted during the imaging process by the inflation of a cuff around the perimeter of the angioscope, and the blood obscuring the image is then displaced by perfusing the area with saline. Angioscopy is often performed in conjunction with angioplasty to assist in placing the angioplasty catheter in the correct position in the artery. The size of the angioscope (<1.8mm) permits safe in-depth study of the stenosised vessels, and the examination of the heart valves. Direct visualisation is said to be able to detect stenosis and its severity more accurately that external imaging (see below). A report by Ramee *et al* (1994) described a detection rate of 36% using angioscopy. The *colour* information is available, due to illumination by a white light source, i.e. the type of thrombus can be identified. Angioscopy has undergone a considerable evolutionary phase, the improvement of optical fibres has permitted development of ever increasing resolution, there are however limitations. The image is produced by illumination of the target, consequently only surface morphology is visible and pathological composition below the surface is unknown. Angioscopy is capable of providing high-resolution myocardial information about damage to the inner vessel wall, and about the presence of thrombus. As currently used, it is not capable of giving information about the deeper layers of the vessel wall, and only limited information about the function and integrity of the endothelium can be obtained.

6.5 Methods of treating coronary stenosis

There are many techniques available to treat coronary stenosis, including angioplasty, coronary bypass and, in minor cases, drug therapy. Angioplasty (section 6.5.1 to section 6.5.3) is one of the most popular forms of treatment. It may be performed under local anaesthesia, and can provide immediate relief in acute cases. The side-effects may however lead to restenosis of the vessel due to damage of the vascular wall during the procedure (section 6.5.4).

6.5.1 Balloon angioplasty

The introduction of angioplasty as a treatment for arterial stenosis has only been regarded as a common surgical procedure since the late 1970's and early 1980's (Myler and Stertzer., 1994). Since its introduction success rates of over 90% have been achieved. The original coronary catheters used were 1.5mm to 2mm in diameter, and comprised of a double lumen: the central lumen permitting pressure measurement and perfusion, whilst the second eccentric lumen was used for balloon inflation and deflation.

Coronary angioplasty involves inserting a guiding catheter from the brachial or femoral artery (Figure 6-5). and manipulating it under X-ray control until the tip lies in the mouth of a coronary artery in the heart. Radio-opaque dye containing iodine can be injected to check the catheter position and to identify the site of restenosis. A fine guide wire is passed through the guiding catheter and manipulated across the restenosis again under X-ray control. Once the guide wire is in position, a balloon catheter is passed over the guide wire through the guiding catheter, to lie across the stenosis (Bourassa *et al.*, 1984). The balloon is then inflated to 600kPa to 800kPa. The balloon is constructed of non-compliant polymer material so that the maximum diameter on inflation does not exceed a specified measurement.

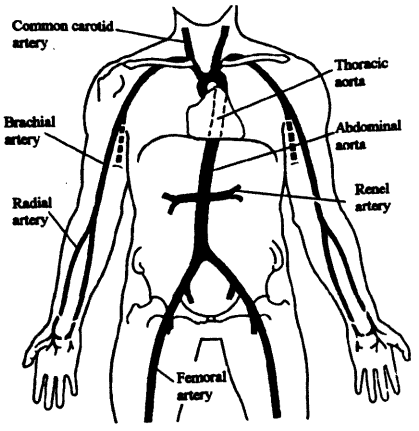

Figure 6-5 The main arteries of the human body
(after Roper., 1987)

6.5.2 Laser angioplasty

The use of lasers in cardiovascular surgery is extensive. A considerable amount of work has been achieved in the medical field regarding the prospect for lasers, and their effects to tissue neighbouring the target area (Forrester., 1994). Applications of lasers in vascular angioplasty may be classified in one of the two following headings:

- Direct laser angioplasty
- Laser assisted angioplasty

Direct laser angioplasty (DLA) involves the use of a laser, Nd:YAG (neodymium-doped:yttrium-aluminum-garnet), argon ion or excimer to ablate occluded vessels. Early research used a Hd:YAG, operating at infrared wavelengths, (1.064μm) and argon ion (488-515nm), in the blue/green part of the spectrum, in a continuous wave mode. The lesion produced by DLA is affected by three factors. The fundamental issue is that the absorption of the light by the tissue is dependent on the wavelength being used. The power of the laser is significant, as is the manner in which the energy is delivered: pulsed or continuous wave. The early use of continuous wave lasers were plagued with problems. The laser boiled the water in the tissues and the resulting lesion lead to perforation of the vessel wall. As a result the medical field has not been quick to adopt the new laser techniques for use in cardiovascular surgery.

Current techniques use pulsed wave lasers, energy is delivered for intervals of only 250 μS and with a power of 50 to 250Watts (White *et al.*, 1993). A catheter delivery system, comprising a number of fibre-optics, is used to channel the light to the occluded artery (Figure 6-6). The catheter is then pulled through the thrombotic region, whilst laser energy is being simultaneously delivered. The process is repeated until the artery is sufficiently recanalised. Although this technique has been successful in treating coronary atheroma, the resulting lumen diameter is limited by the size of catheter used. Consequently DLA is often used in conjunction with balloon angioplasty.

The excimer laser, emitting in the high energy ultraviolet region (308nm), is now used to treat atheromatous arteries and is also used in dentistry (Eduardo *et al.*, 1994) and orthopaedics (Gibson *et al.*, 1994). The shorter wavelengths and the short burst of energy required permit higher precision, and lower temperatures (65°C) to be achieved.

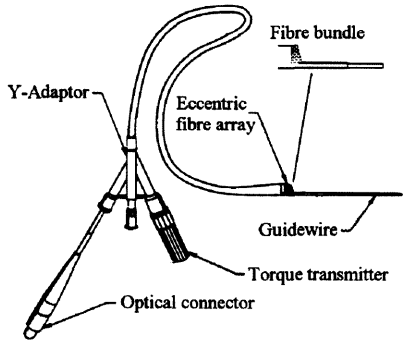

Figure 6-6 A schematic representation of a directional laser catheter. The fibre-optic bundle is steered through the artery using a *torque transmitter* which is able to twist the *fountain pen* tip into position (after Litvack., 1994).

Laser assisted angioplasty (LAA) is most typically referred to as laser balloon angioplasty. The laser is used to heat an angioplasty balloon whilst it is simultaneously inflated, forcing it to rise in temperature from 80°C to 100°C. The applied heat is able to fuse weakened or torn tissue which arises as a result of balloon inflation. The design of a catheter to achieve LAA is a formidable challenge, and holds many problems

which had to be overcome in the early design stages. The laser is potentially high power (>50W) and operates in continuous wave mode in order to maintain the heating effect. Consequently, should the fibre break, the resulting leakage may permit heating of the catheter in the wrong location. This may not only damage the device, but may cause an unwanted lesion in the artery. The balloon must be able to withstand the high temperatures present (90°C to 150°C). Early studies used a continuous-wave argon ion laser (488nm to 514nm), but the tissue penetration was found to be only 0.5mm, not sufficient to fuse tissues (Cheong *et al.*, 1991). A Nd:YAG laser is now used more frequently. The device comprises a fused silica optical fibre with a diffusing tip: a helical fibre wound around a core contained inside the angioplasty balloon. In order for recanalisation to be achieved successfully, the balloon is heated to at least 80°C and maintained for approximately 20 seconds[6] (<150°C to prevent charring).

The success of LAA catheters is attributed to the thermal reshaping of the artery as a result of the cooling process whilst the balloon is still inflated. This prevents elastic recoil of the artery upon balloon deflation. The cost of the catheters is high due to the inherent safety mechanisms required to detect fibre breakage and prevent localised heating in the undesignated areas.

6.5.3 Ultrasound angioplasty

Ultrasound angioplasty differs from the ultrasound used in imaging in the frequency which is used in each application. Doppler ultrasound and imaging is in the frequency range 2 to 30MHz, whilst therapeutic ultrasound is 15 to 30kHz. Ultrasound angioplasty is a method of delivering mechanical energy to the target site without the thermal problems associated with laser angioplasty.

The probe is placed in physical contact with the target and the motion arising from it (20μm to 110μm) rapidly disintegrates the contact site (Siegel *et al.*, 1994). This does not occur if the frequency is too high: the probe oscillation not being

[6]Past research also discusses the heating of the angioplasty balloon by radio-frequency energy. Ionic fluid within the balloon is heated to temperatures up to 100°C using RF waves in the spectrum 100kHz to 300MHz (Fram and McKay., 1994).

sufficient to cause ablation. Ablation occurs due to the generation of heat, the presence of micro-currents on the target surface and micro-bubbles expanding to destroy the structure.

Studies conducted by vascular surgeons have proved the method to be successful. The lack of rigidity of the arterial wall once the calcified region has been removed, means that it is not damaged by the probe. Consequently the stenosis does not reoccur in 80% of treated vessels (Seigel *et al.*, 1993). Problems do arise if the artery is subjected to secondary balloon angioplasty, the trauma to the vessel being considerably higher.

6.5.4 Arterial restenosis and the process of healing

Angioplasty has both long-term and short-term effects, and will not be performed on patients with significant cardiac valve disease or where stenosis has already been treated by previous bypass surgery. The probability of restenosis[7] is reported to be higher in these subjects (Alexander *et al.*, 1993). The initial success of angioplasty is reported to be over 90%, however the quantity of patients suffering from restenosis has not altered significantly. Reports of restenosis vary from 30 to 50% (Preisack and Karsch., 1993).

Restenosis occurs due to the healing process of the vessel wall, and is caused by two pathophysiological processes classified as *early restenosis*: 0 to 3 months, and *late restenosis*: 3 to 6 months. Beyond 6 months and restenosis is less likely to occur (Preisack and Karsch., 1993). The condition arises from the excessive trauma of the vessel and the subsequent vascular damage caused to the vessel lumen during angioplasty. The damage caused is dependent on the type of angioplasty. Balloon angioplasty is theoretically able to compress the plaque on the vessel wall on balloon inflation, in fact the wall is stretched considerably prior to the plaque fracturing or tearing. The result is localised dissection of the arterial wall. The elastic recoil of the vessel permits it to bounce back and split the internal layer (Bonner., 1994). The injury

[7] Restenosis is defined by the National Heart, Lung and Blood Institute as a loss of more than 50% of the initial improvement in the cross-sectional diameter of the vessel immediately after surgery (McBride *et al.*, 1988).

to the calcified plaque results in haemorrage and subsequent thrombosis (Figure 6-7). A report by Van Erven (1991) suggested that acute occlusion is not dependent on the type of angioplasty used. Lasers and heat treatment, used to adhere debris to the arterial wall, severely damage the vessel media and ablate the vascular endothelium. Directional atherectomy attempts to remove the obstruction by cutting into the vessel wall to remove the calcified region, however the resulting lesions have a similar effect to angioplasty (Sketch *et al.*, 1994).

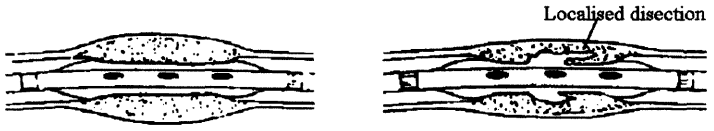

Figure 6-7 Damage of the arterial wall following percutaneous transluminal balloon angioplasty (after Anderson., 1993).

Restenosis originates from the denudation of the vascular endothelium. Platelets are then able to adhere to the sub-endothelium and obstruct further blood flow. Post-mortem studies of vessels post-operative from both human and animal models have observed a considerable reduction in endothelial cells in the treated site (More *et al.*, 1994). Slight contact is sufficient to destroy endothelial cells. The damage leads to cellular profilation and hence the smooth muscle cells migrate towards the centre of the vessel before the endothelium regenerates.

The current methods for the examination of a vessel in the post-operative period involve the removal of the vessel and *in-vitro* investigation. It is not currently possible to perform an *in-vivo* study of the endothelium. Imaging techniques: fluoroscopy and radiography, are used to view the vessel non-invasively, but are limited in detail and resolution. If a vessel is identified to be a candidate for thrombosis, pharmacological measures may be taken to prevent clotting and platelet adhesion to the vessel wall (Anderson., 1993).

6.6 The antibody-antigen reaction

6.6.1 Pathology

The antibody-antigen reaction is the fundamental principle of any mammalian cellular immunity defence system. Each chemical compound is unique in its molecular construction, this part of the substance is the antigen. The immune system of the human body is a learning process. The lymphoid tissue, located in high-risk areas of the body: the gut, pharynx etc, intercepts the antigens of any foreign body and generates antibodies as a counter-measure. Each antibody produced is specific to a particular antigen. Subsequent exposure to the same antigen will trigger a faster response (Guyton., 1981). The antibodies produced are able to bind to the specific antigens to form an *antigen-antibody complex.*

6.6.2 Biologically labelling monoclonal antibodies

A monoclonal antibody, generated *in-vitro,* is able to bind to specific antigens in a similar manner that mentioned above. A technique by Cuello *et al* (1982) described internally labelled monoclonal antibodies containing either a radio-nuclide or fluorescent material (Figure 6-8). The labelling of the antibody does not affect the binding characteristics. Hence if a labelled monoclonal antibody is introduced into the blood stream, a concentration of antibody may be detected by searching for the presence of its biological label. Research by Pringle and deBono[8] (1988) developed monoclonal antibodies able to bind to damaged and regenerating vascular endothelium. The two aforementioned techniques may be combined to provide a method of determining the location of damaged and regenerating vascular endothelium as occurs the in PTCA post-operative period.

[8] Prof. D.P.deBono, Dept. of Cardiology, Clinical sciences wing, Glenfield general hospital, Groby Road, Leicester. LE3 9QP, UK.

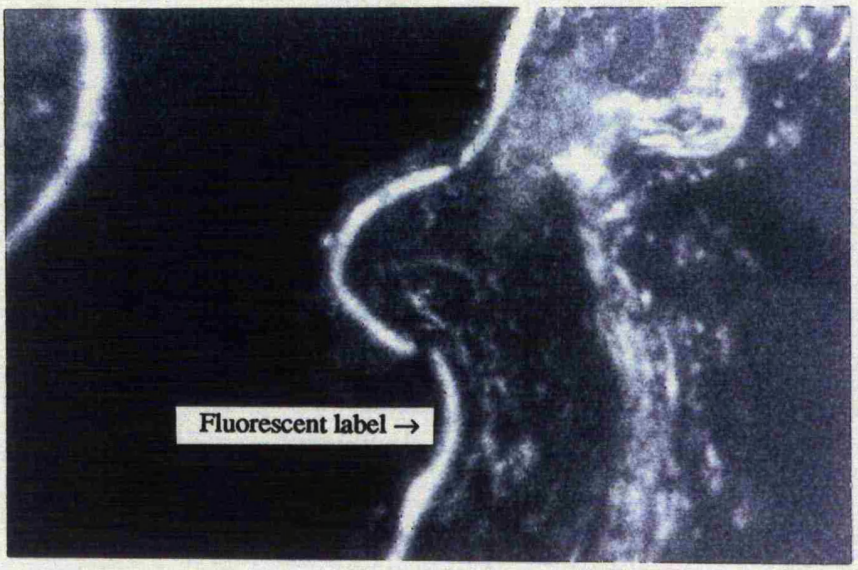

Figure 6-8 Damaged vascular endothelial cells labelled with internally fluorescent labelled monoclonal antibodies. Photograph supplied by Prof. D.P.deBono[8].

6.7 Rationale for the cell damage probe

PTCA as a method of treating atheroma and calcified vessels has a proven record of initial success. Little is known about the healing process of the vessel wall following the operation. The aim of this part of the research was to develop an optical fibre probe, for use *in-vivo*, to monitor the healing process of the tunica interna: specifically the vascular endothelium. Optical fibres are particularly suited to this application for two main reasons:

- Inherent electrical isolation
- Size of final catheter

The development of this probe is in contrast to the former pressure transducer (chapters 2 to 5) as the problem is one yet to be solved. It is not merely an improvement of an existing technology, but a method of overcoming a previously insoluble problem.

The proposed research involved internally labelled monoclonal antibodies treated with an appropriate marker so as to be detectable optically. In comparison with the former pressure transducer for use in the pharynx, the catheter size is particularly

important. Further restriction to blood flow is undesirable as it may cause more serious secondary problems. The significance of electrical isolation is important. Any risk of electric shock must be avoided when dealing with a living body. This device is for use in the cardiac arteries and will be extremely close to the heart itself. Unwanted electrical activity may disrupt the rhythm of the ECG[9].

The technology also differs from the optical fibre pressure transducer in that it is a biosensor, relying on a biological reaction.

[9] ECG: Electrocardiogram - A recording of the electrical activity in the heart

Chapter 7

The design of the endothelial cell damage probe for use in the cardiac arteries

7.1 Introduction

The second type of amplitude modulated sensor addressed in this thesis is presented. The following chapter details the design of an optical fibre biosensor and uses a biochemical reaction to monitor the healing process of the vascular endothelium following PTCA. Two types of optical technology are examined coupled with two types of labelled monoclonal antibody-antigen reactions for detecting vascular damage to the inner lining of the arteries: the endothelium.

Scintillation, intended for use with for use with a radio-labelled antigen found that the emanating radiation from such a system could not provide sufficient sensitivity. A second design is detailed fully using a fluorescent labelled monoclonal antibody as an alternative.

Hardware and software was produced to acquire the data from the optical fibre probe in order to permit analysis in real-time. The selection and design of optical components are also discussed. Experiments were conducted both *in-vitro* and *in-vivo* using simulated and animal models and are summarised in chapter 8.

7.2 Proposed system and project evaluation

In-vivo methods for the examination of the vessel wall during the post-operative period have not, to date, been developed (chapter 6). The design criteria are more restricting in may respects than the optical fibre pressure transducer catheter because it is more invasive and was designed to be inserted by the method described by Bourassa *et al* (1984) and his co-workers, through either the femoral or brachial arteries (chapter 6, section 6.5.1).

- A typical adult human coronary artery has a lumen diameter of approximately 3mm, hence the probe size should not prevent further blood flow: a diameter of no greater that 1mm OD was proposed.

- The probe is highly invasive and the location close to the heart makes the issue of electrical isolation paramount.

- The probe should be disposable due to its close proximity to blood.

- Construction should be rugged and completely non-toxic.

Although the aim of the project was to develop an optical radiation probe able to detect endothelial cell damage, two clearly parallel but different probe designs were envisaged:

- Labelling of monoclonal antibodies using a radio-nuclide.
- Labelling of monoclonal antibodies using a fluorescent material.

For reasons discussed in section 7.3 of this chapter the latter design was chosen for clinical investigation, although a limited series of tests were compiled using radio-nuclides

7.3 The radiation probe

7.3.1 Current techniques for the detection of labelled antibody-antigen reactions

Gamma-emitting radio-nuclides, such as 125I and 111In, are conventionally used to label monoclonal antibodies *in-vitro*. The concentration of the antibody *in-vivo* is determined by viewing the target area of tissue through a gamma-camera. Although this method has in the past been useful for determining the presence of radioactivity, the limited resolution is not sufficient to permit detailed examination of small areas of vascular damage: as occurs in the vascular endothelium during PCTA. The signal-to-noise ratio is limited because of the background radiation emanating from the radioactive dye in the intrathoracic blood pool and pulmonary endothelium (typically iodine) (Prys-Roberts., 1969 and Popma and Bashore., 1994). The signal-to-noise ratio may be improved if the detecting probe is manoeuvred close to the target area.

To reduce effects of background radiation a long range gamma-emitting radio-nuclide may be replaced by a shorter range beta-emitting radio-nuclide such as tritium, making the distinction between the background count and the signal simpler.

Internally-labelled monoclonal antibodies of high specific activity have already been established using the method of Cuello (1982) and his co-workers and may be readily modified for such an application.

Scintillation counting[1] is a technique used in biochemistry to analyse the behaviour of a non-radioactive material by combining it with a similar radioactive material (a tracer) and assuming the two to be identical. The radiation may then be observed to determine the reactions that are taking place. The technique of liquid scintillation counting provides an alternative to such techniques as spectrophotometry (section 7.4.3).

Liquid scintillation counting	Spectrophotometry
Count rate	Optical density
Primary solvent and scintillator	Colour reagent
Specific activity	Concentration
Pulse voltage spectrum	Colour absorption spectrum

Figure 7-1 A comparison of terminology in liquid scintillation counting and spectrophotometry (Neame and Homewood., 1974)

The use of a scintillating probe to detect radiation is not a new idea, past research lead to the development of a fibre-optic coupled scintillation probe designed to measure the decay of plutonium (Swinth *et al.*, 1976). The system used the organic scintillant NaI(TI) which could be excited by low energy photons such as those arising from ^{131}I, ^{125}I, ^{197}Hg, ^{111}Ga etc. The problem with this previous design was the physical size of the final device, the optical fibre being of a diameter of 5mm or more. It also required a considerable level of radiation: 14keV to 150keV to produce light of a detectable level.

[1] Scintillation describes the action of a chemical that emits light when exposed to ionising radiation.

Further to the application in medicine it was envisaged that such a device would be extremely useful in other non-medical applications where low-levels of radiation must be measured without disturbing the measurement site.

7.3.2 Radiation probe feasibility

The final probe was designed ultimately for use in the coronary arteries where the vessel lumen is restricted. The design was hence limited to the current size of angioplasty balloon catheters (volume ~150mm^3). The design discussed by Swinth *et al* (1976) was restricted to available scintillants: solid and liquid, at the time of the experimentation. The efficiency of currently available scintillants has now improved and is currently of the order 60% (see below). Given this improvement, it was hoped that the volume of the former mentioned device be reduced below that specified in the prior investigation (450mm^3).

Prior to experimentation, a series of feasibility calculations were compiled using commercially available scintillants to decide whether radio-labelled monoclonal antibodies could provide sufficient radiation to generate a detectable amount of photons. The envisaged design was that illustrated in Figure 7-2.

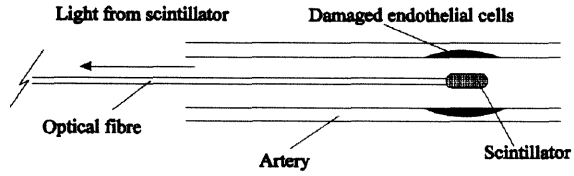

Figure 7-2 An illustration of a possible prototype optical fibre scintillation probe using a scintillator mounted at the tip of an optical fibre

A typical sensor system, such as a low dark current photomultiplier tube, is able to detect approximately 300 photons/sec. Systems more sensitive than this are available, but require highly controlled electrical and optical environments unlikely to be obtained in a hospital. The shape of the scintillator is a cylinder, hence the proportion of light received by an optical fibre of a particular size may be calculated. Given these figures a feasibility study was conducted.

When an electron in the scintillator is excited to a high energy level by the presence of radiation or otherwise, it may release its energy as a photon of a wavelength dependent of the scintillator when it returns to its normal "ground" level. In order to calculate the theoretical level of light captured by an optical fibre the following assumptions were made:

- Light emitted from a molecule did so uniformly in three-dimensional space
- The light travelling towards the receiving optical fibre was not absorbed inherently by the scintillating material

The light flux received by an optical fibre of specified numerical aperture distributed uniformly is defined by the solid angle (in steradians). The solid angle is defined by the angle subtended at the centre of a sphere, radius 'r' by an element 'δA' at the surface of a unit sphere.

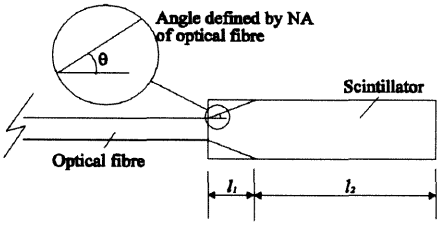

Figure 7-3 A schematic of the theoretical design of an optical fibre radiation probe using a scintillator.

If the diameter of the scintillator approaches that of the optical fibre distance 'l_1' may be neglected, and the light captured by the optical fibre arises only from the column of scintillant of length 'l_2', radius 'r'.

A volume of size ($r\delta\theta.\delta r.\delta x$) emits light as a function of the solid angle using a cylindrical co-ordinate system (Eqn 7-1).

$$\text{Solid angle} = \frac{A_f}{4\pi\left(x^2 + r^2\right)}.r\delta\theta.\delta r.\delta x \qquad \text{(Eqn 7-1)}$$

where

A_f = Cross-sectional area of optical fibre

$\sqrt{(x^2+r^2)}$ = Distance from volume ($r\delta\theta.\delta r.\delta x$) to face of receiving optical fibre

Integrating over area of cylinder forms (Eqn 7-2):

$$\text{Normalised light flux received} = \frac{\int_0^{l_2}\int_0^{R_f}\int_0^{2\pi} \frac{A_f}{4\pi(x^2+r^2)}.rd\theta.dr.dx}{\pi R_f^{\,2}(xl_2)} \qquad \text{(Eqn 7-2)}$$

where

l_2 = Length of column

R_f = Radius of receiving optical fibre

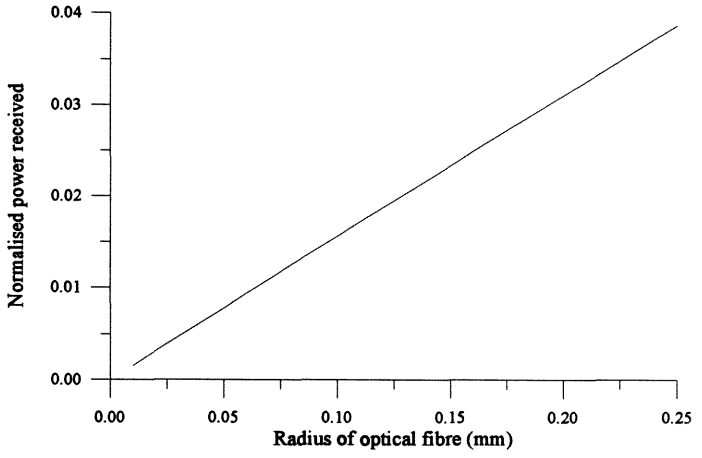

Figure 7-4a The light received by an optical fibre of varying radius when coupled to a column of scintillating material 5mm long, fibre radius wide at 100% efficiency.

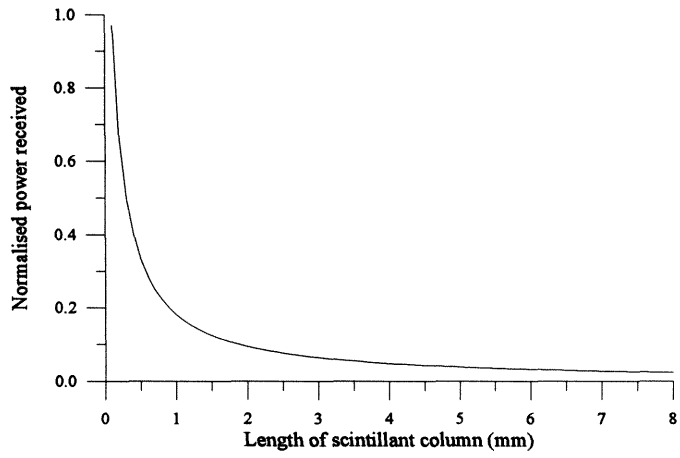

Figure 7-4b The light received by a 0.25mm diameter optical fibre when coupled to a column of scintillating material of variable length assuming 100% efficiency

Figure 7-4 presents two graphs generated by evaluating the integral shown in (Eqn 7-2)[2]. The power received by an optical fibre coupled to a scintillant is dependent on the radius of the optical fibre. A 0.5mm fibre with a source mounted at the tip will receive approximately 3.8% of the light, assuming that the scintillant is fully illuminated and is 100% efficient. The scintillating material further away from the optical fibre is less significant than that closer. This is shown by Figure 7-4b, as the graph is asymptotic to the x axis.

These are purely illustrative calculations. In order to make a quantitative measurement a measure of *photons per unit volume* (efficiency of the scintillant) must also be known.

7.3.3 Preliminary results

In order to investigate the possibility of currently commercially available scintillants to implement a radiation probe for determining endothelial cell damage, a series of preliminary experiments was conducted with a liquid scintillant. A liquid scintillant was chosen because of its higher efficiency than solid state alternatives: a

[2] The diameter of the scintillant was made equal to that of the optical fibre.

sodium-iodide crystal, as used by Swinth *et al* (1976), is typically 2% efficient. It was envisaged that a balloon catheter similar in design to that used in balloon angioplasty be primed with scintillant prior to or during the operation.

A liquid scintillant (Biofluor™, Sigma Chemicals, 1995), a high efficiency emulsifier cocktail, was primed with a Tritium isotope as follows[3]:

0.1 MBeq Tritium : 2.3ml Biofluor

The test sample was then placed into a liquid scintillation counter, along with a standard in order to calibrate the counting equipment and find the efficiency of the liquid scintillation counting system.

Calibration standard data:

Age of standard at time of experiment	:	2789 days
Half life of standard	:	12.4 years
Activity of standard at time of manufacture	:	294.8MBeq

If the half life of tritium and the time elapsed since manufacture is known, it is possible to calculate the theoretical level of radioactivity and hence compare that to the reading taken to calculate the efficiency of the scintillating material.

Decay of tritium: $Y = e^{-\alpha t}$ (Eqn 7-3)

t = time

α^{-1} = Time constant

Theoretical radiation = 192318 counts/sec
Measured radiation = 122150 counts/sec

$$\text{Efficiency of liquid scintillation counter } \zeta \approx \frac{\text{Measured radiation level}}{\text{Expected radiation level}}$$

$$= \frac{122150}{192318} \times 100\% = 63.2\%$$

[3] A Becquerel is equal to one atomic disintegration per second.

The efficiency of the scintillating material was specified by the manufacturer to be approximately 8%.

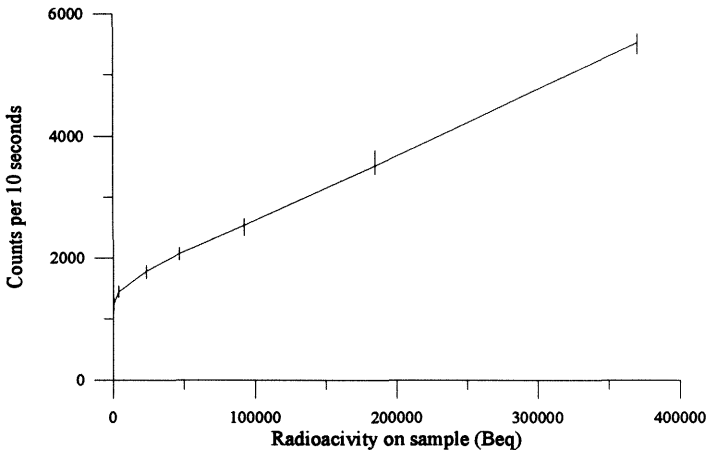

Figure 7-5 The recorded count of a photomultiplier tube as a function of tritium specific activity during ten seconds.

Figure 7-5 illustrates the recorded counts during 10 seconds when using a varying dilution of tritium in a liquid scintillant. A quartz cuvette was placed in direct line with the photomultiplier tube and photons counted for the specified elapsed time[4]. Theoretically a 0.5mm diameter multimode optical fibre should be able to detect 3.3% of this light (Figure 7-4). It is however unlikely as the attenuation of the optical fibre is significant at these short wavelengths, and the scintillating material will scatter and absorb a large percentage of the light emitted.

The theoretical power that a photomultiplier tube (PMT) can detect is defined as the number of photons arriving per second (Eqn 7-4):

$$E_{ph} = \frac{hc}{\lambda} \qquad \text{(Eqn 7-4)}$$

[4] The number recorded by the PMT is not a direct measurement of the number of photons arriving during the elapsed period, purely a figure proportional to that figure.

where E_{ph} - Energy of photon (J)
λ - Wavelength (m)
c - Speed of light in a vacuum (2.9979×10^{8}m/s)
h - Planck's constant (6.626×10^{-34}Js)

This implies that an optical fibre probe connected to equipment able to detect ~ 2×10^{-16} Watts at ultra-violet (300 photons per second, pps) should be coupled to a scintillant generating at least 156250 pps (assuming PMT, scintillant and optical fibre coupling efficiency to be 60%, 8% and 4% respectively). If 1 Beq generates a single photon a 12.5kBeq concentration is required. Labelled monoclonal antibodies are able to generate levels of radioactivity of one order of magnitude less at maximum. It is likely that the concentration would have to be even higher to make the idea feasible.

7.3.4 Discussion

By examination of the data acquired during the experimental analysis shown in Figure 7-5 it may be concluded that a PMT is not an adequate method for determining the quantity of light arising from a scintillator mounted on the tip of a receiving optical fibre. It is possible to measure much lower levels of light that measured in this experiment: Dodd *et al*, (1992) was able to measure 1.2 photons per second. The underlying factor which would however always be cause for concern is the high toxicity of the scintillant. A high efficiency liquid scintillant (≈8%) such as xylene or naphthalene in phenylcycohexane is extremely toxic, and although it may theoretically be pumped into a compliant chamber only when required, balloon rupture into the cardiac or indeed any artery could cause serious damage or fatality. This factor was apparent when conducting the experimentation using Biofluor™. The scintillant vehicle Toluene $C_6H_6CH_3$ was able to quickly dissolve the polymer optical fibre cable and is also carcinogenic if ingested.

7.3.5 Conclusions

The optical fibre radiation probe using scintillation may have applications in other areas of engineering that are not medical in which radiation levels are higher. Currently available materials are not viable for *in-vivo* use for the reasons discussed above. Solid-state plastic or crystalline scintillants are available but have a further

reduced efficiency (<2%) The system may be improved by replacing the polymer optical fibre with that of quartz construction to reduce attenuation at UV wavelengths. The low levels of radiation arising from the labelled monoclonal antibody are not high enough to make the photons detectable without careful design considerations and exposing the inlet window of the PMT for long periods of time.

7.4 The fluorescence probe

To overcome the toxicity and low efficiency problems associated with the radio-labelled monoclonal antibody it was proposed that a fluorescent dye labelled antibody be used as an alternative. The fluorescent marker could then be detected optically by an intravascular probe.

7.4.1 An overview of fluorescence

Fluorescent labelling of tissues is used in cardiology and other medical fields to target specific sites of interest. A report by Bartorelli *et al* (1991) described the use of a helium-cadmium laser (325nm) launched through a quartz optical fibre to distinguish between non-calcified and calcified atheroma for selected targeting of sites for laser ablation. The technique of fluorescence spectroscopy involves the analysis of light returning from the target area in comparison with the light striking it. Spectral analysis of this data defines the fluorescence: typically a high-energy UV laser is used. Expert systems have been developed to provide decision support to evaluate the emitted spectra (Cothren *et al.*, 1994). Systems have also been developed to examine, not the arterial wall, but the constituents of the blood directly: Water, oxidised and deoxidised haemoglobin (Nahm and Gehring., 1994).

Fluorescence is the ability of a material to re-emit a photon at a lower energy (longer wavelength) when struck by a higher energy photon, this is known as Stoke's shift (Wilson and Hawkes., 1989). Phosphorescence is a case of fluorescence where the material is able to re-emit photons a longer time (>~1mS) after the excitation light source has been removed: the electron takes an increased period of time to fall to a lower energy band. Phosphorescence and fluorescence can be measured by a technique

known as time-resolved fluorescence. The material or sample is excited with a short burst of energy (~10nS) and the decay of photons re-emitted is measured (Schneckenburger *et al.*, 1993).

Time-resolved fluorescence was performed *in-vivo* by Schneckenburger *et al*, (1993). Individual mammalian cells contain varying concentrations of photosensitising porphyrin. If the sample is excited with a high power light source, such as a frequency-doubled Hd-YAG laser (532nm), then time-gated microscopic equipment is able to determine the levels of each porphyrin by timing the decay of re-emitted photons at a characteristic wavelength.

Fluorescence is best analysed by quantum theory. Each electron in a material possesses a discrete energy level, E_1, which, when struck by a photon of sufficient energy, will rise one or more levels higher to a level, E_2. A photon is re-emitted when the electron returns to a lower energy band.

$$E_{ph} = \frac{hc}{\lambda} \qquad \text{where } E_{ph} > E_2 - E_1 \text{ for absorption to occur} \qquad \text{(Eqn 7-5)}$$

Since phonons as well as a photon are usually released, the photon is of lower energy, i.e. of longer wavelength.

The unique ability of a fluorescent material to re-emit photons at a different energy to those exciting it make detection of fluorescence an apparently simple task. The standard method, as adopted in this case, is to sample the absorption and emission wavelengths optically and calculate the ratio between the two (Eqn 7-6):

$$\text{Fluorescence (Ratio)} = \frac{\text{Intensity of light emitted at emission wavelength } '\lambda_2'}{\text{Intensity of light absorbed at excitation wavelength } '\lambda_1'} \quad (<1)$$

(Eqn 7-6)

7.4.2 Designing a fluorescent probe for intravascular use

The fundamental difference between the design of the radiation probe and that of the fluorescent equivalent is the manner in which the *internal energy* is not responsible for providing the output signal, i.e. photons do not arise from the probe tip directly as a consequence of a beta particle raising an electron to a higher energy level. Fluorescence represents the release of a photon as a electron falls to a lower energy level having previously been *stimulated* to a higher energy band by an excitation light source at a wavelength characteristic of the fluorescent material used.

The proposed design was considerably simpler than that of the radiation probe discussed earlier. Two probe designs were considered (Figure 7-6), and differ only in the manner in which the fluorescent material is excited.

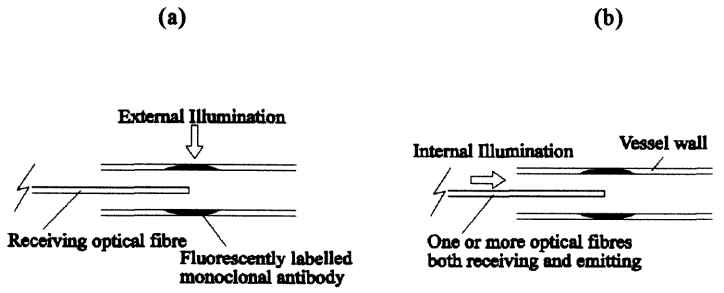

Figure 7-6 The configurations of the optical fibre fluorescent probe using an external and *in-vivo* launched light source.

The main consideration when designing an optical probe for intravascular use is the condition in which the device should operate. The presence of whole blood flowing along the vessel during the study will significantly attenuate the light travelling from the fluorescent target to the probe tip, and in the case of Figure 7-6b, that illuminating the target. The optics, fluorescent material and light sources must be carefully selected.

7.4.3 Fluorescent probe feasibility

Prior to development of the optical fibre probe a series of preliminary investigations and calculations were performed to determine whether the design was more feasible than the radiation optical fibre probe.

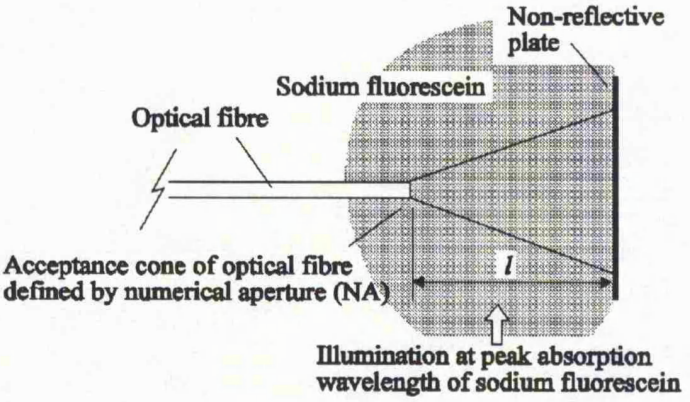

Figure 7-7 Determining the feasibility of the optical fibre fluorescence probe by calculation of the solid angle defined by the acceptance cone of the optical fibre.

It was envisaged that the probe would consist of a modified optical fibre (section 7.4.5.2) and would not contain an active element as in the aforementioned scintillation probe design. By consider the solid angle of each of the elements in the cone length '*l*' (Figure 7-7) it may be seen that:.

$$\text{Normalised light flux received} = \frac{\int_0^{l}\int_0^{x.\tan\left(\frac{\pi}{6}\right)}\int_0^{2\pi}\frac{A_f}{4\pi\left(x^2+r^2\right)}.rd\theta.dr.dx}{\int_0^{l}\int_0^{x.\tan\left(\frac{\pi}{6}\right)}\int_0^{2\pi}rd\theta.dr.dx} \qquad \text{(Eqn 7-7)}$$

where A_f = Cross-sectional area of optical fibre

$\pi/6$ = Acceptance angle of optical fibre

l = Length of cone

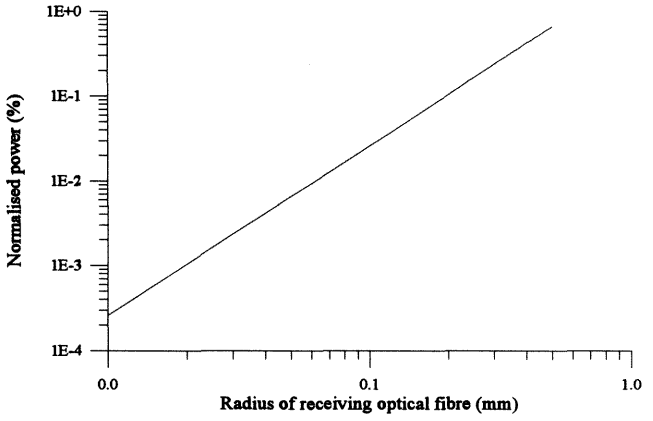

Figure 7-8a The proportion of light received by an optical fibre of varying diameter when immersed in a fluorescing solution (100% efficient) subtending and angle defined by the numerical aperture (NA=0.5) showing a square law.

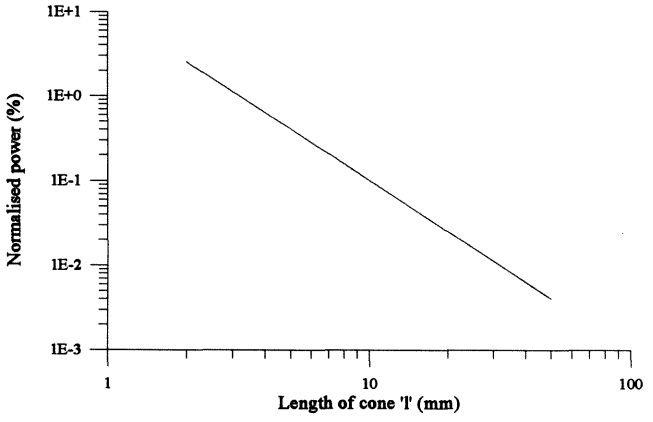

Figure 7-8b The light received by an optical fibre 0.25mm diameter when varying the depth of a cone subtended by the acceptance cone of the receiving optical fibre: cone depth is 50mm (100% efficiency is assumed).

The above figures illustrate the solution to Eqn 7-7, varying the radii of the receiving optical fibre and the depth of the cone subtended by the acceptance cone of the receiving optical fibre respectively. The percentage of light received by the optical fibre increases from 0.04% to 0.16% when the radius is increased from 0.125mm to 0.25mm. When the length of the cone subtended increases, the volume of the material

at a further distance away is not as significant as that closer to the face of the receiving fibre and explains the overall proportion of light falling.

$$\text{Power received} \propto \frac{1}{(\text{Length of subtended cone } 'l')^2} \qquad \text{(Eqn 7-8)}$$

Although the percentage received is low (and will be even lower due to the photon counting technique and the efficiency of the fluorescent material) the fluorescent material may be excited by a light of a higher intensity to compensate. This is the fundamental difference between the fluorescent and radiation probes.

To confirm this hypothesis an experiment was conducted using a fluorescent solution: sodium fluorescein, at varying dilution illuminated by a 20Watt filtered halogen light source. A 0.25mm diameter optical fibre was then lowered into the solution and the light recorded at the excitation and absorption wavelength. The ratio was then calculated to produce a measure of fluorescence.

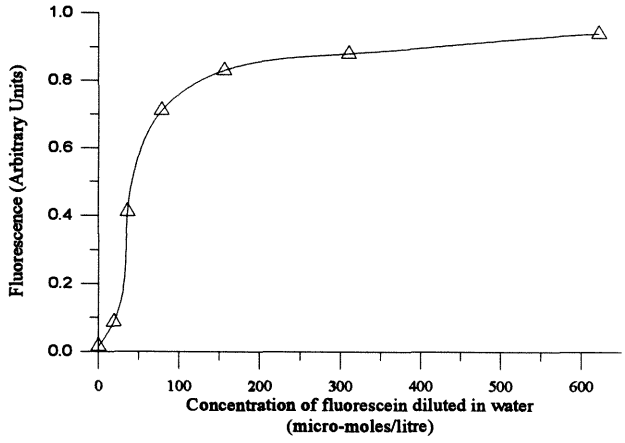

Figure 7-9 Measuring the fluorescence of sodium fluorescein with a 0.5mm diameter optical fibre, NA of 0.5 and a subtended cone of depth '*l*' 50mm plotted on a linear scale

The data clearly illustrates the sodium fluorescein can be detected using narrow gauge multimode optical fibres: 0.5mm diameter. The curve has a plateau region above ~100μMole/l. This is because the vehicle (in this case distilled water, see section 8.2, chapter8) is saturated and cannot dissolve any more solution; hence does not contribute any further fluorescence. This issue is discussed further in chapter 8.

The use of fluorescence as a optically detectable biochemical label is feasible. The selection of the material is dependent on the absorption spectrum of the blood (section 7.4.4), the power of the light source can be increased to compensate for this. The wider selection of commercially available fluorescent materials means that an appropriate non-toxic compound may be found.

7.4.4 Selection of the fluorescent material

Spectrophotometry is used for determining the concentration of an unknown dilution given a control solution at a known concentration. The technique is able to produce a measurement of absorption in arbitrary absorption units (AU), but does not provide information regarding absolute absorption (measured in decibels, dB). In the selection of the fluorescent material and the power of the light source it was necessary to find the absolute value of the optical extinction coefficient (m^{-1}) of the blood. Blood absorption data only appears to have been reported in the literature in arbitrary absorption units. The following procedure was used to establish the absolute absorption spectrum.

Light from a Helium-Neon (HeNe) laser was fired through samples of dilute blood solution of known concentration to determine the extinction co-efficient at 632nm (Figure 7-10). A series of blood / saline dilutions were mixed and loaded into a cuvette: the path length of the laser through the cuvette (not including the cuvette wall was 3mm). Readings were also taken with the cuvette loaded with saline to compensate for absorption not originating from the blood, i.e. in the wall of the cuvette and the saline vehicle of the blood dilution.

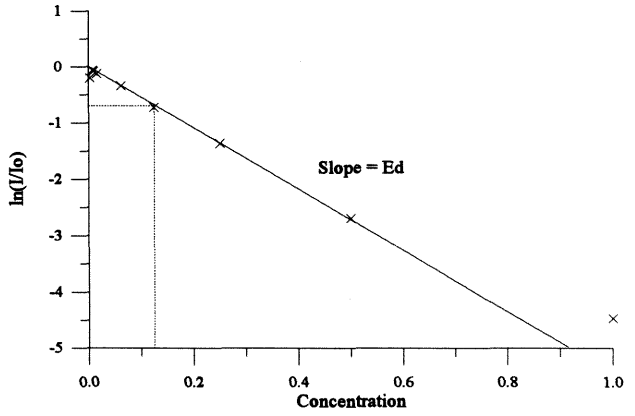

Figure 7-10 The absorption of blood at 632nm at varying concentration

The absorption of monochromatic light in a material is defined by Beer-Lambert's law, stating the intensity of the light at a given distance through the material (Prys-Roberts., 1969) (Eqn 7-9).

$$I = I_o e^{-Ecd} \qquad \text{(Eqn 7-9)}$$

I_o	=	Light intensity at distance zero
E	=	Extinction co-efficient
c	=	Concentration of sample
d	=	Distance through sample

$$\Rightarrow \quad c \propto \ln\left(\frac{I}{I_o}\right) \qquad \text{(Eqn 7-10)}$$

The gradient of this curve (Figure 7-10) is proportional to the extinction co-efficient. The absorption of the blood / saline dilution at higher concentrations is less reliable that that of low concentrations due to the scattering of the light, diverting the light away from the detector.

Extinction co-efficient 'E' at 632nm (Figure 7-10) = $1.95\times10^{3}m^{-1}$

Using a spectrophotometer the absorption of blood at 1:8 concentration was determined to be 91.2AU.

$\therefore$ Extinction co-efficient of blood E_{blood} = 21.34 AU m^{-1} at 632nm

The absorption of blood across the range of the spectrophotometer is now defined and may be expressed in absorption in decibels (dB) from (Eqn 7-11) where:

$$\text{Power 'dB'} = 10\log\left(\frac{I}{I_o}\right) \qquad \text{(Eqn 7-11)}$$

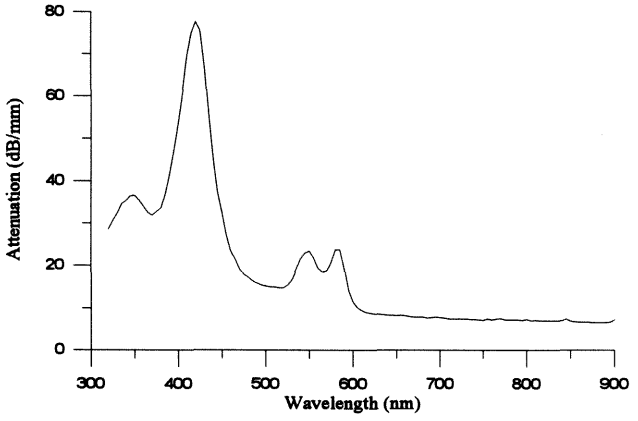

Figure 7-11 The absolute absorption of oxygenated blood from 300nm to 900nm expressed in dB/mm

Figure 7-11 shows that the absorption of blood at unit concentration is considerable, and peaks at ≈420nm. To maximise the efficiency of the system, absorption due to blood should be minimal. This implies two possible operating windows:

- Above 600nm
- 480 to 560nm

Ideally the material selected for labelling the monoclonal antibodies should be selected to have a peak absorption and emission in either of these windows.

Porphyrins naturally exist in the human body and can been seen to fluoresce in the red end of the visible spectrum. A system developed by König *et al* (1992) described the development of an optical fibre probe for determining the level of three types of porphyrin: zinc protoporphyrin (600nm), coproporphyrin (620nm) and protoporphyrin (640nm), in the skin by illuminating the area externally with a krypton ion (Kr^+) laser (406.7nm). The technique was used as a therapeutic aid to assist in the destruction of bacteria acting as cytotoxic sensitisers. An earlier study by Sayer *et al* (1974) described a series of experiments conducted with oxygenated and deoxygenated blood and demonstrated that the porphyrin contained within the haemoglobin was responsible for the series of two peaks shown in Figure 7-11 at 600nm and 650nm. The level of fluorescence detected is dependent on the level of haemoglobin in the artery at the time of the measurement, and hence an unreliable wavelength to select for fluorescently labelling the monoclonal antibody. Biochemically labelled antigens have however been used in the past to determine antibody-antigen reactions: viewed as an increased fluorescence spectra when antibody-antigen binding occurs (Turko *et al.*, 1992).

Sodium fluorescein ($C_{20}H_{10}Na_2O_5$), an inert fluorescent salt, was considered to be more suitable for labelling the monoclonal antibody. It differs from the porphyrins in the respect that the absorption and emission wavelengths are close together in the second low absorption window. Porphyrin is already present in the blood haemoglobin, and it was envisaged that there could be difficulty in separating that naturally present to that labelling the monoclonal antibody (Stryer., 1975). The absorption, and hence peak spectral response of the sodium fluorescein is at 492nm. This is in a lower absorption window than that of UV light (~300nm) which is used to excite porphyrins. UV is attenuated by the haemoglobin more readily (Figure 7-11). For this reason sodium fluorescein was selected to label the monoclonal antibody, and was also used as a dilution of variable concentration during the experimental development of the final probe design. The absorption and emission spectra of sodium fluorescein is depicted in Figure 7-12.

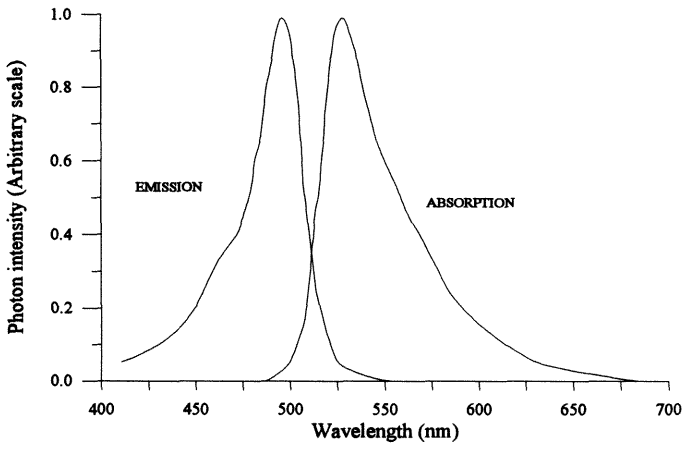

Figure 7-12 The absorption and emission spectrum of sodium fluorescein. (Sigma Chemicals UK Ltd., 1995)

7.4.5 Hardware design and construction

The following section gives full details of the hardware and software developed to control the endothelial cell damage probe withdrawal from the vessel and the data acquisition and analysis. Use of the probe in a clinical environment would require the use of a guide wire (see chapter 6). This includes the selection of the optics and the light source used to excite the fluorescently labelled monoclonal antibodies. A summary of the equipment and its interconnection is given in Figure 7-13.

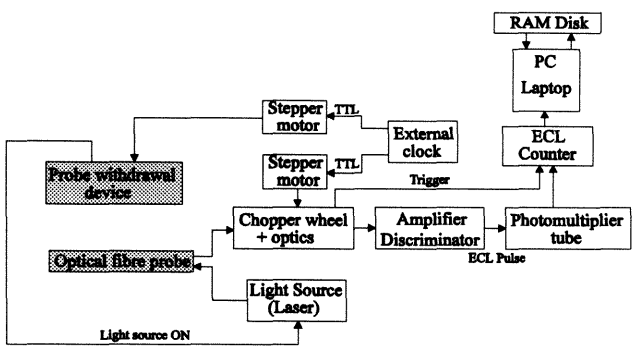

Figure 7-13 The hardware and software interaction and interconnection for the prototype endothelial cell damage probe using a fluorescently labelled monoclonal antibody.

7.4.5.1 The excitation light source

The two fluorescent probes (illustrated in Figure 7-6) required the development of two different types of light source: an external and *in-vivo* device. The simplest method to implement, and that used in the early design stages, was an external source. It was hoped that a high power light source of appropriate excitation wavelength be placed outside the patient whilst simultaneously monitoring the absorption and emission wavelengths of the sodium fluorescein label from an optical fibre probe within the vessel. A 20Watt tungsten halogen dichroic lamp (chosen because of its efficiency at the blue end of the electromagnetic spectrum) was fitted with a 470nm close-band bandpass filter[5] as part of laboratory bench-top tests. For reasons discussed in chapter 8, section 8.3.3.3 it was later replaced with an *in-vivo* launched device given the considerable level of absorption of the tissue of a thickness of 10mm or more: at 492nm the absorption of whole blood was measured to be ~15.7dB/mm using the method described in section 7.4.4.

The *in-vivo* excitation light source must be efficiently focused into the face of the optical fibre carrying the light to target area to provide adequate sensitivity. The dichroic lamp, described above, is designed to focus the visible and UV to a spot (the diameter of which is dependent of the profile of the dichroic reflector) whilst the IR, far-IR and heat passes through the back of the reflector away from the focal point. If such a light source is to be used it must be able to be focused to a point less than the diameter of the optical fibre core, and with a NA less than that defined by the fibre core-cladding interface.

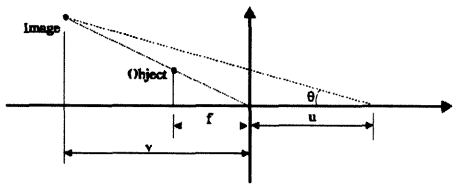

Figure 7-14 Ray diagram of the standard lens equation lens diameter 'ϕ'

[5] The absorption and emission wavelength of sodium fluorescein are separated by 58.8nm, whilst the non-ideal bandwidth of the optical filters were 60nm. The filters were selected to ensure that the skirts of passband of the absorption and emission filters did not overlap significantly.

The implication of the requirement of an optical fibre launched light source initially lead to the development of a compound collimating optical system for the dichroic lamp, however the parabolic profile of the lamp reflector made an apparently simple technique impossible. At its best correctly matched optics can only reduce the image of the source (in this case the tungsten filament) to its original size, and not to a point source (see below):

The standard lens equation : $\frac{1}{f} = \frac{1}{u} + \frac{1}{v}$ (Eqn 7-12)

If angle 'θ' is small

Numerical aperture of optical fibre 'NA_{fibre}' $\approx \frac{\phi}{2u}$ (Eqn 7-13)

Numerical aperture of light source 'NA_{source}' $\approx \frac{\phi}{2v}$ (Eqn 7-14)

$\Rightarrow$ Magnification 'M' $\approx \frac{v}{u}$ (Eqn 7-15)

Lens coupling efficiency 'ζ_{lc}' $= \frac{(NA_{fibre})^2}{(NA_{lens})^2} = \frac{u^2}{v^2} = \frac{1}{M^2}$ (Eqn 7-16)

i.e. the magnification M is fixed by the NA of the source.

Having established that only a parallel beam may be focused down to a point, the obvious choice is that of the laser. The use of the laser also removes problems associated with the filtering of a broad band light source due to its narrow line width. The peak absorption wavelength of the fluorescein is 492nm (Figure 7-12), in order to obtain maximum efficiency the principle wavelengths of the laser should be as close as possible to 492nm. There are three possible viable alternatives:

- **Dye laser** - Tuneable across a wide range of wavelengths, when pulsed it is able to provide up to 50W average.
- **Nd-YAG** - The Nd-YAG has a principal wavelength of 1.064μm, when frequency doubled this may be reduced to 532nm.
- **Argon Ion** - The argon ion gas laser has a series of lines, the closest being 488nm, continuous wave (CW).

The Dye laser is generally of a pulsed type (PW), and usually of extremely high power. Although the power may by reduced, the system may stop lasing if the power is reduced too much (10-20mW, the power may be however be reduced using a neutral density filter). Such high power lasers may cause further vascular damage if launched *in-vivo* puncturing the vessel wall. This was a problem with the early atheromatous plaque ablation techniques when using a PW laser (Litvack., 1994). The frequency doubled Nd-YAG laser will provide a single wavelength, but at 532nm it is extremely close to that of the emission wavelength (550nm). The wavelength is also of a lower energy and may not be sufficient to produce a fluorescent reaction. The optimum solution is the argon ion laser. The active medium is a plasma of excited argon ions, the multiple collisions of the ions within the plasma tube excite them to a series of high energy bands. They are excited still higher into the lasing wavelengths by the introduction of a high current across the plasma tube.

The laser was focused into the fibre using a microscope objective. The NA was chosen so as to be less than that of the optical fibre (NA=0.3, Olympus #103844), and aligned using a custom constructed laser alignment system with 3 degrees of freedom (Schematic in appendix B.1).

7.4.5.2 Construction of optics and probe design

The optical fibre probe *optrode* was designed in consideration for its use in the blood stream. The light rays entering and leaving the optical fibre will be refracted more in a polymer/air or silica/air interface than that in blood[6]. From Snell's law (Powers., 1993):

$$NA_{immersed} = \frac{\sqrt{n_1^2 - n_2^2}}{n_3} \qquad \text{(Eqn 7-17)}$$

where n_1 and n_2 are the refractive index of the core and cladding of the optical fibre, and n_3 is the refractive index of the blood.

[6] For the purposes of the probe design the refractive index of blood was assumed to be that same as that of saline ≈ 1.33 (Kajita *et al.*, 1987).

The design of the optrode tip has been explored extensively by several researchers involved with lasers in medicine (Benner *et al.*, 1991). Depending on the application, the probe tip is designed to either converge or disperse the radiation over the target area. The commonest probe design is the addition of *microbulbs* or *micro-spherical* lenses to the tip of an optical fibre. The bulb-ended surface may then be made either concave or convex to diverge or converge the light respectively.

The endothelial cell damage is on the wall of the cardiac vessel and hence parallel to the neutral axis of the optrode. Given the high absorption of the blood even at the optimised sodium fluorescein wavelengths:490nm and 550nm, the ray path length from the target to the optrode should be minimal, i.e. ideally the ray should be perpendicular to the neutral axis of the optical fibre. A *sapphire* tip is the closest that can be achieved (Fankhauser *et al.*, 1989) (Figure 7-15).

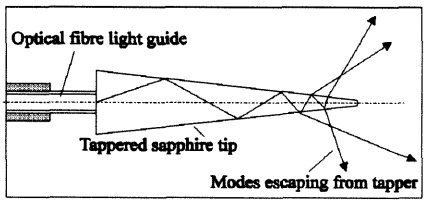

Figure 7-15 The path of a light ray travelling through a sapphire tip (Fankhauser *et al.*, 1989)

The main disadvantage of the design is that the high-order modes are coupled out before they reach the end of the optical fibre and consequently the amount of radiated energy is small. Tapered optical fibres are also expensive and difficult to make in a miniature form (<0.5mm OD).

The final design of the probe used two 0.25mm OD polymethylmethacrylate optical fibres: one to emit the excitation radiation: 488nm from the Ar^+ laser, and a second to receive at 550nm. The duplex pair was then enclosed in a 0.94mm diameter tube which was perfused with saline to form a bolus at the probe tip to assist in reducing the attenuation effects of the blood. The 10μm cladding was dissolved 1mm from the probe tip by dipping it into toluene. The solvent also had the effect of making

the optical fibre face convex further assisting in dispersing the light at the probe tip (Figure 7-16).

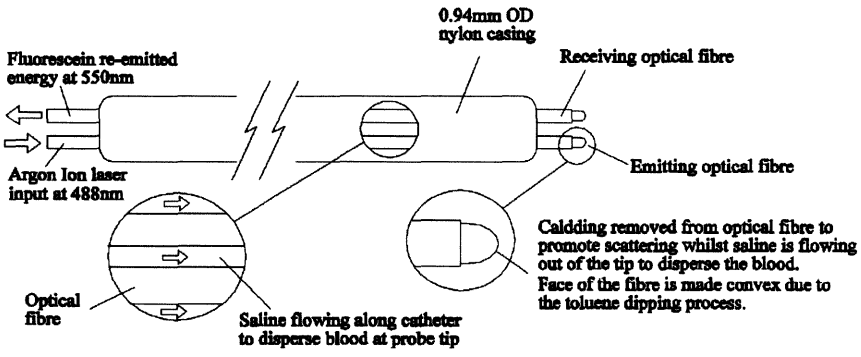

Figure 7-16 The design of the optical fibre fluorescent endothelial cell damage probe with *in-vivo* launched light source

The removal of the cladding means that the high order modes leave the fibre, similarly high order modes will be permitted to enter the optical fibre and will be refracted towards the core as it is the optically denser material. Further details on the optical fibre connectors and modifications are given in appendix B.2, along with materials used in appendix B.3.

7.4.5.3 The beam-splitter

In order to sample the incoming light at the absorption and emission wavelengths of the sodium fluorescein a low-dark-current PMT was fitted with an optical chopper wheel consisting of two bandpass filters at 490nm and 550nm and an opaque blanking plate to provide a means of monitoring the dark current[7].

[7] The input window of the PMT was quartz, selected because of its low attenuation at the blue end of the electromagnetic spectrum. Monitoring the dark current was performed to ensure that the output did not drift due to an excessive amount of light falling on the dynodes.

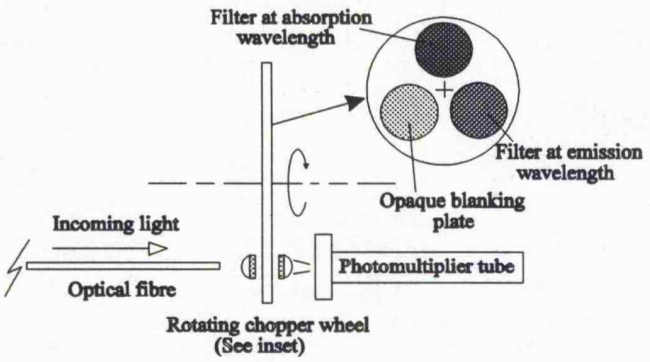

Figure 7-17 The PMT and optical chopper wheel beam-splitter arrangement used for detecting fluorescence.

The light leaving the receiving optical fibre is coupled to the photomultiplier tube from the optical filter with two aspheric crown glass condenser lenses. It is important to ensure that the first lens is matched to the NA of the optical fibre (0.5), and the face of the fibre is located at the focal point of the lenses. Parallel rays will then emerge, passing through the optical filter and into the window of the PMT. The dynodes of the PMT are 10mm in diameter and imply that the NA of the recovered filtered light is not critical. The details of the PMT calibration are given in appendix C.

$$'f' \text{ Number} = \frac{\text{Diameter of lens } 'D}{\text{Focal length of lens } 'l} \qquad \text{(Eqn 7-18)}$$

The diameter D *must* be large enough to ensure that all of the light is captured by the lens when the optical fibre is at the focal point. Hence

$$\tan\theta_c = \frac{D}{2l} = \frac{f}{2} \qquad \text{(Eqn 7-19)}$$

where θ_c = Critical angle of internal reflection

Given the NA of the aspheric lenses and fibres, and the efficiency of the bandpass filters the overall efficiency can be calculated:

NA of aspheric lens = 0.47
NA of optical fibre = 0.50
Efficiency of bandpass filter at centre frequency = 0.4 (specified by manufacturer)

$$\therefore \text{ Coupling efficiency} = \frac{0.47^2}{0.50^2} \times 0.40 \times 100\% = 35.3\%$$

(cf: Eqn 7-16)

Pulses arising from the photomultipler tube are injected into an amplifier discriminator, in order to reject the pulses at low amplitude arising from Johnson noise, and are then counted with a 32-bit ECL (emitter-coupled logic) counter interfaced to a notebook-size PC. The photon counting process is initiated when the ECL counter is triggered from a +5V rising edge and continues until a software determined count duration has elapsed (Figure 7-18).

Mode	Software available photon count times							
Repeated	100ms	200ms	500ms	1s	2s	5s	10s	20s
F.Repeated	1ms	2ms	5ms	10ms	20ms	50ms	100ms	200ms
E.F.Repeated	50μs	100μs	200μs	500μs	1ms	2ms	5ms	10ms

Figure 7-18 The photon count times available from the software controlling the photomultiplier tube triggered either internally or by an external positive clock pulse.

The photomultiplier tube can be configured in three modes: Repeated, Fast Repeated and Extra Fast Repeated. The mode selected is determined by the required photon count time, and whether an external trigger was required (Extra Fast Repeated mode cannot be triggered externally). Increasing the photon count time increases the sensitivity, but also increases the time required to withdraw the probe over a given distance and hence reduces the feasibility to use such a device in an operating theatre. A count period of 1 second was found to be sufficient for the majority of the experiments. The count period is however stated with each set of data in chapter 8.

The use of a single detector means that data must be acquired sequentially whilst the probe is withdrawn back along the artery at a speed synchronous to the chopper wheel. Both the chopper wheel and probe withdrawal device were driven by 1.8° stepper motors. A gray-code shaft-encoder coupled to the chopper wheel and an appropriately programmed EPROM provided 3 pulses per turn and was used to initiate

the photon count sequence for the absorption and emission wavelengths of the sodium fluorescein, and the dark current of the PMT respectively (Figure 7-19).

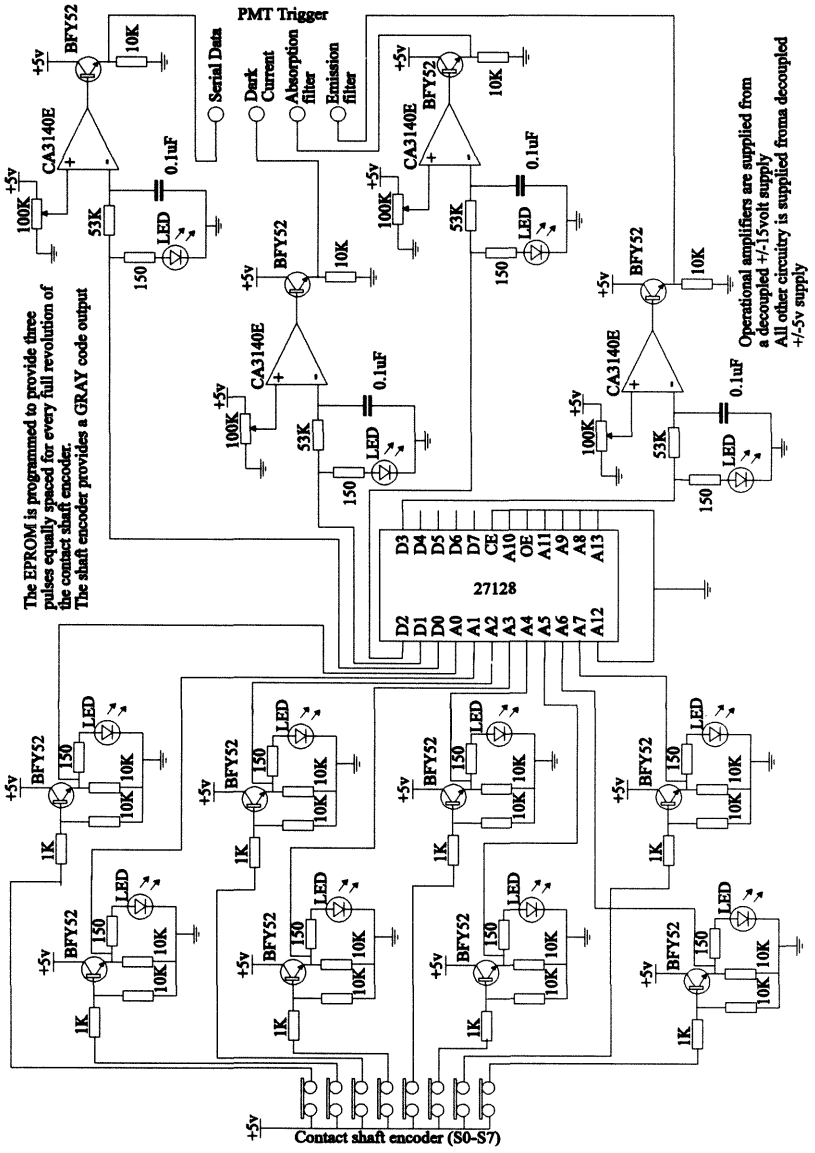

Figure 7-19 A schematic of the endothelial cell damage probe chopper wheel trigger control system.

7.4.5.4 The probe constant velocity withdrawal system.

The location of the probe in the artery is calculated by analysing the time spacing between adjacent samples of data as it is buffered from the ECL counter. A constant withdrawal rate is achieved using a belt and pulley arrangement which in turn is driven by a stepper motor; hence given the physical sizes of the pulleys and the mechanical advantage gained due to the gearing it is possible to calculate the distance covered by the moving probe when feeding each of the stepper motors with a fixed frequency (Figure 7-20).

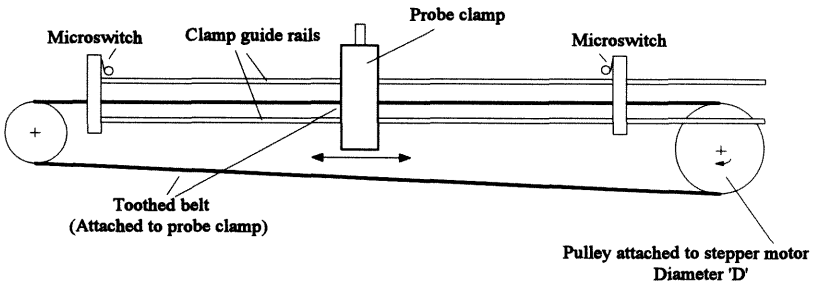

Figure 7-20 A schematic illustration of the optical fibre probe withdrawal device.

Elapsed counting time during 'n' samples = $\left(\frac{n}{3 \times F_{cw} \times S}\right)$ sec (Eqn 7-20)

Velocity of withdrawal device = $\left(F_{wd} \times S \times \pi D\right)$ m/s (Eqn 7-21)

where S = Stepper motor step size as a fraction of a single revolution
F_{cw} = Clock speed of chopper wheel stepper motor
F_{wd} = Clock speed of withdrawal device
D = Diameter of pulley attached to withdrawal device
n = Number of counts in data stream

The distance 'l' representing a serial stream 'n' samples arriving from the chopper wheel is the product of the velocity of the withdrawal device and the time elapsed during 'n' samples:

i.e. $'l' = \left(F_{wd} \times S \times \pi D\right)\left(\frac{n}{3 \times F_{cw} \times S}\right) = \frac{n\pi D F_{wd}}{3F_{cw}}$ m (Eqn 7-22)

Both the chopper wheel and the vascular withdrawal device are driven by identical stepper motors with a step size of 1.8° ($S = 0.005$). It is now possible to calculate the position of the optical probe by calculating the offset from the starting position.

If the probe is to be of practical use to a physician the equipment must be relatively easy to use. For this reason additional control circuitry was integrated into the automatic withdrawal system, consisting of an auto-reverse and manual start feature which was also able to control the light source (Figure 7-21).

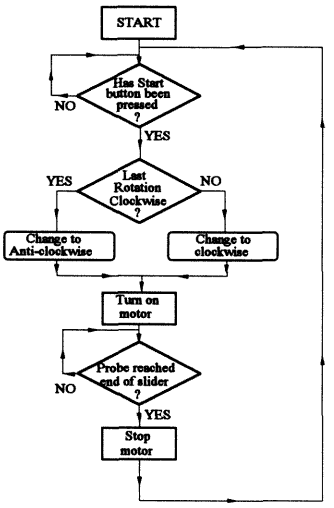

Figure 7-21 Flow chart of withdrawal system control.

The control circuitry was constructed using a *SR flip-flop* arrangement implemented in TTL logic, the change in state of the output can then be used to reverse the direction of the stepper motor at digital level. Micro-switches located at the end of the linear track provided the appropriate logic state to start and stop the stepper motor (Figure 7-22).

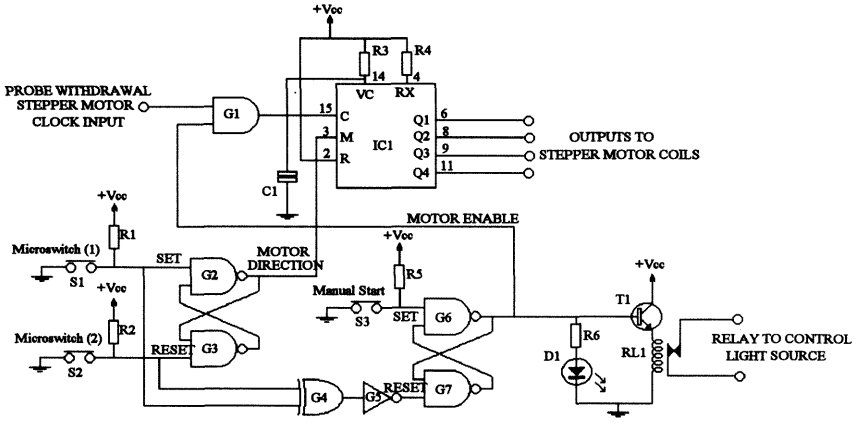

Figure 7-22 The circuit diagram of the optical probe constant speed semi-automatic controller.

7.4.5.5 Software implementation and data acquisition

The operation of the photomultiplier tube was controlled principally at software level, the output being a series of discrete current pulses. In order to take a measurement the photon tube must be assigned a finite time slice during which photon counting occurs (Figure 7-18). During this time it is assumed that all other operations are stopped. The count-rate was minimised to remove non-linearity arising from the PMT *dead time*.

The software provided by the manufacturer of the PMT did was not able to group and display the incoming data to calculate fluorescence in real-time and had to be written specifically for this application. A software package was written in C to solve this problem. The original object code, complied from Quick Basic V4.5 (Microsoft™), was utilised to access the original count routines. The interlinking process at object code level allows the production of a single piece of executable code whilst still using the original hardware control procedures, but with the added advantages of the flexibility of C. Although both languages are written by Microsoft™, the linking of C and Quick Basic yields complications which initially were not

apparent. When producing the final code there must be only one executable address. This is provided by Quick Basic and cannot be changed unlike C which is dependent on the definition of the *main(void)* function. Consequently the entry address exists in Quick Basic and the C code is treated as sub-routine even though it contains the vast majority of the procedures and functions.

C version 5.1 (chosen to be compatible with Quick Basic) is not able to support large arrays. A *huge memory model* and dynamic memory allocation could not be used with Quick Basic as the allocated space deletes the Quick Basic code from within C. To overcome this problem a RAM disk was implemented, the array size is then only limited by the RAM disk allocated memory; the data was then *swapped* as required.

The hardware access routines were read from within Quick Basic and the results passed back to the C for storage and display. The arguments for the functions are of reverse order in each of the two languages and also Quick basic can only support 16 bit addresses when using a call by reference implementation. The functional prototypes of the Quick Basic code declared in C involve the use of *near* pointers with a *Pascal* operator to re-order the arguments.

The function prototype for calling a Quick Basic routine from within C as defined in the C header file:

```
extern int pascal counter(int near *PERIOD, int near *QTY, int near *TRIGGER,
                          int near *FULLSCALE, int near *OFFSET, int near *OPT);
```

When the data acquisition option is selected from the menu the Quick Basic functions are transparent and are simply called from within C, a simplified block diagram of the acquisition software is shown in appendix B.4.

Sample screen outputs are shown in Figure 7-23.

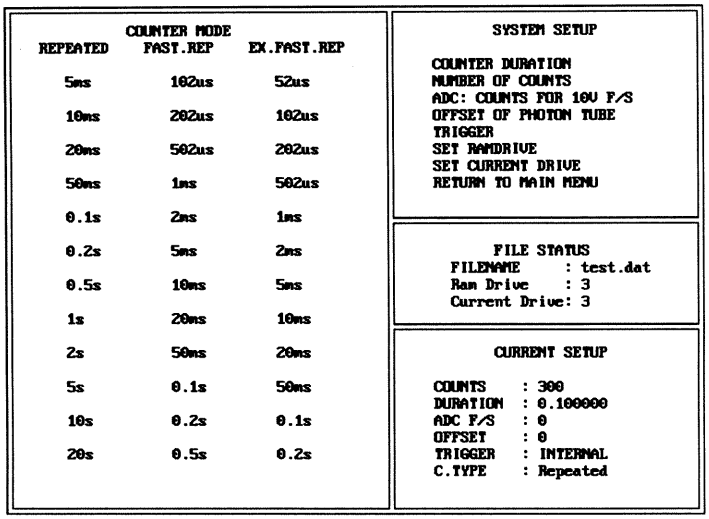

Figure 7-23a The data acquisition software - the setup menu displaying ECL-counter setup options. A similar menu is available for data display, recovery and storage.

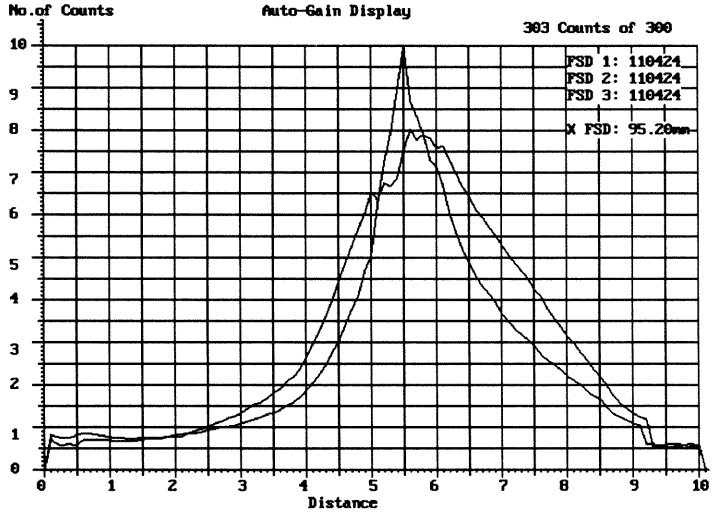

Figure 7-23b The data acquisition software - acquired data recovered from ram-disk displaying the absorption and re-emission of sodium fluorescein.

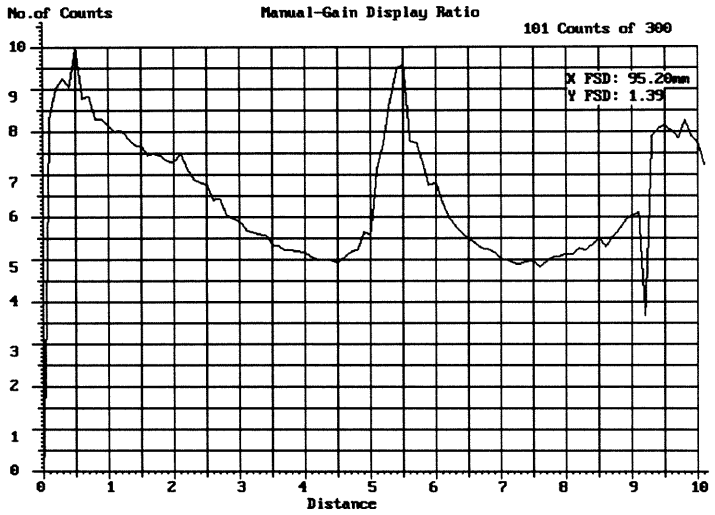

Figure 7-23c The data acquisition software. On-line calculation of the ratio between the intensities of the absorption and emission wavelengths of sodium fluorescein. Centre peak indicates evidence of fluorescence.

7.5 Discussion - Radiation or fluorescence?

The optical fibre fluorescence probe has a far more promising future in this particular application than that using radio-labelled monoclonal antibodies (see section 7.3.4). Its simplicity and lack of active component parts makes the design more viable for *in-vivo* use and the preliminary studies proved that it is possible to detect extremely low concentrations of fluorescein (19μMole/l - chapter 8): increasing the power of the excitation light source at the excitation wavelength increases sensitivity. For this reason the fluorescent concept was considered a worth-while pursuit in the development of a probe to detect endothelial cell damage in the post-operative period of PCTA. The fluorescent optrode design does however require considerably more complicated and expensive optics than that designed on scintillation. The wavelengths of the photons generated from the scintillant are not well defined because of the *cocktail* of chemicals in the manufacture of the material. This means that all of the light

must be captured by the PMT in order to make a measurement, and there is no distinction between wavelengths; the optics are hence less complex.

It is envisaged that as the technology improves, detectors becoming more sensitive, and scintillants more efficient that the radiation probe may again be addressed for an *in-vivo* study. The current main concern is the leakage of the highly toxic scintillant into the blood stream.

A series of further laboratory and clinical trials were conducted on the fluorescein probe to further validate its potential for *in-vivo* use and as a tool for evaluating damage to the cardiovascular wall. These results are presented in chapter 8.

Chapter 8

Validation of the optical fibre endothelial cell damage probe

8.1 Introduction

This chapter summarises the results obtained using the equipment described in chapter 7 obtained during the development of the endothelial cell damage probe biosensor. Experiments were conducted using varying dilutions of sodium fluorescein contained in a *dummy* artery simulating fluorescently labelled endothelial cell damage to confirm the viability and methodology. The experimentation was then extended to using fluorescently labelled monoclonal antibodies bound to damaged endothelial grown *in-vitro* and using mammalian (human, rat and rabbit) models. This involved the use of sodium fluorescein injected into the wall of a harvested vessel, and sodium fluorescein conjugated heparin introduced by a perforated angioplasty balloon.

8.2 Clinical and laboratory methods

It was initially envisaged that the subject area would be illuminated from outside the body. Consequently, during the investigation results were obtained using both an external and *in-vivo* light source. This also permitted earlier laboratory experiments to be conducted without the need for laser safety precautions such as interlocking doors.

A sodium fluorescein solution was prepared at a concentration of 622μMole/l, from here onward referred to as the *control* and was the most concentrated dilution used. The control was then diluted in successive factors of two to form the following:

Dilution of sodium fluorescein (μMole/l)							
Control	Sol^{n} (1)	Sol^{n} (2)	Sol^{n} (3)	Sol^{n} (4)	Sol^{n} (5)	Sol^{n} (6)	Sol^{n} (7)
622	311	156	78	36	19	10	5

Figure 8-1 The dilutions of sodium fluorescein used to simulate varying degrees of endothelial cell damage in the preliminary experimentation

Experiments were not conducted on living tissue and consequently clinical sterilisation was not necessary, however due to the low cost of each device each catheter was deemed to be disposable[1].

8.3 External light source

This first group of experiments is a summary of the investigations performed using an external light source for illuminating the target area containing the fluorescent material.

8.3.1 A simulated artery

8.3.1.1 Method and motivation

A false vessel, simulating endothelial cell damage, was constructed from a length of translucent PVC tubing comparable in size to the diameter of a typical human cardiac artery (≈3mm ID). A helix of transparent narrower gauge nylon tubing (0.25mm ID) was then arranged in 5 turns around the circumference of the former tube. The helix could then be perfused with a sodium fluorescein solution of variable concentration to simulate varying levels of damaged labelled endothelial cells. The optrode, comprising a single 0.25mm polymer optical fibre with a shaped tip (see chapter 7), was then withdrawn at a constant velocity along the vessel past the fluorescent region. The effects of attenuation due to the presence of blood was simulated by filling the device with 0.5ml of deoxygenated venous blood.

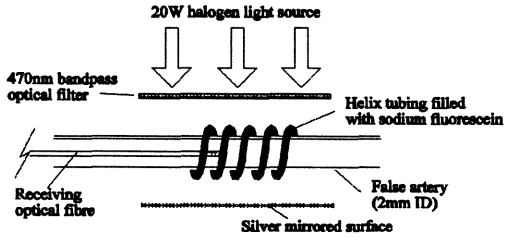

Figure 8-2 A simulated artery excited using a 470nm filtered halogen light source

[1] The figures expressed in this chapter are dimensionless unless otherwise stated due to the ratio between absorption and emission wavelengths calculated to describe fluorescence.

8.3.1.2 Test EL 1 - Saline perfusion

The results illustrated in Figure 8-3a-h show varying concentrations of sodium fluorescein dissolved in distilled water (cf: section 8.2). A simulated artery was enclosed in a light shielded casing and exposed to filtered light: 470nm ±30nm emanating from a 20W halogen light source. A 0.5mm diameter polymethylmethacrylate optical fibre was withdrawn along the vessel over a length of 100mm whilst sampling absorption, emission and PMT dark current at 1mm intervals (300 samples taken in total). The ratio between the absorption and emission wavelengths was then calculated as shown in chapter 7. A 0.25mm ID tube was used for the helix and consisted of 5 turns. The simulated artery was filled with saline and so absorption due to blood flow was not represented.

The peak intensity shown in the centre of each plot: Figure 8-3a-h, corresponds to sodium fluorescein concentrations as shown on the labels of each graph. The peaks of each graph are also summarised and plotted as a function of sodium fluorescein concentration in Figure 8-5 (The former graphs are not shown in the later experiments as they do not yield any further information which cannot be displayed on a peak-intensity plot).

There are three peaks shown on each graph. The centre-most peak (at ≈54mm), corresponds to the sodium fluorescein, whilst the two outer-most peaks are caused by the light source. The light source, being a combination of all visible wavelengths contains radiation at both the absorption and emission wavelength of the sodium fluorescein and cannot be distinguished from fluorescence by sampling each of the two wavelengths and taking the ratio. The combination of the two wavelengths consequently registers an apparent fluorescence. This is shown on both the left-hand-side and right-hand-side of the graphs and is caused by the white light leaking around the side of the filter and onto the vessel. This would not occur *in-vivo*.

The optical fibre will only capture light within its acceptance cone forward of the cleaved face. If the light source is adjacent to the fibre, but outside the acceptance cone it will not be detected. As the fibre face passes the target the light arising from the fluorescein is detected and will then stay in the field of view unless the vessel is bent or occluded. The signal is also attenuated due to the presence of blood. The light

detected will then decay as a function of distance (cf: chapter 4), dependent on the extinction coefficient of the medium through which the light is propagating[2]. This phenomena can be observed if the decay of the peak either side of the maximum value is measured. When using a solution of 622μMole/l (Figure 8-3a) the amplitude of the peak rises from 0.59 to 1.56 over 6.6mm, whilst is takes 17.9mm to return, at which point the amplitude begins to rise because of the white light leakage. The prevention of the light to fall to its original minimum means that the nulls before and after each peak are of different amplitudes and differ by 0.54 (35% of full scale deflection). The longer decay time is apparent on all graphs and is summarised in the table shown in Figure 8-4.

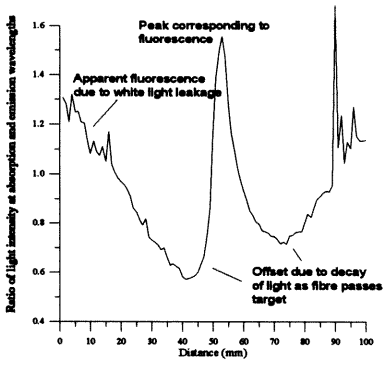

Figure 8-3a Concentration 622μMole/l

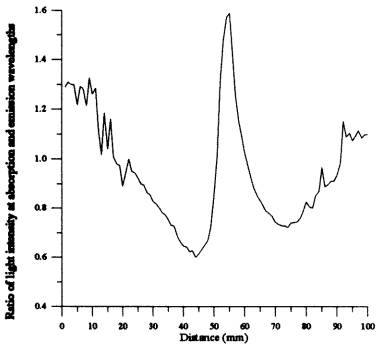

Figure 8-3b Concentration 311μMole/l

[2] This is the ideal scenario, in practice if a light ray strikes the cladding of a fibre from the side it will be refracted. If the transmission angle is such that it is less that the critical angle of internal reflection that particular mode will be contained within the core or cladding and will propagate along the length of the optical fibre

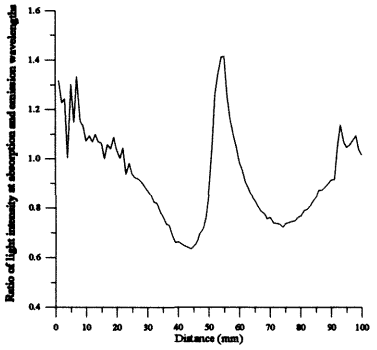

Figure 8-3c Concentration 156μMole/l

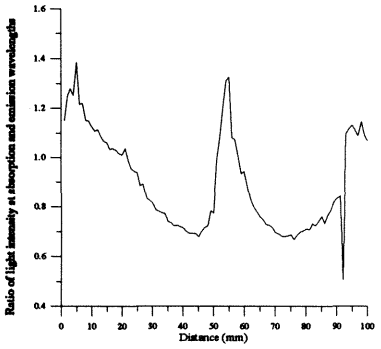

Figure 8-3d Concentration 78μMole/l

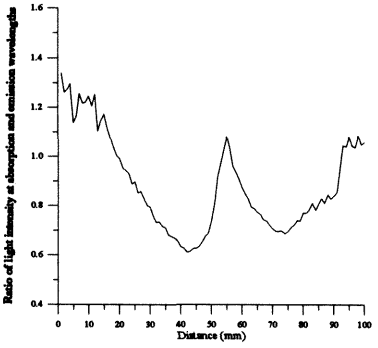

Figure 8-3e Concentration 38μMole/l

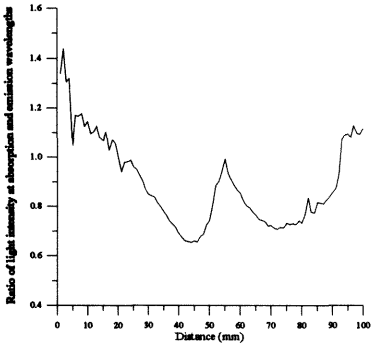

Figure 8-3f Concentration 19μMole/l

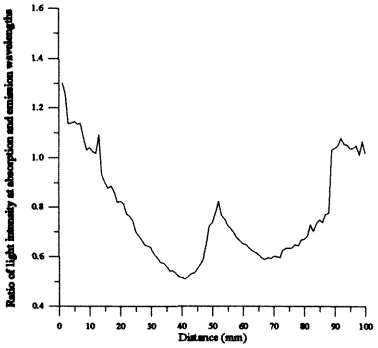

Figure 8-3g Concentration 10μMole/l

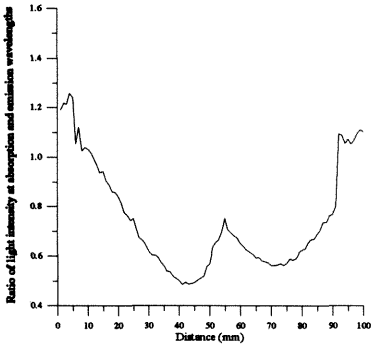

Figure 8-3h Concentration 5μMole/l

Concentration of sodium fluorescein in distilled water (μMole/l)							
622	311	156	78	36	19	10	5
17.9mm	19.2mm	18.6mm	18.3mm	18.4mm	18.0mm	16.8mm	18.3mm

Figure 8-4 A table summarising the distance taken for the amplitude to decay

The absolute quantity of sodium fluorescein present = Concentration × Volume

where volume ≈ Circumference of artery × Cross-sect. area of helix × No. of turns

$= 21.4mm^3$ (21.4μl) (for 5 turns)

The peak amplitude of each plot was plotted against sodium fluorescein concentration and yields a logarithmic relationship (Coefficient of determination, r^2= 0.989) with a gradient of 0.186 (see test EL2). Amplitudes of the data taken using the 622μMole/l and 311μMole/l were similar in amplitude: 1.560 and 1.589 respectively. From this we can conclude that the solution is saturated, and cannot dissolve any further fluorescein. If particles in the fluid have not fully dissolved they will scatter and absorb the light travelling through it, hence attenuating the signal and reducing the fluorescence. This explains the fall in amplitude observed for a concentration increase from 311 to 622μMole/l (see Figure 8-3a and Figure 8-3b).

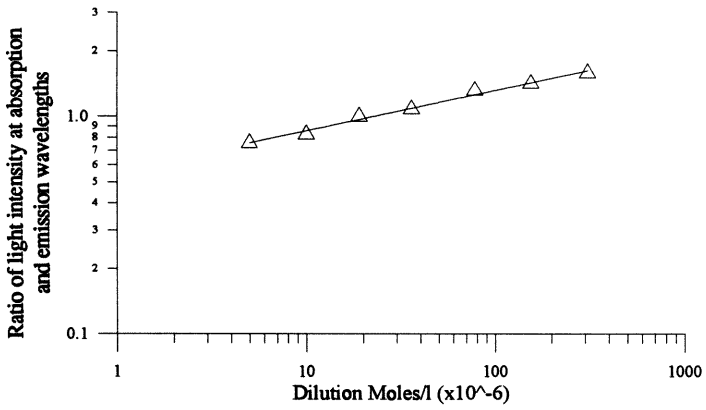

Figure 8-5 The peak fluorescence detected using varying dilutions of sodium fluorescein (unit of dilution are μMole/l)
(Photon count time = 1 second)

According to the definition of fluorescence (section 7.4.1, chapter 7), the ratio between the absorbed and re-emitted light of a fluorescent material should not exceed unity, i.e. the intensity of the light emitted from the Sodium Fluorescein (at 550nm) cannot exceed that it absorbs (at 490nm). This is not the case in Figure 8-5 as it has a maximum value of 1.56. The receiving optical fibre does record the light which the Sodium Fluorescein emits, but it does not measure the light it absorbs, it measures the light remaining. As a result the value produced is a function of fluorescence, but it does not reflect fluorescence directly.

8.3.1.3 Test EL 2 - Venous blood perfusion

In order to produce a more reliable model of the cardiac artery the experiment was repeated with an identical false artery, but with the saline replaced by deoxygenated blood. The oxygen content of the blood haemoglobin affects the optical absorption spectrum in the visible red and infra-red end of the electromagnetic spectrum: deoxygenated haemoglobin and oxygenated haemoglobin begin absorbing at approximately 580nm and 680nm respectively (Prys-Roberts., 1969). Sodium fluorescein (490nm to 550nm) is not affected by these wavelengths.

If the results obtained are compared to that obtained from an artery perfused with saline (Test EL1), the effect of attenuation of the blood can be observed. Figure 8-6a-b illustrates the ratio between the absorption and emission wavelengths for fluorescein concentrations of 622μMole/l and 311μMole/l respectively. The blood has a considerably higher extinction coefficient than that of saline, and consequently when the probe tip traverses past the fluorescent region the decay on the left-hand-side of the peak is much steeper. The trace returns to baseline 2.5mm after the peak value, a reduction of approximately 16mm (see table in Figure 8-4). The secondary peaks, observed on either side of the peak representing fluorescence, have also decreased significantly. When the probe leaves the blood the trace rises sharply to match the amplitude recorded during test EL1 where blood was not present.

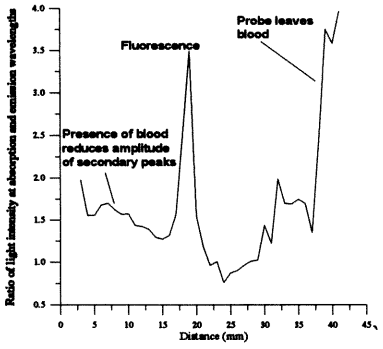

Figure 8-6a Concentration 622μMole/l

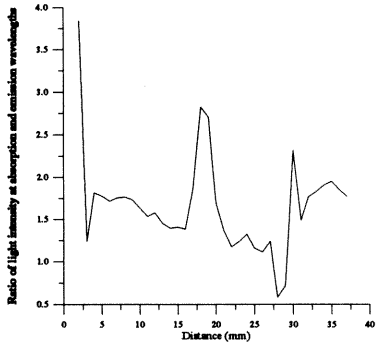

Figure 8-6b Concentration 311μMole/l

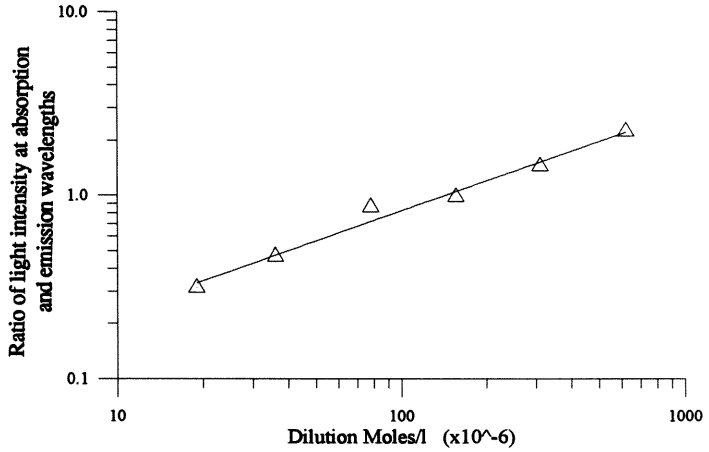

Figure 8-7 The peak fluorescence detected using varying dilutions of sodium fluorescein in an artery perfused with oxygenated blood (unit of dilution are μMole/l) (Photon count time = 1 second)

The results shown in Figure 8-7 show the peak amplitudes of the six most concentrated dilutions of sodium fluorescein in distilled water plotted as a logarithmic relationship. The gradient of the curve has increased to 0.542 and can be attributed to the increased extinction co-efficient. Higher concentrations of sodium fluorescein produce more light which is able to penetrate further through the blood before being

attenuated. This also further validates the steeper decay experienced by the probe as it passes the target.

8.3.1.4 Discussion

Comparison of the two curves illustrated in the above experiments show the significance of introducing the blood into the vessel. If Beer-Lambert's law is considered the decay of light at a specific wavelength through blood is an exponential relationship involving the concentration '*c*' (constant), distance '*d*' (constant) and the extinction coefficient '*E*' which is different for each of the two absorption and emission wavelengths respectively.

$$\text{Fluorescence} = \frac{I_{1e}I_{0a}}{I_{0e}I_{1a}} \propto \frac{e^{-E_e cd}}{e^{-E_a cd}} \qquad \text{(Eqn 8-1)}$$

where I_{1e} and I_{0e} are the intensities of the emission wavelengths at distance 0 and distance 'd'

E_e is the extinction coefficient at the emission wavelength (550nm)

I_{1a} and I_{0a} are the intensities of the emission wavelengths at distance 0 and distance 'd'

E_a is the extinction coefficient at the emission wavelength (490nm)

Given this relationship the correction factor for the presence of blood in the simulated artery is defined. If the extinction coefficient for both were to be equal for both wavelengths the ratio between the intensities should remain constant independent of the presence of blood.

8.3.2 Cellular model

8.3.2.1 Method and motivation

In order to satisfy the research objectives from the original design proposal a series of experiments was conducted using endothelial cells grown and damaged *in-vitro*. The experiment consisted of two halves aimed to produce a set of both expected (Test CM 1) and actual data (Test CM 2). The first experiment was aimed to validate the claim that fluorescently labelled antibodies could specifically bind to damaged and regenerating vascular endothelium and this could be detected by the probe. The second

experiment was used to determine the reduced amount of fluorescence detected due to the labelled cells only existing in one plane, and not the periphery of a vessel.

8.3.2.2 Test CM 1 - Labelled endothelial cells

Experiments by Cuello *et al* (1982) have shown that it is possible to internally label monoclonal antibodies without impairing their binding characteristics. To examine this finding in the present context endothelial cell specific antibodies were prepared. During PCTA the vascular endothelium is damaged around the entire lumen of the vessel, the length of which is determined by the length of the angioplasty balloon used: typical 30mm long. Such damage is difficult to simulate *in-vitro*. Endothelial cells were grown in culture and then scratched along the length of the culture plate. This procedure damages the cells immediately adjacent to the scratch (Figure 8-8).

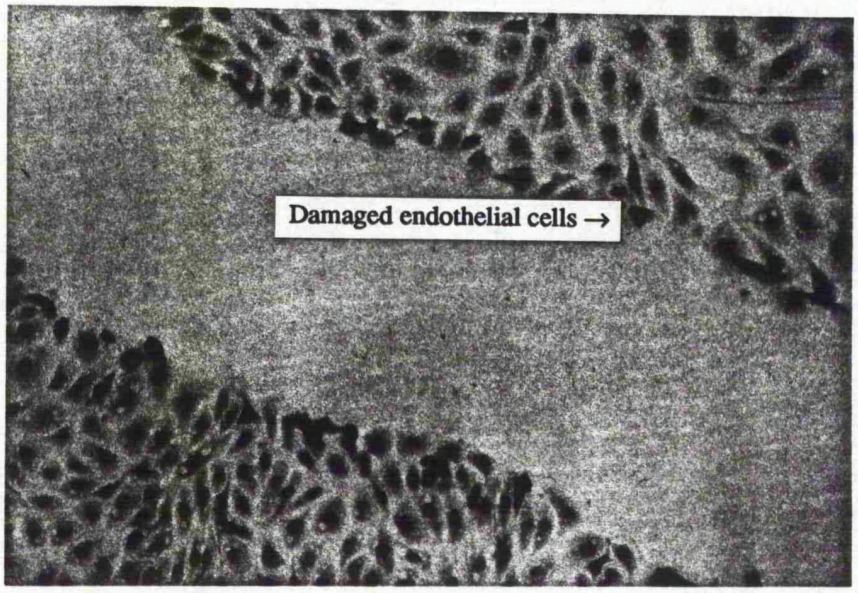

Figure 8-8 Endothelial cells grown *in-vitro* and damaged by scratching the culture plate along its length

The photograph shown in Figure 8-8 shows the scratch on the culture plate and the resulting damaged cells labelled with a visible marker (a darker shade adjacent to the scratch). The cells were then washed with a suspension containing the monoclonal antibodies bound to sodium fluorescein to fluorescently label the damaged region. It was proposed that the damaged region be illuminated from the filtered halogen light source and an optical fibre probe be withdrawn over the subject area.

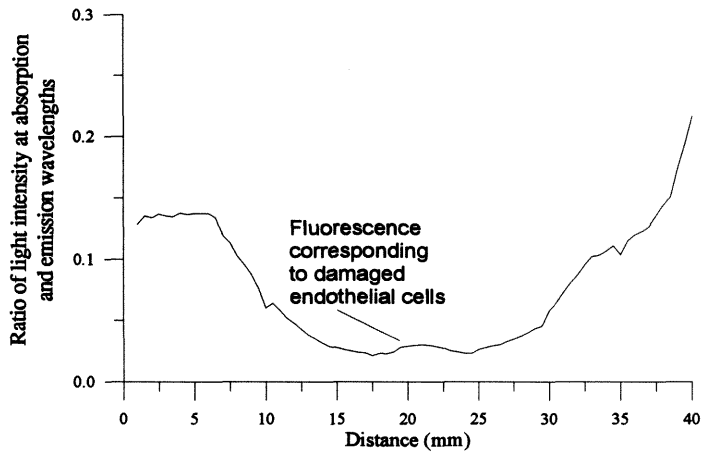

Figure 8-9 The detection of fluorescently labelled endothelial cells when grown and damaged *in-vitro*
(Photon count time = 1 second)

The graph in Figure 8-9 illustrates artefacts due to the non-ideal halogen light source (see test EL 1), shown as peaks or side-lobes on the left-hand-side and right-hand-side of the graph. Fluorescence is shown as a broad peak (3.5mm wide at 21mm distance) at an amplitude of 0.034 when a 0.5mm diameter polymethymethacrylate optical fibre was used to capture the light. The graph shows that using this technique, the sodium fluorescein labelled cells at the sides of the scratch (Figure 8-8) could not be distinguished from one another. If the method of fluorescently labelled monoclonal antibodies were to be adopted in real artery the level of fluorescence would be significantly greater. This is examined during test CM2.

8.3.2.3 Test CM 2 - Glycerol + sodium fluorescein

This experiment was conducted in order to quantify test CM1. The aim of this experiment was to determine the correction factor required to interpolate the results obtained from real labelled endothelial cells to an artery which has been labelled around its periphery.

Sodium fluorescein is an inert fluorescent salt which will only re-emit light when it is dissolved in a solution. To prevent the solution drying and impairing fluorescence

sodium fluorescein was dissolved in glycerol, its high boiling point making it less susceptible to evaporation. 10µl of 600µMole/l (6nMole) of solution was held between two microscope slides and illuminated by the filtered (490nm) halogen light source. A 0.5mm diameter polymethymethacrylate optical fibre was then withdrawn over the fluorescent area and the fluorescence calculated (Figure 8-10).

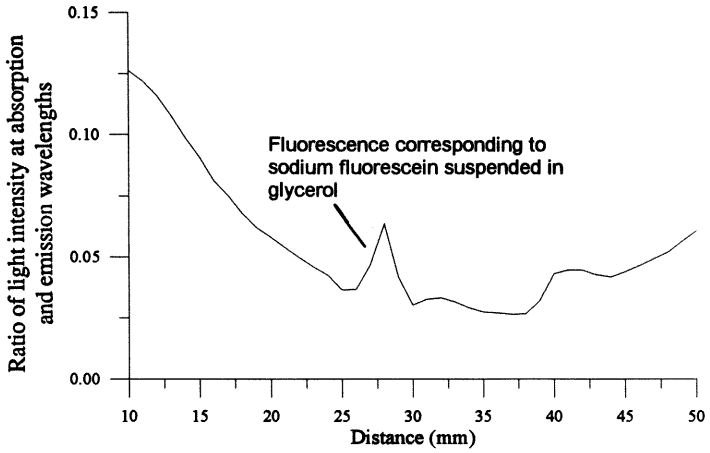

Figure 8-10 Predicting the characteristic produced by fluorescent labelled cell in a single plane parallel to the optical fibre
(Photon count time = 1 second)

The graph above illustrates the level of fluorescence detected when trapping 6nMoles of sodium fluorescein between two microscope slides in order to predict the reduction in signal due to the sodium fluorescein being present in only one plane. The amplitude of the peak is considerably higher than that obtained during test CM1 and is attributed to the increased quantity of fluorescent material in the vicinity of the probe tip: 0.069. This is 202% higher than the value measured from the sodium fluorescein labelled cells.

The measured material (peak amplitude) is not necessarily linearly related to the proportion of the fluorescent material as the location of the probe is significant. The relationship may however be used to determine the expected increase in amplitude if the aforementioned quantity of fluorescein were to coat the inner lining of the vessel. Consider test EL 1:

Amplitude of fluorescence at 622μMole/l = 1.560 (≈1.5 at 600μMole/l)
in false artery perfused with saline.

Amplitude of fluorescence at 600μMole/l = 0.069
in Figure 8-10.

This implies that the signal would increase by at least one order of magnitude due to the increased volume of fluorescein being within the acceptance cone of the receiving optical fibre[3].

8.3.2.4 Discussion

The use of sodium fluorescein to label specific antibodies for binding to damaged endothelial cells can be detected by an optical fibre probe when the cells are grown *in-vitro* and devoid of blood. In an artery, post PTCA, the fluorescent label would be present around the periphery of the vessel lumen and hence of a considerably higher volume than that demonstrated. If exploration is limited to narrow gauge vessels the sensitivity will increase by at least on order of magnitude. The presence of blood in the vessel will attenuate the signal by at least one order of magnitude per mm of blood (chapter 7), but the signal should still be detectable. This feature is not necessarily a disadvantage, the high attenuation of the blood does mean that the probe has to be very close to the target, but it also means that once detected the location of the damage can be very accurately determined.

8.3.3 Mammalian models

8.3.3.1 Method and motivation

The final set of the experiments demonstrated with an external light source (490nm filtered halogen, 20W) was to determine the viability of exciting the subject vessel from outside the patient whilst the intervening tissues were in place: it was envisaged that the patient be in a darkened room and subjected to a high power source

[3] This approximate relationship assumes the optical fibre to be the same distance away from the fluorescent material in each case.

such as a xenon flash lamp. The false translucent arterial model was replaced by harvested human umbilical vessel and the aorta of a recently sacrificed rat.

8.3.3.2 Test MM1 - Umbilical vessel and rat aorta

A 100mm long homogenised umbilical vessel, devoid of blood, was injected with two doses of 0.1ml of sodium fluorescein in distilled water at a dilution of 622μMole/l. The halogen light source was then placed in close proximity of the vessel wall and the probe, consisting of a 0.5mm diameter polymethylmethacrylate optical fibre, withdrawn along its length.

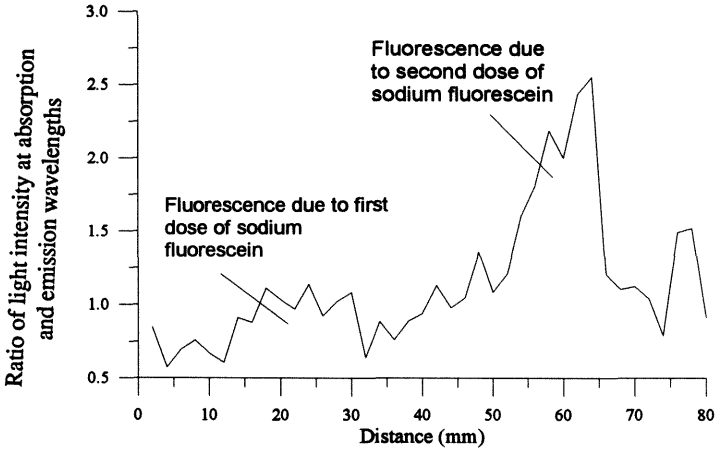

Figure 8-11 The sodium fluorescein injected in 0.1ml doses at 622μMole/l concentration into the wall of an umbilical vessel (Photon count time = 1 second)

The graph shows that sodium fluorescein was detected using an external light source. The vessel wall was approximately 2mm thick, and will significantly attenuate the excitation light source. The fluorescence is visible in the form of two peaks: 1.18 peak between 13mm and 32mm and 2.64 peak between 52mm and 66mm. In both cases an identical quantity of sodium fluorescein was injected, yet in practice the second peak is 124% higher than that of the first. The vessel wall will vary in thickness and the depth that the sodium fluorescein is injected into it will produce a different response. The location of the excitation light source will also effect the sensitivity of the probe as the exciting light source will be attenuated by the intervening tissues.

An experiment was conducted in a similar manner to that described above using a rat aorta. A 0.1ml dose of sodium fluorescein: 622μMole/l, was injected into the tissues adjacent to the vessel wall. The organs and skin were then replaced and the animal illuminated by the halogen light source.

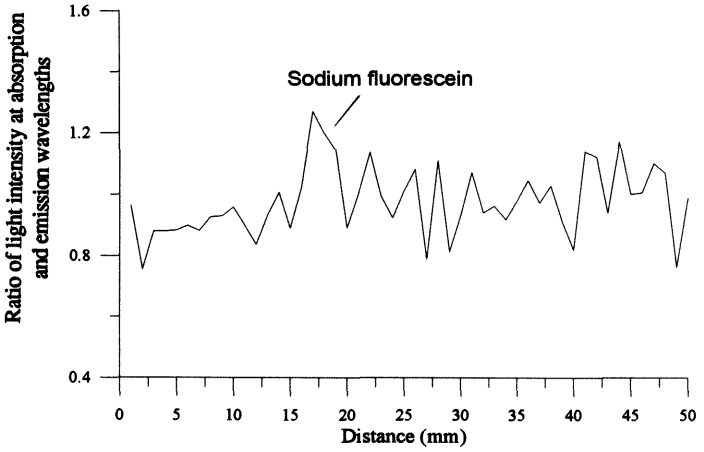

Figure 8-12 Fluorescence of a rat aorta detected by injected 0.1ml of 622μMole/l sodium fluorescein into the tissues adjacent to the vessel wall (Photon count time = 10 seconds)

The fluorescent region is only just visible on the graph as a peak of 1.27 above the average (mean=0.98, standard deviation=0.11) (Figure 8-12). In both of the above graphs photons were captured during a 10 second time interval in order to increase the signal to noise ratio, however the noise is still considerable: 0.3 peak-to-peak. This is due to the low number of photons arriving during the elapsed time: typically only 20 to 30 counts per second were recorded. The reduced number of counts reduces the resolution of the probe and gives the curves a more jagged appearance making the distinction between the presence of a damage fluorescent portion of the artery and a normal artery more difficult. The increased photon count time required to form a reliable diagnosis, proportionally increases the time taken to perform the analysis and will make it eventually become impractical.

8.3.3.3 Discussion

The usefulness of external light source is limited. The intensity of the light permitted to penetrate the vessel wall and excite the target area is highly dependent on the quantity of tissue obscuring the vessel wall. Studies using the rat aorta concluded that an external light source would not be sufficient due to the depth of the coronary arteries beneath the rib-cage: over 50mm. Pulse oximetry works because the selected wavelengths are in the visible red end of the spectrum (in the low absorption window) and the probe relies on determining the absorption of the blood at two specific wavelengths. The porphyrins in the blood mean that fluorescent materials at these wavelengths are impossible to use.

There were also found to be more practical problems of using a continuous light source fitted with the appropriate 490nm optical filter. Even though a dichroic lamp was used to disperse the IR and heat radiation away from the focal point, the heat emanated from the source was sufficient to burn and dry-out the skin. The optical filters was also subjected to extreme heat (>100°C) for which they were not designed and had to be cooled by either forced convection or piping cool water over the surface.

In conclusion the external light source does work where the subject vessel is able to be openly illuminated, but fails where it is surrounded by extraneous tissues. The study was however useful in determining the viability of the system with *in-vitro* labelled endothelial cells, and effects of blood flow in the system. In order to make the device operate *in-vivo* without harvesting the vessel, the external light source was replaced with an alternative *in-vivo* light source (chapter 7).

8.4 *In-vivo* light source

The following section is a summary of the results obtained using an *in-vivo* launched light source, specifically an argon ion laser focused into an emitting optical fibre. During each of the experiments the simulated artery was used with varying dilutions of sodium fluorescein in distilled water. Experiments were performed in both saline and deoxygenated blood and compared to the results obtained using the external, filtered halogen (470nm, ±30nm), light source.

8.4.1 *In-vivo* light source power selection

The power of the laser to be used as the *in-vivo* light source was selected by examination of the sodium fluorescein efficiency, absorption of the blood and the solid angle defined by the receiving optical fibre.

Consider the solid angle:

Assuming the probe is placed in a vessel radius 'R_v' thickness 'C_t' and returning light is only captured if the trajectory of the returning photon strikes the face of the receiving optical fibre cross-sectional area 'A_f', it can be shown that:

$$\text{Flux received by solid angle '}S\text{'} = \frac{\int_{A_2}^{A_1}\int_{R_v}^{(R_v+C_t)}\int_{0}^{2\pi}\frac{A_f}{4\pi\left(x^2+r^2\right)}.rd\theta.dr.dx}{\int_{A_2}^{A_1}\int_{R_v}^{(R_v+C_t)}\int_{0}^{2\pi}rd\theta.dr.dx} \quad \text{(Eqn 8-2)}$$

where

$$A_1 = L + \left(\frac{R_v}{\tan(\pi/6)}\right) \quad \text{and} \quad A_2 = \left(\frac{R_v}{\tan(\pi/6)}\right)$$

C_t = Thickness of cellular wall containing sodium fluorescein
R_v = Radius of vessel
A_f = Cross-sectional area of optical fibre
(see Figure 8-13)

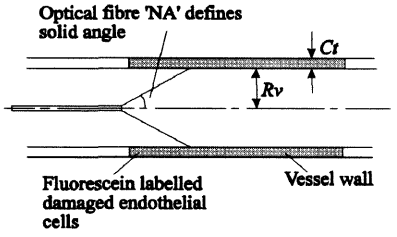

Figure 8-13 A optical fibre enclosed in a coronary vessel showing labelled damaged endothelial cells in the lumen and the solid angle of the optical fibre and a point source on the vessel wall

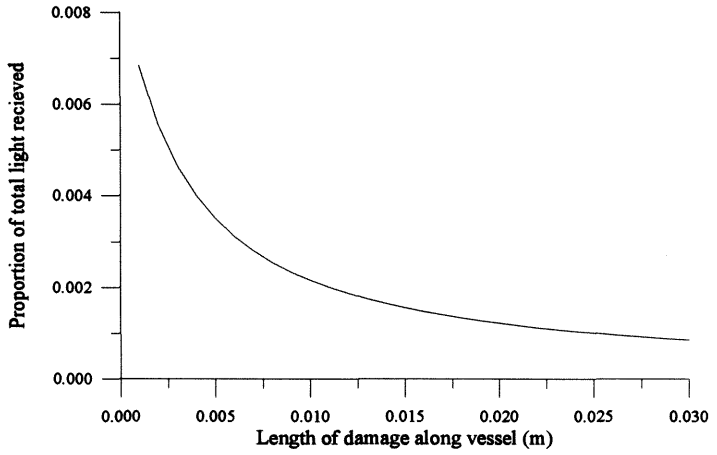

Figure 8-14The proportion of light received by an optical fibre emanating from a cylinder representing endothelial cell damage assuming sodium fluorescein is 100% efficient and the absorption of blood is negligible

Figure 8-14 illustrates the proportion of light received by a 0.25mm diameter optical fibre (NA=0.5) from fluorescing damaged endothelial cells on the surface of the vessel lumen. The vessel diameter was 3mm, with a wall thickness of 0.1mm. The proportion is described as a function of the total amount emitted. A typical angioplasty balloon is 30mm long, and hence approximately 0.1% of the light emitted would be detected (Figure 8-14).

The amount of light re-emitted from the sodium fluorescein is dependent on concentration and the intensity of the source irradiating the fluorescent cells.

Irradiance of surface 'I' = flux per unit area

$$\approx \frac{d\Phi}{dA} \times \Omega \qquad \text{(Eqn 8-3)}$$

where 'Φ' is the flux density over a surface area 'A', and 'Ω' is non-linear variable describing absorption of the blood. This is a complex mathematical problem to solve if Lambert-Beer's law is considered (Prys-Roberts., 1969), but if the emitting optical

fibre is treated as a point source the problem may be simplified. The solid angle from the face of the emitting optical fibre to a point on the vessel wall and back to the receiving fibre can be approximated to be the same if the diameter and location of the optical fibre is the same in both cases.

The intercept of the acceptance cone of the optical fibre in the vessel is defined by the numerical aperture of the fibre. If the flux power distribution across the face of the fibre is uniform the closest point will produce the largest contribution to the total power received (Figure 8-13). The power received by an optical fibre using an identical optical fibre to excite the fluorescent material contained in the vessel wall:

Power reduction 'P_s' $\approx$ (Solid angle)^2 (Eqn 8-4)

$= (1\times10^{-3})^2 = 1\times10^{-6}$

Attenuation of blood assuming the closest point to the face of the receiving optical fibre and within the numerical aperture gives the most significant contribution to the total power received. Considering Beer-Lambert's law (Extinction coefficient of 3.62 for mean attenuation of 15.7dB/mm at 490nm, see chapter 7):

Power reduction 'P_b' $= e^{-Ec\left(R_v/\sin\theta_a\right)}$ (Eqn 8-5)

$= 19\times10^{-6}$

where θ_a is the acceptance angle of the optical fibre (30°), c is unity concentration of blood and the radius of vessel R_v is 1.5mm.

Miscellaneous losses:

Lenses + filters	:	0.35 (section 7.4.5.3)
Fibre loss	:	0.40 (~1dB/m at 490nm) (4m to emit and receive)
Sodium Fluorescein	:	Efficiency $\approx$ 1% (specified by manufacturer)

$\therefore$ Combined efficiency of system $= 2.7\times10^{-14}$

Minimum number of photons detectable[4] by PMT $\approx$ 1000 s^{-1}

$= 3.83\times10^{-16}$W

Hence minimum power of light source required assuming all light is coupled into the emitting optical fibre:

$$\text{Power of laser (minimum)} = \frac{\text{Minimum detectable power}}{\text{Efficiency of system}} \qquad \text{(Eqn 8-6)}$$

$= 14.2$mW

In practice the power was run higher than this to produce the maximum possible signal to noise ratio (100mW). This power level was found to be too high when using an artery perfused with blood due to destruction of the blood proteins (see test PD2/3, section 8.4.2.3). It is also possible probable that the high power will cause cellular damage. This figure assumes that the sodium fluorescein is 1% efficient which is only an approximation.

8.4.2 *In-vivo* probe design

8.4.2.1 Method and motivation

During the course of the probe development two designs were considered.

- **The simplex optical fibre probe** - A bifurcation was constructed using a bundle of 20 125μm diameter multimode polymethylmethacrylate optical fibres split

[4] By definition photons of different wavelengths have a different energy (see section 7.4.1- An overview of fluorescence). For the purpose of this calculation an average was taken between the absorption and emission wavelengths : 490nm and 550nm.

into two equal bundles of 10 evenly distributed optical fibres (Figure 8-15). The probe consisted of a 1mm diameter optical fibre connected to each junction[5].

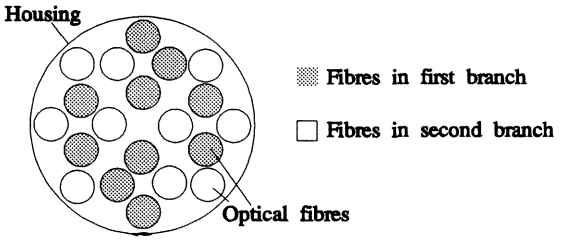

Figure 8-15 The optical fibre bifurcation consisting of 20 optical fibres evenly distributed into two separate bundles.

- The **duplex optical fibre** involved a pair of 250μm polymer fibres. A single fibre was used to receive the light with a second disassociated fibre to emit (see chapter 7. section 7.4.5).

Each of the two probe designs has advantages and disadvantages. The objective is to ensure that the sensitivity of the system is optimum and the size is within the physical constraints of the original specification. It is undesirable to have a intravascular catheter greater than 1mm in diameter as it is both awkward to manipulate and will impair blood flow.

8.4.2.2 Test PD 1 - Simplex probe in saline

The simplex optical fibre probe design is the simplest to envisage. The same optical fibre is used to both receive and transmit light by utilising an opto-coupler to couple the transmitted and returning light into the same optical fibre. The main benefits are the size and cost. The probe consists of a single light guide with a fibre junction outside the body. Although the initial cost is higher due to the coupler the running costs are lower as the probe is cheaper to produce.

[5] Coupling of fibres was performed in conjunction with a layer of refractive index matching gel made from phenylmethyl silicone.

Single mode optical fibre couplers are used with considerable success in transducers using interferometry (Jackson., 1987, see section 1.4.2, chapter 1), and are the integral part of the classic optical fibre interferometer configurations: Fabry-Perot and Mach-Zender.

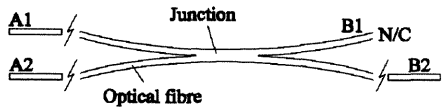

Figure 8-16 An optical fibre bi-directional coupler for using with single mode optical fibre

The termination or insertion loss of a pair of optical fibres can be reduced to levels <0.1dB if the ends of the optical fibre are cleaved and hot welded with high precision apparatus. The loss using a bi-directional coupler is high due to the division of flux at the junction (Figure 8-16). When light travels from a source located 'B_2', it is divided between branches at 'A_1' and 'A_2'. Construction of an optical fibre coupler using a split optical fibre bundle, section 8.4.1, found the loss to be 7.10dB and 6.46dB with the source at the common and 5.15dB and 5.45dB with the source at each of the branches respectively.

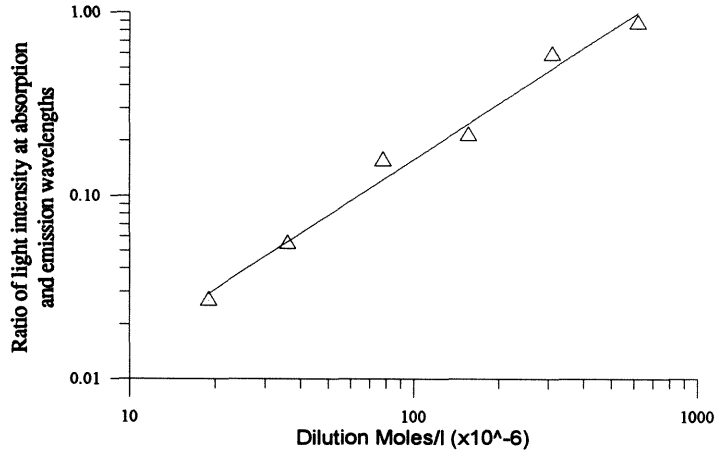

Figure 8-17a The fluorescence of sodium fluorescein contained in a 5 turn helix (section 8.2) using a simplex optical fibre probe (Photon count time = 1 second)

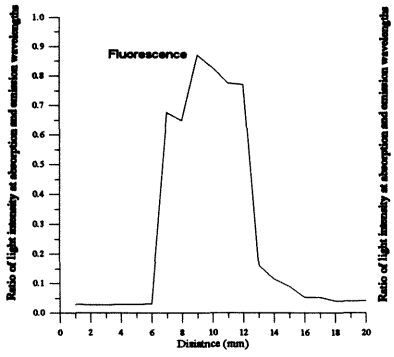

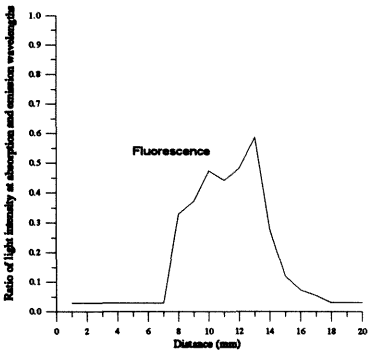

Figure 8-17a Figure 8-17b
The peaks corresponding to the fluorescence of sodium fluorescein in an artery filled with saline using a simplex optical fibre probe design

The plot of fluorescence against concentration is a linear relationship since the gradient of the curve is approximately unity (1.011, R^2=0.985) on a logarithmic scale. Concentration is approximately proportional to amplitude of fluorescence and allows concentration to be calculated directly.

The second main observation is that only a single peak is present. Side peaks on either side of the fluorescent region (≈12mm) are not present (cf: section 8.3.1.2). This is due to the more idealised light source have a bandwidth of ±2nm from the peak emission and the eradication of the broad band light source which leaked *white light* into the target area around the sides of the filter.

The prototype device was constructed from 1mm diameter polymer optical fibre which may not be bent around a radius of less than 50mm without causing serious damage to the cladding. Although it may be envisaged that the final device would be constructed from a narrower optical fibre, the reduction in sensitivity due to the optical coupler is inevitable and cannot be avoided. In order to investigate the *in-vivo* launched light source fully a second design was investigated (below).

8.4.2.3 Test PD 2/3 - Duplex probe in saline and blood

The duplex optical fibre probe was constructed from a pair of 0.25mm diameter polymer optical fibres, chosen because of their comparable size with the former

simplex design when housed in a protective shroud (0.94mm). The reduced fibre cross-sectional area implies that the quantity of light received will be considerably less (0.67% for 1mm OD fibre, 0.039% for 0.25mm OD fibre, chapter 7 figure 7-8a). The light that is collected is coupled directly into the detector without secondary sources of coupling loss originating from the optical coupler. The reduced diameter of the optical fibre and hence the reduced longitudinal stress means that the probe (fibres and shrouding) can be bent through a radius of less than 10mm without permanent damage.

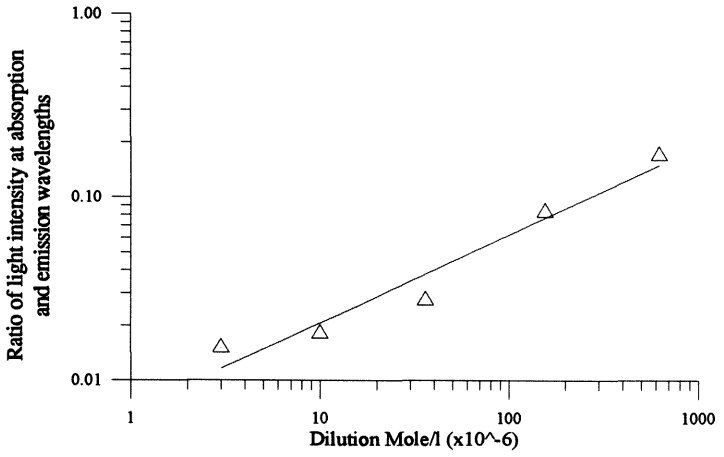

Figure 8-18a The peak fluorescence detected using a saline filled artery filled with sodium fluorescein of varying dilutions using a duplex optical fibre probe (Photon count time = 1 second)

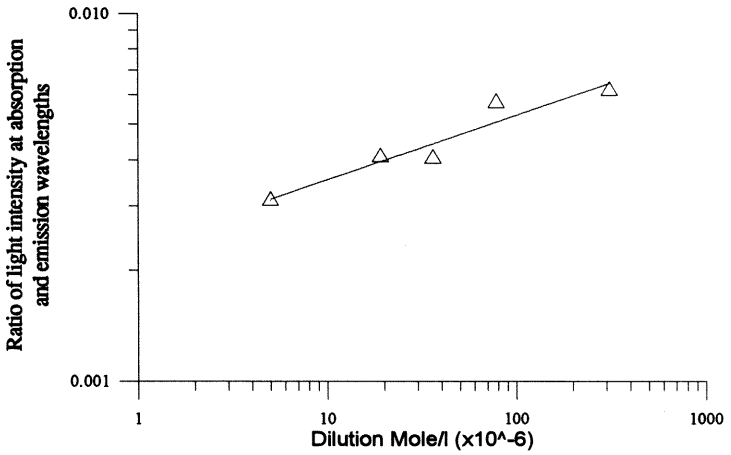

Figure 8-18b The peak fluorescence detected using a blood filled artery filled with sodium fluorescein of varying dilutions using a duplex optical fibre probe (Photon count time = 1 second)

Figure 8-18a and Figure 8-18b illustrate fluorescence detected using the duplex fibre design in a false artery encapsulated in a 5 turn helix of varying sodium fluorescein dilutions. Vessels perfused with saline and blood are depicted.

As was demonstrated in chapter 7 the attenuation of whole blood is considerable (15.7 dB/mm). The replacement of the external light source with the laser means that further attenuation arising because of the intervening tissues between an external light source and the target site does not occur.

Consider the following:

Probe description	Perfusion	Power law exponent 'p' (where $\log(y)=p\log(x)$)	Coeff of determination R^2
Simplex	Saline	1.01	0.99
Duplex	Saline	0.48	0.95
Duplex	Blood	0.17	0.92

Figure 8-19 A table of statistics fitting a logarithmic fit to the data obtained from the simplex and duplex optical fibre probe designs

The gain of the duplex probe with blood falls 36% of its original level when using saline on a logarithmic scale. The coefficient of determination (R^2) falls both

when a smaller diameter fibre is used and when the saline is replaced with blood[6]. This may be attributed to the reduced signal-to-noise ratio due to the reduced solid angle of the fibre acceptance cone and the attenuation of the blood.

8.4.2.4 Discussion

The argon ion laser has proved that it is a viable means of exciting fluorescent material adjacent to the vessel wall both in and out of blood. During the majority of the above experiments the laser power was fixed at 100mW continuous wave and the photomultiplier tube allowed to count for 1 second unless otherwise stated. The maximum power that the laser could deliver was limited by the presence of the blood itself and risk of further injury to the vessel wall. The high energy emanating from the optical fibre tip whilst immersed in blood denatures the blood and caused hard *plaque-like* deposits to build up on the face of the emitting optical fibre over a period of a few minutes seriously impairing its ability to launch light into the target area[7]. Continuous wave argon ion lasers were used in early laser angioplasty techniques, but later disregarded and replaced with pulsed excimer lasers to prevent localised heating leading to further vessel trauma or puncture (Cheong *et al.*, 1991).

8.4.3 Mammalian models - Fluoresceinated heparin

8.4.3.1 Method and motivation

The final experiment conducted again used an animal model to produce the closest approximation permitted to damaged vascular endothelium and was designed to explore the capabilities in a real vessel as far was possible without placing the probe in a living creature (cf. Test MM1)[8].

---

[6] The coefficient of determination (R^2) is the mean-square error of the logarithmic curve fit for each set of data.

[7] Denaturing of the blood occurs when the long protein molecules of the blood are made to unravel by heat or chemical damage.

[8] Damaged endothelial cells could not be examined *in-vivo* because of the animal licence restrictions,

There are a number of unresolved issues when attempting to deliver a drug intravascularly directly into the vessel wall (Hong *et al.*, 1993). The technique is usually performed with a specially perforated angioplasty balloon loaded with drug which is then pressured upon which the drug is released. The blood flow and only a semi-permeable vessel wall means that only a fraction of that delivered is retained in the vessel, the quantity of which has not been accurately measured. To simulate fluorescence arising from labelled endothelial cells the drug was replaced by fluorescein labelled heparin. 20mg/ml of commercial heparin was conjugated with fluorescein isothiocyanate (FITC) at a concentration of 50μg per 1mg of heparin. The conjugate was purified by ion-exchange chromatography (affinity chromatography): a PD-10 column was eluted with a phosphate buffered saline (ph7.4). The purified conjugate was then diluted (see below) and concentration verified by spectrophotometry[9].

8.4.3.2 Test FH1 A simulated artery

The experiment was conducted in two halves. Firstly a calibration was carried out using a saline filled false artery (section 8.2) to ensure that the fluoresceinated heparin was fluorescing at 550nm when excited at 490nm, and the binding of the two chemicals had not altered the spectral characteristic. The heparin was then used in conjunction with a length of recently harvested rabbit iliac artery.

[9] Due to the purification process the dilution concentrations are specified in international unit (IU) where 1000 IU=6mg/ml. Moles/l=Weigtht(g)/Molecular weight, hence 1IU=0.3μMole/l where the molecular weight = 20,000.

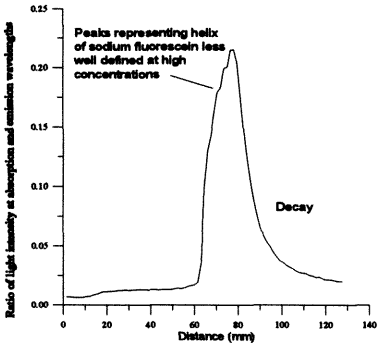

Figure 8-20a
Fluorescence of heparin at 500IU

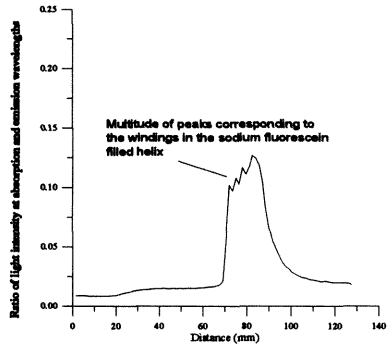

Figure 8-20b
Fluorescence of heparin at 310IU

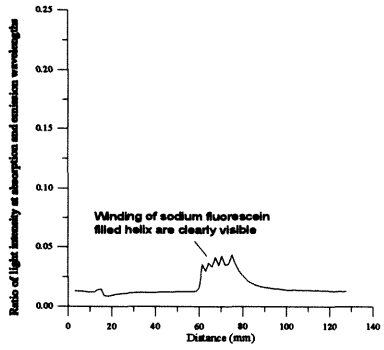

Figure 8-20c
Fluorescence of heparin at 80IU

Figure 8-20a-c illustrate the fluorescence detected using the false artery perfused with saline in conjunction with the *in-vivo* light source. In order to improve the resolution the probe was withdrawn in 0.5mm steps (cf: Figure 8-6). The power of the laser was adjusted to provide 100mW of continuous power and tuned to 488nm using a Brewster prism. As the concentration of the sodium fluorescein is reduced the peak at the centre of each characteristic falls in amplitude and follows the characteristic logarithmic relationship Figure 8-20d.

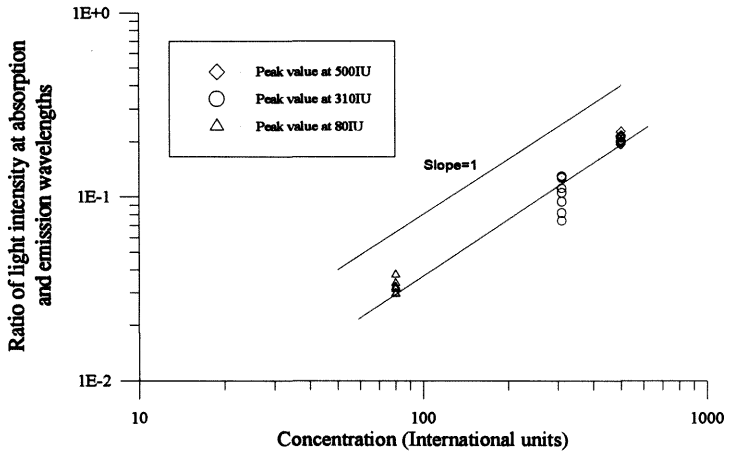

Figure 8-20d A summary of the results obtained from fluoresceinated heparin at 3 concentrations: 80IU, 310IU and 500IU. The probe was withdrawn along the vessel 8 times for each concentration (Photon count time = 1 second)

The graphs also show improved clarity of the image due to reduced concentration. Figure 8-20a shows a sharp peak: 0.22 at 78mm, followed by a decay which has been present in all of the experiments conducted in the false artery perfused with saline (section 8.2). Preceding the maximum is a series of shoulders which in later traces (at lower concentrations) manifest as separate peaks. Each peak corresponds to a single turn of the sodium fluorescein laden helix around the plastic artery. As the concentration decreases the definition of the probe increases. The presence of saline in the replacement of the blood permits light arising from adjacent turns to overlap and blur the image. When blood replaces the saline the higher absorption should sharpen the image, although the amplitude will be lower.

A series of eight sample passes were performed in each vessel at the three concentrations, the results of which are summarised in Figure 8-20d and Figure 8-21.

Sample #	Mean 'μ'	Standard Dev 'σ'	Coeff of variation σ/μ	Concentration IU
1	0.2085	0.0102	0.0487	500
2	0.1060	0.0215	0.2027	310
3	0.0322	0.0026	0.0793	80
Unknown	0.0411	0.0046	0.1110	-

Figure 8-21 A summary of results obtained from varying dilutions of fluoresceinated heparin

The viability of the system for recognising solutions of unknown concentration given series of controls of known dilutions was investigated. The data obtained showed that the peak fluorescence detected in dilutions of 500IU (sample #1) and 80IU (sample #3) were distributed so a single standard deviation was within 4.9% and 7.9% of the mean respectively ($(\sigma/\mu)\times100\%$). The curve plotted during sample #2 produced a coefficient of variation of 0.2027 assuming the data is distributed normally. This highly diverse data was attributed to the conditions under which the sample was analysed. It was the first sample to be analysed at which time the laser had not stabilised and the power delivered was not constant.

A curve was plotted for the three known dilutions and a fourth of unknown concentration deduced using a new false artery. The unknown was presented to be 80IU of fluorescein when the experiment was complete, and hence a peak wavelength ratio identical to sample #3 was expected. Given the mean and standard deviation of sample #3 the probability of the mean value of the unknown sample (0.0411) occuring is the same concentration is approximately 0.3%. Since this probability is extremely small (> 3 SD from the mean) it is clear that the two samples were either of slightly different concentrations of the artery used during the second experiment produced different results due to differences in construction. It is impossible to make an identical artery in each case, and although the same artery could be used for all experiments it was though unreliable to do so due to the heparin remaining bound to the wall of the helix during successive experiments even when flushed.

It can be concluded that in order to make repeatable readings it is extremely important to monitor the conditions under which the experiment is conducted, i.e. the probe is located in the same position in the vessel during successive investigations.

8.4.3.3 Test FH2/3 - Rabbit iliac artery

The second half of the experiment involved introducing conjugated heparin into the aorta of an anaesthetised rabbit during blood flow using a perforated angioplasty balloon by the technique described by Hong *et al* (1993). The iliac artery was then removed, flushed with saline and suspended between the lumen of two modified arterial catheters. This produced a 50mm working section through which the optical fibre probe could be passed. The arrangement was then enclosed in light shielded housing and the probe withdrawn along the vessel sampling absorption and emission wavelengths at 0.5mm intervals for photon count times of 1 second. The procedure was performed on two rabbit iliac arteries, 3mm ID, laced with fluoresceinated heparin 60IU and 400IU concentrations. It was surmised that the heparin would stick to the vessel wall and enter the tunica media where-upon its fluorescent label would be detectable by the probe.

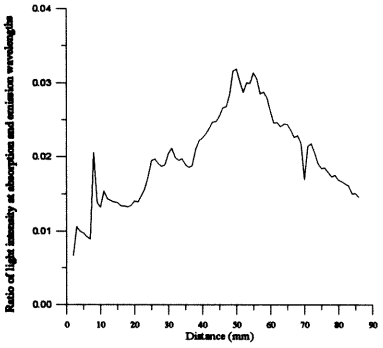

Figure 8-22a

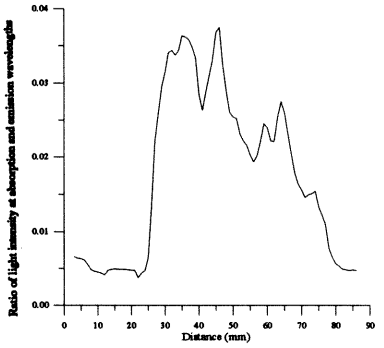

Figure 8-22b

The fluorescence of fluoresceinated heparin introduced into a rabbit iliac artery through a perforated angioplasty balloon at dilution s of 60IU and 400IU respectively

The diagrams shown in Figure 8-22a and Figure 8-22b are the profiles of fluorescence along the length of the vessel for concentrations of 60IU and 400IU respectively. The amplitude of the signal increased from 0.0319 to 0.0375 (an increase of 17.5%). The method proved that not only could the probe detect fluorescence emanating from the vessel wall which may arise from damaged endothelium, but the probe may also be useful for the analysis of local drug delivery (see discussion section). A set of 8 passes were performed on each of the two arteries. The signals obtained

from each were seen to steadily degrade with each successive withdrawal and may be caused by the probe tip degrading the vessel wall and dispersing the heparin, or by the heparin diffusing out of the tunica media (Figure 8-23).

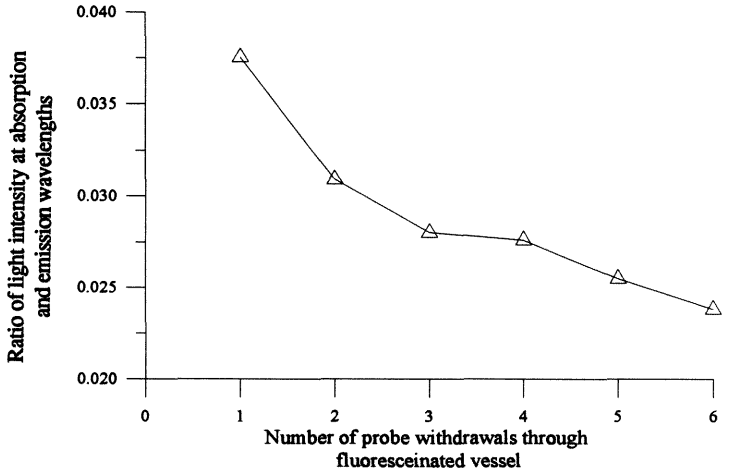

Figure 8-23 The degradation of the peak fluorescence corresponding to the fluoresceinated heparin after repeatedly withdrawing the probe along the vessel

If the probe is to be used in surgery the design of the catheter is extremely important as it should disrupt the vessel wall as little as possible so that measurements are repeatable.

8.4.3.4 Discussion

The optical fibre fluorescence probe has shown that it may be feasible for use in a real mammalian artery. Although experiments with labelled damaged endothelial cells *in-vivo* were not performed directly, fluorescence of a level comparable to that expected from labelled cells was detected. The manufacture of the fluoresceinated conjugate in the laboratory on closer inspection was extremely inefficient, and it was suspected that only 1:38 parts of fluorescein bound to the heparin. Although this does not affect the experiment conducted in the false artery, the sodium fluorescein being dissolved in the heparin, it does affect the results obtained using the rabbit artery. The fluorescence detected is dependent on the heparin binding to the vessel wall. If the heparin is not bound to the sodium fluorescein a peak will not be detected. If the

binding is inefficient the signal-to-noise ratio will increase by a factor of 38 when the process is refined, making the probe 38 times more sensitive than it is currently, i.e. 1.5IU would be easily detectable.

The results also have emphasised the inefficiency of the drug delivery system using a perforated angioplasty balloon. The leakage of the drug into blood stream produces a broad dispersed peak which is not as distinct as the idealised simulated model. The majority of the drug is washed away by blood flow, and only a small percentage reaches the target site.

The conditions under which the experiment were performed were not favourable to the probe due to the requirement to harvest the vessel from the body. The tissues shielding the vessel from an external light source (see section 8.3.3.2) are advantageous for the *in-vivo* light source as the background photon count due to spurious light is reduced.

The design of a probe for intravascular use in a real patient is important if the results are to be repeatable. If the probe repeatably rubs the endothelium the endothelial cells will be damaged impairing the healing process (More *et al.*, 1994). It is envisaged that a further probe design may use a second transparent tube, shielded from the blood, to act as a guide and preventing the tip striking the vessel wall.

8.5 Discussion

The main disadvantage of the fluorescent probe relative to the radiation apparatus described in the early part of chapter 7 is the susceptibility of the system to absorption of the blood. Prior arterial catheter designs have attempted to displace the blood from the target area using a catheter perfused with saline. This technique is often used in conjunction with angioscopy to produce a clearer image of atheromatous arteries (Ramee and White., 1994). The technique does however rely on maintaining a seal between the catheter and the vessel wall. Such a seal is difficult to maintain, and if poorly defined will permit an unknown dilution of blood and saline to form around the catheter; the absorption of light due to the unknown dilution is thus unknown and the measurement is meaningless. In order to make quantitative measurements the diameter of the artery must be known and the probe must be kept either adjacent to the vessel

wall or in the centre. Given the known position it is then valid to pass saline or a similar solution into the blood stream at a known flow rate in order to dilute the blood.

The use of the system on a clinical basis requires the design to be refined. The photomultiplier tube is the obvious detection device as its high gain could not be rivalled until recently. Avalanche photo diodes were mentioned in the initial project proposal but the gains of such devices cannot match that of the PMT: a typical gain of a PMT is 1.3×10^6 with a quantum efficiency (QE) of 20% at the blue end of the electromagnetic spectrum. The main disadvantage is the high photon count time required to produce a fluorescence characteristic from a low amplitude signal with a reasonable resolution. The PMT selected had a background dark current count of 700 counts per second at maximum gain (see graphs in appendix C). Increased photon count time increases the time taken to withdraw the probe and hence the time taken to perform the analysis. Stability was also found to be a problem during the construction of the apparatus. When exposed to excessive light the dark current of the device will rise significantly and deems the device unusable for at least 24 hours. The current advancement in charge-coupled devices (CCD) technology makes the replacement of the photomultipler equipment with such a device viable. CCDs are currently used for imaging applications in medicine and astronomy, but their high sensitivity could make them suitable for this application (Kim *et al.*, 1993 and Holton., 1994).

It is desirable to use an excitation light source disassociated to the detector and outside the body, however due to the high attenuation of the blood, vessel wall and intervening tissues this is not possible: at least one order of magnitude per millimetre in whole blood. The blood has a lower absorption in the red end of the electromagnetic spectrum. In order to exploit this the sodium fluorescein would ideally be replaced with a material of an appropriate emission wavelength such as occurs in porphyrins (Stryer., 1975). The excitation wavelength is still in the UV and is not able to penetrate the tissues satisfactorily. The experiments conducted were confined to the laboratory containing the argon ion laser which was not portable as it was 3 phase and water cooled. This meant that the experimentation was restricted. It was not possible to conduct an experiment in a living animal model, i.e. in blood flow, due to the restrictions of the animal licence. The best approximation was achieved given the conditions available. Future work would include the replacement of the water-cooled

laser with either an air-cooled or solid state alternative. Ar^+ lasers are now available at powers up to 150mW which are both air-cooled and may be supplied from a mains supply (240V AC). The availability of solid state semiconductor lasers has to date been limited due to the non-existence of an appropriately doped semiconductor with a bandgap able to produce laser light towards the blue end of the electromagnetic spectrum. Currently available devices have a life-time limited to 9 minutes, new devices using double heteroscructures are able to produce life-times of 10,000 hours at wavelengths 450nm to 520nm in continuous or pulsed wave mode (Sony Corp. Res. Centre, 1994). It was felt however that when available such lasers would not be suitable as they are not able to provide sufficient power to overcome the attenuation of the blood: currently available devices at these wavelengths are not usually able to deliver more than a few milliwatts of power.

The optical fibre fluorescent probe is not limited purely for examining localised damage to the vascular endothelium, it may be used for any application (biomedical or otherwise) where a fluorescent material is present. The size of the probe does however make it a candidate for an *in-vivo* catheter. It has been suggested that such a device could be used for measuring either blood flow or local vascular drug delivery. A drug can be delivered to a vessel directly using a perforated angioplasty balloon. If the drug is linked to a fluorescent label the quantity of the drug which has penetrated the vessel can be examined. The probe would measure the quantity of drug left at the site at given times after the treatment. Blood flow could be quantified by placing a small quantity of fluorescent dye into the blood stream and timing it to travel a specific distance. If this were to be combined to the pressure transducer described in chapters 3 to 5 both blood pressure and blood flow may be quantified. The Department of Cardiology is particularly interested in this application and have sought further funding from the British Heart Foundation to carry out further experiments both on rabbits and man. The optical fibre to light source coupling optics are to be made more efficient and the probe miniaturised in order to reduce obstruction to blood flow in living tissue.

The endothelial cell damage probe differs from the pressure transducer catheter in the respect that the main expense is in the optical, detection apparatus and laser equipment. The probe comprises of only two optical fibres and connectors. The

disposability of the device is more relevant because of its highly invasive nature in the blood stream and so low cost is desirable.

8.6 Conclusions

The research into the optical fibre vascular damage probe has significantly contributed to the understanding of the use and detection of monoclonal antibodies labelled with both radio-active and fluorescent biological markers. Clearly this research has opened a wider research horizon than was first predicted, it holds a promising future, particularly that of the fluorescence probe. The development of monoclonal antibodies able to recognise specific antigens, is a recent research development in itself, the integration of such technology with that of optical fibres should lead to a completely disposable catheter which would be a useful diagnostic aid to the cardiologist.

This investigation has shown how optical fibre technology has been able to overcome a previously insoluble problem. Optical fibres are thus not only able to assist the physician, and so provide a means of performing investigative and therapeutic surgery more efficiently, but also allow totally new procedures to be undertaken.

Chapter 9

Conclusions, comparisons and further work

9.1 Introduction

The research discussed in this thesis has involved the investigation of two optical fibre sensor systems developed to aid in the diagnosis of specific clinical disorders: Obstructive Sleep Apnoea Syndrome (OSAS) and Arterial Restenosis (AR). The selection of the transducers for the investigation have contrasted the design considerations which must be evaluated when constructing a system for *in-vivo* use (Figure 9-1).

Description of property	Obstructive sleep apnoea syndrome	Arterial Restenosis
Transducer principle	Physical	Chemical
Modulation principle	Amplitude	Amplitude
In-vivo use	Semi-invasive	Highly-invasive
Transduction element	Complex (Physical movement)	Simple (Polished fibre)
Disposability	Yes (but expensive)	Yes
Manufacturing time	13 Hours	2 Hours

Figure 9-1 A table contrasting the differences of the transducers designed to assist in the diagnosis of OSAS and AR.

Both of the systems designed were constructed so as to be portable, data acquisition being performed on a *notebook size* computer, but that of the endothelial cell damage probe was limited due to the laser (safety and size). The two systems enable a contrast to be made between two amplitude modulated extrinsic sensors, using a chemical biosensor and a physical sensor as vehicles to examine the potential

application of optical fibre transducers for *in-vivo* use. Optical fibre sensors are not only useful in offering an alternative transducer system to commercial devices (e.g. in OSAS), but they are also able to access parameters previously unmeasurable (e.g. in AR). Moreover the data can be obtained in real-time and, if an experienced clinician is present, the patient can be diagnosed immediately.

9.2 Summary of pressure transducer design lessons

The principle of determining the site of airway collapse by pressure measurement is not a new idea, and has been investigated by several researchers (Skatvedt., 1993 and Tvinnereim and Miljeteig., 1992). Early research used a saline or air-filled tube to transmit the pressure signal to a remote site as pressure transducers were not sufficiently small to be housed in a catheter at that time. The development of silicon *micro-structure* technology has however now made this possible, and the advantages of the optical fibre as a miniature sensor not are so apparent. The miniaturisation of micro-structures and micro-machines to sizes of only a few microns is a formidable achievement. The cost of such devices for *in-vivo* use is high and consequently it is unlikely that it can be deemed disposable.

The optical fibre pressure transducer catheter (described in chapter 2 to chapter 5) was approximately 3mm in diameter (the widest point being the pressure isolation collars: 3.5mm). The main limitation encountered during the research was that of the materials equipment and knowledge. The main housing of the catheter was a hydrophobic PVC tube, with a lumen of less than 2mm. If this tubing were to be replaced by a thinner walled tube then the device would be narrower than any commercially available device, or any solid state device containing as many transducers. The other important issue is that of the so far unbreached limits of the transducer and catheter design. The main factor in the design of the optical fibre pressure transducer, once the location of the fibres in the housing with respect to the reflective transduction element had been determined, was the volume of gas contained inside the transducer. If sensitivity is to be maintained the volume of this gas must be maintained; hence a reduction in diameter must be compensated by increasing the

length of the transducer. The transducer was able to fulfil the original design criteria, and although investigation was not conducted on patients suffering from OSAS, the analysis performed on locally anaesthetised patients instructed to perform breathing exercises did distinguish palatal vibration associated with snoring. The model was further improved by conducting an investigation on six patients under general anaesthesia with a cross-section of abnormal and normal airways. Pressure waveforms describing oral and nasal breathing, airway obstruction, palatal vibration (snoring) and peristalsis were observed.

In conclusion, this transducer has not yet reached its theoretical limit for miniaturisation. Previous pressure transducer designs with optical fibres have been constructed with outer diameters of 350μm (Emanuelsson *et al.*, 1991) for intravascular use, however the measured pressures were greater (30mmHg to 70mmHg for systolic and diastolic respectively in a stenosised coronary artery). The final pressure transducer was able to resolve pressures of 10Pa, and is one of the more novel achievements (see section 9.5.1.1). The system was also able to overcome problems arising from macro-bending losses.

9.3 Summary of endothelial cell design lessons

The development of the endothelial cell damage probe (chapter 6 to chapter 8) has demonstrated how optical fibre technology is able to address an issue previously unsolved by former methods[1]. The use of antibodies, enzymes and similar agents for locating specific biological compounds in immunocytochemistry is one of the potentially most exciting areas of medical research. Two optical topologies were initially considered using radio-labelled and fluorofluor-labelled antibodies to detect damaged endothelial cells respectively. The technology investigated differs from that of the pressure transducer in the respect that it is still in its infancy. The use of the radio-nuclide to label the monoclonal antibody was possible *in-vitro*, but the apparatus for

[1] The endothelial cell damage probe is novel, and consequently protected under British patent: patent application number 9413769.2 (1994).

in-vivo detection was not feasible. The gain of the detection apparatus was not sufficiently high, and more importantly the available chemicals were so toxic that leakage into the blood stream would always be cause for concern. The use of a fluorescent label has made the investigation of a damaged coronary artery possible by taking real-time measurements, and hence removing the need for expensive histological investigations. Moreover the miniaturisation offered by the use of the optical fibre means that the recovery time of the patient is considerably shorter than if a more invasive investigative technique were to be used. Investigations were conducted on both simulated and mammalian vessels perfused with both blood and saline. The main disadvantage of the probe using fluorescence was its susceptibility to attenuation by the blood. This can be compensated by increasing the power of the excitation light source, but it should not be increased such that the blood is denatured at the probe tip. A scheme adopted by Warren *et al* (1995) integrated an A-mode Doppler probe and a optical fibre spectrophotometer into the same arterial catheter designed to detect fluorescence arising from arterial plaque. The distance information provided by the Doppler probe could then be used to compensate for the attenuation of the blood between the probe tip and target.

The design of the endothelial cell damage probe uses *state-of-the-art* optics, and although the efficiency may be improved slightly by further research the gains will be small in comparison to those available for the pressure transducer as the photon detection apparatus is the best available at the current time (see section 9.5.1.2).

9.4 Discussion

One of the most important issues to be addressed in the construction of a unit for *in-vivo* use is its disposability ease of sterilisation. The levels of cleanliness for each of the two devices are different in each case because of the differing invasive nature. The upper airway and gastric tracts are arguably the most contaminated part of the human body, and contain a multitude of normally harmless bacteria. Consequently the pressure transducer does not need to be *medically sterile*, although it does need to be *clean* and free of pathogenic organisms. In comparison the endothelial cell damage

probe penetrates the blood vessels, and contamination on the probe will be transferred into the blood stream. Autoclaving is the most common method for sterilising a device for *in-vivo* use and involves passing the equipment through superheated steam. This would destroy the polymer optical fibre used in both of the transducers. For this reason both transducers would ideally be disposable, and hence cost should be kept low. The fundamental difference between the two systems is the manner in which the pressure transducer is of complex design, where the endothelial probe is extremely simple: comprising only two optical fibres. This difference is also reflected in the design of the associated hardware. The pressure transducer uses relatively cheap emitters and receivers: approximately £20 each (a single transducer costing £60 in optical components). For a seven channel device £420 covers the cost of the optical components. Although the endothelial cell probe is simpler by the nature of its design, it requires *state-of-the-art* optics (collimating lenses and optical filters), a high power argon ion laser (£8000) as well as the photomultiplier tube. In contrast the expense of the pressure transducer catheter is markedly more in comparison with the passive biosensor. The complexity of the design makes the manufacture of each pressure device extremely expensive, and requires a great many man-hours to construct (Figure 9-2). In contrast the endothelial probe was constructed in 2 hours (not including polishing of optical terminations).

Transducer preparation	Optical fibre preparation	Construction of skeleton	Addition of connectors	Addition and latex preparation
1 hr	2 hrs	2.5 hrs	3 hrs	2.5 hrs

Figure 9-2 The distribution of time for construction of a seven channel optical fibre pressure transducer not including the time taken to polish the optical fibre connectors and waiting for adhesives to cure.

A lesson learnt from the construction of both devices was the importance of ensuring that not only are the materials used for construction able to interact, but they are also suitable for long term storage. This was a particular problem with the pressure transducer catheter. The housing of the catheter was a hydrophobic PVC tube, and consequently the latex used in the final dipping process would not adhere to it. To overcome this problem the surface of the tube was oxidised by heat treatment (see

appendix A.2). A less obvious design consideration was the interaction of the cured latex with the silicon sealants used to isolate the adjacent pressure chambers in the catheter. The sealant was initially able to maintain an air-tight seal for a shelf life of approximately one week, however beyond this the latex began to disintegrate. This was found to be caused by the chemicals in the sealant combining with ambient UV light which then attacked the latex. The problem was solved by replacing the sealant with an acrylic alternative. Such problems were also encountered in the construction of the biosensor. The liquid scintillant, used in the preliminary research, began to dissolve the probe tip over a period of 2 to 3 minutes, and caused the optical fibre to fracture. This was not a problem with the fluorescent probe, as there was no need for an active element. The final design of both devices had an indefinite shelf life if the catheters were kept clean, dust caps intact and, in the case of the pressure transducer, in a dark dry container and not exposed to excessive heat.

One of the most important considerations when designing a device, optical or otherwise, for *in-vivo* use is the study of the environment in which it is designed to operate, e.g. intravascular, intramuscular etc. The pressure transducer takes measurements from both the upper airway and the oesophagus and is subjected to a considerable amount of mechanical shock due to the presence of swallowing and coughing manoeuvres, and the ensuing peristaltic waves. Peristalsis has the effect of persistently pulling on the catheter in the direction of the stomach. There was also concern about the temperature change and the presence of fluid and mucus in the airway impairing the operation of the diaphragm to transfer pressure through the wall of the catheter and onto the transduction element. Although there is a temperature change in the airway during respiration, the time constant of the device was such that drift was negligible (17Pa). It was also found that the nose adequately saturated the air with water vapour by the time it had reached the level of the soft palate (the site of the airway collapse due to OSAS), and consequently mucus did not collect and congeal on the catheter housing.

The endothelial cell damage probe design had potential problems because of its *highly-extrinsic* design. Both probes are extrinsic in the respect that light is able leave an emitting optical fibre, strike a target and the return to a second optical fibre collecting the incoming light, but in the pressure transducer the light is not intended to

leave the confines of the transducer housing. The cell probe relies on laser light passing through the arterial blood to strike a target. It was found that it the laser was run at high power (>100mW) the proteins in the blood were destroyed and a denatured *calcified-like* deposit would form on the face of the emitting optical fibre due to the high power density of the laser light in the optical fibre core (2.04W/mm^2, assuming all light is coupled into fibre core of diameter 0.25mm).

The insertion of an *in-vivo* catheter into the airways and blood stream not only subjects the patient to differing levels of risk, but it also varies the susceptibility of the catheter to signal degradation due to the interaction of the catheter with the body fluids in tissue. The semi-invasive nature of the catheter and its location in the naso-pharynx means that accumulation of mucus and other secretions in the airway is unlikely due to the air being almost completely saturated with water vapour by the time it reaches the pressure transducers; consequently mucus does not have to opportunity to hard around the periphery of the catheter impairing the operation of the pressure transmitting diaphragm. The endothelial cell damage probe however is subjected to considerably more harsh conditions, and will be susceptible to the accumulation of platelets and fibrin on the end of the catheter. This phenomenon was encountered by Spencer *et al* (1995) when developing a catheter-tip PO_2 sensor for use in pre-term infants. Although it did not impair the operation of that particular sensor drastically the highly extrinsic nature of the endothelial cell damage probe may be a potential problem. Rolfe (1994) suggested a technique to coat the probe with a cellular layer to prevent this occurring, and may be an area for further work.

The patient investigations conducted established the importance of making a conscious patient comfortable with the surroundings as this will directly effect the validity of the reading. This was apparent in the case of the pressure transducer, where peristaltic waves can distort the signal. This did not occur in the anaesthetised patient.

The optical fibre sensor has many advantages over conventional measurement techniques, the details of which are presented in chapter 1. It is important to realise that there are also some important potential disadvantages in using optical fibres in the design. One of the main advantages of the optical fibre are its dielectric properties. Conversely this means that should any part of the sensor require electrical power, extra

conductors have to be integrated into the catheter. An example of this could be the requirement of a temperature sensor in the single channel pressure transducer to compensate for temperature change. Optical fibre technology is in its infancy, and although it potentially holds many benefits over conventional sensors techniques applications are currently limited because the optics involved are often expensive.

The explosion of data collected by physical and biological sensors such as those discussed above emphasise the need for adequate computer and decision support systems to analyse the data. Both of the systems presented are candidates for semi-automated computerised decision support systems using a knowledge-based expert system. This would be a worthwhile and useful area for further work. Research into optical fibres and their associated optical components: opto-couplers, detectors etc, is expanding and the technology is not yet established. As a consequence future gains made in the technology of optical systems could be expected to be large in comparison with established technologies. This will make decision support and data storage even more important.

9.5 Further work

Optical fibres is currently one of the fastest growing fields in engineering, and consequently previously impractical ideas may be worth further evaluation in future years (e.g. the optical fibre endothelial probe using scintillation, chapter 7).

9.5.1 Engineering based

9.5.1.1 The pressure transducer

Although the optical fibre pressure transducer catheter did not suffer from some of the practical design limitations, such as sensitivity, that were due to the limitations in the technology some practical problems were found. The seven transducers encased in the catheter required 21 optical connectors to be disconnected every time the catheter needed changing. It is envisaged that a future design would encompass an *optical fibre ribbon cable* to decrease the set-up time. The second main disadvantage again arises from the pre-calibration stage which must be performed prior to each measurement.

The data from this procedure is later used for scaling in order to make a quantitative measurement. Although the calibration cannot be avoided if the recording is going to be accurate, further software development would make the system more *user-friendly* for the clinician. Such a package could include auto-scaling, auto-ranging and data acquisition. Given further evaluation of the data obtained, research could be extended into creating a knowledge-based decision support system for the apparatus to aid in the diagnosis.

The construction of the device presented a formidable material challenge. Further investigation, and the adoption of the idea on a commercial basis could foreseeably reduce the size of the device to less than 2mm (smaller than any currently commercial or researched alternative (Skatvedt., 1993)). As well as the single transducers being made smaller, the latex sheath encapsulating the catheter can also be improved (Figure 9-3) and shaped such that the addition of sealants to isolate adjacent chambers is not necessary.

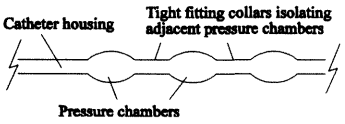

Figure 9-3 The improved pressure transducer diaphragm

9.5.1.2 The endothelial cell damage probe

The development of the charge-coupled device (CCD) for low-level light detection would offer a solid state alternative to the photomultiplier tube and remove the need for long photon count times. It would also not require long recovery times should it be exposed to an unacceptably high light level. The CCD can provide higher gains than the Avalanche Photodiode (APD) which is the current commercially available solid state alternative.

The light source used was a liquid-cooled, 3 phase argon ion laser. This wavelength (488nm) is the optimum solution for the selected sodium fluorescein biological label, but the laser rating was over specified (750mW peak), and cumbersome to use. Although systems using high power lasers cannot be considered portable without first addressing the necessary safety issues, the replacement of the

system with a lower power (100mW) air-cooled, mains powered system is more desirable. Alternatively a HO^{3+} or Pr^{3+} doped optical fibre laser could be used. Poole (1992) reported the availability of a laser able to deliver laser light at 491nm (cf: 492nm required to stimulate Sodium Fluorescein). For limited use such a system could be made portable if the safety criteria were satisfied (BS EN60601(2.22) and BS EN60825: laser safety).

The final criticism is the semi-automated nature of the measurement procedure, with further research the system could be made fully automatic by implementing the control for the probe withdrawal device at software level.

9.5.2 Medical based

9.5.2.1 The pressure transducer

In order to evaluate the system fully a large study of patients (50 or more) both with abnormal and normal airways, and sufferers from OSAS should be studied. The statistical results from these studies can then be used to comment on the usefulness and reliability of such a system for routine overnight sleep study.

Once the ability to localise airway collapse is confirmed, patients previously thought unsuitable for palatal surgery by conventional means (radiology) (see chapter 2) will be investigated and, if deemed suitable, subjected to operation. The outcome will be evaluated by further sleep studies and questionnaire.

9.5.2.2 The endothelial cell damage probe

In order to conduct a fuller evaluation of the probe, it would be useful to conduct a series of experiments in blood within a mammalian vessel using antibody labelled endothelial cells, having previously damaged the vessel with an inflated angioplasty balloon. This experiment was not conducted due to the restrictions of the animal licence, however such an investigation would combine all of the ideas and results present throughout this document.

The probe is not limited purely to the detection of endothelial cells labelled by a fluorescent material. Applications may extend to measuring blood flow and local vascular drug delivery systems (see chapter 8, section 8.4.3.4 for further details).

9.6 *In-vivo* optical fibre sensors - the future?

Sensors are used as either part of a therapeutic procedure, or just to assist in the diagnosis of the patient. To examine the potential for optical fibre sensors for *in-vivo* use is it useful to identify first the parameters which can be measured with existing techniques, and then examine whether they are candidates for measurement by fibre optic transducers. The most obvious set of transducers which are applicable to physiological measurement are physical sensors measuring pressure, temperature, flow, displacement and force. There are very many locations in the human body where such measurements can take place, but in each case the measurement is fundamentally the same, although the static and dynamic requirements will differ in each case. A good example is that of pressure whereby the pressure range and size of the catheter is dependent on the measurand and the measurement site.

Chemical and biochemical sensors or *biosensors* can be considered to be a subsidiary of the *primary* physical sensors in the sense that they modulate physical parameters to measure molecular changes: colour change for example. The wide range of biochemical-reactions, particularly the highly-specific antibody-antigen reactions, suggests that biosensors will have a major role in biochemical sensing. The ability of biochemical reactions to produce optically-detectable changes suggests that optical fibre biosensors will become an attractive technology in the future.

The availability of biological parameters to measure is limited only by the imagination of the physician. Prior to this research it would have been almost impossible to foresee the need for an endothelial cell damage probe in the arteries. Biochemical sensors measure properties such as tissue damage (chapters 6 to 8), biochemical composition, pH, chemical affinity and biochemical interaction. The choice of available chemicals is constantly increasing. In contrast the pressure transducer would have been perhaps easier to envisage as it is less obscure.

The field of optical fibres and their associated optical components is extremely dynamic. Manufacturing techniques are constantly improving making the standard of the equipment better and the cost lower. The infancy of the technology means that the gains in optical fibre sensors will be large in comparison with established technology. Some of the most promising fibre optic systems are those associated with oncology,

where optical fibre sensors are used to analyse tumour cells. This is performed by fluorescence or pH mapping of an area of tissue (Baldini and Mignani., 1994). This use of optical fibre parameters allows access to previously unmeasurable parameters.

9.7 Concluding remarks

Two amplitude modulate extrinsic optical fibre sensors have been presented. The optical fibre pressure transducer offers an alternative device to measure a physical parameter which is accessible with commercially available equipment, but which has the potential for further miniaturisation so making it a candidate for further development in order to replace existing commercial devices. The method of catheter construction and the physical transduction element is novel. The endothelial cell damage probe accesses a parameter previously unquantifiable and is novel in its entirety. It provides a means of conducting real-time analysis of the arterial vascular wall without subjecting the patient to a long recovery period in hospital.

This chapter argues that it is important for researchers to gain a clear understanding of the environment in which the transducer is to operate, and the key fields of development as outlined. The research discussed is a contribution to the *international* effort in the development of optical fibre sensors for use in the human body, by taking two specific examples of a biochemical and physical sensor and using them as vehicles to examine some of the major design considerations.

The systems discussed are both prototype designs, but both the pressure transducer catheter and the endothelial cell damage probe should be a viable as they stand for assisting in the diagnosis of obstructive sleep apnoea syndrome and arterial restenosis respectively.

References

[1] M.Aizawa (1991), Principles and applications of electrochemical and optical biosensors, Analytica Chimica Acta, **250**(1), pp.249-256

[2] M.B.Alexander and K.P.Brin (1993), Balloon angioplasty in coronary artery disease: Recent advances, Primary cardiology, **19**(11), pp.42-54

[3] H.V.Anderson (1993), Restenosis after coronary angioplasty, Disease-a-month, **39**(9), pp.615-670

[4] M.A.Arnold (1985), Enzyme-based fibre optic sensor, Anal. Chem, **57**, pp.565-566

[5] L.Badimon *et al* (1992), Endothelium and atheroslerosis, J. of hypertension, **10**(2), pp.s43-s50

[6] F.Baldini and A.G.Mignani (1994), *In vivo* biomedical monitoring by fibre optic systems, Proc. of 10th optical fibre sensors conference (Scotland), SPIE, **1**, pp.80-89

[7] F.Baldini *et al* (1987), Model for an optical fibre pH sensor, NATO ASI Series E: Applied sciences, **132**, pp.437-443

[8] A.L.Bartorelli *et al* (1991), *In-vivo* human atherosclerotic plaque recognition by laser-excited fluorescence spectroscopy, J.Am. Coll. Cardiol, **17**(6), pp.160B-168B

[9] C.S.Beardsmore *et al* (1982), Assessment of the catheter-tip pressure transducer for use in infant lung function tests, Med. Biol. Eng. Comput., **20**, pp.657-660

[10] R.E.Benner *et al* (1991), Light distributions from diffusing optical fibre tips, Lasers in the life sciences, **4**(2), pp.103-113

[11] J.W.Berthold (1994), Historical review of microbend fibre optic sensors, Proc. of SPIE 10th optical fibre conf (Scotland), **1**, pp.182-186

[12] H.K.Bhullar (1992), Computerised extraction and analysis of data from medical records: an examination of QT dispersion in the electrocardiogram, Ph.D Thesis, University of Leicester, pp.1.8-1.18

[13] R.E.Bicking (1982), A survey of pressure transducer technology, Medical device and diagnostic industry, **4**(10), pp.49-55

[14] W.J.Bock (1992), GaAs-based fibre optic pressure sensor, IEEE Trans on Instrum and Meas, **41**(1), pp.68-78

[15] J.Bonner (1994), Keeping the blood flowing, The New Scientist, **1931**, pp.32-35

[16] M.G.Bourassa *et al* (1984), Percutaneous balloon angioplasty, **in** Recent advances in cardiology (9th Ed), Edited by: D.J.Rowlands, Curchill Livingstone, Chapt.7, pp.193-212

[17] T.D.Bradley (1986), Pharyngeal size in snorers, nonsnorers, and patients with obstructive sleep apnea, N.Engl.J.Med, **315**, pp1327-1331

[18] M.Brenci and F.Baldini (1992), Fibre optic optrodes for chemical sensing, Proc. of 8th Int. Conf. in optical fibre sensors, IEEE lasers and electro-optics soc, pp.313-319

[19] S.L.Brooks and A.P.F.Turner (1987), Biosensors for measurement and control, Measurement and conrol, **20**, pp.37-43

[20] W.Cheong *et al* (1991), Laser balloon angioplasty, Clin. Reviews in biomed eng, **19**(2-3), pp.113-1466

[21] N.S.Cherniak and D.W.Hudgel (1988),*The upper airway muscles*, Their role in sleep-related respiratory dysrhythmias, **in** Control of breathing during sleep and anaesthesia, edited by W.A.Karczewski *et al*, Plenum Press (USA), pp.29-37

[22] J.D.S.Chu *et al* (1964), Lung compliance and lung volume measured concurrently in normal full-term and pre-term infants, Pediatrics, **34**, pp.525-532

[23] V.C.Colussi *et al* (1994), Fluorescence distribution of hematoporphyrin derivative in rats normal tissue, Phys. in Med. and Biol, Abstr. World Congress on Med. Phys and Biomed. Eng (Rio de Janeiro, Brazil), **39a**(1), pp.154

[24] R.M.Cothren *et al* (1994), Prospective evaluation of autofluorescence spectroscopic diagnosis of dysplasia *in-vivo* using a probability-based algorithm, Phys. in Med. and Biol, Abstr. World Congress on Med. Phys and Biomed. Eng (Rio de Janeiro, Brazil), **39a**(1), pp.143

[25] R.L.Crumley *et al* (1987), Determination of obstructive site in obstructive sleep apnea, Laryngoscope, **97**, pp.301-308

[26] A.G.Crenshaw *et al* (1989), A new *transducer-tipped* fibre-optic catheter for measuring intramuscular pressures, J. of orthopaedic research, **8**, pp.464-468

[27] A.C.Cuello *et al* (1982), Immunocytochemistry with internally labelled monoclonal antibodies, Proc.Acad.Sci (USA),**79**, pp.665-669

[28] C.Dafu *et al* (1993), Optical-fibre pH sensor, Sensors and actuators A, **12**(1), pp.29-32

[29] C.Dickens (1836), The posthumous papers of the pickwick club, Chapman and Hall (London)

[30] S.J.Dodd *et al* (1992), Quantitative light emission as a probe of electrical treeing processes, IEEE Proc. 4th Int. Conf. on conduction and breakdown, Italy, pp.308-312

[31] N.J.Douglas (1990), Upper airway imaging, Clin. Phys. Phyiol. Meas, **11**, Suppl.A, pp.117-119

[32] J.E.Drorbaugh *et al* (1963), Compliance of the lung during the first week of life, Am. J. Dis. Child, **105**, pp.63-69

[33] T.Duncan (1987), Physics A textbook for advanced level students (2nd Ed), John Murray publishers Ltd, pp.232-243

[34] C.P.Eduardo *et al*(1994), The usage of the laser in dentistry, Phys. in Med. and Biol, Abstr. World Congress on Med. Phys and Biomed. Eng (Rio de Janeiro, Brazil), **39a**(1), pp.139

[35] H.Emanuelsson *et al* (1991), Initial experiences with a miniaturised pressure transducer during coronary angioplasty, Catheterization and cardiovascular diagnosis, **24**(2), pp.137-143

[36] F.Fankhauser *et al* (1989), Integrated optical fiber systems - some theoretical aspects, International Ophthalmology, **13**(4), pp.239-242

[37] J.T.Fell (1988), Surface and interfacial phenomena, in Pharmaceutics: The science of dosage form design, edited by M.E.Aulton, Churchill Livingstone, Chapt.4, pp.50-61

[38] J.S.Forrester (1994), Laser Angioplasty: Current and future prospects, in Textbook of interventional cardiology (2nd Ed), edited by E.J.Topol, W.B.Saunders Company, **2**, 1994, pp.959-965

[39] J.C.Fothergill *et al* (1988), Optical and electrochemical detection of DNA, Biomaterials, **9**, pp.66-70

[40] D.B.Fram and R.G.McKay (1994), "Hot" balloon angioplasty, in Textbook of interventional cardiology (2nd Ed), Edited by: E.J.Topol, W.B.Saunders Company, **2**, pp.821-825

[41] W.A.Gambling (1991), Optical fibres for sensors, Sensors and actuators A, **A23**(1-3), pp.191-196

[42] W.A.Gambling and S.B.Poole (1988), Optical fibres for sensors, in Optical fibre sensors: principles and components, Edited by J.Dakin and B.Culshaw, Artech house Inc, pp.249-261

[43] H.Gastaut *et al* (1965), Etude polygraphique des manifestations episodiques (hyniques et respiratoires) diurnes et nocturnes du syndrome de Pickwick, Rev. Neurol, **112**, pp.573

[44] R.C.Gauthier and J.Dhliwayo (1992), Birefringent fibre-optic pressure sensor, Optics and laser technology, **24**(3), pp.139-143

[45] K.F.Gibson *et al* (1994), Controlled laser ablation of bone cement, Phys. in Med. and Biol, Abstr. World Congress on Med. Phys and Biomed. Eng (Rio de Janeiro, Brazil), **39a**(1), pp.148

[46] J.P.Golden *et al* (1994), An evanescent wave biosensor - part II: Fluorescent signal acquisition from tapered fibre optic probes, IEEE Trans. on Biomed. Eng, **41**(6), pp.585-591

[47] K.T.V.Grattan (1987), Recent advances in fibre optic sensors, J. Int. Meas. Confed, **5**(3), pp.122-134

[48] K.T.V.Grattan (1989), New developments in sensor technology - fibre and electro-optics, Measurement and control, **22**, pp.165-175

[49] C.Guilleminault and M.Partinen (1990), Obstructive sleep apnea syndrome, Raven Press Ltd (New York), pp71-98

[50] A.C.Guyton (1981), Textbook of medical physiology (6th Ed), W.B.Saunders Company, Chapt.15 & 18, pp.176-181, 206-231, 479-481

[51] Z.M.Hale and F.P.Payne (1994), Fluorescent sensors based on tappered single-mode optical fibres, Sensors and actuators B, **17**(3), pp.233-240

[52] E.F.Haponik *et al* (1983), Computerized tomography in obstructive sleep apnea, AM. Rev. Respir. Dis, **127**, pp.221-226

[53] F.M.Haran (1994), Bend loss oscillations in single-mode optical fibre high order recoupling, Optics Communications, **108**(1-3), pp.55-59

[54] A.L.Harmer (1987), Guided wave chemical sensors, OFS NATO ASI Series E: Applied sciences, **132**, pp.210-219

[55] P.Hauri (1977), Current concepts: The sleep disorders, Scope publications,, pp.6-20

[56] E.Hecht (1987), Optics (2nd Ed), Addison-Wesley publishing company, pp.153-167

[57] P.Horowitz and W.Hill (1990), The Art of Electronics (2nd Ed), Cambridge University Press, Chapt.4, pp.263-284

[58] W.C.Holton, (1994), CCD Technology has brought profound changes to the world of bioimaging, Biophotonics, **1**, pp.45-51

[59] M.K.Hong *et al* (1993), Feasibility and drug delivery efficiency of new balloon angioplasty catheter capable of performing simultaneous local drug delivery, Coronary artery disease, **4**(4), pp.1023-1027

[60] R.L.Horner *et al* (1989), Pharyngeal size and shape during wakefulness and sleep in patients with obstructive sleep apnoea, Quarterly J. of Med, **72**(268), pp.719-735

[61] D.W.Hudgel (1993), Properties of the upper airway during sleep, ENT Journal, **72**(1), pp.42-45

[62] D.W.Hudgel (1992), Mechanisms of obstructive sleep apnea, Chest, **101**(2), pp.541-549

[63] D.W.Hudgel and C.Hendricks (1988), Palate and hypopharynx - Sites of inspiratory narrowing of the upper airway during sleep, AM Rev. Respir. Dis., **138**, pp.1542-1547

[64] D.A.Jackson (1987), Overview of fibre-optic interferometric sensors, Inst. Phys: Short meeting on fibre optic sensors (Scotland), IOP Publishing Ltd, **7**, pp.1-22

[65] D.A.Jackson *et al* (1992), Three phase current measurement using a hybrid current sensing technique, Proc of 8th optical fibre sensors conference (USA), IEEE lasers and electro-optic soc., pp.426-429

[66] D.A.Jackson and J.D.C.Jones (1986), Extrinsic fibre-optic sensors for remote measurement: part one, Optics and laser technol., **18**(5), pp.243-252

[67] Jenrick *et al* (1989), Amiga 3D graphic programming in Basic, Abacus publishing (Germany), Chapt.2, pp.7-18

[68] H.J.Jeong *et al* (1994), Polarisation characteristics of mode locked fiber laser gyroscope, Proc. of 10th optical fibre sensors conference (Scotland), SPIE, **1**, pp.124-127

[69] N.B.Jones and G.Papageorgiou (1988), Optical fibre sensors: smaller, cheaper, faster, Sensor review, **8**(1), pp.19-22

[70] A.Ju and A.S.Siddiqui (1993), Theory of a novel high-sensitivity optical-fibre gyroscope, IEEE J. of Optoelectronics, **140**(2), pp.150-156

[71] F.Kajiya *et al* (1987), An optical-fibre laser doppler velocimeter and its application to measurements of coronary blood flow velocities, Medical progress through technology, **12**(1-2), pp.77-85

[72] Y.V.Kamami (1994), Outpatient treatment of sleep apnoea syndrome with CO_2 laser assisted UPPP, J. of Otolaryngology, **23**(6), pp.395-398

[73] C.K.Kao (1988), Optical fibre-Its prognosis and its economic impact, in Optical fibre, Peter Peregrinus Ltd, pp.146-151

[74] M.D.Kaplan *et al* (1985), Vascular recanalization with the argon ion laser: the role of blood in the transmission of laser energy, Lasers in surgery and medicine, **5**(3), pp.275-279

[75] S.P.Keenan *et al* (1994), Long-term survival of patients with obstructive sleep apnea treated by uvulopalatopharynoplasty or nasal CPAP, Chest, **105**, pp.155-159

[76] S.E.Kim *et al* (1992), Silicon differential pressure transducer line pressure effects and compensation, ISA, **212**, pp.809-820

[77] M.H.Kim *et al* (1993), Open electrode CCD UV/XUV sensistive detectors for astonomy, Dept. of Engineering and Astronomy, University of Leicester, Report 93-27, Chapt.2, pp.4-8

[78] C.Köhl (1990), Alteration of airway wall temperature during different inhalation procedures, J. of Aerosol. Sci., **21**(S2), pp.S415-S417

[79] Y.Koite *et al* (1992), Measurements of mesopharyngeal pressure in patients with obstructive sleep apnea, Adv.Otorhinolaryngol., **47**, pp.260-266

[80] K.König *et al* (1992), Fluorescence detection and photodynamic activity of endogenous protoporphyrin in human skin, Optical Engineering, **31**(7), pp.1470-1474

[81] T.Kudoh (1991), An integrated miniature capacitive pressure sensor, Sensors and actuators A, **29**, pp.185-193

[82] M.T.Laine *et al* (1994), A modification on the pressure-flow technique for measuring breathing of cold air and its effect on nasal cross-sectional area, J. of orthodontics and denofacial orthopedics, **105**(3), pp.265-269

[83] M.L.J.Landsman *et al* (1978), A fibre optic reflection oximeter, Pflügers Archiv: European J. of Physiol., **373**, pp.273-282

[84] T.Leuthner (1994), Development system for pulse oximetry, Med. & Biol. Eng. & Comput., **32**(1), pp.596-598

[85] Y.Libo and Q.Anping (1991), Fiber-optic diaphragm pressure sensor with automatic intensity compensation, Sensors and Actuators. A, **28**, pp.29-33

[86] L.Lindström (1970), Miniaturised pressure transducer intended for intravascular use, IEEE Trans. on Biomed. Eng., **17**(3), pp.207-219

[87] F.Litvack (1994), Excimer laser coronary angioplasty, in Textbook of interventional cardiology (2nd Ed), edited by E.J.Topol, W.B.Saunders Company, **2**, 1994, pp.840-853

[88] K.Lossnitzer *et al* (1984), Myocardium vessels, calcium, Knoll AG (Ludwigshafen), 1984, pp.51-101

[89] G.Loudon (1991), Advances in knowledge based signal processing: a case study in EMG decomposition, Ph.D Thesis, University of Leiecester, pp.2.1-2.2

[90] R.Lydic and J.F.Biebuyck (1988), Clinical physiology of sleep, American physiological society, Chapt. 7, pp.97-123

[91] R.T.Lyon *et al* (1987), Vessel, Plaque and lumen morphology after transluminal balloon angioplasty, Ateriosclerosis, **7**, pp.306-314

[92] B.D.Maccraith *et al* (1993), Fibre optic sensor based on fluorescence quenching of evanescent-wave excited ruthenium complexes in sol-gel derived porous coatings, Analyst, **114**(4), pp.385-388

[93] B.D.Maccraith and F.J.McAleavy (1994), Water detection using fluorescent thulium-doped fluoride fibre pumped by low cost semiconductor laser, Proc. of SPIE 10th optical fibre conf (Scotland), **1**, pp.90-93

[94] G.B.J.Mancini, Digital coronary angiography in the evaluation of interventional techniques, in Textbook of interventional cardiology (2nd Ed), edited by E.J.Topol, W.B.Saunders Company, **2**, 1994, pp.1033-1051

[95] W.McBride *et al* (1988), Restenosis after successful coronary angioplasty: Pathophysiology and prevention, New England J. of Medicine, **318**(26), pp.1734-1737

[96] P.McGeehan (1987), The market for fibre optic sensors: chemical, biological and biomedical potenetial, IOP short meetings: Fibre optic sensors, Inst. of Phys., **7**, pp.139-147

[97] D.S.McNally *et al* (1992), Development and validation of a new transducer for intradistal pressure measurement, J. Biomed. Eng., **14**, pp.495-498

[98] D.L.Meadows and J.S.Schultz (1993), Design, manufacture and characterisation of an optical fibre glucose affinity sensor based on anhomogeneous fluorescence energy transfer assay system, Analytica Chimica Acta, **280**(1), pp.21-30

[99] R.S.Medlock (1987), Fibre optic intensity modulated sensors, NATO ASI Series E: Optical fibre sensors, **132**, pp.131-141

[100] W.B.Mendelson *et al* (1977), Human sleep and its disorders, Plenum Press (USA), pp.1-20

[101] A.G.Mignani and M.Brenci (1991), Optoelectronic devices: fibre-optic sensors for biomedical and environmental applications, Bioptics: Optics in biomedicine and environmental sciences, **1524**, pp.272-289

[102] W.J.Moore (1974), Physical Chemistry (5th Ed), Longman, Chapt.11, pp.479-481

[103] R.S.More *et al* (1994), Temporal vessel wall changes in an experimental model of angioplasty, J. of pathology, **73**, pp.319-324

[104] J.D.Muhs (1992), Silicone rubber fibre optic sensors, Photonics Spectra, Laurin Publishing Co., July Issue

[105] J.D.Muhs *et al* (1991), Overview of silicone-rubber fibre-optic sensors and their applications, SPIE: Dist. and multiple fibre optic sensors, **1586**(1), pp.107-116

[106] R.K.Myler and S.H.Stertzer (1994), Coronary and peripheral angioplasty: Historic perspective, in Textbook of interventional cardiology (2nd Ed), edited by E.J.Topol, W.B.Saunders Company, **1**, 1994, pp.171-185

[107] W.Nahm and H.Gehring (1994), Multicomponent analysis of time-resolved NIR spectroscopy for *in-vivo* determination of arterial blood components, Phys. in Med. and Biol, Abstr. World Congress on Med. Phys and Biomed. Eng (Rio de Janeiro, Brazil), **39a**(1), pp.142

[108] R.Narayanaswamy (1994), Chemical transducers based on fibre optics for environment monitoring, Science of the total environment, **135**, pp.103-113

[109] K.D.Neame and C.A.Homewood (1974), Introduction to liquid scintillation counting, Butterworths (London), Chapt.1-3, pp.1-48

[110] W.W.Nichols and M.F.O'Rourke (1990), McDonald's blood flow in arteries: theoretical, experimental and clinical principles (3rd Ed), Edward Arnold (London), pp.1-7, 130-137 & 216-250

[111] A.Ourmazd *et al* (1983), Thermal properties of highly birefingent optical fibers and preforms, Applied optics, **22**(15), pp.2374-2379

[112] P.A.Payne (1987), Skin: *In vivo* imaging, in Concise encyclopedia of biological and biomedical measurement systems, Edited by P.A.Payne, Pergamon Press, pp.353-354

[113] J.L.Pepin *et al* (1992), Somnofluoroscopy, computed tomography, and cephalometry in the assessment of the airway in obstructive sleep apnoea, Thorax, **47**, pp.150-156

[114] A.Perlin (1992), Single optical fibre transducer for pressure measurement, Neurological Research, **14**(1), pp.62-68

[115] G.D.Pitt *et al* (1985), Optical-fibre sensors, IEE Proceedings, **132**(4), Pt.J, pp.214-248

[116] S.B.Pool (1992), Applications of specific optical fibres and fibre devices for optical fibre sensors, Proc of 8th optical fibre sensors conference (USA), IEEE lasers and electro-optic soc, pp.274-278

[117] J.J.Popma and T.M.Bashore (1994), Qualitative and quantitative angiography, in Textbook of interventional cardiology (2nd Ed),Edited by E.J.Topol, W.B.Saunders Company, **2**, pp.1052-1068

[118] T.V.Potts and A.Petrou (1991), Argon laser initiated resin photopolymerization for the filling of root canals in human teeth, Lasers in surgery and medicine, **11**(3), pp.257-262

[119] J.P.Powers (1993), An introduction to fibre-optic systems, Aksen Assoc. Incop. Publishers (Boston, USA), 1993, Chapt.2 & 3, pp.17-44 & 45-102

[120] M.B.Preisack and K.R.Karsch (1993), The paradigm of restenosis following percutaneous transluminal coronary angioplasty, European heart journal, **14**(l), pp.187-192

[121] P.H.Priest (1979), Selection of pressure transducers for hydraulic - a review of current techniques and their application, I.Mech.E, June issue, pp.96-81

[122] M.B.Pringle and C.B.Croft (1993), A grading system for patients with obstructive sleep apnoea - based on nasendoscopy, Clin. Otolaryngol, **18**, pp480-484

[123] S.Pringle and D.P.deBono (1988), Monoclonal antibodies to damaged and regenerating vascular endothelium, J.Clin.Lab.Immunol, **26**, pp.159-162

[124] C.Prys-Roberts (1969), The measurement of cardiac output, Brit. J. of Anaesth, **41**, pp.751-760

[125] J.R.Qian *et al* (1994), Spun linear birefringence fibres and their sensing mechanism in current sensors with temperature compensation, IEE Proc. optoelectronics, **141**(6), pp.373-380

[126] K.Rajanna *et al* (1993), Pressure transducer with Au-Ni thin-film strain gauges, IEEE Trans on Elect Devices, **40**(3), pp.521-524

[127] S.R.Ramee and C.J.White (1994), Percutaneous coronary angioplasy, in Textbook of interventional cardiology (2nd Ed), edited by E.J.Topol, W.B.Saunders Company, **2**, chapt.67, pp.1123-1135

[128] A.Ramirez (1969), Registration of intravascular pressure and sound by a fibre optic catheter, J. of appl. Physiol, **26**(5), pp.679-683

[129] A.Rechtchaffen & A.Kales (1968), A manual of standardised terminology, techniques and scoring system for sleep stages in human subjects, National Institutes of Health Publication No.204, pp.1-12

[130] T.A.Roberts and R.L.Burton (1992), Piezoelectric pressure transducer technique for oxidizing atmospheres, Rev. Sci. Instrum, **63**(7), pp.3787-3788

[131] D.O.Rodenstein *et al* (1990), Pharyngeal shape and dimensions in healthy subjects, snorers, and patients with obstructive sleep apnoea, Thorax, **45**, pp.722-727

[132] D.O.Rodenstein and D.C.Stânescu (1986), The soft palate and breathing, AM Rev. Respir. Dis., **134**, pp.311-325

[133] A.J.Rogers (1988), Essential optics, in Optical fibre sensors: principles and components, Edited by J.Dakin and B.Culshaw, Artech house Inc, pp.57-61

[134] P.Rolfe (1994), Cellular engineering: progress and future prospects, , Phys. in Med. and Biol, Abstr. World Congress on Med. Phys and Biomed. Eng (Rio de Janeiro, Brazil), **39a**(1), pp.227

[135] N.Roper (1987), Pocket medical dictionary (14th Ed), Churchill Livingstone, pp.294-295

[136] T.V.Santiago and N.H.Edelman (1986), Breathing disorders of sleep, Churchill Livingstone, pp157-163, 181-193

[137] S.Satomura (1959), Study of flow patterns in the peripheral arteries by ultrasonics, J. Acoustic Soc, Japan, **15**, pp.151-158

[138] P.Sayer *et al* (1974), Fluorescence of blood protoporphyrin in the presence of haemoglobin, Biochemical medicine, **10**(1), pp.24-35

[139] H.Schneckenburger *et al* (1993), Time-resolved *in-vivo* fluorescence of photosensitising porphyrins, J. of photochemistry and photobiology, **21**(2/3), pp.142-147

[140] P.W.Serruys *et al* (1994), Intracoronary doppler, in Textbook of interventional cardiology (2nd Ed), edited by E.J.Topol, W.B.Saunders Company, **2**, chapt.66, pp.1069-1121

[141] J.W.Sheppard *et al* (1991), Evaluation of the upper airway in patients with obstructive sleep apnea, Sleep, 14(4, pp.361-371

[142] R.J.Siegel *et al* (1994), Ultrasound angioplasty, in Textbook of interventional cardiology (2nd Ed), edited by E.J.Topol, W.B.Saunders Company, **2**, pp.931-943

[143] R.J.Siegel *et al* (1993), Clinical trial of percutaneous peripheral ultrasound angioplasty, J. of the american college of cardiology, **22**(2), pp.480-488

[144] Sigma Chemicals UK Ltd (1995)., Biochemicals organic compounds for research and diagnostic reagents, Product catalogue, pp440-442 & pp.1941-1942

[145] A.V.Silva and M.M.Werneck (1994), Fibre optic pH sensor, Phys. in Med. and Biol, Abstr. World Congress on Med. Phys and Biomed. Eng (Rio de Janeiro, Brazil), **39a**(1), pp.159

[146] O.Skatvedt (1992), Continuous pressure measurements in the pharynx and eosophagus during sleep in patients with obstructive sleep apnea syndrome, Laryngoscope, **102**, pp.1275-1280

[147] O.Skatvedt (1993), Localization of site of obstruction in snorers and patients with obstructive sleep apnea syndrome: A comparison of fiberoptic nasopharyngoscopy and pressure measurements, Acta. Otolaryngol (Stockh), **113**, pp.206-209

[148] O.Skatvedt and J.Groegaard (1994), Inspiratory pressures in the newborn and 6 and 12 weeks old children in different sleeping positions, Arch Dis in Child, **71**, pp.138-140

[149] M.H.Sketch *et al* (1994), Extraction Atherectomy, **in** Textbook of interventional cardiology (2nd Ed), edited by E.J.Topol, W.B.Saunders Company, **1**, chapt.38, pp.678-684

[150] Sony Corp. Res. Centre (1994), Japan aims for blue laser by 1996, Opto and laser europe, **14**(1), pp.7

[151] J.R.Stradling (1993), Clinical presentation of obstructive sleep apnoea, **in** Handbook of sleep-related breathing disorders, Oxford medical publications, pp.65-81

[152] A.M.Smith (1987), Technology overview: optical fibre biological and chemical senors, IOP Short meetings, **7**, pp.23-30

[153] A.Spencer *et al* (1995), *In vivo* assessment of catheter-tip PO_2 sensor: sampling lumen fabrication, Med & Biol Eng & Comp, **33**(2), pp.157-162

[154] W.B.Spillman (1982), Multimode fibre-optic pressure sensor based on the photoelastic effect, Optics Letters, **7**(8), pp.388-390

[155] E.N.D.Stenow and P.A.Öberg (1994), Design and evaluation of a fibre-optic sensor for limb blood-flow measurements, Physiological measurement, **15**(3), pp.261-270

[156] L.Stryer (1975), Biochemistry (2nd Ed), Freeman and Co. (USA), Chapt.21, pp. 506-508

[157] P.M.Suratt *et al* (1983), Fluoroscopic and computerised tomographic features of the pharyngeal airway in obstructive sleep apnea, AM. Rev. Respir. Dis, **127**, pp.487-492

[158] K.Swinth and J.Ewins (1976), Biomedical probe using a fibre-optic coupled scintillator, Medical Physics, **3**(2), pp.109-112

[159] M.Taniguchi *et al* (1991), Basic study on possibility for application of optical fibre to interferometry, IEEE Trans on Opt Eng, **5**, pp.135-137

[160] L.Tenerz *et al* (1991), A fibre-optic silicon pressure microsensor for measurements in coronary arteries, International conference of solid state sensors and actuators, San Francisco (USA), pp.1021-1023

[161] M.J.Thorpy and J.Yager (1991), The encyclopedia of sleep and sleep disorders, Facts on file Ltd (UK), pp.40-41, 98-99, 169-170

[162] G.Thursby *et al* (1992), A novel fibre refractive index sensor using resonance shift phenomena, Proc. of 8th optical fibre sensors conference, IEEE Lasers and optics soc, pp.197-200

[163] G.J.Tortora and N.P.Anagnostakos (1990), Principles of anatomy and physiology (6th Ed), Harper and Row publishers (New York, USA), Chapt.21, pp.603-608

[164] P.M.Tracy (1991), Intrinsic fibre-optic sensors, IEEE Trans on Indust Appl, **27**(1), pp.96-98

[165] T.Tran (1994), Methods for the evaluation and classification of transient signals from noisy data, Ph.D Thesis, University of Leicester, Chapt.3, pp.3.1-3.4

[166] I.V.Turko *et al* (1992), Direct antigen detection in Langmuir-Blodgett films of immunoglobulin G modified with coproporphyrin-I, Analytica Chimica Acta, **256**(1), pp.21-26

[167] M.Tvinnereim and H.Miljeteig (1992), Pressure recordings - A method for detecting site of upper airway obstruction in obstructive sleep apnea syndrome, Acta.Otolaryngol (Stockh), **492**, pp.132-140

[168] L.Van Erven *et al* (1991), Arterial wall injury, arterial wall healing and restenosis, Lasers in medical science,**6**(3), 1991, pp.271-279

[169] M.P.Varnham *et al* (1983), Polarimetric strain gauges using high birefringence fibre, Electronics letters, **19**(17), pp.699-700

[170] B.F.Waller *et al* (1992), Coronary balloon angioplasty dissections: "The good, the bad and the ugly", J. of the American college of cardiology, **20**(3), pp.701-706

[171] R.E.Walsh *et al* (1972), Upper airway obstruction in obese patients with sleep disturbance and somnolence, Ann. Intern. Med., **76**, pp.185

[172] S.Warren *et al* (1995), Combined studies and fluorescence spectroscopy for physico-chemical imaging of atherosclerosis, IEEE Trans. on Biomed Eng, **42**(2), pp.121-132

[173] J.Watson (1989), Optoelectronics, Van Nostrand Reinhold (International), Chapt.6, pp.108-120

[174] J.F.Whidborne *et al* (1994), Algorithms for solving the method of inequalities - A comparative study, Leicester University Internal report (Dept. of Engineering), Report 94-17Aug, pp.5-8

[175] J.Wilson and J.F.B.Hawkes (1989), Optoelectronics: An introduction (2nd Ed), Prentice Hall, Chapt.3, pp.76-112

[176] C.J.White *et al* (1993), Holmium: YAG laser-assisted coronary angioplasty with multifibre delivery catheters, Catheterization and cardiovascular diagnosis, **30**, pp.205-210

[177] T.H.Wilmhurst and J.Shah (1994), PC processor for plethysmograph airway resistance and thoracic gas volume measurement, Med. & Biol. Eng. & Comp., **32**, pp.342-348

[178] R.A.Wolthuis *et al* (1991), Development of medical pressure and temperature sensors employing optical spectrum modulation, IEEE Trans on Biomed Eng, **38**(10), pp.974-981

[179] B.T.Woodson and M.R.Wooten (1992), A multisensor solid-state pressure manometer to identify the level of collapse in obstructive sleep apnea, Otolaryngol. Head. Neck. Surg., **23**(1), pp.651-656

[180] P.G.Yock *et al* (1994), Intravascular ultrasound, in Textbook of interventional cardiology (2nd Ed), edited by E.J.Topol, W.B.Saunders Company, **2**, chapt.68, pp.1136-1152

Appendix A

The pressure transducer hardware and software components

A.1 Latex manufacture

The catheter manufacturing process requires a latex tubing of 3mmØ and 4mmØ which may be cut to length as required. The latex is formed on a polished stainless steel rod, either of 3mmØ or 4mmØ, depending on the size of the tubing to be made.

The former is warmed to 70°C and lowered into the latex solution (#AL340, Dunlop adhesives) and held for 60 seconds before being slowly withdrawn at a slow steady rate so as to allow the excess material to drain off the former. Once removed the former should be allowed to air dry (5-10 minutes) and then immersed into a coagulant solution (20% acetic acid in methanol) and immediately removed, the methanol in the coagulant will promote fast evaporation. The pre-coated former may now be dipped as many times as is necessary to produce the required thickness of latex, dipping in coagulant between dips. When the desired thickness has been achieved the former should be heated to 70°C for one hour to promote the cross-linking process of the latex.

The removal of the latex was achieved by coating the dipped former with french chalk. 130mm lengths may then be slowly rolled off the former, suitable for enclosing six transducers in the catheter, adding more french chalk as they come off.

NOTE: It may be necessary to pre-dip the former several times, stripping the latex each time, to encourage the latex to adhere to the former better during later dips.

A.2 Heat treatment of hydrophobic tube

PVC tubing 3mmØ OD and 3mmØ ID (#800/000/180, Portex UK Ltd) is used for the basic catheter body, however its hydrophobic properties will not permit it to be coated in latex as part of the catheter finishing process unless it is heat treated. The tubing is placed in a oven for twelve hours at 80°C.

A.3 Modification of optical connectors

The optical fibre amphenol used to connect the catheter to the electronics is dependent on the PIN diodes and emitting LEDs used. The catheter described in this thesis used standard SMA devices and connectors, SMA series 905. The ferrule hole was opened to 350μm to accommodate the 250μm optical fibre and epoxy resin used in the design (a ceramic ferrule is not suitable for this purpose, a stainless steel device must be used: Tech Optics Ltd, #905-150-5001).

The optical fibre connector is supplied as a three part device, including the amphenol, a crimp connector and a strain relief shroud. As the device is designed to accommodate silica fibres enclosed in a protective jacket, the sheathing of which is designed to fit into the crimp connector, the device must be modified to accommodate a single 250μm optical fibre. A 150mm length of fine bore polyethylene tube (#800/100/500, Portex UK Ltd) was slid into the ferrule along with the uncrimped crimp housing, this was then held in place by quick setting epoxy resin before the protective shroud was slid over the whole construction (Figure A-1).

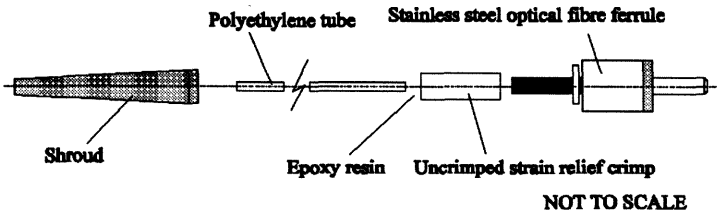

Figure A-1 A schematic of a modified SMA905 stainless steel amphenol

A.3.1 Catheter construction - Layout of individual transducers

When constructing the seven channel pressure transducer a bench-top plan was drawn on a large plate of aluminium on which the catheter was constructed. Figure A-2 shows the distances apart that the individual transducers should be in the final device (ie: six transducers spaced 20mm apart, with a seventh placed 200mm from the sixth), and also where the main upper body of the catheter starts (5mm away from transducer #1). Each transducer is allocated a 10mm window, see plan below (Figure A-2).

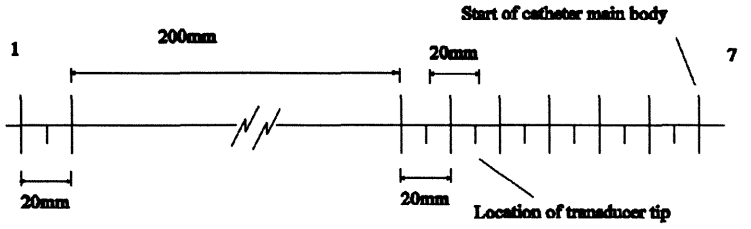

Figure A-2 The pattern for catheter construction.

Seven of the pigtailed transducers should be taped onto the pattern so that the tip of each lies in the correct position within its allocated window. The catheter body can then be assembled.

A.3.2 Diagrams of connecting and fibre terminator blocks

Seven lengths of 90mm 0.76mm∅ ID autoclavable nylon tubing (# 800/200/175, Portex UK Ltd) are fed over each of the three sets of fibres that correspond to each of the transducers and secured in place using silicone sealant (#RTV118, GE Adhesives). A SMA905 optical connector is slid over each of the optical fibres grouped in sets of three corresponding to 'M', 'L' and 'S' of each transducer. The SMA905 connectors are slid over the fibres and the termination enclosed in a fibre-optic clamp (Figure A-3). The clamps and the ferrules may now also be filled with epoxy resin, clamped shut and the whole assembly allowed to cure for twenty-four hours. The seven clamp are then secured in a fibre optic clamp holder (Figure A-4).All polished connectors should be covered with dust caps to prevent contamination at a later date.

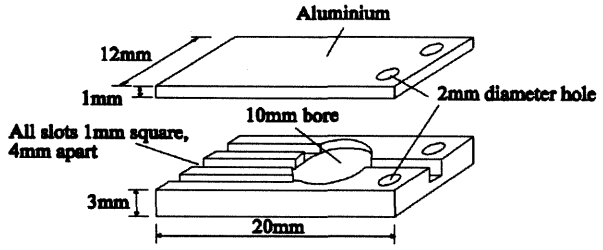

Figure A-3 Schematic of the optical fibre connector clamp (×7 for one catheter)

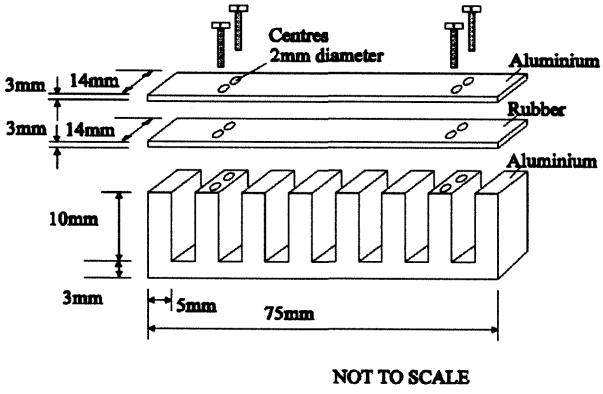

Figure A-4 Optical fibre connector clamp holder (×1 for one catheter).

A.3.3 Materials used in catheter construction

Name	Supplier	Purpose / Notes
Epoxy Resin 555-027	RS Components	Secure optical connectors and sealing individual transducers
Titanium Dioxide TiO_2 (Fine grade)	British Drug Houses Ltd	Coat pressure transducer transduction element
Latex Rubber #AL340	Dunlop adhesives	Sheath for catheter, and final dipping
Propan-2-ol $(CH_3)_2CHOH$	Hogg laboratory supplies	Cleaning all equipment coated with silicone gel after use
Sylgard 527 silicone dielectric gel	Dow Corning	Pressure transducer transduction element
Flexible acrylic sealant (C42513)	Evo-stik	Forming pressure seals between latex sheath and catheter housing
Silicon sealant RTV 118	GE Silicones	Forming pressure seals between the catheter housing and optical fibres
Cyanocrylate	Locktite	Holding reinforcing members in place inside catheter housing
Nylon tube 0.76mmID (#800/200/175)	Portex UK Ltd	Constructing individual pressure transducers
Polyethylene tube (#800/100/500)	Portex UK Ltd	Guiding optical fibre into ferrule of SMA905 connector
PVC tube 3mmOD (#800/000/180)	Portex UK Ltd	Main catheter body
Polymethylmethacrylate Optical fibre 0.25mm	Optronics	Pressure transducer construction

Figure A-5 A table summarising the main materials used in the construction of the optical fibre pressure transducer catheter

A.4 Supplementary circuitry details

The following section gives design details of the low-pass filter hardware used for the optical fibre pressure transducer. The second order voltage-controlled voltage-source 'VCVS' filter is active, containing two-capacitors, two resistors and an operational amplifier (Figure A-6b). The values of these components may be selected to choose the pass and stop-bands of the filters, successive stages may be cascaded together to produce filters of higher orders.

The VCVS circuit is able to emulate a Bessel filter by choosing the values for 'R' (Figure A-6a) in accordance with the table in Figure A-7.

Poles	Bessel VCVS filter	
	f_n	K
1-2	1.781	1.024
3-4	1.835	1.213
5-6	1.956	1.593
7-8	2.192	2.184

Figure A-6(a)
Coefficients for calculation of Bessel filter

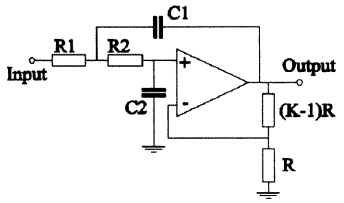

Figure A-6(b)
Circuit for a VCVS filter

No. Poles (Bessel)	f_{3dB} (Hz)	Step rise time (0-90%) (sec)	Over-shoot (%)	Settling time (Sec)		Stopband attenuation	
				to 1%	to 0.1%	$f=2f_c$	$f=10f_c$
2	1.0	0.4	0.4	0.6	1.1	10 (dB)	36 (dB)
4	1.0	0.5	0.8	0.7	1.2	13 (dB)	66 (dB)
6	1.0	0.6	0.6	0.7	1.2	14 (dB)	92 (dB)
8	1.0	0.7	0.3	0.8	1.2	14 (dB)	114 (dB)

(-3.0dB at f_C=1.0Hz)

Figure A-7 The time-domain performance of a Bessel filter
(Horowitz and Hill., 1990)

Each VCVS filter contains two sets of passive components, and is able to provide two poles of the filter. The Bessel lowpass filter selected was eighth order to achieve a sharp cut-off. The settling time (to within 0.1%) and rise time are affected, but only differ by 0.1% and 0.3% respectively. The overshoot increases for the lower order filters, but is a minimum of 0.3% (a reduction of 0.1% from 2nd order) when implemented as eighth order. The most significant feature is the higher attenuation due to the sharper cut-off: a difference of 4dB at twice the corner frequency and 78dB at ten times the corner frequency. Successive stage are cascaded by changing the constant K and fundamental frequency f_n as shown in the table in Figure A-6a.

$$\text{Filter centre frequency } 'f' = \frac{1}{2\pi RCf_n} \qquad \text{(Eqn A-1)}$$

cf: Figure A-6a

The value of the resistors R and $(K-1)R$ (Figure A-6b) are calculated and correspond to the values calculated from Eqn A-2 describing the Bessel filter.

Bessel filter $$H(j\omega) = \frac{\beta_n(0)}{\beta_n(s)}$$ (Eqn A-2)

where $\beta_n(s)$ is the Bessel polynomial of order 'n'.

Appendix B

Endothelial cell damage probe hardware and software

B.1 The laser alignment system for an SMA905 optical fibre

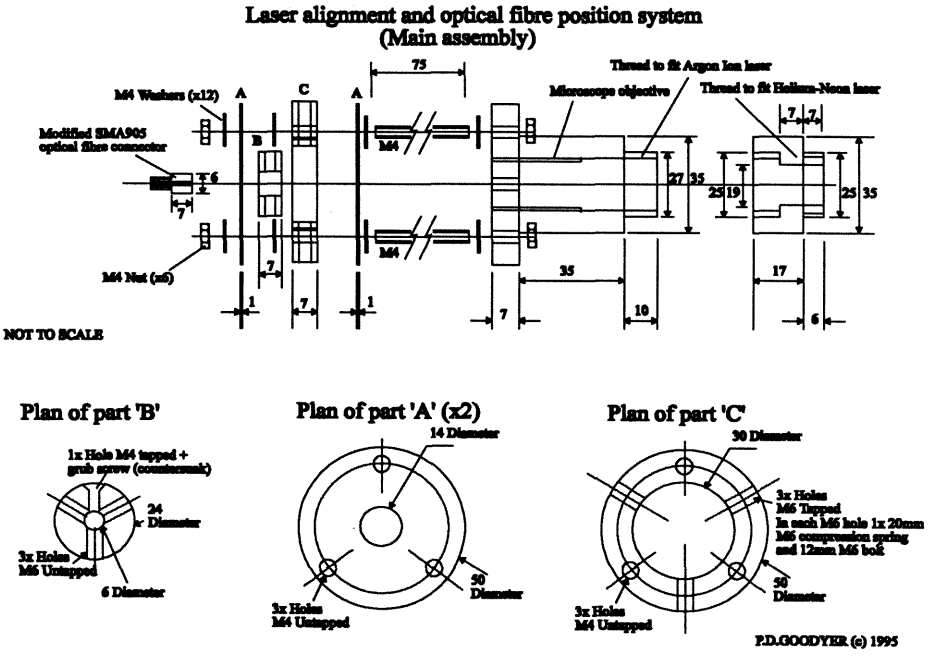

Figure B-1 A schematic of the laser alignment system with six degrees of freedom for focusing the Argon Ion laser into an optical fibre fitted with a SMA905 optical connector

B.2 Construction of the probe

The probe construction is considerably simpler than the former pressure transducer catheter, and does not require heat treatment in order to allow any chemicals to interact. The probe comprises to 0.25 polymer optical fibres. The first fibre is terminated to a SMA905 optical connector (see section A.3) and connects to the laser alignment system (Figure B-1). The second fibre passes into a custom built connector comprising a optical fibre connector (supplied by RS components, Figure B-3) with the tip removed and replaced by a 55mm long length of pito tube.

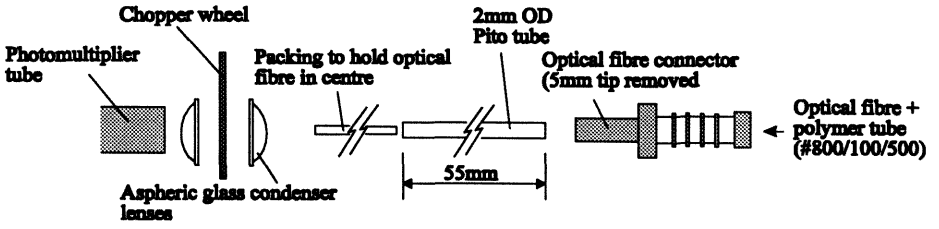

Figure B-2 A schematic of the optical fibre connectors and optics arranged to focus the incoming light into the photomultiplier housing

B.3 Materials used during research

Name	Supplier	Purpose / Notes
Toluene	Sigma Chemicals Ltd	Dissolving optical fibre tip
Polymethylmethacrylate Optical fibre 0.25mm	Optronics	Endothelial cell damage probe receiver and transmitter
Pito-tube (2mm OD)	Stored material	Modification of optical connector
Optical connector #456-598	RS Components	Connection of optical fibre to photomultiplier tube
Nylon tube 0.76mmID (#800/200/175)	Portex UK Ltd	Endothelial cell damage probe housing
Sodium Fluorescein	Sigma Chemicals Ltd	Simulating arterial damage

Figure B-3 A table summarising the main chemicals used during the development of the endothelial cell damage probe

B.4 Implementing the software for the endothelial cell damage probe

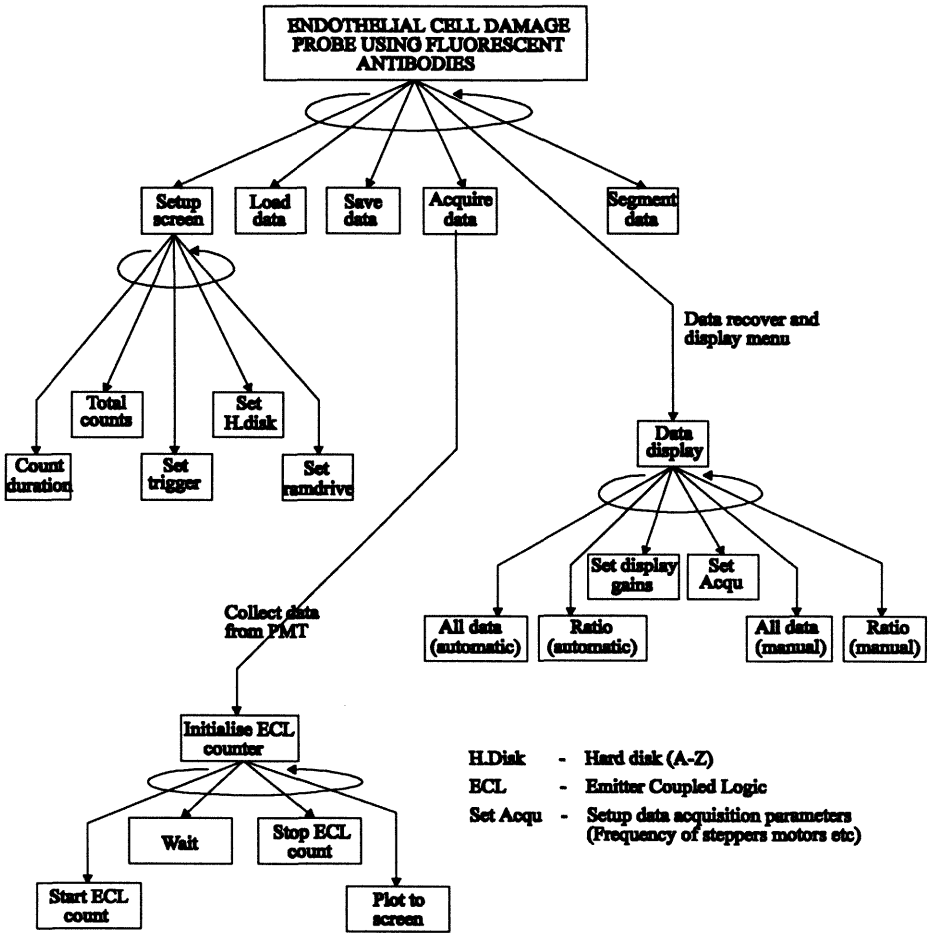

Figure B-4 A block diagram of the endothelial cell damage probe acquisition and display software (written in C 5.1, Microsoft™)

Appendix C

Additional data on the photomultiplier tube and sodium fluorescein

C.1 Characteristics of the low dark-current PMT

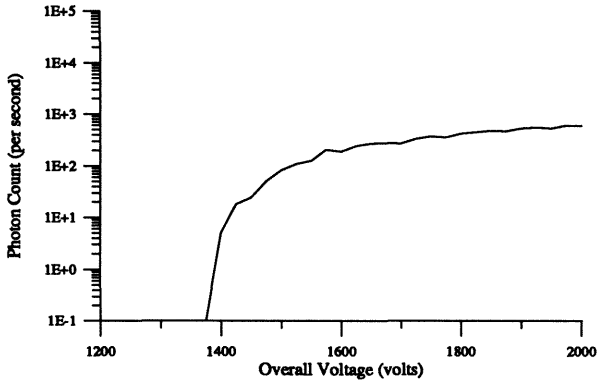

Figure C-1 The operating plateau of the photomultiplier tube dynodes obtained during calibration

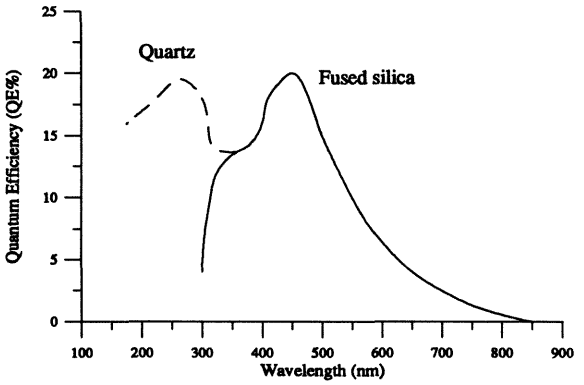

Figure C-2 Comparison of the quantum efficiency of the low dark-current photomultiplier tube when fitted with a fused silica and quartz photon inlet window

Appendix D

P.D.Goodyer, J.C.Fothergill, N.B.Jones, D.P.deBono (1994), Optical fibre probes for measuring endothelial cell damage in arteries, Phys. in Med. and Biol, Abstr. World Congress on Med. Phys and Biomed. Eng
(Rio de Janeiro, Brazil), **39a**(2), pp.572

OPTICAL FIBRE PROBES FOR MEASURING ENDOTHELIAL CELL DAMAGE IN ARTERIES

P.D.GOODYER[†], D.P.De BONO[‡], J.C.FOTHERGILL[†], N.B.JONES[†],

University of Leicester, Departments of Engineering[†] and Cardiology[‡], University Road, Leicester, LE1 7RH, UK

A small diameter optical fibre sensor for measuring endothelial cell damage in the aorta, coronary arteries and similar vessels is being developed. The objective is to study *in-vivo* changes during the healing of vascular endothelium following percutaneous balloon angioplasty. Two optical technologies have been investigated both of which attempt to utilise the ability of monoclonal antibodies to recognise specific antigens associated with damaged endothelium. The antibodies are given a 'label' which can be detected at close range by an arterial catheter.

Preliminary research involved the labelling of the antibodies with a gamma-emitting radio-nuclide such as 125I or 111 In. Laboratory tests showed that this was not feasible because of the toxicity of the scintillants; an alternative fluorescent antibody marker was therefore used. The subject area of tissue is illuminated at the excitation wavelength of the fluorescent material and a ratio between the excitation and emission wavelengths is then taken. An increased ratio is detected if there are any damaged endothelial cells local to the probe.

The system was tested using a simulated arterial wall perfused with red blood cells, a human umbilical cord and a recently sacrificed rat. The fluorescent material (fluorescein) was excited by a 40W halogen light source, external to the artery, transmitted through a filter at the excitation wavelength. In the artificial artery 45 picomoles of fluorescein could be detected, but in the mammalian arteries detection was only achieved down to 0.04 micromoles. These preliminary results suggest that the technique will be useful but could be improved by using an excitation light source introduced *in-vivo* through another optical fibre. This will avoid attenuation in local vascular tissues.

Such probes do have a place in cardiological applications, but it is limited in this particular application by the

speed of the catheter past the point of injury as a function of photon counting time: an increased speed results in a loss of resolution. For the lowest levels of fluorescein a speed of 0.5 mm/s was used.

Appendix E

P.D.Goodyer, J.C.Fothergill, N.B.Jones, D.P.deBono (1994), Fibre optic probes for studying cell damage in the arteries, Proc. of XIII IMEKO world congress: from measurement to innovation, International measurement confederation (Torino, Italy), **3**, pp.2503-2508

Appendices

OPTICAL FIBRE PROBES FOR STUDYING CELL DAMAGE IN THE ARTERIES.

P.D.GOODYER†, D.P.De BONO‡, J.C.FOTHERGILL†, N.B.JONES†,

University of Leicester, Departments of Engineering† and Cardiology‡,

University Road, Leicester, LE1 7RH, UK

Abstract

Research is underway to develop an optical fibre probe for the detection of beta-gamma radio biological markers and that of the fluorescence type when linked to the antigens of damaged endothelial cells. Preliminary research involved the exploitation of scintillation properties of both a solid state and liquid scintillant, a series of feasibility experiments were conducted and a prototype probe developed. Results indicated that although a probe would be theoretically possible a similar method using a fluorescent marker would overcome many problems associated with background noise and toxicity.

Experimentation involved the use of a simulated artery which was illuminated using an external or *in-vivo* light source .The vessel was then perfused with red blood cells and the optical probe withdrawn along its length. Using an external 40W halogen light source a minimum of 45 picomoles of Fluorescein was detectable. However the used of an Argon Ion laser lead to considerable improvements in sensitivity and resolution. Further experimentation also involved the use of an animal model in the form of a recently sacrificed rat, and human umbilical cord.

Keywords: Optical Fibre Biosensor, Fluorescence, Scintillation, Monoclonal Antibody, Endothelium

1. INTRODUCTION

Percutaneous Balloon angioplasty is a well established technique for treating atheromatous stenoses in coronary blood vessels. A surprisingly small amount of research has been undertaken on the pathology and effects of a dilated balloon on the vessel wall in human vessels, because of the low mortality rate of such operations. Even if the post-operative vessel can be examined post-mortem, this does not provide the physician with any information about the healing process or what leads to restonosis. The aim of the work was to attempt to monitor the healing process of the cardiovascular lumen following balloon angioplasty.

The cardiac artery is an extremely sophisticated vessel consisting of several types of cell. Although the reasons why complete or partial occlusion of vessels may occur are not discussed here such vascular obstruction can clearly have drastic effects, effects which may re-emerge if the healing process is not monitored [1]. The development of the optical fibre cell damage probe is based on the ability of monoclonal antibodies to latch onto the antigens of the damaged cells of the vessel lumen. The inner lining of the cardiac vessel is comprised of a layer of *endothelial cells* which collectively completely covers the inner wall of the vessel to make the Endothelium, it is these cells which are damaged during balloon angioplasty and are the target of the antibody. Prior to introduction into the blood stream the antibodies may be given a *biological label* which may then be detected optically: a concentration of the label indicates a concentration of antibody and hence of damaged cells.

2. THE OPTICAL FIBRE SCINTILLATION PROBE.

Scintillation is widely exploited in radiation cameras to detect gamma-emitting radio nuclides such as 125I and 111In. However, although this technique has been useful in the past for looking at large areas of tissue to provide an overview of the problem, its limited resolution prevents close detailed examination of small tissue areas. The use of scintillation as a method of detecting radiation is not a new idea, past research lead to the development of a fibre-optic coupled scintillation probe designed to measure the decay of plutonium [2]. The problem with this previous design was the physical size of the final device, the optical fibre being of a diameter of 5mm or more. The ultimate aim was to reduce physical size of the probe so as to make it viable for intravascular use.

In order to achieve high enough sensitivity and resolution a photomultiplier tube configured as a photon counter was coupled to a receiving optical fibre probe consisting of a high speed counter-timer board connected to a 486DX PC.

A fused quartz cuvette was filled with a tritium / scintillant dilution and placed in a closed light-proof container in front of a low dark count quartz window photomultiplier tube. A set of one hundred samples was taken with the scintillant solution both present and replaced with an empty identical cuvette which was matched at the UV end of its absorption spectrum. The dilution was then varied in order to calculate the efficiency of the photon counting process, Fig1:

Liquid scintillation counting to calculate efficiency of photomultiplier tube.

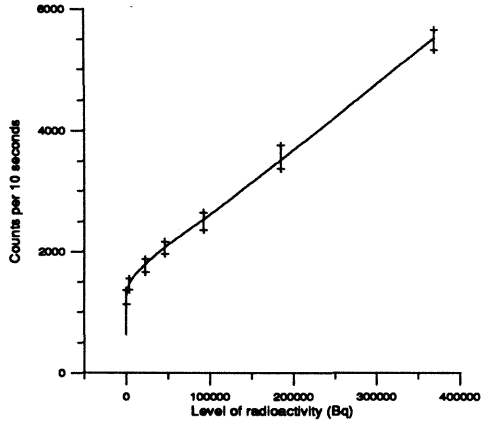

Fig. 1 The photon count of a tritium and scintillant cocktail when using a ten second counting window

The optical fibre can only receive light which lies within its acceptance cone , any light outside this region will pass through the side of the fibre, the angle of incidence being higher than that of the critical angle required for total internal reflection. The volume of fluid used during the experiment was designed to be comparable to that of the volume of an angioplasty balloon, a typical balloon size being: 20mm long × 3mm in diameter

When struck by a beta particle the scintillant will emit light in all directions in three dimensional space. The intensity received by the optical fibre can be calculated by examining the solid angle (in steradians). The

solid angle is defined in terms of the angle subtended at the centre of a sphere radius 'r' by an element 'δA' at the surface of a unit sphere .

The proportion of the total light received by the optical fibre is:

$$P(x_1, x_2, x_3, A, \Phi) = \left(C \int_{x_3}^{x_2} \int_{0}^{x.\tan(\Phi)} \int_{0}^{2\pi} \frac{A}{4\pi\left[(x - x_1)^2 + (x\tan(\Phi))^2\right]} r.d\theta.dr.dx \right) \times \text{Photons per unit volume}$$

where	x1	-	Solid angle calculation limit
	x2	-	Top of cone defined by NA of optical fibre
	x3	-	Bottom of cone defined by NA of optical fibre
	A	-	Cross-sectional area of receiving optical fibre.
	Φ	-	Acceptance angle of optical fibre

This only represents two to three percent of the light emitted by the scintillant given the small diameter of the optical fibre. Further complications arise due to the scintillation occuring at the UV end of the electromagnetic spectrum. High energy UV is readily absorbed by most materials.

2.1 Optical fibre scintillation probe - Results & discussion.

There was found to be a detectable change in mean count rate using a ten second sample window in conjunction with 370KBeq sample, however such a high level of radioactivity would rarely be seen to occur when using monoclonal antibodies. Considerably lower levels of radiation would not be detectable above the noise floor of the Photomultiplier Tube, and may also be swamped by other sources of noise such as spurious background radiation arising from the intrathoraic blood pool.

It can be argued that there is a case for further research into the development of a scintillant-based optical fibre radiation probe using a light detector with a much lower noise floor. The underlying factor which would always be cause for concern is the high toxicity of the scintillant. A high efficiency liquid scintillant (≈ 8%) such as xylene or naphthalene in phenylcyclohexane is extremely toxic, and although theoretically able to be pumped into a compliant chamber only when needed, balloon rupture into the cardiac or indeed any other artery could cause serious damage or fatality. This was particularly apparent when conducting the experimentation using Biofluor™, the scintillant vehicle Toluene C6H5CH3 quickly dissolved the tip of the polymer optical fibre and is also carcinogenic.

3. THE OPTICAL FIBRE FLUORESCENCE PROBE.

Fluorescence is the ability of substance to emit light at a given wavelength whilst being stimulated by a second wavelength at a higher energy [3]. The ability of a fluorescent material to re-emit photons at a different wavelength to those striking it makes the detection of fluorescence an apparently simple task. The standard method, as adopted in this case, is to implement a beam splitting device which is able to optically sample the data at the absorption and emission wavelengths and then take a ratio between the two (Fig 2):

$$\text{Fluorescence (Ratio)} = \frac{\text{Intensity of light emitted at emission wavelength } '\lambda_2'}{\text{Intensity of excitation source at excitation wavelength } '\lambda_1'} \qquad (<1)$$

Appendices

Before experimentation was initiated, the fluorescent compound used as the substitute for the biological label was selected so as to be optimised with respect to the absorption spectrum of whole human blood. Considering the medical complications when using toxic chemicals (section 2) an important part of the design criteria was the non-toxic nature of any chemicals used in the prototype probe . Sodium Fluorescein, a relatively inert fluorescent salt, was used to simulate fluorescing damaged endothelial cells.

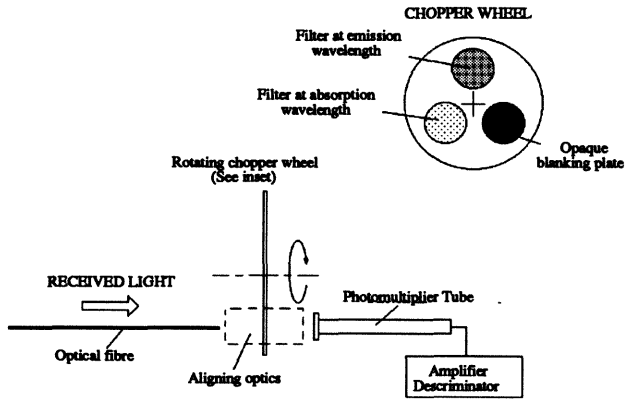

Fig. 2 The optical chopper wheel used for detecting fluorescence of Fluorescein via an optical fibre.

The optical chopper wheel is an important feature of the design, the main requirement being the band separation between each of the filters in order to distinguish the emission and absorption wavelengths of the fluorescein. The lower energy emission wavelength and the excitation wavelengths are separated by only 60nm, and would hence imply high order filters. The ideal optical filter would only let through the required frequency without attenuating the signal. This however is impossible in practical engineering terms and the signal to noise ratio of the output is a function of the practical bandwidth of the filter.

3.1 The fibre optic transillumination probe.

The excitation light source is placed outside the body and penetrates though the skin and other intervening blological tissues into the vessel wall and lumen from where it is transmitted to a light detector via one or more intravascular optical fibres. This is the simplest design of all of the fluorescent probes to construct, however particular attention must be paid to the light source because of the attenuation of blood and tissues. Preliminary experiments used a 40W halogen light source with a close band optical filter to reject any wavelengths close to that of the emission wavelength of the fluorescein which may swamp the signal.

A false vessel simulating endothelial cell damage was constructed from a length of translucent tubing (figure 3), comparable in size to that of a typical human cardiac artery (≈2mm∅) and a helix of narrower gauge tubing (0.25mm∅ ID) arranged around its circumference in several turns. The helix could be filled with a fluorescein solution of variable concentration and the simulated vessel perfused with red blood cells as a first approximation to that of a real artery. A probe consisting of a single polymethylmethacrylate optical fibre was then placed into the vessel, illuminated and withdrawn at a constant velocity whilst sampling at the appropriate wavelength (490nm and 550nm). Using the artificial artery the system was able to detect a minimum of 45 picomoles, a typical plot is shown in figure 4.

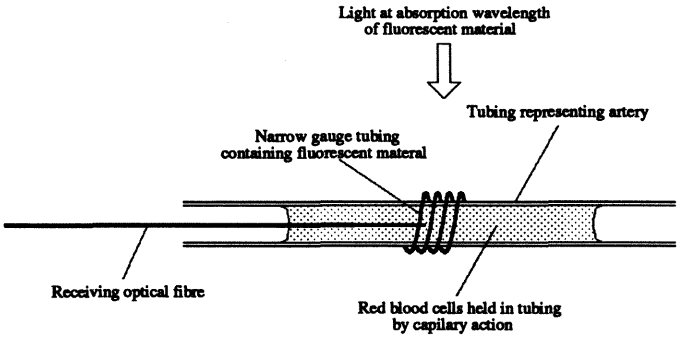

Fig 3. A simulated artery perfused with red blood cells.

The optical sampling of absorption and emission wavelengths of fluorescein.

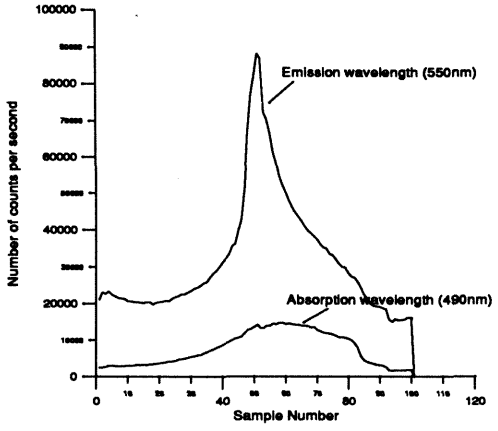

Fig. 4 The absorption and emission wavelengths of 10µl of a 622µMole/l solution, using a simulated artery (Red cells not present).

Following confirmation that a fluorescent material can be detected with red blood cells present, experimentation was extended to involve that of real mammalian tissue. Experiments were conducted with a length of human umbilical cord devoid of blood and a vessel in a recently sacrificed rat in order to investigate the problems associated with using an external light source to excite the fluorescein. In each case a subject area of tissue in close proximity of the vessel wall was injected with 10ml of 622µMole/l solution, the neighbouring tissues were then replaced prior to being illuminated from the halogen light source. 0.04µMoles of solution could be detected, the poor efficiency being attributed to the high attenuation of the tissues. Although the optical probe did detect fluorescence its efficiency is considerably reduced when other tissues are present; a fact which becomes more significant if the level of endothelial cell damage and hence quantity of fluorescent

material is small. The solution is to develop a probe which is able to both launch and received light, thus in this case removing the problems of extraneous tissues completely. The only source of attenuation being the blood.

3.2 The fibre optic photo-excitation probe.

In order to improve efficiency a further optical probe was developed in the form of two prototypes designed to launch directly to the sight of interest via another optical fibre. The first design comprised a bifurcation formed from a split optical fibre bundle; hence only one optical fibre was required at the probe tip. Unfortunately this design is not ideal due to the halving of the optical energy on its return journey back to the photo detector at the bifurcation. The second device was simpler in design, introducing a second neighbouring fibre isolated from the first through which to carry the source. Again the probe is not ideal: the introduction of a second optical fibre results in a doubling of probe diameter.

The *in-vivo* light source chosen was an Argon Ion laser having a principle wavelength of 488nm, just below that of the optimum absorption wavelength of the fluorescein at 493nm, above this wavelength and the energy of the photons would not be sufficient to cause fluorescence. The laser has advantages over a broad band light source: complications from localised heating damaging the end of the optical fibre do not occur and the high degree of parallelism permits the beam to be readily focused onto the face of the optical fibre. Both the duplex and simplex optical fibre probe design was investigated using the simulated artery and were able to detect concentrations of below 45 picomoles. The system sensitivity can be improved by increasing the power of the laser, practical limitations being only that of the risk of further vascular damage as a result of the laser. The choice of the probe design can be dictated by the physician depending on the application of the probe, narrow diameter vessels best being investigated by as smaller probe as possible: 0.25mm in diameter using a single optical fibre.

Detection of fluorescence using a duplex optical probe with an Argon Ion laser

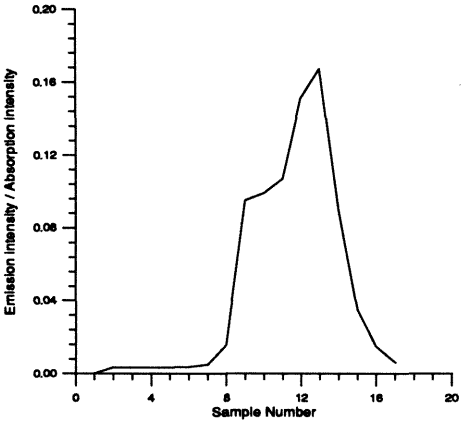

Fig. 5 The photo-excitation optical fibre probe using a duplex polymer optical fibre coupled to a 10mW Argon Ion laser, 10µl of 300µMoles/l solution..

Appendices

4. CONCLUSIONS & SUMMARY OF RESULTS.

The ultimate aim of the project was to detect endothelial cell damage. Although this is difficult to simulate using a mammalian vessel, endothelial cells can be grown to culture and treated in the laboratory with monoclonal antibody marked with a fluorescent biological label. Once cultured, the cells were scratched to create localised surface damage. As in the transillumination probe the subject area was then illuminated from an external light source and the probe withdrawn over the damaged area. The resulting ratio between the emission and absorption wavelengths did indicate fluorescence, however the signal was extremely small. This signal level would be considerably improved by the use of the optical fibre light source.

The optical fibre scintillation probe does have a future in the transducer market, but the toxicity of the chemical make such a system impractical for use in biomedical applications. The system may be improved by the use of quartz optical fibre, reducing attenuation at the UV wavelengths, and also by choosing a more efficient scintillant. There is a compromise in probe design. Solid state scintillants are less toxic but are also less efficient. Clearly the use of such a solid state device will be restricted to application were levels of radiation are high.

The optical fibre fluorescence probe can be implemented safely in several biomedical applications. A large number of fluorescent materials are inert. The sensitivity of such a probe can be improved significantly using a laser light source, which also removes problems associated with the optical filters. Both of the optical fibre photo-excitation probe designs were constructed so as to be of comparable physical size: the simplex type using a 1mm diameter fibre, and the duplex device using a pair of 0.25mm diameter optical fibres contained within a 1mm diameter tube. The sensitivity of the simplex device was considerably higher than that of the latter. This can be attributed to the increased cross-sectional area of the receiving optical fibre. Although a higher background count will be present, because of the internal reflections of the bifurcation the signal to noise ratio is higher.

Research into the reduction of the probes physical size is still continuing. Work also proceeds in other biomedical applications using fluorescence, such as the monitoring of local vascular drug delivery.

References

[1] Topol, E., Textbook of interventional cardiology, W.B.Saunders Company, London, 1994, p.171-185

[2] Swinth, K, and Ewins, J.,Biomedical probe using a fibre-optic coupled scintillator, 3 (1976) 109-112

[3] Hirschlaff, E., Fluorescence and phosphorescence, Methuen& co Ltd, London, 1938, p.26-39

Contact point: PROF N.B.Jones, Department of Engineering, University of Leicester,
Leicester, Leics. LE1 7RH (England).
Tel: (++44) (533) 522550 Fax: (++44) (533) 522619

Appendix F

P.D.Goodyer, J.C.Fothergill, A.H.Gershlick, N.B.Jones, D.P.deBono (1995), A fluorescence sensor for investigating vascular damage, Sensors and their applications VII, Instrum. sci. and techn. grp of Phys, (Dublin, Ireland), Accepted for publication

A fluorescence sensor for investigating vascular damage

P D Goodyer, J C Fothergill, A H Gerschlick, N B Jones and D P de Bono

Department of Engineering, University of Leicester, Leicester LE1 7RH, U.K.

Abstract. An optical fibre probe is being developed to detect radiation from fluorescein attached to endothelial cells using biological macro molecules. Endothelial cells grown in-vitro, when damaged, have been successfully labelled with macro molecules carrying fluorescein. Two different methods of exciting the fluorescein are reported, external illumination via a 40W halogen light and in-vivo illumination from an Argon Ion laser. Measurements have been made in simulated arteries, in animal models, and in human umbilical artery. The experiments indicate that an in-vivo probe for monitoring cell damage is possible.

1. Introduction

1.1. Endothelial cell damage in arteries

The cardiac artery is a complex structure consisting of several types of cell. The innermost layer is made up of endothelial cells. These arteries can become obstructed by atheromatous stenoses which can often be treated by Balloon Angioplasty. This operation damages the endothelial cells and the return of vascular obstruction after operation can occur with drastic consequences. It is important to monitor the healing process of these cells both for research purposes and for prognostic reasons (Preisack and Karsh 1993).

This project aims to find means to monitor the damage caused by this operation and the subsequent healing process. It is proposed that antibodies specific to endothelial cells be introduced into the bloodstream and that these antibodies are labelled in such a way that the extent of damage can be measured.

1.2. Measurement of damage

If labels can be attached to the damaged cells using monoclonal antibodies or other macro molecules it would then be necessary to show that a scheme can be devised to detect the markers. The substance chosen for the markers was sodium fluorescein since this is well tolerated by the body and has a peak spectral response in a low absorption window of blood.

The solution proposed is to excite the fluorescein by injection of light energy and to observe the fluorescent response with a fibre optic probe. The displacement of the probe in the artery and the intensity of the response can thus be used to estimate the degree and range of cell damage.

1.3. Demonstration of principle

In order to demonstrate the feasibility of the proposed scheme it is necessary to establish whether the markers can be successfully attached to the damaged cells and also that the fluorescein can be detected in the concentrations expected. It must be noted that the measurements need to be made in the presence of oxygenated blood and so account has to be taken of attenuation due to that.

Two sets of experiments are reported; one which shows that fluorescein can be attached to damaged endothelial cells in preference to undamaged endothelial cells and the fluorescence detected, the other which shows that fluorescein can be detected in suitable concentrations in simulated and real arteries.

2. Experiments

2.1. The detection of damaged cells in-vitro

2.1.1. Preparation of the cells

Experiments by Cuello et al (1982) have shown that it is possible to internally label monoclonal antibodies without impairing their binding characteristics. To examine this finding in the present context endothelial cell specific antibodies were prepared. Endothelial cells were then grown in culture. The cell layer was scratched on the culture plate and the plate was washed with a suspension containing the monoclonal antibodies labelled with fluorescein.

2.1.2. Measurement of fluorescent response

Fluorescein absorbs energy at 490 nm and emits energy at 550 nm. A scheme was devised in which a filtered light source was used to illuminate the plate and an optical fibre was drawn across the plate to detect the fluorescent response. Appropriate filters and detectors were designed to measure the detected light at 490 nm and 550 nm and the ratio taken. Figure 1 shows the apparatus for controlling the position of the fibre and for measuring the light energy. Figure 2 shows the ratio of the intensity at the two wavelengths as a function of distance. The increased response at the location of the damage is clearly seen. Further details are available from Goodyer et al (1992).

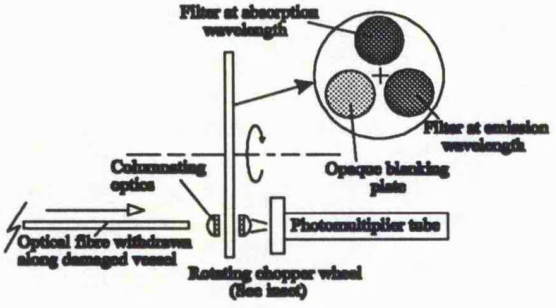

Figure 1. The apparatus for controlling the position of the optical fibre and acquiring the light energy.

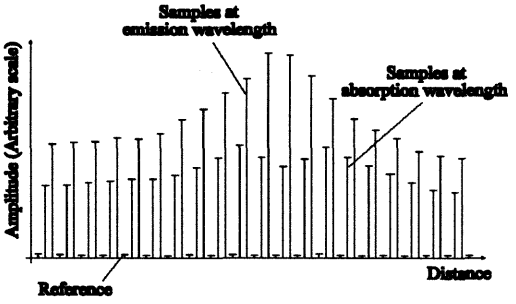

Figure 2. The intensity of the two wavelengths as a function of distance.

2.2. Measurements of fluorescence in simulated cardiac arteries

2.2.1. External illumination

In these experiments a false vessel was constructed from a length of translucent tubing comparable in size to that of a typical human cardiac artery (≈2mmØ ID) and a helix of narrower gauge tubing (0.25mmØ ID) arranged around its circumference in several turns. The helix could be filled with a spectrum fluorescein solution of variable concentration and the simulated vessel perfused with red blood cells as a first approximation to a functioning real artery. A probe consisting of a single polymethylmethacrylate optical fibre was then placed into the vessel, illuminated and withdrawn at a constant velocity whilst sampling at the appropriate wavelength (490 nm and 550 nm). Using the artificial artery the system was able to detect a minimum of 45 picomoles of fluorescein.

Figure 3 shows a specimen fluorescein response as a function of displacement. Further details are available from Goodyer et al (1994).

Following confirmation that a fluorescent material can be detected with red blood cells present, experimentation was extended to involve real mammalian tissue.

Experiments were conducted with a length of human umbilical cord devoid of blood and a vessel in a recently sacrificed rat in order to investigate the problems associated with using an external light source to excite the fluorescein. In each case a subject area of tissue in close proximity to the vessel wall was injected with 0.1 ml of 622μMole/l solution, the neighbouring tissues were then replaced prior to being illuminated from the halogen light source. 0.04μMoles of solution could be detected, the poor efficiency being attributed to the high attenuation of the tissues.

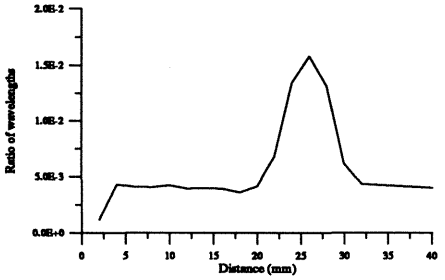

Figure 3. The ratio of wavelengths corresponding to fluorescence (5μMole/l dilution).

2.2.2. Internal illumination

The in-vivo light source chosen was an Argon Ion laser having a principle wavelength of 488nm, just below that of the optimum absorption wavelength of the fluorescein at 493nm. The laser light is introduced via a fibre optic. The laser has advantages over a broad band light source in that complications from localised heating damaging the end of the optical fibre do not easily occur and the high degree of parallelism permits the beam to be readily focused onto the face of the optical fibre. The system sensitivity can be improved by increasing the power of the laser, practical limitations being only that of the risk of further vascular damage as a result of the laser.

Fluorescein was linked to heparin in varying dilutions and introduced into the aorta of a live rabbit by a perforated angioplasty balloon. It was hoped that the heparin would adhere to the vessel wall and be detectable by the fluorescent probe once the vessel had been harvested from the animal. Using this technique the peaks corresponding to 60IU/ml and 400IU/ml concentrations of fluorescein were detected[1]. Figure 4 shows that a good response has again been observed in this case.

The fluorescein plus heparin solution was also investigated using the aforementioned simulated artery. The dilutions of 500IU/ml, 310IU/ml and 80IU/ml were easily detected using a saline filled simulated artery.

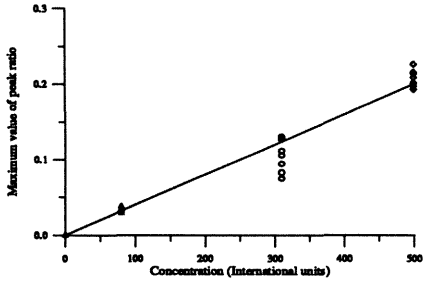

Figure 4. The peak of the ratio of the emission to absorption wavelengths using varying dilutions of fluorescein with heparin.

[1]The technique for linking fluorescein and heparin is yet to be refined.

3. Conclusions

These pilot experiments have shown that it is possible to get biological macro molecules labelled with fluorescein to bond with damaged endothelial cells. Further it has been shown that it is possible to detect the fluorescein in appropriate dilutions in situations and conditions very similar to those expected in living human cardiac artery. The use of heparin as a carrier of the fluorescein is possible. Exciting the fluorescein by external illumination is possible but may not be practicable due to the high attenuation of the tissue. In-vivo excitation by Argon Ion laser looks like a more promising alternative approach.

4. References

A.C. Cuello *et al* (1982), Immunocytochemistry with internally labelled monoclonal antibodies, Proc. Nat. Acad. Sc. (USA), **29**(1), pp.665-669

P.D. Goodyer *et al* (1994), Fibre optic radiation probe and the study of vascular damage, EPSRC Research Grant Report: GR/F80777, Dept. of Engineering, University of Leicester

M.B. Preisack and K.R. Karsch (1993), The paradigm of restenosis following percutaneous transluminal coronary angioplasty, European Heart Journal, **14**(1), pp.187-192.

Appendix G

A.H.Gershlick, P.D.Goodyer, L.Kenyon, D.P.deBono, N.B.Jones, J.C.Fothergill (1995), Fluorescein-labelled drugs: a new method of detecting their *in-vivo* concentration after local delivery, J. of Cardiology, Submitted for publication

FLUORESCEIN-LABELLED DRUGS: A NEW METHOD OF DETECTING THEIR *IN-VIVO* CONCENTRATION AFTER LOCAL DELIVERY?

A.H.Gershlick[†], P.D.Goodyer[‡], L.Kenyon[†], D.P.deBono[†], N.B.Jones[‡], J.C.Fothergill[‡]

The Academic Department of Cardiology[†] and Department of Engineering[‡], University of Leicester, University Road, Leicester, LE1 7RH, UK

Abstract

There are a number of unresolved issues in the developing area of local drug delivery. One important aspect prior to large randomised trials in man is developing a way of detecting how much of the intended drug is retained in the artery wall. To investigate methods of determining local drug concentration we have developed and used a fluorescein detecting probe to determine whether different local concentrations of heparin could be detected in a simulated artery. 20mg/ml of commercial heparin was conjugated with fluroescein isothiocyanate (FITC) at a concentration of 50μg per mg of heparin. Conjugate alone was obtained by passage through a PD-10 column and eluted with phosphate buffered saline (pH 7.4). The conjugate was diluted, 1in 2 and 1 in 10, and the concentration of heparin determined by spectrophotometry. The final concentrations of heparin in the fluoresceinated-heparin conjugate were 80IU/ml, 310IU/ml and 500IU/ml. Each concentration of conjugate was in turn placed in a plastic tube (diameter 0.76mm) wrapped ×5 around a second plastic tube (diameter 3mm) designed to simulate local drug deliver in an arterial wall. Emission and absorption wavelengths were obtained for each concentration using a fluorescein probe and photomultiplier. The emission / absorption ratio peaks were measured eight times for each concentration and the mean (SD) were 0.208 (0.01) for 500IU/ml, 0.106 (0.02) for 310IU/ml and 0.03 (0.002) for 80IU/ml (r^2=0.98). A straight line curve could be drawn. An unknown was also infused and the peak ratio measured at 0.04 (0.005) which corresponded to 102IU/ml (±10%). The unknown heparin concentration was measured at 80IU/ml.

We have developed an accurate and simple method of potentially detecting local concentration of a drug after its delivery to the vessel wall. Further studies are ongoing.

Appendix H

P.D.Goodyer *et al* (1995), The design and development of an optical fibre probe for measuring endothelial cell damage in the arteries, IEEE Trans. Biomed Eng, Submitted for publication

THE DESIGN AND DEVELOPMENT OF AN OPTICAL FIBRE PROBE FOR MEASURING ENDOTHELIAL CELL DAMAGE IN THE ARTERIES.

P.D.GOODYER†, D.P.de BONO‡, J.C.FOTHERGILL†, N.B.JONES†, A.GERSHLICK‡, R.AGGARWAL‡

†Department of Engineering, ‡Department of Cardiology,
University of Leicester, University Road,
Leicester, LE1 7RH, UK

Abstract -

Design and development of an optical fibre sensor for measuring endothelial cell damage in the aorta, coronary arteries and similar vessels is described. The sensor is intended for the study of *in-vivo* changes during the healing of vascular endothelium following percutaneous balloon angioplasty. Two optical technologies have been investigated both of which attempt to utilise the ability of monoclonal antibodies to recognise specific antigens associated with damaged endothelium. The antibodies are given a label which can be detected at close range by an arterial catheter.

Preliminary research involved the labelling of the antibodies with a gamma-emitting radio-nuclide such as 125 I or 111 In [1]. Laboratory tests showed that this was not feasible because of the toxicity and poor efficiency of the scintillant; an alternative fluorescent antibody marker was therefore used. The subject area of tissue is illuminated at the excitation wavelength of the fluorescent material and a ratio between the excitation and emission wavelengths is then taken. An increased ratio is detected if there are damaged endothelial cells local to the probe.

The system was tested using a simulated arterial wall perfused with red blood cells, a human umbilical cord and a sacrificed rat. The fluorescent material (sodium fluorescein) was excited by a tungsten halogen light source, external to the artery, transmitted through a filter at the excitation wavelength; later an Argon Ion laser was used to transit the light directly to the site also via an optical fibre. In the artificial artery 45pmoles of sodium fluorescein could be detected, but in the mammalian arteries detection was only achieved down to 0.04μmoles.

1 Introduction

The use of percutaneous balloon angioplasty as a treatment for atheroma in both the coronary and peripheral blood vessels is now a common surgical technique. Although research into the pathology of vascular wall damage following balloon angioplasty has been conducted [2], results are limited due to the lack of mortality arising from the angioplasty. In at least 25% of the patients treated, restenosis re-occurs in the recanalised vessels [3]. A method for monitoring the progress of healing inside the vessel lumen, in particular the endothelium, has not been available up until now. Recent research in our laboratories has lead to the development of monoclonal antibodies able to recognise specifically the antigens of the damaged endothelial cells making up the endothelium on the inner vessel wall. The inner lining of the cardiac vessel comprises a layer of *endothelial cells* which completely covers the inner wall of the vessel to make the endothelium, it is these cells which are damaged during balloon angioplasty and are the target of the antibody. Prior to introduction into the blood stream the antibodies may be given a label which may then be detected optically: a concentration of the label corresponds to a concentration of antibody and hence of damaged cells.

The equipment developed is ultimately for use *in-vivo* within the lumen of the coronary arteries and so must be inert, non-toxic and, as far as is possible, without any side-effects. Two parallel lines of investigation were developed, each with significantly different optical technologies:

- Radio-nuclide labelling, detectable by scintillation counting.
- Fluorescent dye labelling detectable by photon counting.

2 Methods and materials

2.1 Development of a scintillation probe

Preliminary investigations concentrated on a scintillation probe as conventional techniques label monoclonal antibodies with radioactive gamma-emitting radio-nuclides, such as 125 I or 111 In which can then be detected by Geiger Müller apparatus, or a radiation camera. It was anticipated that this probe would be able to locate the sites of damaged endothelium more accurately than a radiation camera. The probe was based on a scintillation crystal mounted at the tip of an optical fibre which could then be passed into the damaged artery [1]. When the probe was moved close to the area of interest the resulting radiation excited the scintillant and the level of the resulting light measured.

Preliminary tests with gamma-emitting radio-nuclides proved this design to be unsatisfactory when investigating small areas of vascular damage in the cardiac vessels. Problems originate from the relatively high level of background radiation in the intrathoracic blood pool and pulmonary endothelium. The poor signal-to-noise ratio can be improved by the use of beta-emitting radio-nuclides with a higher specific activity. The short range of the beta radiation would mean that the probe would have to be mounted on a very fine vascular catheter in order to get close enough to the damaged site; hence removing some of the background problems.

A feasibility study was conducted using the liquid scintillant Biofluor™ (Sigma Chemicals UK Ltd), a high efficiency emulsifier cocktail, which was able to detect radiation. The volume of fluid used during the scintillation probe development was designed to be comparable to that of the volume of an angioplasty balloon, a typical balloon size being 20mm long × 3mm in diameter. When struck by a beta particle the scintillant will emit light in all directions in three dimensional space; only a small proportion of this light will be captured by the optical fibre.

It was found that much higher levels of radiation (~22kBeq) than could be expected from the antibody labelling (maximum 2kBeq) were required in order to be detectable using a sensitive photomultiplier detection system. An optical fibre can only accept light incident on its end from within a given solid angle known as the *acceptance cone*. Any light outside this cone will pass through the side of the fibre, the angle of incidence being higher than that of the critical angle required for total internal reflection. This reduced the sensitivity of the device to a level which was not felt to be viable using current technology.

As the construction of low loss optical fibres, and the methods for measuring extremely low levels light improve the system may become more viable. This would not however remove the problem of the high toxicity of the scintillation material: leakage into the blood stream would always be cause for concern.

2.2 Development of a fluorescence probe

An alternative design to that of scintillation again uses internally labelled monoclonal antibodies, but this time labelled with a fluorescent marker [4]. An optical fibre probe may be passed along the lumen of the damaged vessel and the level of fluorescence recorded. The fundamental difference between the optical fibre scintillation probe and the fluorescent equivalent is the manner in which the internal energy of each system may be viewed. The light arising from the scintillating material in the first design is purely a function of the radiation level and hence indirectly the quantity of endothelial cell damage, the fluorescent material however may be excited by as little or as much energy at a given wavelength as is necessary to achieve a given sensitivity.

Fluorescence is characterised by the ability of a material to re-emit light at one wavelength, *emission wavelength*, whilst being excited at a lower (higher energy) wavelength, *absorption wavelength*. The ratio between these two wavelengths describes the fluorescence of the material.

3 Experimental arrangement.

3.1 Selection of fluorescent biological label

The fluorescent material to be used as the label must be carefully selected. The fluorescent probe has some disadvantages over that of scintillation, the most obvious being the significance of the haemoglobin and other blood constituents as sources of attenuation: defined by the Lambert-Beer law [5]. The level of attenuation

is a function of the absorption spectrum of whole blood, and consequently the fluorescent label must be chosen in the lowest possible attenuation window.

The absorption spectrum of blood was measured using a spectrophotometer over the range 300nm to 900nm; this is shown in Figure H-1. Note this graph is rather unusual as the attenuation units are absolute (dB/mm) and not arbitrary absorption units (AU) as is usually presented. Two regions of lower attenuation were examined as a basis for fluorescent material selection: greater than 650nm and between 450nm and 550nm. Two materials were considered for use as a biological label: porphyrins (excited by UV and re-emitting in the red and infra-red) the other sodium fluorescein (excited at 490nm, and re-emitting at 550nm). Although both materials are potentially suitable as a marker, the porphyrin must be excited in the ultra-violet end of the spectrum which is readily absorbed by the oxygenated haemoglobin, porphyrins are also naturally present in the blood and though difficult to separate [6]. An appropriate monoclonal antibody had been previously labelled with sodium fluorescein under laboratory conditions using the technique described by Pringle et al, 1988 [7]. Although sodium fluorescein is not ideal, ie: not in the window of minimum absorption (>650nm) it is in the window between 450nm and 550nm. It should also be noted that the sample described below (Figure H-1) is that of venous blood and not arterial. Although there will be differences in the absorption characteristic between the two the most significant source of attenuation will arise from the haemoglobin which is present any where in the blood stream.

Figure H-1

A Sodium Fluorescein solution was used to both simulate labelled monoclonal antibody and also later to mark the antibodies themselves. The simulated artery was used as part of a feasibility study to design the optical fibre probes. Two designs are discussed; the fundamental difference between the two is the manner in which the target tissue and hence the sodium fluorescein is illuminated.

3.2 The Apparatus

In order to separate the absorption and emission wavelengths of the sodium fluorescein, the light arriving from the optical fibre probe must be sampled at the appropriate wavelengths. The probe first probe design comprised a 0.25mm diameter polymethylmethacrylate optical fibre. The output of which was collimated and filtered by two close band optical filters before being collected by the detection equipment.

Figure H-2

The low levels of light involved imply that a photomultiplier tube (PMT) with a low dark current is an appropriate method of detection. The PMT was configured in photon counting mode and interfaced to a notebook size PC for portability. The chopper wheel was rotated at a well defined velocity using a 1.8° stepper motor (Figure H-2). Pulses arising from the photomultiplier tube are injected into an amplifier discriminator in order to reject pulses at low amplitudes caused by noise and ensure they are all of equal amplitude. The pulses are then counted by a 20MHz, 32 bit emitter-coupled logic (ECL) counter interfaced to a notebook PC. The photon count period is adjusted by the software.

To relate the optical information and hence the level of fluorescence to the location of the optical probe inside the lumen, a catheter withdrawal device was constructed and synchronised to the counting apparatus. Stepper motors were used in both the withdrawal device and chopper wheel, the input frequency of which can then the used to provide catheter location information.

The assembled system sampled the incoming light at the two wavelengths along the length of the vessel at regular intervals. The ratio of the received light flux to that emitted was then used to compute an indication of fluorescence, and the time spacing between each of the samples was used to determine the location of the optical fibre within the vessel (Figure H-3).

Figure H-3

3.3 Design of the optical probe

Variations in catheter design are defined primarily by the light source: illumination *in-vivo* or by an external means. A bifurcated, duplex or optical fibre bundle may be used to incorporate the light source and the receiving apparatus into a single catheter. Alternatively the subject area of tissue may be illuminated from outside the body, provided the correct wavelength is used. The second simpler approach was used initially in an attempt to establish the viability of the system. A model vessel was illuminated using the arrangement in Figure H-4. The diameter of the tubing was chosen so as to be comparable to that of a human cardiac artery. A length of secondary narrow gauge tubing was then wrapped around the *simulated artery* in a helix; the number of turns being variable, provided a means of adjusting the quantity of fluorescent material encapsulating the tubing. A control sodium fluorescein solution was then pumped around the outer diameter of the vessel. For the purpose of the experiment the apparatus was placed in a dark environment and flooded with light at the absorption wavelength. The tubing was then perfused with red blood cells and a receiving optical fibre withdrawal along its length past the fluorescent region.

Figure H-4

The absorption of the intervening tissues when using an external light source is significant. A prototype probe was developed designed to guide light directly to the sight of interest using another optical fibre. A second neighbouring fibre, isolated from the first, was introduced to carry the source. The *in-vivo* light source chosen was an Argon Ion laser having a principle wavelength of 488nm which is very close to the optimum absorption wavelength of the sodium fluorescein: 493nm. The laser has advantages over a broad band light source: complications from localised heating damaging the end of the optical fibre do not occur and the high degree of parallelism permits the beam to be focused easily onto the face of the optical fibre. The system sensitivity can be improved by increasing the power of the laser; practical limitations being the risk of further vascular damage and the denaturing the blood at high powers.

The Argon Ion laser as the monochromatic light source was a class four, water cooled, Spectra-physics laser, having a maximum output of 750mW, although it was not found to be necessary to run it at this power. The beam was focused into the emitting optical fibre by a microscope objective with a numerical aperture of 0.3. The power of the laser and the elapsed photon counting time may both be increased to improve sensitivity, however changing such parameters requires a re-calibration of the system.

Complications arise when the probe is immersed in a fluid, in this case blood or saline (section 4), having a different refractive index to that of air. The introduction of a fluid such as saline or blood at the point where the light leaves or enters the core reduces this numerical aperture (Eq^n 1):

$$\text{Numerical aperture 'NA'} = \frac{\sqrt{n_1^2 - n_2^2}}{n_3} = \frac{\text{NA in air}}{n_3} \qquad \text{-Eq}^n\ 1$$

Where n_1 and n_2 are the refractive index of the core and cladding of the optical fibre and n_3 is the refractive index of the blood.

In order to improve the scattering of the light leaving the emitting optical fibre, and conversely that received, a small length of the cladding (1mm) from the end of the probe was dissolved by a solvent to increase the NA at the probe tip (Figure H-5).

When struck by the appropriate wavelength a particle of fluorescent material will re-emit as a point source. The light then seen by an *observing* optical fibre will by described by the solid angle between the observers field of view and the source. This phenomenon implies that less than one percent of the light will be

collected by an optical fibre just millimetres away (fibre diameter = 0.25mm). The removal of the cladding effectively improves the field of view, ie: the numerical aperture of the optical fibre.

Figure H-5

3.4 Mammalian tissue models.

The simulation of endothelial cell damage by the substitution of living tissue with a sodium fluorescein filled helical tube was useful as a feasibility study, but it do not prove whether the system will work with the living endothelium. In order to apply the techniques discussed in section 2, a series of further studies were conducted *in-vitro* and with mammalian vessels.

Endothelial cells were cultured and stained with a sodium fluorescein and glycerol solution (600μMole/l). The sample was the illuminated by an external source (section 3) and the optical fibre probe withdrawn over the surface.

The final set of experiments involved the use of rabbit aorta. Fluorescein with heparin was introduced into the living animal by a perforated angioplasty balloon. The animal was then terminated and the aorta removed. The probe was then withdrawn along the vessel. Unlike the above experiments the *in-vivo* launched light source (Argon Ion laser) was used to excite the material to overcome the absorption of the intervening tissues.

4 Results.

4.1 Artificial vessels

A sodium fluorescein solution was prepared at a concentration of 622 μMoles/l, here after referred to as the *control* and was the most concentrated. The control was then diluted in successive factors of two and the experiment repeated on the simulated artery. In each case the simulated artery was prepared with either red blood cells or saline with a five turn helix containing sodium fluorescein encapsulating the lumen. The absorption effects of the vessel wall were neglected. A real mammalian artery has endothelial cells only on the absolute surface of the inner circumference of the vessel.

The idealised model also took no account of distance. The amount of the sodium fluorescein was calculated from the volume of the helical tube and the concentration of the solution.

Figure H-6a-b

Figure H-6a and Figure H-6b illustrate results using the simulated PVC artery (figure 5) perfused with whole blood with an external and *in-vivo* launched light source respectively. In each case the artery was illuminated at the absorption wavelength of the sodium fluorescein, and the optical probe drawn along the length of the vessel: 2mm OD. It was assumed that the probe followed a similar path for each scan, making results comparable with one another.

The results illustrate the differences of using the external light source, constructed from a halogen lamp fitted with a 490nm close band optical filter, and the *in-vivo* launched Argon Ion laser at 488nm. The use of a well defined light source (laser) makes the separation of the absorption and emission wavelength simpler and more efficient, the excitation wavelength is no longer a broad band of wavelengths, but a narrow line of ~ ± 2nm. Ideally the subject vessel should be in total darkness, ensuring that the only light being received is that re-emitted by the fluorescent material. The probes design for use *in-vivo* is simplifies the problem, the body attenuating all but the brightest of light sources before the it penetrates into the wall of the vessel under study. The laser light source is a considerable improvement over a filtered incandescent source.

4.2 Mammalian vessels

4.2.1 In-vitro studies using an endothelial cell model

Endothelial cells were grown *in-vitro* and the petri dish scratched along its length. Monoclonal antibody was then introduced and treated by the method described by Pringle and deBono, 1988 [7]. The cells were then placed in a dark room and illuminated at 490nm with the external light source.

Figure H-7

The external illumination of the subject area produces a peak on each side of the centre peak. The use of the Argon Ion laser should remove this problem. The peak indicating the presence of the sodium fluorescein is low in amplitude, and it may be that a low level of fluorescence may not be visible using a short photon counting time (< 1 second). The power of the light source and the photon count time can be increased to increase sensitivity

4.2.2 *In-vivo* studies using mammalian model

To further simulate endothelial cell damage as occurs in balloon angioplasty, fluorescein linked to heparin was introduced into the aorta of a rabbit by a perforated angioplasty balloon. The heparin penetrates the tunica media of the vessel and should be detectable by the probe once the vessel is harvested. A calibration was performed on three concentrations: 60IU, 310IU and 500IU[2].

Figure H-8a-b

Figure H-8 shows the calibration curve and the a typical peak recorded corresponding to the sodium fluorescein labelled heparin held in the media of the vessel wall. The fluorescence is clearly visible as a peak in the centre of Figure H-8 of amplitude 0.8. These levels of fluorescence are similar to that one would expect from labelled endothelial cells coating the periphery of the vessel lumen. Although the experiment was devoid of blood the apparatus was not operating at its limits of sensitivity.

5 Discussion

The aim of the experimentation was to determine whether a labelled monoclonal antibody is practical as a means of locating endothelial cell damage in the coronary arterial wall following Percutaneous Transluminal Coronary Angioplasty (PTCA) using optical fibres. The feasibility study has simulated endothelial damage by varying the concentration of the dye contained within a helix of narrow gauge tubing encapsulating a false vessel. The two experiments with the saline and whole blood/ heparin perfused false arteries were able to compare the effects of the presence of blood in a vessel. Once the receiving optical fibre has passed the target the Lambert-Beer law [5] relates the absorption of the blood and the distance to the signal; the result is a decaying offset once the fibre has passed the fluorescence. The absorption of blood at the ultra-violet end of the spectrum is so large that the offset is quickly attenuated.

The laser light source has some clear advantages over that of the filtered halogen source. The manufacturing methods of optical filters means that although the passband of a bandpass filter maybe narrow,

---

[2] Due to the purification process the dilution concentrations are specified in international unit (IU) where 1000 IU=6mg/ml. Moles/l=Weigtht(g)/Molecular weight, hence 1IU≡0.3μMole/l where the molecular weight = 20,000

it is not ideal. The transmission even in the centre of the passband is typically only 40% (specified by manufacturer, Oriel, UK). This means that any external light source is not only likely to distort the signal by emitting in the emission band of the sodium fluorescein, but when light is present in the broad band light source (halogen lamp) it will be greatly attenuated. In practice it was also found that the light source, being of high power, became very hot over several minutes even if forced convection and a dichroic reflector was used. Although this did not prove to be a problem in the presence of the false artery it had the effect of drying the tissue out if the experiment was allowed to run for too long. Although a high power flash, such as a xenon arc lamp, was considered it was felt that the coupling efficiency would still be too small to make it worth while. This hypothesis was validated by the use of a recently terminated rat. In a similar manner to the umbilical cord the vessel had injected into the wall a series of 0.1ml doses of sodium fluorescein (622µMole/l). With the external organs pealed back the subject area was illuminated from the halogen light source and the probe withdrawn. Having detected the presence of sodium fluorescein all external organ and skin were then replaced and the animal re-illuminated. The signal was not visible to the probe even when the PMT count time was increased to ten seconds. The light source was attenuated almost completely over the 40mm of tissue between the light source and aorta. The 20watt light source was increased to 150watt. The heat emanating from the source at close range was unacceptably high, and it was felt that close proximity would seriously damage the tissues.

6 Conclusions

The optical fibre fluorescence transducer clearly holds some major advantages over that of the scintillation probe, in particular the probe with the integrated *in-vivo* optical fibre launched light source. Although the radio-labelled monoclonal antibodies have be used by radiation cameras, the level of resulting radiation required to excite the scintillant is unacceptable. The efficiency and toxicity of currently available scintillants imply that such a system would not be practical for use in the body. The scintillant may be injected into a compliant chamber immediately before use, however leakage into the blood stream would always be cause for concern. Future advances in the development of safer and more efficient scintillants may permit the research to be re-examined but currently such a probe is not suitable for biomedical applications.

The replacement of the radio-labelled monoclonal antibody with that of a fluorescent marker does appear to be viable for biomedical use. The fluorescent material however must be carefully chosen so as not to harm the patient, particularly as the probe is highly invasive intended for use in the coronary arterial system. Experiments deduced that a laser excitation light source should be used. The external light source is limited in its applications, although the tungsten halogen lamp was able to produce results, in order for the system to be useful in the real world the lamp would have to be of an extremely high power to penetrate the tissues surrounding the damaged vascular endothelium.

It is also important to note that the laboratory experiment was conducted in surroundings not favourable to the probe. The high gain of the detection apparatus leaves the probe susceptible to spurious signals originating from sources other than that of the laser and the sodium fluorescein. When using the probe in a real patient the tissues enclosing the damaged vessel will shield the probe tip from any ambient light, further increasing the signal-to-noise ratio of the system.

The main disadvantage of using a fluorescent dye as a biological marker as an alternative to a radio-nuclide is the attenuation effects of the blood and surrounding tissues, as illustrated in Figure H-1. Beta particles or gamma rays are not significantly effected by the presence of blood, but the signal arriving at the receiving optical fibre from the scintillant has a direct relationship to the level of radiation, and hence to the degree of vascular damage. A powerful laser, able to deliver 750mW of continuous power at 488nm was available, but it is not desirable to simply attempt to overcome absorption through the use of increasing powerful lasers. The probe was designed to be small (the two prototype designs using a simplex and duplex arrangement being 1mm and 0.94mm in diameter respectively) in order to ensure that the blood flow was not severely obstructed, especially important in the cardiac vessels. If the probe is to produce repeatable results, measures must be taken to either ensure that the quantity of blood between the tip of the probe is minimal or that it is displaced during the measurement. Guide wires are used as part of many catheterization surgical techniques, including angioplasty, and indeed play an important role in *keyhole* surgery. It is possible to envisage that such a system may be implemented not only to guide the probe into the correct artery, but also to ensure that it is drawn back close to the vessel wall, perhaps held in place by a partially inflated balloon.

Alternatively a steady flow of saline would produce a bolus at the probe tip, and hence an operating window within which the effects of attenuation due to the presence of blood are considerably decreased due to its dilution. The perfusion of the device would also assist in preventing the adhesion of platelets to the cleaved face of the optical fibres which may reduce collection and emission efficiency.

7 Bibliography

[1] K.L.Swinth and J.H.Ewins (1976), Biomedical probe using a fibre-optic coupled scintillator, Medical Physics, **3**(2), pp.109-112

[2] R.T.Lyon *et al* (1987), Vessel plaque and lumen morphology after transluminal balloon angioplasty, Arteriosclerosis, **7**, pp.306-314

[3] M.B.Preisack and K.R.Karsch (1993), The paradigm of restenosis following percutaneous transluminal coronary angioplasty, European heart journal, **14**(1), pp.187-192

[4] A.C.Cuello, J.V.Priestly and C.A.Milstein (1982), Immunocytochemistry with internally labelled monoclonal antibodies, Proc. Nat, Acad Sc.(USA), **20**, pp.665-669

[5] C.Prys-Roberts (1969), The measurement of cardiac output, Brit. J. Anaesth, **41**, pp.751-760

[6] L.Stryer (1975), Biochemistry (2nd Ed), Freeman and Co. (USA), Chapter.21, pp.506-508

[7] S.Pringle and D.P.deBono (1988), Monoclonal Antibodies to Damaged and regenerating Vascular Endothelium, J.Clin. Lab. Immun., **26**, pp.159-162

8 Authors

Paul D. Goodyer was born in London England in 1971. In 1989 he attended the University of Leicester, England and was awarded a first class B.Eng.(Hons) degree in Electrical and Electronic Engineering in 1992. He is presently in his final year reading for a Ph.D. in Biomedical Engineering, continuing this postgraduate study at the same university. Current research interests include the development of optical fibre sensors and the use of lasers and optics in biomedical and high voltage applications.

David P. deBono obtained a B.A. (Cambridge) in 1968 (1st class Hons in parts Ia and Ib Medical Sciences Tripos, 1st class Hons Natural Sciences Tripos part II Biochemistry). M.A Cambridge, M.B, B.Chir 1971. MRCP 1973. MD Cambridge 1979, FRCP (Ed.) 1982, FRCP (Lond) 1990. Currently British Heart Foundation Professor of Cardiology, University of Leicester. Professional interests include outpatient and inpatient care, cardiac catheterisation, coronary angiography and angioplasty. Particularly interested in acute coronary thrombolysis, and in aspects of coronary artery disease.

John C. Fothergill, a senior lecturer in Engineering, obtained his doctorate from UCNW, Bangor in 1979 in *Electronic Properties of Biopolymers*. From 1979 to 1984 he worked for STL in Harlow (now BNR Europe) on high voltage power cables. His interests include high electric field effects, optical fibre sensors for both biomedical and high voltage environments, and intelligent signal processing techniques.

N.B. Jones was born in Liverpool in 1941. He obtained his B.Sc. in Electrical Engineering from Manchester University in 1962, was a graduate apprentice with BICC, obtained a M.Eng degree from McMaster University, followed by more industrial experience with Westinghouse in Canada. He obtained a D.Phil. degree in Control Engineering from the University of Sussex in 1968, and worked on various aspects of bioengineering there until 1984, specialising in control and signal processing applied to neurology and vascular surgery. He was director of the Sussex Centre for Medical Research for ten years. He is now Professor of

Engineering at the University of Leicester, where he is continuing research in biomedical signal processing and instrumentation.

Anthony Gershlick MB. BS FRCP. qualified in 1977 from St. Mary's Hospital, London and trained in basic science at the London Hospital, Whitechapel and in clinical cardiology in the National Heart Hospital and The London Chest Hospital, London. He was appointed Senior Lecturer in Cardiology at the University of Leicester in 1989. Present appointment Consultant Cardiologist and Hon. Senior Lecturer. Interests include the role of platelets in Cardiology and the importance of local drug delivery.

Rajesh Aggarwal is at present a British Heart Foundation Clinical Research Fellow / Honorary Registrar in Cardiology, Division of Cardiology, University of Leicester and Glenfield Hospital Leicester. He graduated MD ChB from the University of Edinburgh in 1987. Postgraduate qualifications: MRCP (UK), 1991

9 Acknowledgements.

SERC, Research grant No: GR/F80777

British Lung foundation

Figures

Figure H-1

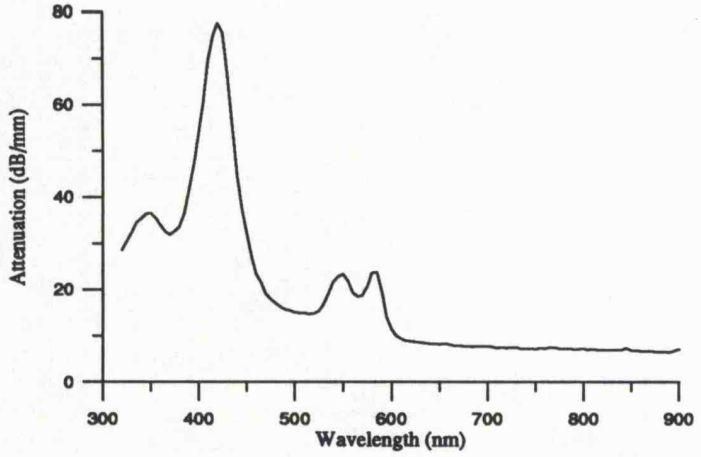

Figure H-2

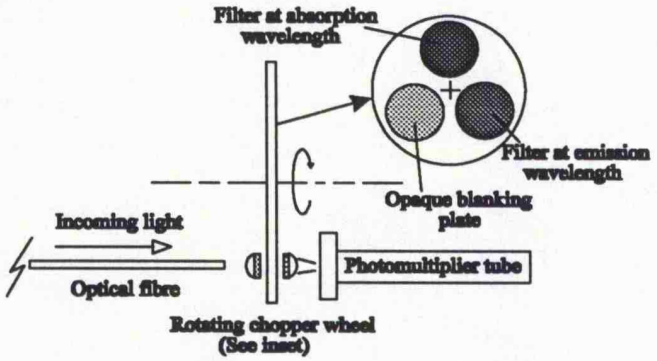

Figure H-3

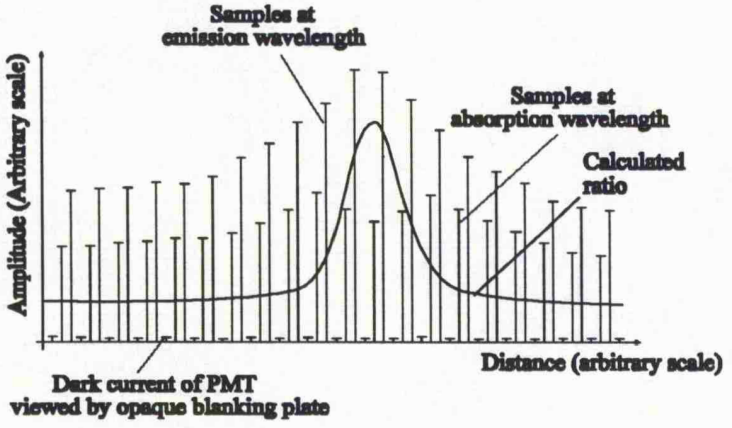

Figure H-4

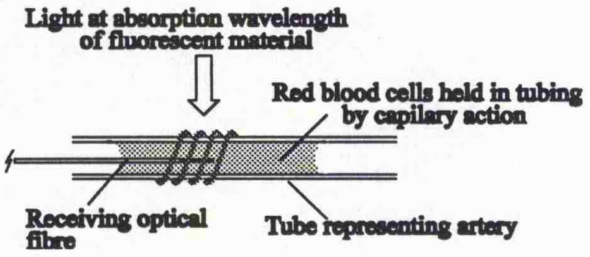

Figure H-5

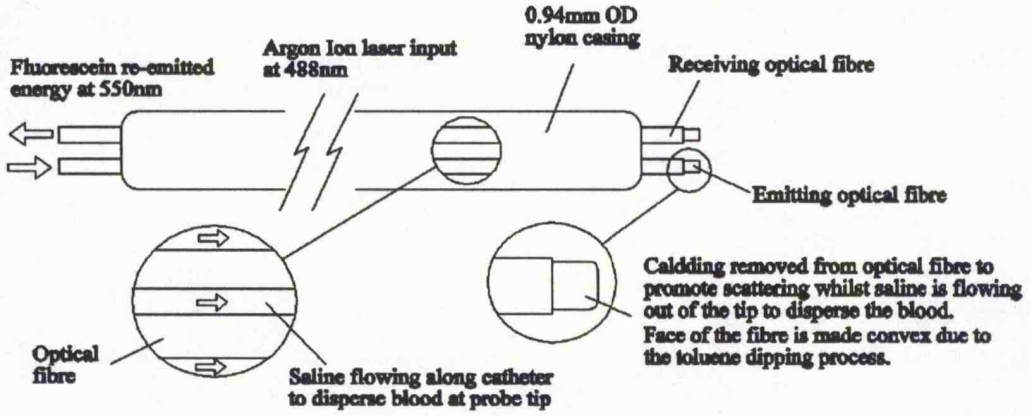

Figure H-6a

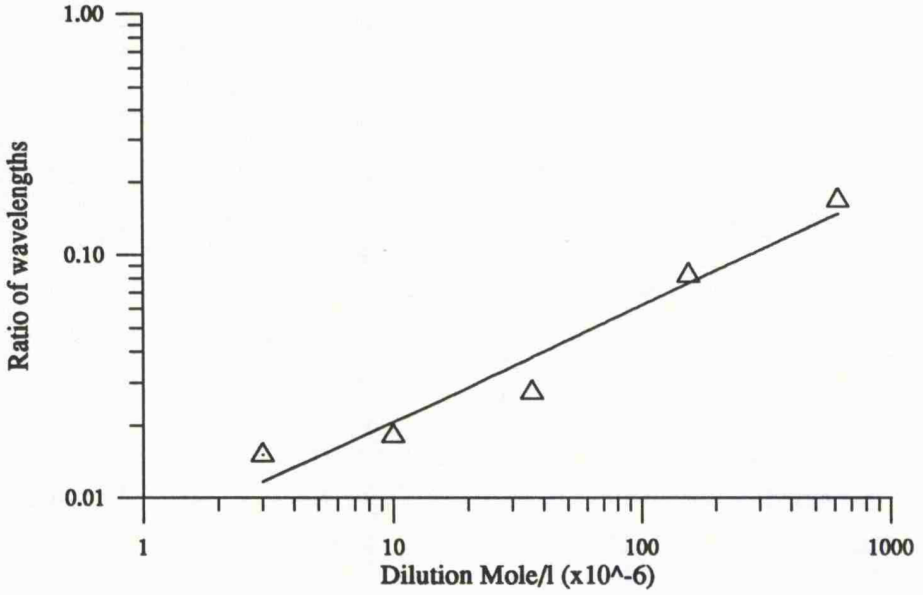

Figure H-6b

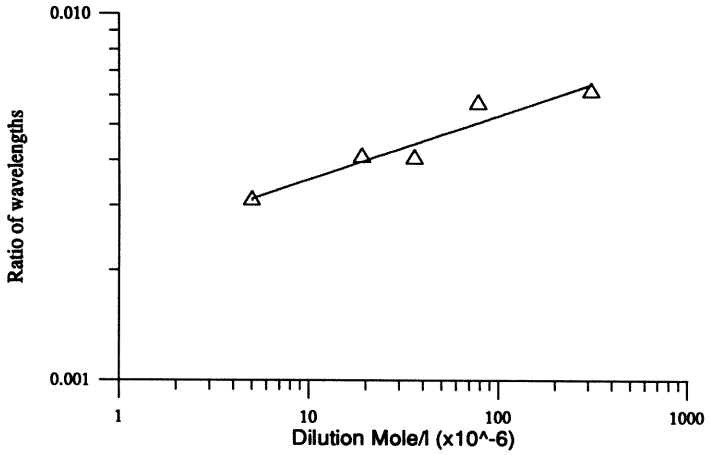

Figure H-7

Photo of stained endothelial cells

Figure H-8a

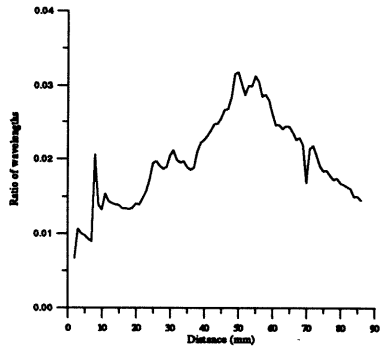

Figure H-8b

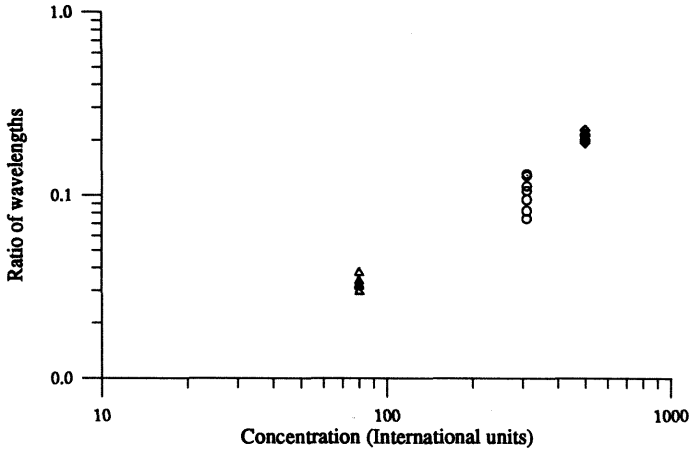

Captions -

Figure 1. The absorption spectrum of whole blood.

Figure 2. The photon multiplier tube and its associated optics assembled to count photons at selected wavelengths.

Figure 3. A single revolution of the optical chopper wheel exposes the photon multiplier tube to a blocking plate and the two filters, to produce a set of three counts.

Figure 4. Preliminary tests using a simulated artery contracted from PVC tubing perfused with blood.

Figure 5. The final design of the optical fibre endothelial cell damage probe.

Figure 6a. Saline perfused artery encapsulated in a 5 turn helix (0.76mm ID).

Figure 6b. Heparin and blood perfused artery encapsulated in a 5 turn helix (0.76mm ID).

Figure 7. The fluorescein stained endothelial cells. Excited by a 490nm external filtered light source.

Figure 8a. Fluorescence of 60IU fluoresceinated heparin in a rabbit aorta

Figure 8b. A summary of the results obtained from fluoresceinated heparin at three concentarions:60IU, 310IU and 500IU used for probe calibration

Keywords -

Cell damage, optical fibre, Fluorescence, Monoclonal antibody, Biosensor

Appendix I

P.D.Goodyer *et al* (1995), The design of an optical fibre pressure transducer for use in the upper airways, IEEE Trans. Biomed. Eng, Submitted for publication

Appendices

THE DESIGN OF AN OPTICAL FIBRE PRESSURE TRANSDUCER FOR USE IN THE UPPER AIRWAYS.

P.D.GOODYER†, J.C.FOTHERGILL†, N.B.JONES†, C.D.HANNING‡

†Department of Engineering, ‡Department of Anaesthesia

University of Leicester, University Road,

Leicester LE1 7RH.

Abstract -

The development of an optical fibre transducer for use in biomedical applications has been presented. The design was targeted for use in the upper airways of patients with sleep disorders stemming from partial or total occlusion of the airway. The transducer preliminary specification was suited for that of upper airway manometry: a resolution of 10Pa over the range ±5kPa, a single transducer being less than 0.94mm in diameter.

Amplitude modulated optical fibre sensors are susceptible to loss due to bending of the fibre core and cladding. The design of the transducer uses a series of three optical fibres, one emitting and two receiving, the combination of the two receiving optical fibres is used to reduce effects of light loss: a bend radius of 50mm is typical for the insertion into the naso-pharynx. The transducer transduction element is a silicone gel coated with reflective titanium dioxide, the meniscus deforms under pressure and modulates the intensity of light reflected back into the receiving optical fibres.

The main disadvantage of optical fibre pressure transducers is their susceptibility to temperature drift. Temperature in the airway rarely changes more than 17°C. The frequency of breathing and the high thermal mass of the catheter means that temperature drift in this application is not significant, and will cause an insignificant error of 12Pa.

The transducer produced is cheap to produce, and may deemed disposable: approximately $20 in material costs (using current manufacturing techniques this can be halved). The system has the added advantage of being electrically, magnetically and chemically passive. The potential for miniaturisation is limited only by the mechanical strength of the optical fibres as mechanical problems associated with fragile elastic membranes do not apply.

1 INTRODUCTION

Optical fibre transducers are of considerable interest to physicians as the patient is intrinsic electrically isolated from the electronic circuitry[1]. The signal is not affected by background electromagnetic radiation (arising from NMRI for example), the devices may be very small and may be capable of measurements not possible with other techniques. Constant improvements in optical fibres and associated emitters and receivers have maintained interest in this area. This paper describes the development of an extrinsic optical fibre pressure sensor, specifically designed to aid in the diagnosis of the collapse of the human upper airway as typically occurs during Obstructive Sleep Apnoea Syndrome.

2 SENSOR REQUIREMENTS

Obstructive Sleep Apnoea Syndrome (OSAS) was first identified by Gastaut [1], as the involuntary occlusion of the human upper airway whilst asleep[3]. It was found to be the cause of periodic hypoxaemia and sleep fragmentation. During sleep the muscles, including those of the upper airway, relax. This is particularly significant in deeper and REM sleep. During inspiration, the ensuing negative gauge pressure causes the airway to collapse. The patient wakes momentarily (a *micro-arousal*), tone returns to the muscles and the obstruction is overcome.

The airway may collapse either at the palate, behind the tongue or at both sites [2]. Successful treatment demands that the site of obstruction be identified reliably. Preliminary studies suggested that pressure measurement at different sites in the airway during sleep could permit the site of obstruction to be deduced [3,14].

The specification for a suitable system required a number of transducers to be incorporated into a single catheter so that measurements could be made at several sites simultaneously. A total of seven transducers were thought necessary, one at the tip of the catheter placed in the oesophagus to measure pressure in the chest, and six arrayed over 20mm intervals to measure the pressure from the back of the nose to just above the larynx [4]. The outside diameter of the catheter should not be greater than 3mm for straightforward insertion into the airway through the nose using a local anaesthetic spray. This implied a diameter for individual sensors of a maximum of 1mm. Polymethylmethacrylate multimode optical fibre, as used in this study, is available at 125μ m diameter. The size to which the transducer may be produced is only limited by the mechanical strength of such optical fibres.

The transducer had to be capable of measuring gauge pressures in the range +5kPa to -5kPa (-500mm to +500mm of water gauge pressure) with a resolution of 10Pa (1mm of water pressure). The accuracy did not need to be very high, perhaps ±5% in order to observe systematic trends. A bandwidth of approximately 40Hz without signal distortion was required. It had to be very flexible with a minimum bend radius of approximately 50mm without loss of accuracy.

3 EXISTING DESIGNS OF TRANSDUCERS.

There are various types of optical fibre pressure transducer, however each type relies upon a transduction element which physically moves or changes in some way in response to pressure which can then be detected optically [5,6,7].

Previous research in our laboratory led to the replacement of the pressure sensitive diaphragm transduction element [8] with a saline or similar fluid [9] which was contained in a small length of tube at the end of either an optical fibre bundle, single or pair of optical fibres. It was this previous research which was the starting point of the development of this new sensor.

The final individual transducer had to be of reasonable size so as to be integrated into a narrow catheter, housing at least seven devices. Due to the tight physical constraints of the specification, the number of optical fibres within the catheter should be minimal; hence a separate optical fibre bundle for each individual transducer is not feasible. Ideally the final transducer would consist of a single fibre which could be used to both receive and transmit light to and from the reflective surface. Since the system is amplitude modulated, if the light is attenuated by any source other than the transduction element a *phantom* pressure will be recorded [10]. A solution was found using two optical fibres at different locations to detect the light reflected off the transduction element [8]. Assuming that each of the two optical fibres losses the same amount of light, the problem of light loss during bending can be overcome. A second design feature is associated with the high sensitivity required to detect the low pressure changes arising from a typical respiratory signal. As the housing containing the transduction element falls in size the practicality of a diaphragm as the transduction element becomes less feasible. The small cross-sectional area requires such a diaphragm to be so thin and elastic that it would be extremely fragile and easily damaged. The transducer discussed in this paper replaces the diaphragm with a gel or fluid, depending on the operating conditions of the transducer.

---

[3] *Apnoea* is defined as the cessation of breathing for ten or more seconds.

4 THE DESIGN OF THE OPTICAL PRESSURE TRANSDUCER

4.1 Orientation of the optical fibres in the transducer housing.

Research led to the development of an optical fibre sensor which used two wavelengths to describe pressure, and hence two different detectors with a peak response at the two wavelengths, the output being the difference between the two [11]. A pressure change led to the change in amplitude of each of the two wavelengths detected. This method was able to compensate for light loss. In order to understand the advantage of using two receiving optical fibres instead of just one it is useful to examine a simple amplitude modulated optical fibre displacement transducer (Figure I-2a).

Figure I-1A -Figure I-1B

The displacement transducer consists of a single emitting optical fibre, and a second receiving; this gives rise to three distinct operating zones (as shown on Figure I-2b) labelled '1', '2' and '3' respectively. The first zone is a *dead spot* and occurs when the fibres are too close to the reflecting surface. Light emitted from an optical fibre emanates within a cone whose solid angle is a function of the numerical aperture and the cross-sectional area of the fibre. Similarly, only light within this *cone of acceptance* can be successfully launched into an optical fibre. In the dead spot zone the projections of the cones onto the reflecting surface do not overlap. The second zone occurs when the reflecting light traverses across the face of the receiving fibre: the projections of the cones partially overlap. In this zone the gain is potentially very high and may be suitable for applications where the displacement of the reflecting surface is small. The width of zone '2' is a function of the diameter of the core of the optical fibres. Zone '3' is a more desirable for the design of the pressure transducer, not only is it wider, but the positions of the optical fibres are less critical. It can be approximated by an inverse square law, the received light being a ratio between the cross-sectional area of the receiving optical fibre and the effective area of the emitted light at a fixed distance away (Eq^n 1).

Having chosen the appropriate part of the operating characteristic, in this case zone '3', it is important to ensure that the transducer does not wander into any other zone which may give a false reading (see Figure I-2b). If the receiving optical fibre gets too close to the reflective surface the reading will begin to fall into zone '2', if this occurs there will be two displacements, and hence two pressures, at which the reading will be the same. The incorrect reading is rejected by offsetting the emitting optical fibre from those receiving by a distance 'l_1' (Figure I-2).

Figure I-2

Hence, assuming the inverse square approximation :

$$\text{Intensity of light '}\Gamma\text{' at distance '}l_1\text{'} \propto \frac{1}{(2x+l_1)^2} \qquad \text{-(Eq}^n\text{1)}$$

The distance from the emitting optical fibre to that receiving, via the reflective surface, is $2x+l_1$ which implies that the path length can never fall to zero. If distance 'x' is set to at least half the sum of the distance defined by zones '1' and '2' of the operating characteristic (Figure I-1b), zones '1' and '2' will never be reached.

The second stage of the design process was the introduction of a second auxiliary optical fibre in a different location and at a different distance from the transduction element. The transducer is ultimately for use in the upper airway and intended to be introduced via the nasal cavity before passing the soft palate, epiglottis and into oesophagus. As a result we would expect the transducer to bend through at least 90°. If both receiving optical fibres are located in roughly the same position in the catheter they should bend through the same radius of curvature, and hence suffer the same losses. The ratio between them should remain the same if the fibre is

not bent too far. The location of the second receiving optical fibre is important. If it is placed too far away from the reflective surface an unacceptably low light level will be detected making it worthless as a reference, however too close and the difference will be so small that the high gains in the pre-amplification stages may make the system unstable and force it too close to the noise floor.

Intensity 'I_1' at distance 'l_1' $\approx \frac{k_1}{(2x+l_1)^2}$ -(Eq^{n}2)

Intensity 'I_2' at distance 'l_2' $\approx \frac{k_2}{(2x+l_2)^2}$ -(Eq^n 3)

$\therefore$ Ratio between intensity $\frac{I_1}{I_2} = \frac{k_1(2x+l_2)^2}{k_2(2x+l_1)^2}$ -(Eq^n 4)

where 'k_1' and 'k_2' are constants of proportionality (cf: Figure I-2).

4.2 Choice of the fluid or gel used for the transduction element.

The other main difference between this transducer and others is the replacement of the flexible diaphragm with a gel. The composition of the gel and its location in the transducer tip is an important factor in the design process. The replacement of the standard pressure sensitive diaphragm is not a new idea [9], designs in the past have discussed replacing the diaphragm with saline or a similar fluid. Saline as the reflecting medium does work, although reflectivity and hence sensitivity is low and, as a consequence, the transducer is very susceptible to noise unless the electronics are designed very carefully. Preliminary experiments involved the use of *'white liquids'*. This is problematic as white liquids as such do not exist, they are either emulsions (which have a tendency to *crack*) or suspensions which inevitably settle out over time. A more fundamental problem was found when using a low viscosity fluid as the transduction element. The transducer becomes very susceptible to sudden shock which sharply jars the fluid and either drastically changes its operating characteristic and sensitivity or ruins the transducer all together by displacing the fluid from the transducer tip. A soybean oil emulsion was however used in the early stages of the experimentation, the results of which are shown in section 6.

Given the considerable problems of using a low viscosity fluid, a suspension or otherwise, to reflect the light an inert silicone gel was used. The composition of the gel is an important factor in the design process, the frequency response of the final transducer being dependent on the mechanical properties, specifically Young's modulus, of the gel. The gel, being transparent, was coated on the surface closest to the optical fibres by micro-spheres of fine grade titanium dioxide. Ideally such particles should be suspended in the gel, however the addition of such particles increases the Young's modulus and hence decreases the frequency response. (Fine particles tend to provide nucleation sites for polymer crystallisation, thus increasing the crystallinity and modulus). Once the gel had cured and secured itself in position the three optical fibres were mounted at the appropriate distances from the coated meniscus.

5 EXPERIMENTAL

In order to quantify the steady-state characteristics and the frequency response of the pressure transducer the arrangement shown in Figure I-3 was used to acquire data from the catheter on seven channels simultaneously. The output of each device was scaled and displayed in real-time.

Figure I-3

Appendices

5.1 Static characteristics

A series of experiments was conducted to determine static characteristics. A single channel optical fibre transducer, as described in section 4, was constructed and subjected to a series of static pressures. The transducer was placed in an enclosed pressure chamber and exposed to atmospheric pressure. All pressures were then measured using a water filled manometer with respect to the atmospheric pressure on the day of the measurement. The pressure was changed in the pressure chamber by adjusting the volume of air using an air loaded syringe.

Figure I-4

The output, which is derived from the difference in light intensities from the two fibres, is plotted as a function of pressure in Figure I-4. This experiment has been repeated for many such transducers and similar results have been obtained.

In order to produce a transducer which is usable as a clinical tool, the output must be either linear or predictable. The output from the transducer is clearly not linear over a wide range, however it may be approximated to be linear over a limited working characteristic of ±3kPa (±300mm of water pressure).

5.2 Dynamic characteristics

In order for the transducer to be effective in measuring the respiratory signals associated with Obstructive Sleep Apnoea the transducer should respond to the bandwidth of the dynamic pressure changes associated with the fluttering of the soft palate during snoring. Typically this is 20Hz. In order to minimise noise the output was fitted with a low pass filter at 100Hz.

Frequency response was measured in two ways. The first was to feed in a pressure signal produced from a mechanical shaker fitted with a white noise generator. Both had a frequency response which was known to be flat to at least 1kHz. The transducer was then placed in a chamber fed by the shaker and the output recorded using a digital signal processor acquisition system. The fast Fourier transform of the signal was then calculated. A second method of measuring frequency response was used to confirm the mutual results. An enclosed speaker was fed with a pure tone at a selection of frequencies. Both the optical transducer and a secondary transducer with known frequency response, were used to measure the pressure in the enclosure. The two techniques gave very similar results. Bode plots, as shown in Figure I-5, indicate the frequency response of the transducer system using titanium dusted silicone gel. The response was seen to be flat up to 100Hz, whereupon the effect of the 100Hz filter is observed.

As described in section 5, transducers were also developed using a *white* low viscosity fluid as the transduction element. These transducers were not suitable for this application as large sudden changes in pressure (perhaps caused by coughing) resulted in the liquid moving within the tube. This resulted in either changing the calibration curve or making the transducer unusable. As they may be suitable for other applications and their frequency response was expected to be better this was also measured. The frequency response characteristic of a transducer primed with a soybean oil 10% fat emulsion (Intralipid®, Kabi Pharmacia Ltd.) was measured with the 100Hz low-pass filter disabled. This are shown in Figure I-6.

Figure I-5A - Figure I-5B

Figure I-6

5.3 Quantification of temperature stability

The main disadvantage of the optical fibre pressure transducer is the temperature dependency. Temperature was quantified by performing a series of two experiments aimed to determine the drift of the output with respect to temperature and the thermal mass of the catheter body. The transducer design principle involves the compression of a column of gas which is also prone to expansion and contraction due to temperature change.

In order to make quantitative measurements, temperature must be either constant, compensated for or the thermal mass of the transducer should be such that the device temperature cannot change significantly during respiration (0.2Hz minimum). The time constant '*T*' of the single channel device was measured to be 0.3 seconds and 78 seconds in the seven channel device [4]. If the transducer is considered to be a first order system (Eq^n 5):

$$H(j\omega)=\frac{1}{1+j\omega T} \qquad \text{-(Eq}^n\text{ 5)}$$

The temperature change of the airway is dependent on the whether the subject is breathing orally or nasally. If the subject is in warm ambient conditions (≈20°C) in the worse case the temperature change will be 10°C [12]. A 17°C temperature change (difference between airway mucosa and inhaled air) was measured to be equivalent to a pressure change of approximately 200Pa in the steady state given a working range of ±500Pa. Due to the time constant the effect of temperature drift is reduced to 6% of the steady state temperature change for the multiple channel device given the respiration is 0.2Hz approximately in a sleeping adult. This implies an insignificant error of 12Pa (1.2mm of water pressure in conditions unfavourable to the device).

6 DISCUSSION

The fundamental difference between the optical fibre pressure transducer without an elastic diaphragm and the alternatives with a diaphragm, optical or otherwise, is the ability to change the reflective medium readily to tailor characteristics to a particular application. The use of a soybean oil emulsion produced a good frequency response, flat up to 0.5kHz (Figure I-6). Unfortunately the low viscosity of the fluid made it unsuitable for use in the upper airways. The introduction of the gel as the reflective medium, although more stable has a lower frequency response. The selection of the gel as the reflective medium, has produced a pressure transducer whose output is stable and predictable.

The static characteristics, shown in Figure I-4, illustrates the non-linearity of the system. The gel, acting as the transduction element, is unable to physically move within the vessel containing it, it is only able to deform. The gel adheres to the transducer wall and consequently the curvature will change with respect to pressure which is non-linear.

The sensitivity of the transducer is a function of the volume of air contained behind the fluid meniscus, and hence the transducer measures pressure with respect to the conditions under which the transducer was first sealed and the gel was in equilibrium inside the housing. This means that the If such a transducer is to be used in the upper airway, the efficiency of the nose as a humidifier and heater / cooler is important in achieving a reliable measurement which is repeatable. The change in temperature of the air inhaled and exhaled is dependent on oral or nasal breathing. The time constant of the device, especially in the system devised to house seven transducers (78 seconds) means that temperature effects can be neglected (error of 12Pa). The clinical and temperature results obtained from this transducer are reported by Goodyer and co-workers in references [4] and [13].

One of the advantages of an optical transducer in the past over that of a similar mechanical or electrical alternative was their size. Transducers by Skatvedt *et al* [14,3] have developed miniature transducers for assessment of the upper airways, however this technique offers an alternative disposable device. The initial cost of the pre-amplification circuitry, optical components and associated instrumentation was approximately $1500. The transducers were produced for approximately $150 each for a seven channel device. A single channel system was $300 and $20 for the single channel instrumentation and catheter respectively. It is hoped

that current modern manufacturing processes should reduce this cost to half of this amount. The pressure range is ±5kPa with a resolution of 10Pa. The size of a single transducer makes it a candidate for measuring pressures in more isolated areas of the human body. Suggested further applications include oesophageal and rectal manometry, and also arterial and venous measurements to determine pressure and flow. The researchers envisage a seven channel device less than 2mm in diameter by refinement of the manufacturing and material techniques.

7 REFERENCES

[1] C.Guilleminault, and M.Partinen, "Obstructive Sleep Apnoea Syndrome", *Raven Press,* Chapter 1, 1990

[2] D.A.Hudgel, Properties of the upper airway during sleep, *ENT Journal*, Vol.71, No.1, pp.42-45, 1993

[3] O.Skatvedt, "Continuous pressure measurements in the Pharynx and Oesophagus during sleep in Patients with OSAS", *Laryngoscope.*, Vol. 102, pp.1275-1280, 1992

[4] P.D.Goodyer, J.C.Fothergill, C.D.Hanning and N.B.Jones, "A multiple channel optical fibre pressure transducer for use in Obstructive Sleep Apnoea: Clinical investigations ", To be submitted for publication April 1995

[5] A.Lekholm, "Optoelectronic transducer for intravascular measurements of pressure variations", *Med. and Biol. Eng.*, Vol.7, pp.333-335, 1968

[6] W.J.Bock, "GaAs-Based Fibre-optic Pressure Sensor", *IEEE Trans Instr and Meas.*, Vol. 41, No.1, pp.68-71, 1992

[7] P.M.Tracy, "Intrinsic Fibre-optic sensors", *IEEE Trans Indust Appl.*, Vol. 27, No.1, pp.96-98, 1991

[8] R.A.Wolthuis, "Development of medical pressure and temperature sensors employing optical spectrum modulation, *IEEE Trans. biomed. Eng.*, Vol.38, No.10, pp.974-981, 1991

[9] G.Papageorgiou, and N.B.Jones., "Optical sensors: Smaller, Cheaper, Faster", *Sensor review: IFS Publications*, Vol. 8, No.1, pp.19-22, 1988

[10] J.W.Berthold, "Historical review of microbend fiber optic sensors", *Proc. of 10th Optical fibre sensors conference (Scotland),* IOP Publications, pp.182-186, 1994

[11] Y.Libo, and Q.Anping, "Fibre-optic diaphragm pressure sensor with automatic intensity compensation", *Sensors and Actuators A*, Vol. 29, pp. 29-33, 1991

[12] C.Kohl, "Alteration of airway wall temperature during different inhalation procedures", *J. of Aerosol Science*, Vol.21, No.S2, pp.415-417, 1990

[13] P.Goodyer, "The design of optical fibre sensors for *in-vivo* use: with applications in obstructive sleep apnoea syndrome and arterial restenosis", *PhD Thesis*, University of Leicester, Chapter 5, 1995

[14] O.Skatvedt and J.Groegaard., "Inspiratory pressures in the new-born and 6 and 12 weeks old children in different sleeping positions", *Arch Dis in Child*, Vol.71, pp.138-140, 1994

8 AUTHORS

Paul D. Goodyer was born in London England in 1971. In 1989 he attended the University of Leicester, England and was awarded a first class B.Eng.(Hons) degree in Electrical and Electronic Engineering in 1992. He is presently in his final year reading for a Ph.D. in Biomedical Engineering, continuing this postgraduate study at the same university. Current research interests include the development of optical fibre sensors and the use of lasers and optics in biomedical and high voltage applications.

John C. Fothergill, a senior lecturer in Engineering, obtained his doctorate from UCNW, Bangor in 1979 in *Electronic Properties of Biopolymers*. From 1979 to 1984 he worked for STL in Harlow (now BNR

Europe) on high voltage power cables. His interests include high electric field effects, optical fibre sensors for both biomedical and high voltage environments, and intelligent signal processing techniques.

Christopher D. Hanning graduated BSc, MB, BS from St Bartholomew's Hospital in 1972. He has been Senior Lecturer in Anaesthesia to the University of Leicester since 1981. His clinical and research interests encompass patient monitoring and the investigation and treatment of sleep disorders.

N.B. Jones was born in Liverpool in 1941. He obtained his B.Sc. in Electrical Engineering from Manchester University in 1962, was a graduate apprentice with BICC, obtained a M.Eng degree from McMaster University, followed by more industrial experience with Westinghouse in Canada. He obtained a D.Phil. degree in Control Engineering from the University of Sussex in 1968, and worked on various aspects of bioengineering there until 1984, specialising in control and signal processing applied to neurology and vascular surgery. He was director of the Sussex Centre for Medical Research for ten years. He is now Professor of Engineering at the University of Leicester, where he is continuing research in biomedical signal processing and instrumentation.

9 ACKNOWLEDGEMENTS

The authors are grateful to the British Lung Foundation and Simms Portex (UK) for supporting the development of this transducer and to the EPSRC for a scholarship for P.D.Goodyer.

Appendices

Figures

Figure I-1a

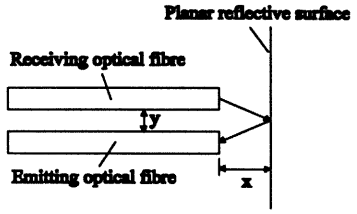

Figure I-1b

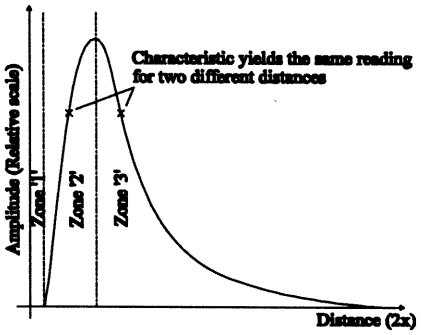

Figure I-2

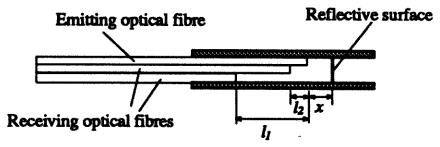

Figure I-3

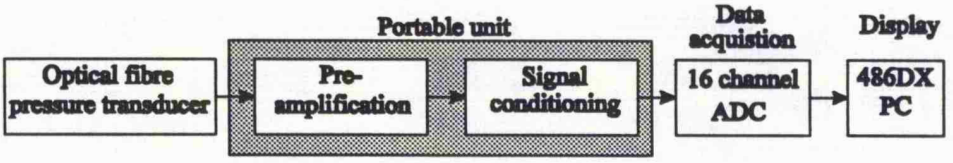

Figure I-4

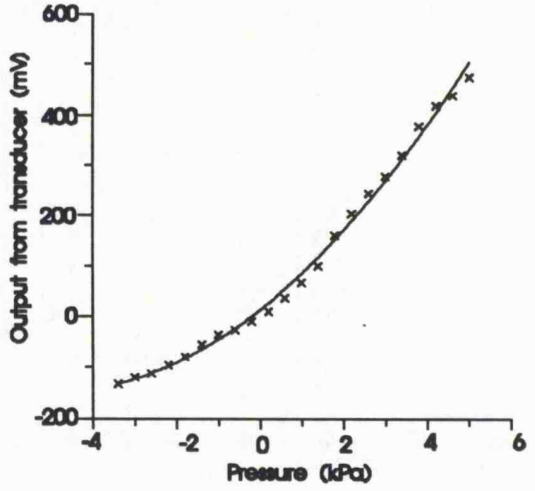

Figure I-5a

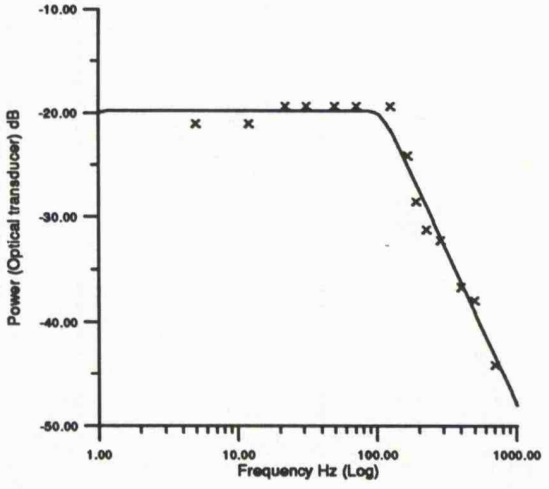

Figure I-5b

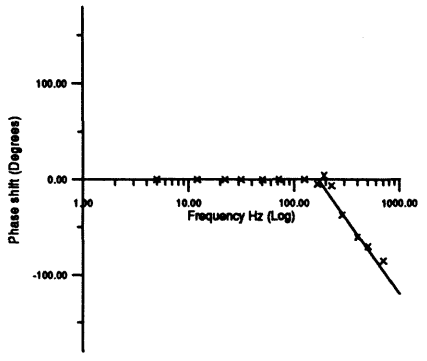

Figure I-6

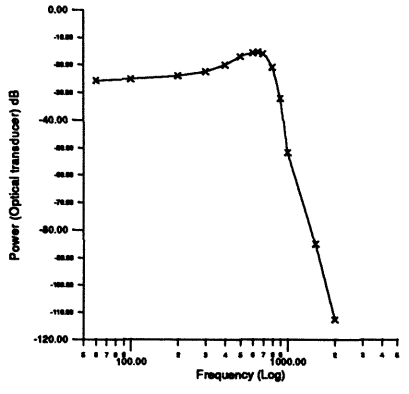

Captions:

Fig. 1a. An optical fibre displacement transducer using a single emitter and receiver.

Fig. 1b. The output characteristic of a simple optical fibre displacement transducer as illustrated in fig 1a.

Fig. 2. A schematic diagram of an optical fibre pressure transducer designed to overcome amplitude modulation induced problems by optical fibre micro-bending.

Fig.3 A block diagram of the pressure transducer and data acquisition system.

Fig. 4. Output from an optical fibre pressure transducer over a wide range (<±4kPa ,< ±400mm of water) illustrates non-linearity.

Fig. 5a-b. The frequency response of the optical fibre pressure transducer when using a gel as the transduction element, output filtered at 100Hz for respiratory applications.

Fig. 6. The frequency response of an optical fibre pressure transducer using an intralipid emulsion as the transduction element to improve the frequency response.

Appendix J

P.D.Goodyer, J.C.Fothergill, N.B.Jones, C.D.Hanning (1995), An optical fibre pressure transducer for use in obstructive sleep apnoea, British Journal of Anaesthesia, Submitted for publication

AN OPTICAL FIBRE PRESSURE TRANSDUCER FOR USE IN OBSTRUCTIVE SLEEP APNOEA

P.D.GOODYER†, J.C.FOTHERGILL†, N.B.JONES†, C.D.HANNING‡

†Department of Engineering, ‡Department of Anaesthesia

University of Leicester, University Road,

Leicester LE1 7RH.

Abstract

A catheter containing seven optical fibre pressure transducers has been constructed with an external diameter of 3mm. One transducer is located at the tip whilst the remaining six are spaced 20mm apart between 200mm and 300mm from the tip. The transducers had a resolution of 10Pa (1mm of water pressure) in the range ±5kPa (±500mm of water pressure). The catheter was designed specifically for insertion into the upper airway of patients with Obstructive Sleep Apnoea Syndrome to facilitate diagnosis and treatment.

Pressure profiles of a small group of normal subjects were measured under both local and general anaesthesia. The catheters were placed so that the tip was in the oesophagus and the six transducer array was in the upper airway from posterior nasopharynx to hypopharynx and confirmed by visual inspection.

Preliminary analysis after equilibration showed that phasic respiratory pressure changes could be measured at all points. Cardiac and peristaltic pressure changes were seen from the distal (oesophageal) transducer. During episodes of simulated and natural snoring, high frequency pressure changes could be seen from transducers adjacent to the palate with a change in waveform suggestive of flow limitation and partial airway obstruction.

We concluded that the catheter should be a useful tool for the investigation of upper airway obstruction. Further clinical studies are warranted.

Keywords - Obstructive Sleep Apnoea, Optical fibre, Pressure transducer, Snoring

1 Rationale - Obstructive Sleep Apnoea Syndrome

Obstructive Sleep Apnoea Syndrome (OSAS) is a common condition characterised by two symptoms, snoring and daytime sleepiness. Snoring represents partial obstruction of the airway with fluttering of the palate and pharyngeal wall. In some patients the airways collapses completely: level of the palate or behind the tongue or both. The subject struggles to breathe for 20 to 60 seconds and then arouses from sleep. As the airway opens, a loud snort or "heroic snore" is emitted. After a few breaths the subject falls asleep and the sequence is repeated, often several hundred times each night. The arousals (known as micro-arousals) are so short that the subject does not remember them and the fragmentation of the sleep reduces its quality leading to daytime sleepiness. OSAS has been studied extensively by several reviewers, and is not reviewed fully in this paper (Crumley *et al*, 1987,. Sheppard *et al*,1991 and Hudgel, 1992).

Previous research has developed a multitude of pressure transducers suitable for insertion into the upper airway as a means of determining the pressure profile and hence regions of abnormal airway narrowing (Skatvedt, 1993 and Tvinnereim *et al*, 1992). Given this pressure profile it should then be possible to determine the extent of the collapse, whether it is correctable by surgical means and the type of surgery appropriate. Due the potential miniaturisation of optical fibre pressure transducers it was proposed that an array of devices be integrated into a catheter to analyse the pressure from the nasal pharynx to the top of the oesophagus. The use of imaging (CAT, NMRI etc) to monitor airway collapse has been used by several physicians for this purpose (Pepin *et al*, 1992). The ultimate goal of the project was to produce a device which may be used along with the imaging techniques to validate the diagnosis of the severity of the collapse.

2 Equipment

2.1 Design specification

Once OSAS has been identified, it is usual to admit the patient to take part in an overnight sleep study during which several physiological parameters are monitored:

- Sound using a microphone (snoring).
- Blood oxygen saturation using pulse oximeter.
- Abdominal movement during respiration.
- Body trunk movement on the mattress.
- Airflow through nose and mouth.

It was proposed that the optical fibre pressure transducer ultimately be inserted as part of this study.

The design of the multi-channel optical fibre pressure transducer stemmed from the development of a single channel optical fibre pressure transducer without an elastic membrane (Jones and Papageorgiou, 1988). In order to produce a reasonable resolution along the upper airway it was decided that there should be seven transducers integrated into a catheter of a diameter of ideally no more than 3mm in diameter. It was stipulated that six of seven transducers in total be equally spaced at 20mm intervals and situated from the back of the nasal cavity to the hypo-pharynx whilst the seventh, being 200mm from the bottom-most transducer, should lie mid-oesophagus. The resolution of the transducers should be able to distinguish ideally 10Pa (1mm of water pressure) over the range ±5kPa (500mm of water pressure).

A single pressure transducer, able to satisfy this criteria has already been development, and is described in an earlier paper (Goodyer *et al*, 1995). It was proposed that seven single channel pressure transducers be integrated into a catheter housing to meet the above specification. Snoring, characteristic of OSAS sufferers, has a frequency of 15 to 20Hz. The pressure transducer used had a nominal frequency response of 500Hz, however this was limited to 100Hz using a low-pass filter to reduce noise.

3 The pressure transducer catheter.

The construction of the catheter posed a formidable materials challenge. The highly invasive nature of its application means that all materials used in the catheter should be harmless should any part become detached from the main body and ingested. The pressure transducer and catheter housing was either nylon or PVC, and sealants, adhesives etc were checked to ensure they were non-toxic (acrylic if possible). The final surface finish of the catheter is extremely important if it is to be inserted into the patient through the nose as it will lacerate the nasal mucosa. An open-ended catheter is also unsuitable for use in the airway due to problems with mucus and other secretions accumulating in the pressure inlet. Both problems were solved by enclosing the device in a flexible membrane. A series of seven balloons along the catheter length were used, each chamber being isolated from its neighbours. In order to minimise the volume of the catheter the pigtailed devices were staggered. This means that for a given cross-section through the catheter, particularly near the upper most transducers, there will be both the transducer housing and a number of optical fibres running from transducers further down the catheter (Figure J-1). In order to monitor the location of the transducer in the upper airway each device was given a radio-opaque marker[4], it should however rarely be necessary to take an X-ray as long as the depth of penetration of the catheter into the oesophagus is known.

[4] Radio-opaque markers were fitted above transducer '7', between transducers '5' and '6' and above transducer '1'. The marker comprised a small strip of gold leaf secured around the transducer housing. The X-ray, being able to distinguish between materials by their density, also revealed the shadow of the block of sealant isolating adjacent transducers.

Figure J-1

The signal conditioning electronics and optics were split between two boxes. A small box was designed for placement next to the patients head during the study, which enclosed the pre-amplification stages, optical emitters and receivers. This was then connected to the other larger half of the equipment which contained the signal processing circuits and power supplies. This in turn was connected to the ADC and the acquisition system. It was felt important to split the electronics into two modules not only to reduce the risk of electrical interference, but also to make the patient feel more comfortable with the equipment. The data was acquired and displayed in real-time on the computer screen.

Figure J-2

Figure J-2 illustrates the seven channel pressure transducer connected to the pre-amplification circuitry. The box also contains a earth protected oscillator driving the fibre optic emitters.

4 Preliminary clinical evaluation

In order to test the catheter design a series of preliminary studies were undertaken on a small group of people with both normal and abnormal airways. The group varied in age and the anaesthetic administered was adjusted depending of the subject. The catheter was calibrated by placing it into a pressure chamber connected to an analogue pressure gauge and air loaded syringe. The pressure was slowly increased and decreased over the range ±500Pa (±5mBar). The seven pressure transducers were monitored simultaneously to ensure the sensitivity of each was identical.

4.1 Measurements using local anaesthesia

The subject was seated in a relaxed upright position and the nasal airway and soft palate anaesthetised with Lignocaine spray. The transducer was passed in through the nostril, through the nasopharynx and back behind the soft palate and tongue. When the tip of the transducer was at the back of the throat it was swallowed into the oesophagus with the aid of water (the catheter was marked at various distances along its length to monitor how far into the oesophagus the transducer had penetrated). The transducer was held in place by either tape or the subject himself to ensure peristalsis did not pull the device further towards the stomach.

When the transducer was in position, transducer '1' being anchored mid-oesophagus, reading commenced. Due to the consciousness of the subject, and hence the high level of airway and gastric activity, it was found necessary to introduce the catheter ten minutes prior to the measurements being taken. This allowed the oesophagus to become used to the presence of the catheter and also the temperature of the device to stabilise. When the patient was relaxed a series of respiratory exercises were performed. These involved normal and heavy breathing, and also simulated snoring and airway obstruction.

Figure J-3a **Figure J-3b**

Figure J-3a is the pressure reading observed at transducer number 3, located behind the soft palate, and shows partial airway obstruction. This was simulated by tipping the head back in a horizontal position and instructing the subject to breath heavily through the nose to promote vibration of the soft palate as occurs during snoring. A fundamental low frequency respiratory waveform (0.25Hz) with an amplitude of 350Pa is shown[5]. There is evidence of *snoring* on the inspiratory part of the waveform. Snoring is seen as a high

[5] The output is AC coupled and consequently has a mean value of 0Pa.

frequency component in the trough of waveform. When examined closer it was measured to be of the frequency range 15-20 Hz, considerably higher than any other waveform associated with respiration.

Figure J-3b is the pressure observed in the distal transducer located mid-oesophagus (400mm beyond the entrance to the nose). The main dominant feature observed was that of cardiac contraction. This has the effect creating a higher frequency component on the waveform (1.4Hz). The figure also shows a peristaltic wave. The patient was instructed to swallow, and the speed of the ensuing peristaltic wave was calculated by timing the group velocity of the wave as it passed transducers 6 and 7 which were spaced 200mm apart. The velocity was calculated to be 46mm/s.

In total six studies were undertaken with patients under local anaesthesia. It was found possible to derive the location of the transducer in the gastric tract purely by observing the waveform. Other waveforms observed included pressure inversion if the transducer was passed through the sphincter into the stomach, i.e. below the diaphragm.

Although it was possible to introduce the catheter with only a local anaesthetic, the anaesthetic did wear off within twenty minutes. This meant that more anaesthetic had to be induced. In order to alleviate the problem it was proposed the KY Jelly™, previously used to lubricate the catheter, be replaced by Lignocaine jelly.

4.2 Measurements using general anaesthesia

The second stage of the investigation was to introduce the catheter into an unconscious patient under general anaesthetic and attempt to isolate particular respiratory features associated with OSAS that could not be simulated on conscience patient.

Five patients were selected for a preliminary investigation. The catheter and pre-amplification box were taken into the operating theatre and inserted into the patient twenty minutes before the end of the operation (which was not sleep related) to allow it to stabilise. The location of the device in the pharynx was checked by visual inspection to ensure the second top-most transducer was level with the uvula. The patient was then brought into recovery and a set of readings taken prior to them coming out of the anaesthetic. A notebook size PC was used to acquire the data, making the whole system more portable, and transportable into the operating theatre if necessary.

The patient arrived in recovery under general anaesthetic. Recording of the pressure profile was then undertaken during a ten minute slot prior to him or her becoming completely conscious.

Figure J-4

Figure J-4 shows a sample output from transducers '1' to '4' and '7'. The patient was male and in his mid-fifties with a history of an abnormally narrow airway and snoring. All graphs are AC coupled, and hence have a mean value of 0Pa.

If the patient had a normal airway and was not either snoring or obstructing in any way we would expect all of the six upper transducers to provide a similar signal of steadily increasing amplitude further down the airway (Koite *et al*, 1992). This patient does not have a normal airway, and by examining each of the traces it is possible to see features associated with partial or total obstruction of the throat. Transducer '1' does not appear to show any main features of interest, other than a single cycle of a typical respiratory signal. As we progress further down the airway, to transducer '2' there is clear evidence of snoring. In a similar manner to Figure J-3a, snoring is seen as a high frequency component corresponding to the *fluttering* of the soft palate during inspiration. This was measured and in this particular patient measured to be 20Hz. The inspiratory part of the waveform also shows a peak close to its centre in Figure J-4b, this becomes a null followed by a plateau region in Figure J-4c and Figure J-4d. The plateau can be explained by flow limitation. If the patient is fully or partially obstructing the air will be prevented from flowing along the airway. If the inspiratory signal is examined in close detail it appears that during the onset of inspiration the palate does indeed begin to *flutter* characteristic to snoring. This then leads to partial obstruction of the upper airway, at which point snoring stops

and flow is limited. The expiration part of the cycle then forces the airway fully open. The plateau of the expiration waveform, shown between 2.5 and 4.5 seconds on Figure J-4b, c and d, is not a saturation but an indication of constant flow rate. Transducer '7', situated in mid-oesophagus, does illustrate the respiratory signal but due to its location behind the heart there is also a considerable amount of cardiac artefact (cf: Figure J-3b).

Figure J-5

Results from a non-snoring patient (Figure J-5) showed that transducers '1' to '6' detected a lower amplitude waveform without the high frequency artefacts associated with snoring or plateau in the inspiratory part of the cycle. The absence of obstruction means that the measured waveforms were purely due to the airflow passing each transducer. The reference transducer '7' displayed a similar level of cardiac artefact as that shown in Figure J-4e, the respiratory signal was however again of considerably lower amplitude.

5 Discussion

The main criticism of pressure transducers for this application is their susceptibility to temperature drift. The catheter has a large thermal mass, and the time constant was measured to be 78 seconds. The quantity of drift is dependent on the change of the airway temperature during inhalation and expiration. This is a function of the ambient airway temperature and the rate and depth of breathing (Köhl, 1990). Given a worst case of a 15°C temperature change, at a nominal breathing rate of 0.2Hz the error was calculated to be ≈17Pa.

It may be argued that there are many pressure transducers on the market, there are few that are sufficiently small in size to fit into the airway (Skatvedt, 1992 and Skatvedt, 1993). Airway manometry has been studied in the past, but often with a lower number of pressure points, a lower sensitivity and a lower frequency response. The optical transducer described in this paper had a diameter of 3mm, seven pressure points, a sensitivity of 10Pa over the range -5kPa to +5kPa with an accuracy of 1% and a bandwidth of 100Hz. The researchers envisage a bandwidth of greater than 1kHz for future devices.

The use of the device in a small group of subjects under either local or general anaesthesia highlighted the importance of the tranquillity on the clarity of the waveform. If the subject is aware that the catheter is present, the ensuing peristaltic waves from swallowing and otherwise are more frequent. This agitates the transducers and makes the waveform for difficult to quantify. It was found that in order to produce a clean set of data the subject should be allowed to relax for at least ten minutes with the catheter in place prior to acquisition. If the catheter is to be used in real patients as part of a sleep study it was concluded that it would have to be used in conjunction with a mild sedative to allow them to sleep. It is hoped that the catheter may then be used in conjunction with the other sleep study monitoring techniques in order to produce a reliable diagnosis of OSAS.

The potential for miniaturisation with a fibre optic transducer is greater in many transducer applications, pressure measurement being one of them. The application of optical fibres to the study of OSAS is particularly suitable for a number of reasons. The optical fibre is made from a dielectric material, and hence has a zero risk of electric shock and electromagnetic interference. This means that a catheter constructed from optical fibre for *in-vivo* use may be readily used with other biomedical technologies, for example Nuclear Magnetic Resonance Imaging (NMRI). The technology is still in its infancy, further development will reduce the size of the device to less than 2mm in diameter.

6 Conclusions and summary

The trial and use of an multiple optical fibre pressure transducer catheter has been demonstrated as a feasibility study, and some preliminary data arising from snoring and airway obstruction have been presented.

The transducer has proved that it is able to produce a profile of upper airway and oesophageal pressure by monitoring seven points along the airway and oesophagus. On inspection of the data air flow impairment was measured as was the high frequency change in air pressure associated with snoring. Analysis of data from all transducers should lead the trained physician to deduce the site of the upper airway collapse.

In order to validate the transducer fully it is necessary to study a larger group of real patients. A series of overnight sleep studies with patients suspected of having sleep disorders is planned, the results of which will be published in due course.

7 Glossary of terms

ADC - Analogue to Digital Converter

CAT - Computer Aided Tomography

OSAS - Obstructive Sleep Apnoea Syndrome

NMRI - Nuclear Magnetic Resonance Imaging

8 Bibliography

R.J.Crumley *et al* (1987), Determination of obstructive site in obstructive sleep apnoea, Laryngoscope, **97**, pp. 301-308

P.D.Goodyer *et al* (1995), The design of an optical fibre pressure transducer for use in the upper airways., IEEE Trans Biomed Eng, Submitted for publication, paper #7082

D.W.Hudgel (1992), Mechanisms of obstructive sleep apnea, Chest, **101**(2), pp.541-549

N.B.Jones and G.Papageorgiou (1988), Optical fibre sensors: smaller, cheaper, faster, Sensor review, **8**(1), pp.19-22

C.Köhl (1990), Alteration of airway wall temperature during different inhalation procedures, J. of Aerosol Sci, **21**(S2), pp.S415-S417

Y.Koite *et al* (1992), Measurements of meospharyngeal pressure in patients with obstructive sleep apnea, Adv.Otorhinolaryngol, **47**, pp.260-266

J.L.Pepin *et al* (1992), Somnofluoroscopy, computed tomography, and cephalometry in the assessment of the airway in obstructive sleep apnoea, Thorax, **47**, pp.150-156

J.W.Sheppard *et al* (1991), Evaluation of the upper airway in patients with obstructive sleep apnea, Sleep, **14**(4), pp.361-371

O.Skatvedt (1992), Continuous pressure measurements in the pharynx and oesophagus during sleep in patients with obstructive sleep apnea syndrome, Laryngoscope, **102**, pp.1275-1280

O.Skatvedt (1993), Localisation of site of obstruction in snorers and patients with obstructive sleep apnea syndrome: A comparison of fiberoptic nasopharyngoscopy and pressure measurements, Acta. Otolaryngol (Stockh), **113**, pp.206-209

M.Tvinnereim *et al* (1992), Pressure recordings - A method for detecting site of upper airway obstruction in obstructive sleep apnea syndrome, Acta Otolaryngol (Stockh), **492**, pp.132-140

9 Authors

Paul D. Goodyer was born in London England in 1971. In 1989 he attended the University of Leicester, England and was awarded a first class B.Eng.(Hons) degree in Electrical and Electronic Engineering in 1992. He is presently in his final year reading for a Ph.D. in Biomedical Engineering, continuing this postgraduate

study at the same university. Current research interests include the development of optical fibre sensors and the use of lasers and optics in biomedical applications.

John C. Fothergill, a senior lecturer in Engineering, obtained his doctorate from UCNW, Bangor in 1979 in *Electronic Properties of Biopolymers*. From 1979 to 1984 he worked for STL in Harlow (now BNR Europe) on high voltage power cables. His interests include high electric field effects, optical fibre sensors for both biomedical and high voltage environments, and intelligent signal processing techniques.

Christopher D. Hanning graduated BSc, MB, BS from St Bartholomew's Hospital in 1972. He has been Senior Lecturer in Anaesthesia to the University of Leicester since 1981. His clinical and research interests encompass patient monitoring and the investigation and treatment of sleep disorders.

Barrie Jones was born in Liverpool in 1941. He obtained his B.Sc. in Electrical Engineering from Manchester University in 1962, was a graduate apprentice with BICC, obtained a M.Eng degree from McMaster University, followed by more industrial experience with Westinghouse in Canada. He obtained a D.Phil. degree in Control Engineering from the University of Sussex in 1968, and worked on various aspects of bioengineering there until 1984, specialising in control and signal processing applied to neurology and vascular surgery. He was director of the Sussex Centre for Medical Research for ten years. He is now Professor of Engineering at the University of Leicester, where he is continuing research in biomedical signal processing and instrumentation.

10 Acknowledgements

The authors would like to thank the following: **The British Lung foundation** for their financial support and assistance during the research, **EPSRC** for the scholarship for P.Goodyer's Ph.D. **Anthony Piper** (biomedical technician) for assistance during construction and preliminary experimentation.

Figures

Figure J-1

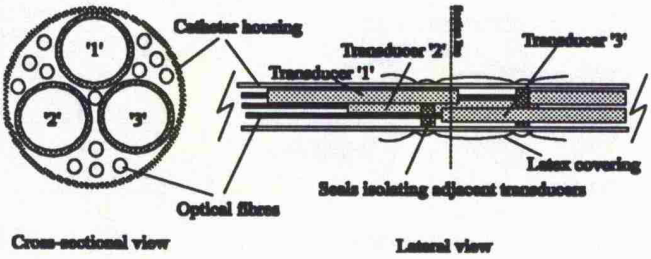

Figure J-2

Photograph of bedside apparatus

Figure J-3a

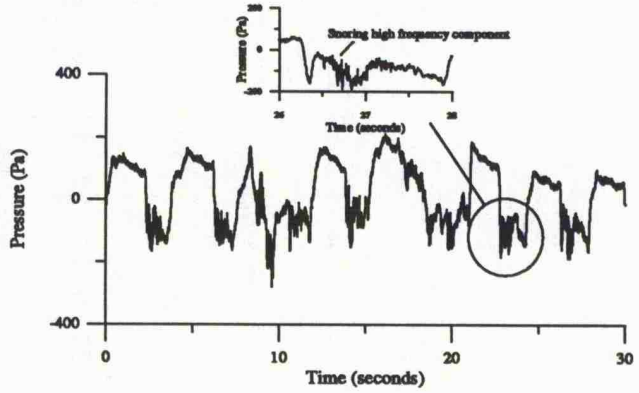

Figure J-3b

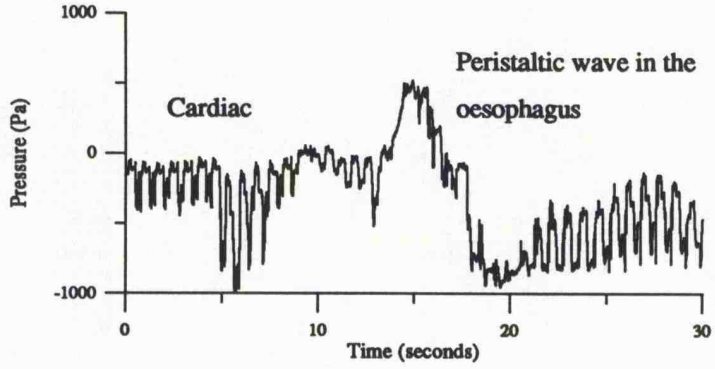

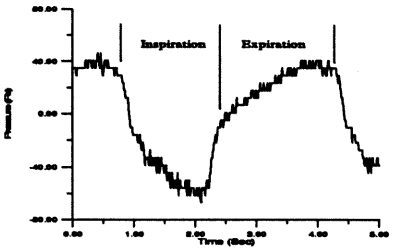

Figure J-4a

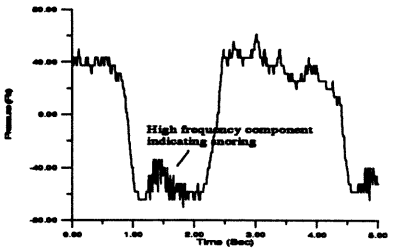

Figure J-4b

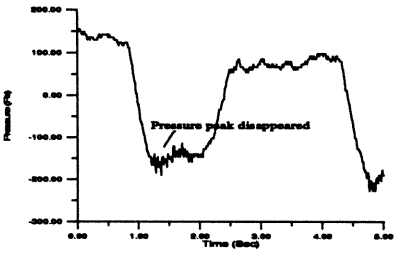

Figure J-4c

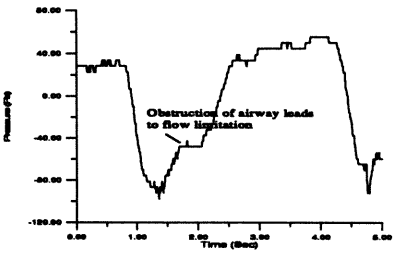

Figure J-4d

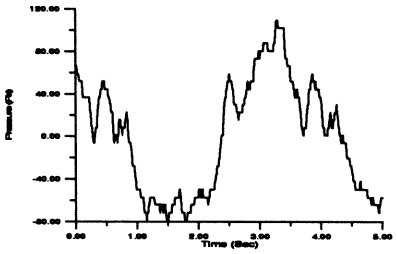

Figure J-4e

Patient Number	Sex	Build	Age	Observations
Patient 1	F	Slim	52	Normal airway. Low amplitude signals observed but steady increase in pressure 17Pa, 38Pa, 55Pa and 108Pa for transducers number 3 to number 6 detected.
Patient 2	M	Slim	65	Oral breathing observed, patient breathing normally. Transducers detecting 50Pa at the back of the throat, increasing to 400Pa for transducer number 6.
Patient 3	M	Heavy	55	Obstructing and snoring. Flow limitation observed on inspiratory flow. Evidence of soft palate vibration at 21.2Hz also detectable.
Patient 4	F	Medium	65	Obstructing and snoring. Waveforms showed large pressure swing (200Pa), also evidence of flow limitation, tissue collapse and palatal vibration.
Patient 5	M	Medium	57	Apparently breathing normally, but pressure transducer showed evidence of collapse at the back of the tongue

Figure J-5

Captions

Figure J-1 The construction of a catheter containing seven optical fibre pressure transducers shown as a side view and cross-section (Not to scale).

Figure J-2 A photograph of the constructed catheter containing seven optical fibre pressure transducers and the pre-amplification box.

Figure J-3a The optical fibre pressure transducer located 200mm from the entrance to the nose. Simulated snoring arising from the vibration of the soft palate in a locally anaesthetised subject.

Figure J-3b The distal optical fibre pressure transducer is located 400mm from entrance to the nose in mid-oesophagus.

Figure J-4a Transducer '1' located above the soft palate

Figure J-4b Transducer '2' located at the soft palate

Figure J-4c Transducer '3' 20mm away from transducer '2'

Figure J-4d Transducer '4' 40mm away from transducer '2'

Figure J-4e Transducer '7' located mid-oesophagus.

Figure J-5 A table summarising the results obtained from five patients under general anaesthesia.

Appendix K

Papers currently being wiritten

K.1

P.D.Goodyer, C.D.Hanning, J.C.Fothergill, C.Secker, N.B.Jones (1995), The development of a seven channel optical fibre pressure sensor for determining the site of collapse in obstructive sleep apnoea, British Journal of anaesthesia, To be submitted as conference paper

K.2

C.Secker, P.D.Goodyer, C.D.Hanning, J.C.Fothergill, N.B.Jones (1995), Clinical trials of an optical fibre pressure sensor for diagnosing obstructive sleep apnoea, British Journal of anaesthesia, To be submitted as conference paper